Development of a Wave Energy Basin to Maximize Wave Energy Conversion

by

Felipe Guerrero Martínez
16117727

Thesis presented in partial fulfilment of the requirements for the degree of Master of Engineering at the University of Stellenbosch

Department of Civil Engineering,
University of Stellenbosch,
Private Bag X1, Matieland 7602, South Africa

Supervisor: Mr G. Toms

March 2012

Declaration

By submitting this thesis electronically, I declare that the entirety of the work contained therein is my own, original work, that I am the owner of the copyright thereof (unless to the extent explicitly otherwise stated) and that I have not previously in its entirety or in part submitted it for obtaining any qualification.

Signature: .....
F. Guerrero M.

Date: March 12^{th}, 2012
.....

Abstract

Significant efforts have been made by researchers to enhance wave energy for extraction, and a number of wave energy devices have been proposed and prototypes have been built. To better understand wave energy conversion technology and its interaction with the resource (waves), a new device classification is proposed: *Wave interference* devices, *wave collector* devices and *wave resonance* devices.

In a similar line of investigation, the development of a wave energy basin to enhance wave energy conversion is investigated. The concept considers a shoreline-based resonant basin that makes use of the research on properties of the devices already classified. The interaction of a wave energy converter device inside the basin is not considered.

Results from physical and numerical modelling are promising. The wave energy density is increased by a factor of 2.9, but it is limited to a narrow wave frequency band.

The concept of a wave energy basin to enhance wave energy conversion can lead to further research. Wave energy resources might be increased even more by constructive wave interaction between radiated waves from wave energy converters and incoming waves within a resonant basin.

Opsomming

Aansienlike pogings is deur navorsers gemaak om golfenergie te verbeter vir ontginning, en 'n aantal golfenergie toestelle is voorgestel en prototipes is reeds gebou. Vir verdere navorsing word golfenergie-omskakelingstegnologie en die interaksie met die bron (golwe) as 'n nuwe toestelklassifikasie voorgestel: Golf-inmengingstoestelle, golf-versamelaarstoestelle en golf-resonansie toestelle.

In 'n soortgelyke lyn van ondersoek, is die ontwikkeling van' n golfenergie-kom om golfenergie-omsetting te verbeter ook ondersoek. Die konsep stel 'n kuslyn-gebaseerde resonante skottel voor wat gebruik maak van die navorsing en eienskappe op die toestelle wat reeds geklassifiseeris. Die interaksie van 'n golfenergie-omsettingstoestel binne die kom is nie oorweeg nie.

Resultate van die fisiese en numeriese modellering is belowend. Die golfenergie-digtheid is met 'n faktor van 2.9 verhoog, maar dit is beperk tot 'n smal golffrekwensieband.

Die konsep van 'n golfenergie-kom om golfenergie-omsetting te verhoog, kan lei tot verdere navorsing. Die golfenergie-bron kan verder verhoog word deur 'n konstruktiewe golf-interaksie tussengolwe wat van die energie-omsetters uitgestraal word, en die inkomende golwe binne 'n resonante kom.

Acknowledgements

I would like to express my sincere gratitude to the following people and organisations:

Mr Eddie Bosman, for his help with my application to the MSc programme on Coastal and Port Engineering at the University of Stellenbosch, and for his interest in wave energy. Mr Geoff Toms, my study leader, for his valuable comments on this thesis. The DHI, for providing an academic license for Mike 21 BW and technical support. The CSIR, for providing one of their wave tanks for this thesis, for preparing the wave tank and for setting up the paddles.

My shoreline crew: Suzanne van Zyl, for her valuable and voluntarily help and classes on the software *Sketch-up* to produce some of the sketches in this thesis. My friend Lorenzo Cerda, for showing me the "light" on LaTeX and linux OS, and for sending me the paper on resonators by Valembois.

And last but not least, to my office mate Christopher Baret and my "koffie boet" Matthys Saayman, for all those litres of coffee brewed, and for making my life a lot easier.

Dedications

A mi Padre†
y a mi Madre

Table of Contents

List of Figures

List of Tables

Nomenclature

Constants

$\pi =$ 3.141 592 654
$\rho =$ 1 025 $[kg/m^3]$ Density of sea water
$g =$ 9.81 $[m/s^2]$ Acceleration of gravity
$\gamma_e =$ 0.5772 Euler's constant

Units

J	Joule (work)	$[\mathrm{N \cdot m}]$
W	Watt (power)	$[\mathrm{J/s}]$
Wh	Watt hour (energy)	[3600J]
kW	kilowatt $= 1 \cdot 10^3$ Watts	
MW	megawatt $= 1 \cdot 10^6$ Watts	
GW	gigawatt $= 1 \cdot 10^9$ Watts	

Variables

η	Elevation of the water surface relative to the still water level	[m]
η_b	Backward waves η	[m]
η_f	Forward waves η	[m]
ω	Wave angular or radian frequency $(= 2\pi/T)$	[rad/s]
A_f	Amplification factor	[ ]
C	Courant number $(= c\Delta t/\Delta x)$	[ ]
c	Wave celerity	[m/s]
C_r	Reflection coefficient	[ ]
c_g	Wave group celerity	[m/s]
h	Water depth	[m]
$\overline{E}$	Average wave energy density	$[\mathrm{J/m^2}]$
f	Wave frequency $(= 1/T)$	[Hz]

H	Wave height	[m]
H_s	Significant wave height	[m]
H_{rms}	Root mean square wave height	[m]
k	Wave number ($= 2\pi/L$)	[rad/m]
K_r	Reflection coefficient	[ ]
K_s	Shoaling coefficient	[ ]
L	Wave length	[m]
$\mathcal{L}$	Capture width	[m]
n	Ratio of group celerity to phase celerity	[ ]
$\overline{P_{abs}}$	Mean wave power absorbed by a *WEC*	[kW]
T	Wave period	[s]
F or P_w	Wave energy flux or wave power	[kW/m]

Acronyms

CSIR Council for Scientific and Industrial Research, South Africa.
DHI Danish Hydraulic Institute
GDP Gross domestic product
OWC Oscillating water column
SWL Still water level
WEC Wave energy converter

Subscripts

o deep water

Terms and Definitions

The resource

Bathymetry. Topography of the sea floor.

Constructive wave interference. Interaction between fixed structures and incoming waves that results in an increase in wave energy.

Regular or monochromatic waves. Wave train with constant wave height and period.

Exploitable wave energy resource. Average wave power propagating in a fixed direction and limited to a multiple of four times the average wave power, i.e. for a constant wave period this is twice the incoming wave height (Folley and Whittaker, 2009).

Unexploitable wave energy resource. Excess wave power that cannot be extracted by a WEC, due to device or wave farm hydrodynamics (Folley and Whittaker, 2009).

Standing wave. Resulting pattern of waves travelling in opposite directions or head-on waves reflected by a vertical barrier.

Wave power

Amplification factor (A_f). Ratio between measured wave heights (or amplitude) at a point to the incoming wave height (or amplitude). In terms of wave energy density, the wave energy density would be modified by a factor of A_f^2 for linear waves, since $\overline{E} \propto H^2$.

Wave power. Time-averaged energy flux in a system of water waves (Pitt, 2009).

Wave energy resource. Wave power which occurs at a particular position or in a particular area integrated over whatever time scales are of interest (Pitt, 2009).

Mean wave power. Wave power averaged on the wave period.

Wave energy conversion

Point absorber. *WEC* with a symmetrical oscillating body.

Pitch. Rotational movement of a floating body around an axis parallel to the wave front.

Heave. Vertical motion of a floating body.

Wave tank. Basin used in hydraulic laboratories to model wave interaction with structures. Waves are generated by a wave maker.

WEC (Wave Energy Converter) device. Piece of machinery that houses a *PTO* system to absorb wave energy and convert it to electric energy.

PTO (Power take-off system). Mechanical equipment that is attached to an electric generator that allows it to draw energy (from waves). It is designed to be easily connected and disconnected. Types of *PTO* include hydroelectric turbines, air turbines, linear electrical generators and pump-to-shore systems (adapted from Wikipedia).

Wave energy farm. Arrangement of wave energy devices moored closely one to each other in order to maximise the capture of wave energy from the incoming wave front.

Chapter 1

Introduction

1.1 Background

The production of renewable energy from ocean waves is not a new idea, and proof of this is the first technique patented in France back in 1799 by Pierre Girard and son (Clement *et al.*, 2002). With the oil crisis in 1973, a new interest in wave energy research developed worldwide, promoting some of the most quoted wave energy researchers in the western world: Kjell Budal (†1989) and Johannes Falnes from the Norwegian Institute of Technology; David Evans from the Bristol University; Michael French from the University of Lancaster; Michael E. McCormick from the U. S. Naval Academy; Chiang C. Mei and John Newman from the MIT; and Stephen Salter from the University of Edinburgh.

South Africa was not excluded. A near-shore device, the Stellenbosch Wave Energy Converter *(SWEC)*, was designed in the early 1980's (Retief *et al.*, 1982) to suit local conditions. Investigations were abandoned within 10 years with the reduction in oil prices and consequent lack of research and development (R&D) funding.

Currently there are more than a thousand wave energy converter (*WEC*) devices that have been patented in Japan, North America and Europe. Nevertheless, only a few prototypes have been built and there is no well-proven device available commercially to date.

Today it is not only the price of oil that is driving the development of renewable energy sources. It is the need to diversify the energy matrix and also a long-term effect: emissions of greenhouse gases into the atmosphere, mainly carbon dioxide (CO_2) from the combustion of fossil fuels. The world energy supply to date is dependent on fossil fuels. Fortytwo percent of global energy generation is fuelled by coal (IEA, 2010), and coal power plants account for 28% of global CO_2 emissions. China is the second largest energy consumer, after the USA, with 15% of global energy use, and coal is the primary energy source, at 69% in 2000

(Wang *et al.*, 2011*b*). The world's biggest economies, which are also the biggest energy consumers, are the main contributors to CO_2 emissions. In descending order, the countries that contribute the most to global CO_2 emission are: China, USA, India, Russia, Japan and Germany (CDIAC, 2007). The European Union as a whole would be ranked third.

In South Africa, coal fuels 93% of electricity production (IEA, 2010), and in spite of the fact that it was ranked by the World Bank as the 31^{st} world economy in terms of GDP in 2009, it is the 13^{th} largest CO_2 emitter in the world (CDIAC, 2007).

Due to the above facts and concerns, a number of countries are changing their policies aimed at reducing the carbon footprint of their economies to a greater or lesser extent, giving room and incentives for the production of renewable energy.

Within this context, the South African government is already promoting a shift in energy generation to some extent away from coal towards renewables. As part of this policy, the *IRP-2010* or Integrated Electricity Resource Plan for South Africa 2010 to 2030 (DoE, 2010) was published for public review. A balanced scenario for 2030 is proposed, considering 33% of new capacity from renewable sources (16% in total, excluding a 6% Hydro), and 9% new capacity of coal-based load. With this plan, the coal contribution to energy generation would be reduced to 48% by 2030.

In terms of renewables, the *IRP-2010*, which is to be revised every two years, considers onshore wind energy capacity up to 5 GW by 2019 and solar power up to 600 MW by 2019. After 2019 it would depend on the maturity of the technology and pricing. It is interesting to note that wave energy conversion is not considered or mentioned in the *IRP-2010* report.

From the global wave energy resource estimates of Barstow (2008), the areas of highest overall offshore wave energy in the southern hemisphere are located off South Africa, Southern Chile, South and South West Australia and New Zealand. This wave energy resource is more stable if compared with locations elsewhere. The same author whows that the minimum monthly wave power relative to the annual wave power is higher and the ratio between the 100-year significant wave height and the mean wave height is lower if compared with the North Atlantic and North Pacific.

This effect can be better understood with the help of Figure 1.1, in which the oceans relative to each other and to land masses are shown with an accurate scale. The South Pacific, South Atlantic and Indian Oceans are the largest water surfaces on the Earth. Moreover, they are connected by the Southern Ocean that surrounds Antarctica (at the centre of Figure 1.1). This provides a large surface ocean area

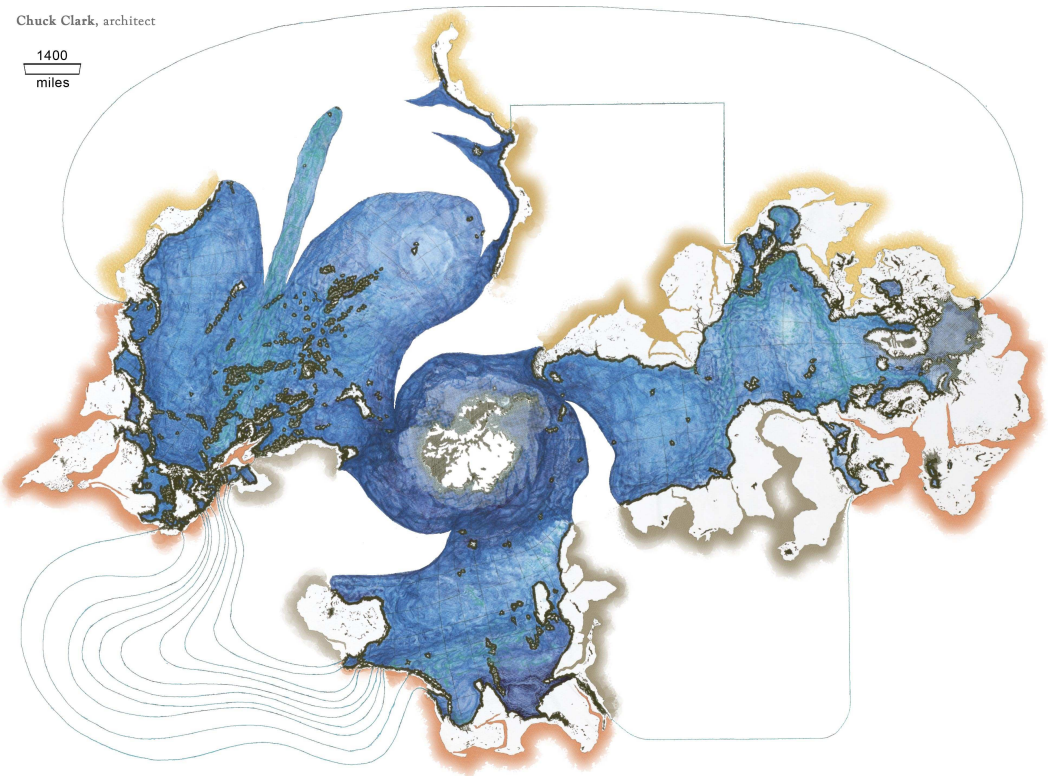

Figure 1.1: Spilhaus projection of the ocean watersheds drawn by Clark (2008) after J.P. Snyder. The overall proportion of land to water, the relative proportion of each ocean to the others, and the proportions, shape and size of the particular watersheds, relative to each other, are accurate. The map folds to a globe.

to produce and store wave power from the surface wind.

In South Africa, it was found from the work of Joubert (2008) that the South West Coast is exposed to the highest wave power, with an average wave power of approximately 40kW per metre wave crest. The rest of the South African coast is exposed to average wave power of between approximately 18 kW/m and 23 kW/m. For context, the first commercial wave energy conversion plant, Mutriku, was inaugurated in July 2011 in the North of Spain. This plant was integrated into a breakwater with an average wave energy resource of 7kW/m (Tease *et al.*, 2007).

1.2 Problem statement

In general terms, any project that requires the construction of facilities in the marine environment is a challenge in itself. For wave energy conversion developments

there are four main technical issues:

1. `Project location`. The first one is in relation to the location and its accessibility to existing supporting infrastructure for construction and maintenance of the facilities. Wave power is comparatively higher at exposed locations further away from land or in remote and inaccessible areas where there is a lack of infrastructure. Particularly for wave energy projects, the distance to the national power grid or final consumer is also relevant.

2. `Harsh marine environment`. The marine environment is aggressive and dynamic in terms of wind and wave loads, humidity and corrosion of steel and reinforcements, marine growth, abrasion and movable sea floor in coastal areas.

3. `Impacts on the environment`. The third difficulty is the potential environmental impact that should be considered from the start of any *WEC* development. Although it is not a direct technical difficulty in design, it is necessary to obtain environmental permits and to achieve a renewable and sustainable solution. The most typical impacts on the environment (Thorpe, 1999; Cruz, 2008) are noise, aesthetics, navigation hazard and impact on the marine flora and fauna.

4. `The resource`. A main problem is the manner in which the energy resource (waves) presents itself at the chosen site for wave energy extraction. Wave power is proportional to wave height squared and to the wave period, both of which are variable in space and time. Closer to the shore, wave heights are dissipated by breaking and wave directions are transformed due to wave interaction with the sea floor.

Considering the first three main technical issues as general types of problems for any type of marine works, the specific main problem in wave energy developments is the resource variability, as previously stated by Cruz (2008): The technical challenge is "*to convert the time varying incident power, to useful electrical power or into some useful repository of power storage*".

The problem of resource variability can be seen from three aspects (Clement *et al.*, 2002):

- `Irregularity in wave conditions`. Ocean waves are irregular in amplitude, frequency and direction, and also have hourly, daily and seasonal fluctuations. The power input is random and power output needs to be delivered in a constant fashion and when it is needed.

- `Slow motion`. Electric generators have to convert slow-motion waves into electricity at higher frequency to feed the power grid. A simple example would be to consider waves with a constant wave height and wave period (regular or monochromatic waves): then for typical ocean waves with a period of 10 s, this is a wave with a frequency of 0.1 Hz, and the electric generators have to convert the available wave power to match the 50 Hz of the power grid. This requires the generation of electrical energy at a frequency 500 times higher than the input wave energy.

- `Extreme events`. Extreme weather conditions impose large loads on the structures that need to be sized for survivability without necessarily increasing the capture of wave power.

The resource variability aspect also brings new challenges, in terms of the resource assessment and prototype scales for wave energy developments.
To quantify the resource, the average wave power usually is used as a parameter for comparison purposes between sites. Unfortunately this parameter is misleading, since it takes into account unexploitable wave energy. The exploitable wave energy resource is a better parameter (Folley and Whittaker, 2009), and is defined by the device or wave farm hydrodynamics and its plant rating. The wave energy resource is then technologically and economically limited, rather than only restricted by the available resource itself.

Finally, wave period defines the size and scale of the devices. This means that a device designed for the North Atlantic Ocean or the North Sea needs to be resized and built larger to be efficient offshore of the South African coastline. Indeed, the longer periods of the South African wave resource means longer wavelengths and even slower motions.

1.3 Objectives

The general objective of the study was to determine the feasibility of a shoreline-based basin designed to modify the wave energy resource. This was in order to reduce the resource variability of the incoming waves, as stated in 1.2, and then to maximize the power production by one or more wave energy devices deployed within the basin.

The specific objective of the investigation was to determine whether a special basin with a specific geometry open to the sea can increase the local wave energy density by trapping sea waves, and whether it is feasible to be used to maximize wave energy extraction.

1.4 Limitations

From the previous section, the investigation was aimed at enhancing the wave conditions in a basin in order to maximize wave energy extraction. The main limitations of this study would be in the validity of the wave theory used and in the assumptions made in the model to simplify the geometry of the basin.

An effect that will not be modelled is the impact of *WECs* on the basin dynamics. It is expected that a *WEC* operating at resonance would radiate waves that might couple with the basin waves, also at resonance, changing the wave pattern inside the basin. This is an effect that depends on the design of the *WEC* itself and also on the interaction between them if more than one. These are both subjects that are beyond the scope of this study.

1.5 Significance of the study

The design premise of the proposed basin is to minimize the problems identified in 1.2. In this regard, the proposed basin can be referred as an enabling technology for wave energy conversion, and the aim would be to:

1. *Work as an accumulator*, allowing *WECs* to extract wave energy from a more constant distribution of wave heights in time. For a given incoming wave energy flux, the system is expected to increase the wave energy density, reducing the irregularity in wave amplitude.

2. *Reduce the structural loading in the event of extreme weather conditions.* Physically it is possible to restrict the maximum wave heights by limiting the water depths. Also, the project location and the orientation of the entrance of the basin can reduce the exposure to storm waves. The *WECs* to operate inside this system can then be designed with less risk of damage from extreme storms, reducing *WEC* construction costs and increasing survivability.

Besides the above, the location of the basin would provide secondary effects that should be considered, as follows:

1. Potential environmental impacts on the shoreline.

2. A shore-based basin might reduce the *WEC* installation and maintenance costs, since access would be easier.

3. A basin allows the operation of different types of WECs inside the basin.

4. An increased number of WECs per unit of surface area reduces the demand for ocean surface.

5. A basin can also be used as a testing facility. The *WEC* technology might be improved over time, but could still utilize the same basin.

This basin is not a *panacea* for wave energy extraction, since it is adding the construction cost of the basin and would be limited to the available room along the shoreline. In spite of this, the concept of a wave energy basin is considered promising.

1.6 Thesis overview

This introduction (Chapter 1) presents technical problems in wave energy conversion, as well as the objectives, limitations and significance of this thesis.

Following the Introduction, the literature review is presented in Chapter 2. Wave energy absorbers are presented from the point of view of the resource rather than the characteristics of the device. A WEC device classification is proposed based on its interaction with the incoming waves. Based on this classification, common characteristics between wave energy absorbers are evident. Potential wave interactions that can be enhanced in a basin are proposed.

In Chapter 3 the methodology of the investigation is explained, starting from a proposed basin layout to maximize wave energy conversion. Details of physical experiments and numerical model studies are described.

Chapter 4 presents the results of both the physical and numerical experiments. A discussion of the results follows.

Finally, in Chapter 5 significant conclusions are drawn and further studies are proposed.

Chapter 2

Literature review

2.1 Introduction

The idea of a basin to maximize wave energy conversion sounds expensive to build, but it is appealing to increase wave energy density for better availability to wave energy converter (WEC) devices. Besides, a shoreline basin would provide easy access for maintenance.

Wave energy extraction is a complex, dynamic 3D process. In this process the hydrodynamic effects used by the power take-off (PTO) system are specific to the WEC design. Hence it is necessary to observe and understand what has been done in wave energy conversion before attempting to improve the wave conditions inside a basin.

Wave energy converters at different development stages are listed in Khan and Bhuyan (2009). Special attention was given to $WECs$ that are at a similar design stage. From those WECs, 16 were selected because they have a prototype, are representative of a type of WEC, and there is enough information publicly available. These 16 wave energy converter devices are presented by their interaction with waves to increase the capture of wave power by the PTO system.

The power capture performance of a wave energy device can be measured by the capture width. Capture width ($\mathcal{L}$) is by definition the ratio between the total mean power absorbed by the wave absorber and the mean power unit of the wave front (P_w) of the incident waves. The device then captures an amount of $\mathcal{L}P_w$. This index is widely used in wave energy conversion, and can be seen as a bulk index of wave energy converter performance.

The review of wave energy conversion devices leads to a proposal for a new WEC classification, based on the interaction of the device with the resource (waves) rather than on characteristics of the device. This literature review is organized on

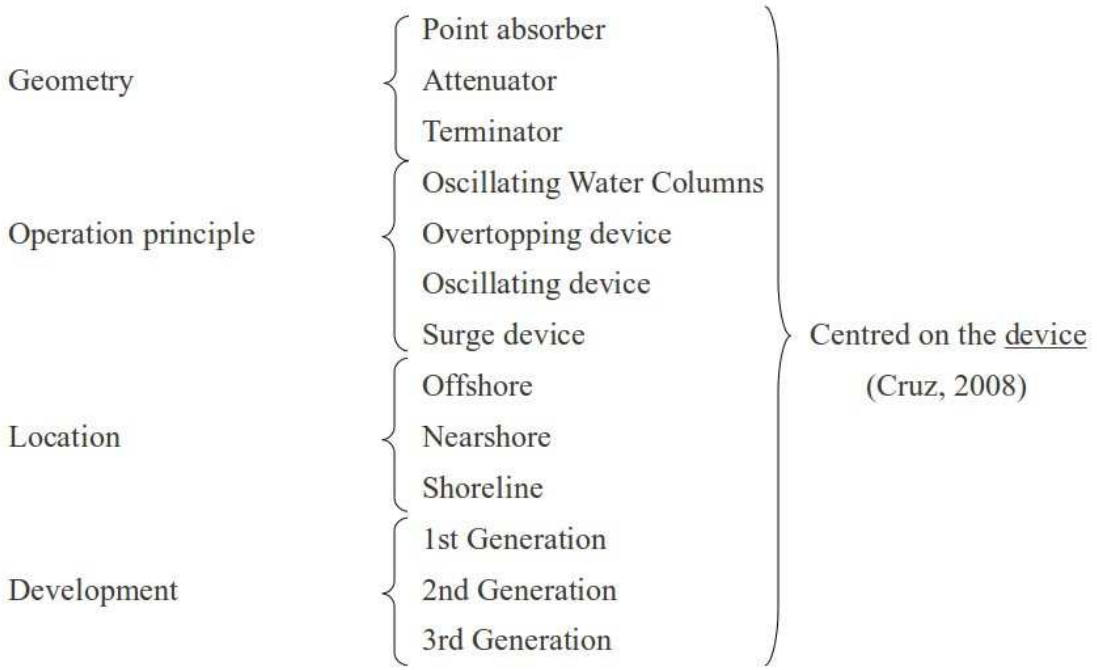

Figure 2.1: Classification of wave energy converters based on properties of the device (Cruz, 2008).

the basis of this new classification.

This chapter concludes with the most suitable wave interaction to be enhanced within a basin to maximize wave energy conversion.

2.2 Classification of wave energy converters

Classifications of wave energy converters (*WECs*) are typically based on the geometry, its principle of operation and the location of the device (Cruz, 2008; Falcao, 2010). These classifications are illustrated in Figure 2.1. From the geometry, a *WEC* can be classified as a point absorber, an attenuator or a terminator. The principle of operation of the *WEC* defines if it is an oscillating water column (*OWC*), an overtopping, oscillating or surging device, and the device can be located offshore, nearshore or at the shoreline. An alternative classification considers the status of development of the device: first-, second- and third-generation systems (Cruz, 2008). All of these classifications are centred on the device.

To improve the wave energy resource for extraction in a basin, it is necessary to understand the way in which the *WEC* interacts with the resource to extract en-

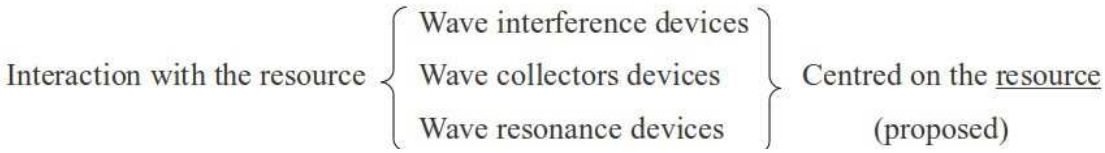

Figure 2.2: Proposed new classification of wave energy converters based on the interaction of the device with the resource.

ergy. For this purpose, a complementary classification is proposed centred on the resource rather than on the device, as shown in Figure 2.2. These interactions are basically *wave interference*, *wave collection* and *resonance*. These three interactions are present to a greater or lesser extent in every *WEC* design. An optimum *WEC* design should optimise these abilities.

Representative *WEC* devices that have prototypes are grouped and presented by their main ability to *interfere* with the incoming waves, to *collect* or focus waves at a point or area, and to amplify the water surface elevation by *resonance*.

2.3 Wave interference

For an oscillating system to be a good wave energy extractor, it should also be able to be a good wave generator when driven by external energy. Waves generated by an oscillating body should cancel the transmitted or reflected waves for maximum extraction (Falnes and Budhal, 1978). Hence, *wave interference* needs to be of a destructive nature to be useful for wave energy absorption. As illustrated in Figure 2.3, a body oscillating in heave and pitch, driven by external energy, can transmit a wave that completely absorbs an incoming wave.

In the case of a *point absorber*, when it extracts energy from incoming waves it generates circular waves radiating away from the submerged surface of the oscillating body (Falnes, 2002), as illustrated in Figure 2.4. These radiated waves therefore limit the device performance, since they are generated by the device work.

Similarly, Falnes and Budhal (1978) introduced the term *dynamic reflection*. Dynamic reflection takes place when an oscillator generates waves opposite in direction to the incoming waves, but shifted in phase to generate a *standing wave* with a *node* at the oscillator.

2.3.1 Constructive wave interference of fixed structures

The superposition of linear regular waves heading in opposite directions produces a *standing wave* pattern. This can happen offshore by waves coming from different

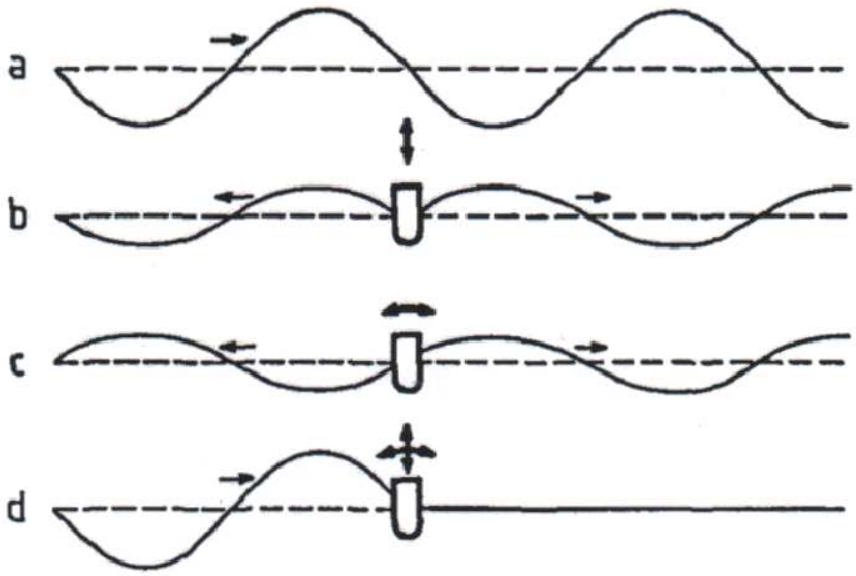

Figure 2.3: Wave interference by an oscillating body (Falnes and Budhal, 1978). a) incident wave, b) symmetric wave generated by an oscillating body in heave, c) antisymmetric wave generated by an oscillating body in pitch, and d) superposition of waves from a), b) and c) completely absorb the incident wave.

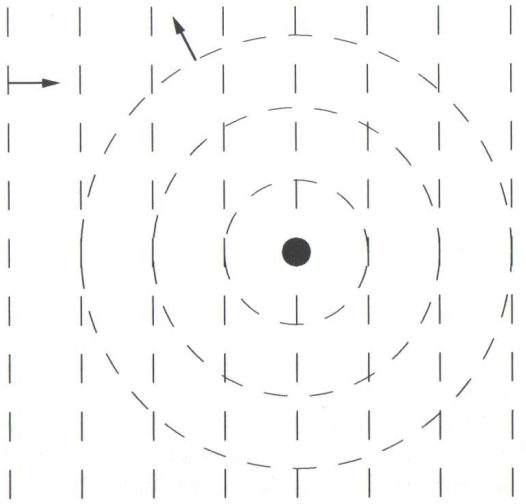

Figure 2.4: Wave pattern of two interfering waves seen from above (Falnes, 2002).

generation zones, nearshore by reflected waves from a reflecting coastline, or within a harbour due to wave reflection from vertical quay walls.

The wave energy storage $\overline{E}$, also called wave energy density, in a *standing wave* pattern is twice the incoming average wave energy (Holthuijsen, 2007; Falnes, 2007),

$$\overline{E}_{standing} = \rho g(\overline{\eta_f^2} + \overline{\eta_b^2}) = 2\rho g\overline{\eta_f^2} = 2\overline{E}, \tag{2.3.1}$$

with η_f and η_b the forward and backward water surface elevations respectively. This is considering an ideal fully reflective vertical wall without dissipation ($\eta_f = \eta_b$) and head-on waves.

On the other hand, the wave energy transport $\overline{F}$, or average wave energy flux, is zero at the antinodes, since no energy is transmitted forward at a vertical wall,

$$\overline{F}_{standing} = 0. \tag{2.3.2}$$

In the case of partial reflection, the reflected water surface elevation η_b would be a fraction of the incoming water surface elevation η_f. In terms of the reflection coefficient, $C_r = \eta_b/\eta_f$ with $0 \leq C_r \leq 1$. In this case, the wave energy storage on a *standing wave* pattern with partially reflected head-on waves becomes

$$\overline{E}_{standing} = (1 + C_r^2)\overline{E} \tag{2.3.3}$$

and the wave energy transport or flux is

$$\overline{F}_{standing} = (1 - C_r^2)\overline{F} \tag{2.3.4}$$

which for perfect reflection ($C_r = 1$) becomes zero, as in the particular case of equation 2.3.2 (Holthuijsen, 2007; Falnes, 2007). Typical values of reflection coefficients for different structures can be found in Thompson *et al.* (1996).

Waves at an angle produce a slightly more complicated pattern. The resultant oscillation of two wave fronts at an angle of 45° is illustrated in Figure 2.5. This particular *standing wave* pattern has nodal lines at an angle and antinodes on single points.

A similar pattern is formed in front of a vertical wall by incoming waves at an angle. The main difference is that nodal lines are not fixed. Nodal lines perpendicular to the wall travels along the wall (pattern movement in Figure 2.6), producing a wave along the wall, as shown.

On the other hand, a fully reflective structure like a vertical wall with head-on waves and no absorption will reflect all the incoming wave energy, opposite in direction and with the same phase. A *standing wave* will be generated with an anti node at the wall. If a symmetrical oscillating body in heave (point absorber) is

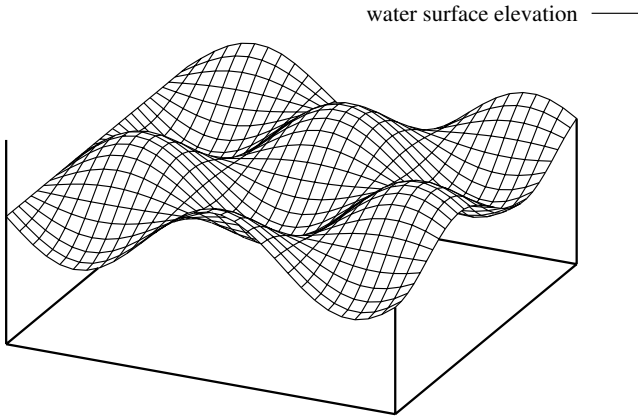

Figure 2.5: Superposition of waves at an angle of 45°.

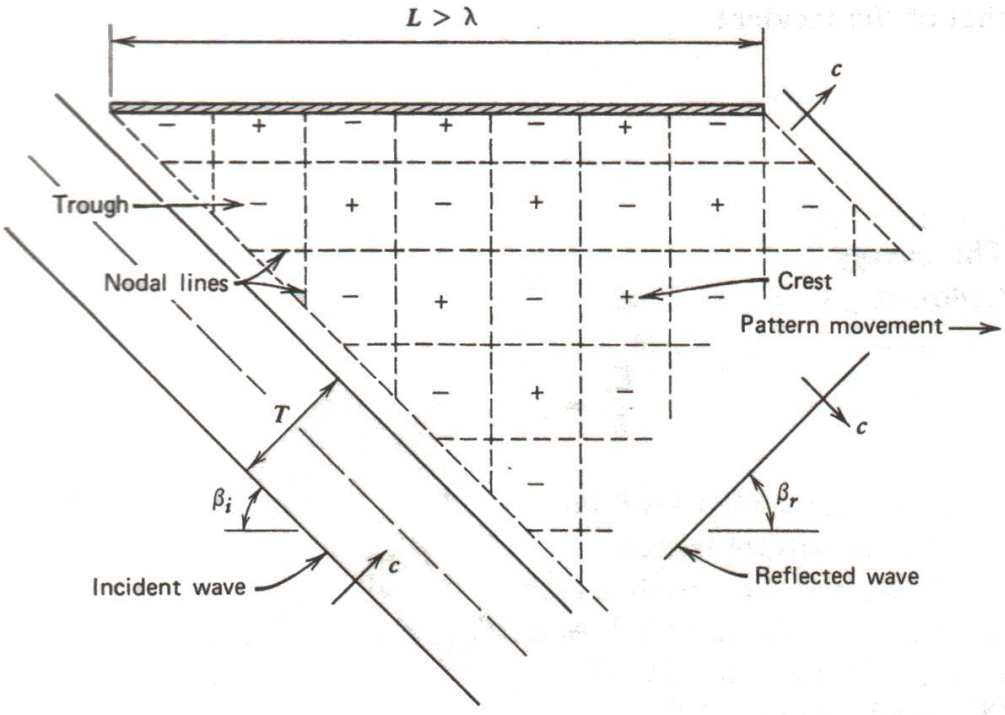

Figure 2.6: Perfectly reflected oblique wave pattern from a finite vertical barrier (McCormick, 2007).

located at an *antinode* in front of this reflective wall, the potential for wave power absorption increases. In contrast, if it is located at a node it drops to zero (Evans, 1988).

The effect of the local shoreline on a wave energy converter was studied by Brito-Melo *et al.* (2000). This research focused on the effect of the local *bathymetry* on the performance of an *oscillating water column (OWC)* device by using a boundary element method. In a similar line of investigation, Martins-Rivas and Mei (2007) studied linear diffraction by an *OWC* chamber located at the head of a breakwater.

Wave scattering from an *OWC* chamber at the head of a breakwater was studied by Martins-Rivas (2008), and an *OWC* on a cliff coastline was reported by Martins-Rivas and Mei (2009). In both cases a linear hybrid element method was used, which was based on potential flow, radiation boundary conditions and the inclusion of the effects of the *OWC* chamber on the velocity potential. In the first case, it was noticed that the response of the system depends strongly on the angle of incidence, and in the second one, the capture length was doubled due to coastal reflection.

From these references, wave interference is also relevant in terms of the structures nearby a *WEC*. The superposition of incoming waves, radiated waves from the *WEC* device, and scattering of waves from nearby structures or the shoreline affects the overall performance of the wave energy converter device.

Similarly to oscillating bodies, radiated waves from fixed structures such as vertical walls or a reflective coastline can contribute to increasing the wave power capture. The main difference would be that a single coastal structure absorbs energy only by dissipation. Hence, in this case it is not possible to invert the phase of the incoming waves.

In conclusion, in this thesis the term *constructive wave interference* is used to define the interaction between fixed structures and incoming waves that results in an increase in wave energy.

2.3.2 Wave interference devices

Wave energy converters that fall into this category are basically oscillating bodies that, through their motion, absorb power, but at the same time radiate waves that interfere with the incoming waves. These absorbers can be floating, submerged or fixed to the bottom, and generally the destructive interference is enhanced when the absorbers operate in an arrangement of units (Falnes and Budhal, 1978).

The first wave absorber that succeeded in interfering destructively with the incoming waves was the Salter Duck of Salter (1974). The effect is clearly seen in the

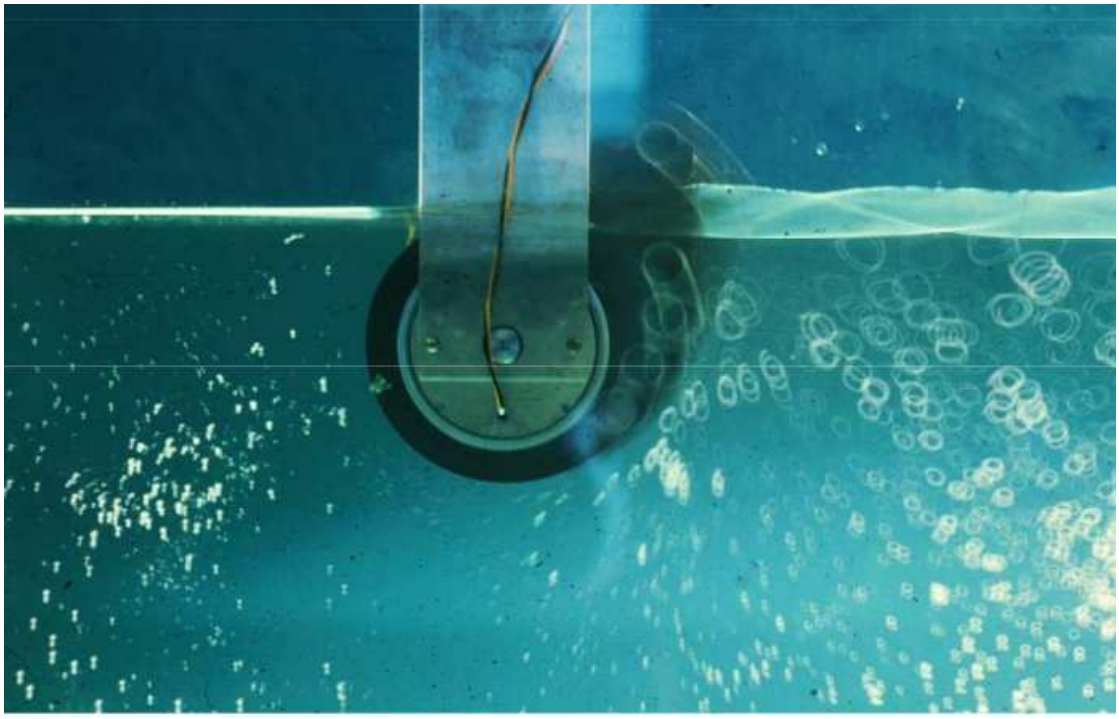

Figure 2.7: Destructive interference of the Salter Duck (Salter, 1974). Time exposure with tracing fluid showing size of reflected and transmitted waves (photo by Jamie Taylor in 1976).

slow shutter speed photo by Jamie Taylor in 1976 (Figure 2.7). The asymmetric Salter Duck in *pitch* interferes with the incoming waves, but radiates no energy in the wave direction, absorbing most of the wave power. Hence, the more effective the device, the fewer waves are radiated away from the device in the wave direction.

An analogue effect to the Duck was achieved by the Pelamis wave energy converter, shown in Figure 2.8. Provided by four or five cylindrical sections, the joints allow a restricted vertical and lateral movement by an orthogonal pair of inclined axes from vertical and horizontal, as illustrated in Figure 2.9. The motion between adjacent sections drives hydraulic compressors at the hinges (Cruz, 2008). The combined motion, similar to the motion of a snake, produces a characteristic radiation pattern in which the motion of the buoyant sections reinforces waves in a prescribed direction and cancels others, while the waves move along the device (Figure 2.10). This pattern increases the theoretical maximum capture width of the Pelamis up to half a wave length, which is three times (π) more effective than a floating buoy with the same volume (Cruz, 2008).

Figure 2.8: Pelamis *WEC* allows vertical and lateral motions to increase capture width. Bottom right: Pelamis at a dry-dock (http://www.pelamiswave.com).

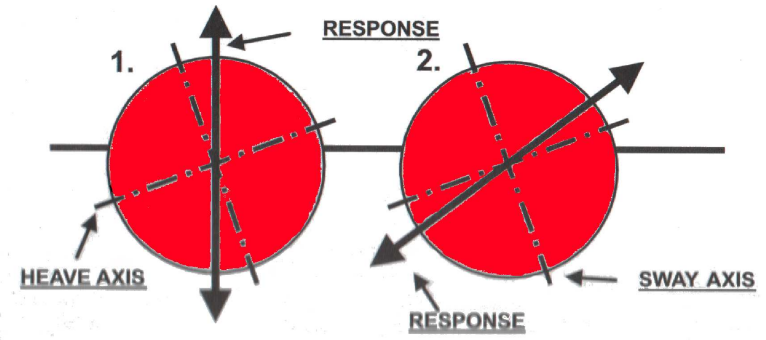

Figure 2.9: Schematic response of a cross section of the Pelamis *WEC*. Response under non-resonant (1) and resonant (2) modes.

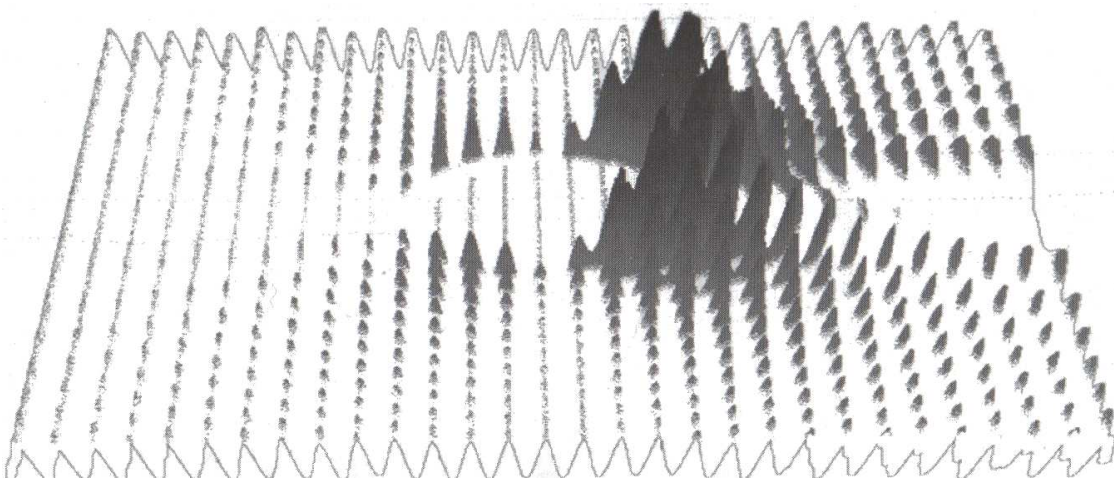

Figure 2.10: Wave interference of the Pelamis *WEC* (Cruz, 2008).

There are other two subgroups of oscillating wave absorbers that interfere with the incoming waves: floating and submerged symmetrical oscillating bodies.

Floating symmetrical oscillating bodies are buoys, of different size, shape and power take-off systems, that radiate waves as illustrated in Figure 2.4. This allows an increase in maximum capture width to the incoming wave length divided by 2π (Cruz, 2008). There are several designs of buoy absorbers, such as the IPS buoy or the Power Buoy, shown in Figure 2.11.

Submerged symmetrical wave absorbers also radiate waves in a similar pattern to the floating ones, such as the Arquimedes Wave Swing (Figure 2.12) or the CETO-3, shown in Figure 2.13 (left). In these cases the devices are submerged but close to the water surface, where the wave energy is higher. A CFD model of the interaction between the submerged sphere of the CETO-3 *WEC* and the incoming waves is shown in Figure 2.13 (right). Short waves radiate from the oscillating body.

Figure 2.11: Oscillating devices: the IPS buoy (Weinstein, 2006) (left) and an arrangement of Power Buoys devices (artist's impression) (right).

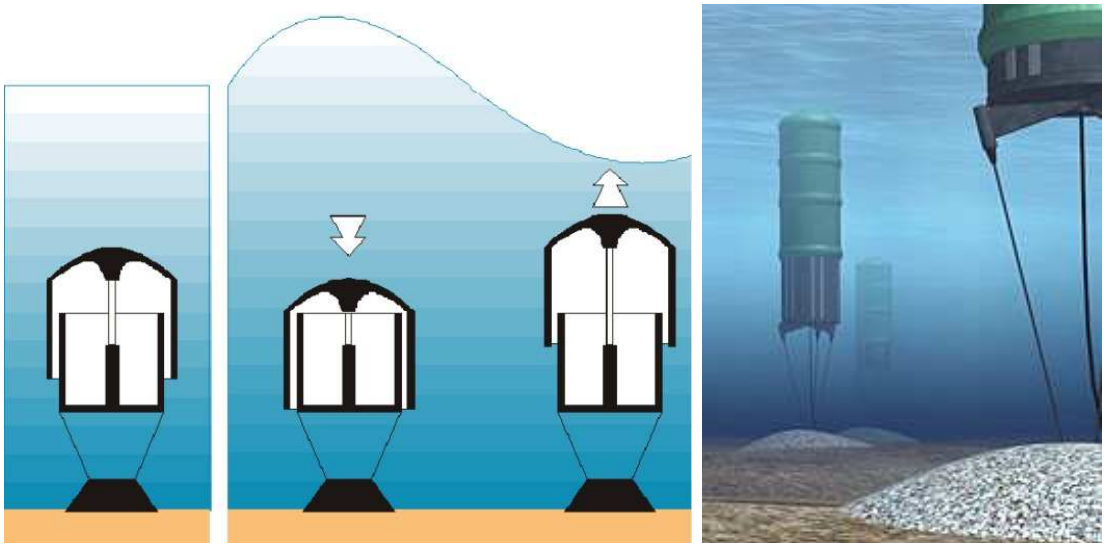

Figure 2.12: Submerged oscillating wave energy device with a linear generator, the Arquimedes Wave Swing (http://www.awsocean.com and Polinder *et al.* (2005)).

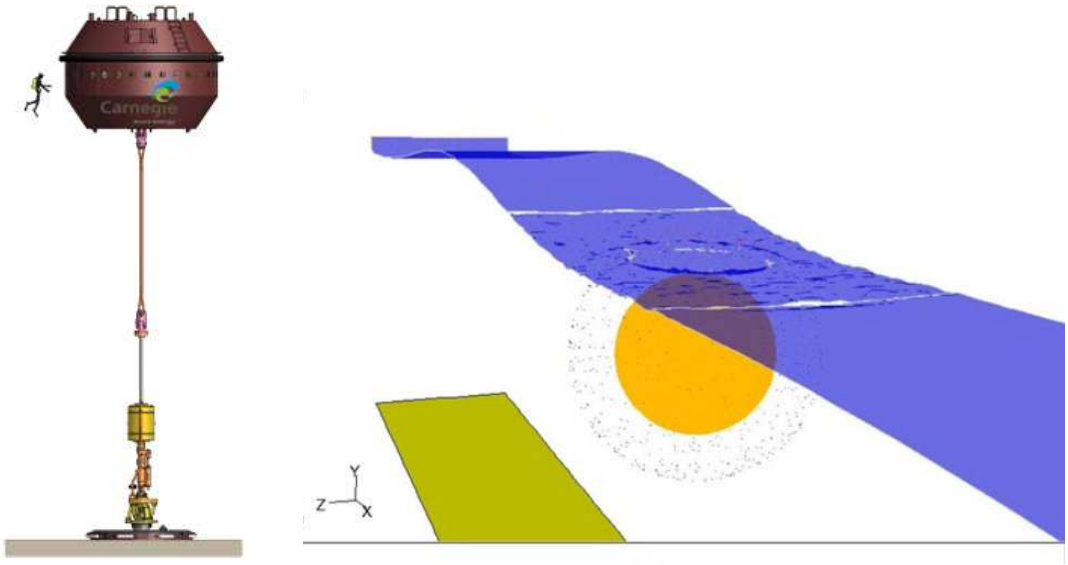

Figure 2.13: CFD model of the interaction between the bottom fixed and submerged sphere of CETO-3 WEC (left) and the incoming waves. The PTO system pumps sea water to shore (http://www.carnegiewave.com).

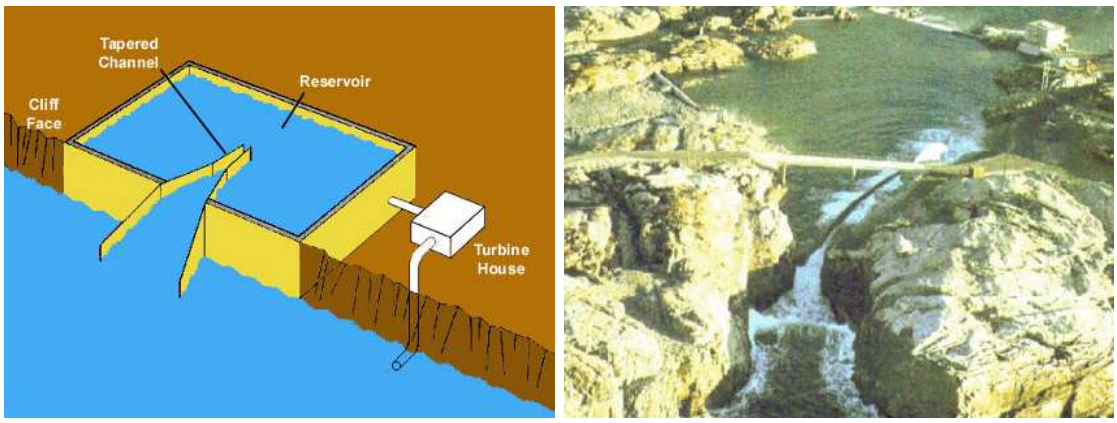

Figure 2.14: Tapered channel (Tapchan) funnels waves to fill a reservoir by overtopping.

2.4 Wave collector devices

Wave collectors are wave energy devices with appendices or structures with the ability to increase the available wave power levels at the converter. A way to achieve this is to increase the overall width of the device by means of reflectors to focus the wave power at the location of the wave absorber.

A wave collector can be found in nature as rocky gulleys, where the wave power is concentrated by the narrowing sides of the gulley and a favourable near-shore bathymetry. The effectiveness of the collector for wave power absorption depends on its shape, size and degree of exposure to wave power, i.e. water depth and slope, orientation, entrance width, bottom roughness and, of course, local wave climate.

Man-made wave collectors can also be structures or appendices designed to increase the wave energy absorber capture width. Narrowing channels, wave reflectors and bottom mounds are types of wave energy collectors that have been designed, built or proposed, as presented below.

2.4.1 Narrowing channel

A wave collector in front of a wave absorber is effective. The collector provides increased levels of wave power per metre wave front at the device for the same offshore wave power. This can be done by narrowing the distance between the side walls in a channel, utilising a natural gulley, or by focusing the wave energy into an area by refraction or reflection. The purpose is to reduce the width of the wave front for a constant level of wave energy flux.

An example of this wave power capture structure is the Tapchan, illustrated in

Figure 2.15: Tapchan rocky gulley and tapered channel. Left: Waves funneled at the rocky gulley (bottom right), then at the tapered channel (centre) to fill the reservoir by overtopping (top left). Photo from Falnes and Hals (1999). Right: Aerial view of the collector and channel after decommission (Google Earth).

Figure 2.14. This *WEC* has two narrowing channel effects. Firstly, a natural rocky gulley funnels wave power into a channel entrance and, secondly, the man-made channel (the Tapered channel) also narrows, but this time to gradually absorb wave power. The channel collector was built for the 350kW tapered channel that operated in Tofiestallen, Norway, from 1985 to 1991 (Brooke, 2003).

The narrowing effect of a rocky gulley is site specific, depending on gulley plan shape, size and bathymetry. The plan shape of the natural gulley and narrowing channel can be seen in Figure 2.15.

At the end of the natural gulley, the narrowing channel has 6 m to 7 m water depth with a flat bottom. Vertical concrete side walls extend up to a height of 2 m to 3 m above mean sea level (Brooke, 2003). The channel funnels waves and increase the wave energy levels. The increased water surface oscillation spills over the sides of the channel to fill a reservoir, reported to have an area of 8,500 m^2. The hydraulic head drives a generator.

After this design, another Tapchan device of 1.1 MW installed power was proposed to be built in Indonesia, the INDONOR's TapChan power plant. The project was abandoned after the financial crisis in late 1997 (Brooke, 2003)

In the case of the proposed 1.1 MW power plant in Indonesia, the wave collector dimensions were 126 m long with a maximum width of 124 m. The narrowing channel (tapered channel) was designed to -8 m chart datum (CD), 60 m long with a maximum width of 7 m (Falnes, 2005).

A balance of energy between planes perpendicular to the wave direction and at both ends of the channel leads to $b_1\overline{F_1} = b_2\overline{F_2}$ with $\overline{F} = nc\overline{E}$. This is without losses and channel widths on its ends b_1 and b_2. The power capture at the narrow side of the channel then becomes $\overline{F_2} = \overline{F_1}b_1/b_2$, which is a linear gain in wave energy capture. The drawback is that it requires a long structure to minimise wave reflections and gradually increase wave power.

The Pendulor shown in Figure 2.16 is another example of a wave collector. Convex vertical walls funnel wave energy into a chamber where the *PTO* system is located (Wang *et al.*, 2011*b*).

A natural gulley is also a collector. A slowly narrowing gulley cross-section and shoaling increase the wave energy density. Oscillating water column prototypes that use this effect are the 75kW Queens University of Belfast device , the 400kW Pico plant in Figure 2.17 (Falcao, 2000), and the 40kW plant at Sansei shown in Figure 2.18 (Hagerman, 1992).

As mentioned in Section 2.3, the research of Brito-Melo *et al.* (2000) focused on the effect of the local shoreline on a *WEC*. The wave energy converter studied was the *OWC* of Pico Island, illustrated in Figure 2.17. The numerical model of the *OWC* chamber was extended to include the rocky gulley (Figures 2.19 and 2.20).

The main advantage of devices built on natural gulleys is that a relatively small size device make use of the existing natural rock to increase the capture of wave power. The disadvantage is the natural gulley itself: it is site specific and water depths and slopes can limit the incoming wave energy by early wave breaking.

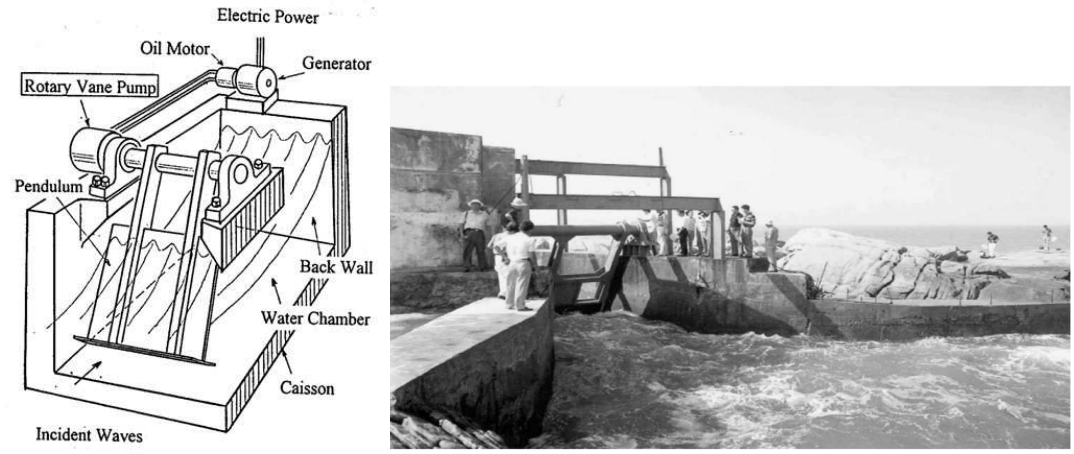

Figure 2.16: Funnel effect of the Pendulor wave energy converter. Left: concept sketch of the mechanical parts. Right: 100kW Pendulor prototype with convex walls at Daguan Island (Wang *et al.*, 2011*b*).

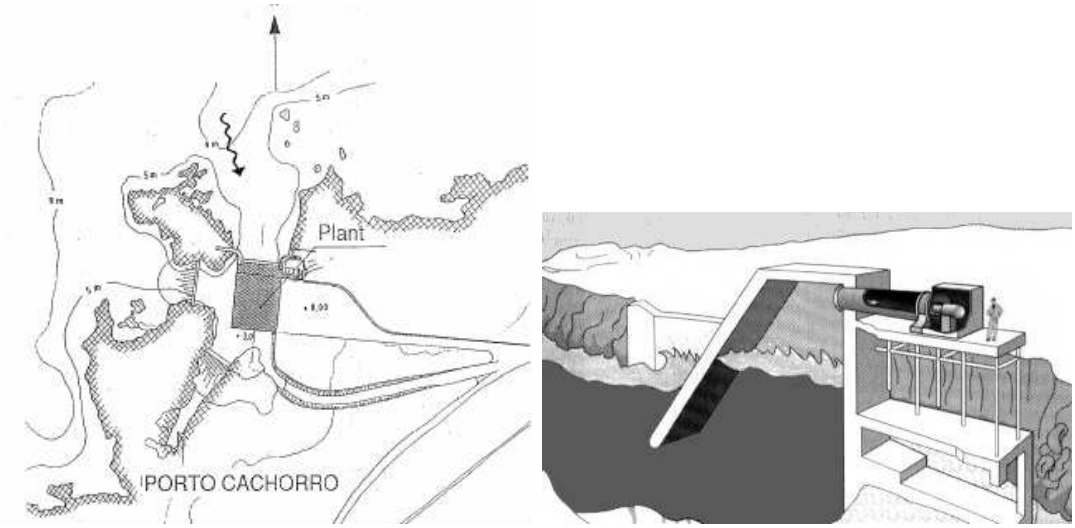

Figure 2.17: Gulley effects of the OWC in Pico Island at the Azores. Left: Plan location of the 400kW *OWC* prototype. Right: sketch of the chamber and air turbine (Falcao, 2000).

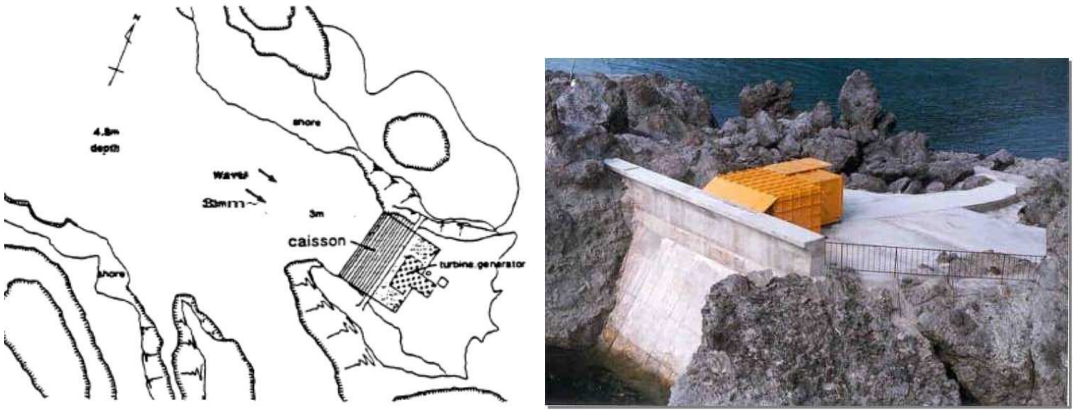

Figure 2.18: Gulley effects of the 40kW *OWC* Sansei. Left: plan location. Right: bird's eye view of the prototype (Hagerman, 1992).

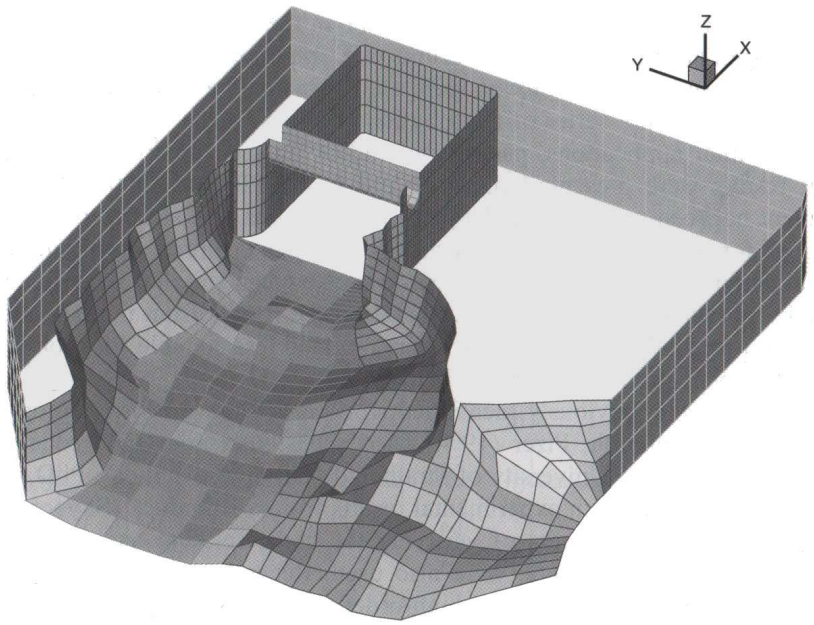

Figure 2.19: Rocky gulley included in the model of the Pico Island OWC (Brito-Melo *et al.*, 2000).

Figure 2.20: Pico Island *OWC* from Google Earth. Azores Archipelago.

Figure 2.21: Wave reflectors on a 1:4.5 prototype scale of the Wave Dragon overtopping device (Kramer and Frigaard, 2002; Sorensen *et al.*, 2003).

2.4.2 Wave reflectors

Wave reflectors are another means to "collect" wave energy and increase capture width. The objective is to focus wave power at a point or area by wave reflection. The advantage, if compared to narrowing channels, is that they can be shorter for the same level of power capture.

A floating wave reflector was designed for the Wave Dragon *WEC* shown in Figure 2.21. In this floating devices, wave reflectors are appendices on each side of a reservoir. Wave energy is reflected towards the ramp and fills the reservoir by overtopping waves. The *PTO* system is a low head hydraulic turbine. The plan shape of the reflectors must be parabolic, with the focus at the ramp. Floating *WECs* can be moored and exposed to more energetic offshore waves. Since wave energy decays exponentially with depth, the draft of floating reflectors is relevant to utilize the higher energy levels on the ocean surface.

According to Kramer and Frigaard (2002), the configuration tested in the physical and numerical models gave efficiencies of 130% to 140%. The efficiency figures of the reflectors were calculated as the mean power at the centre cross-section (at the ramp of width 2c in Figure 2.22) divided by the power of the undisturbed incoming wave. From this definition it can be said that the calculated efficiencies (130% to 140%) are mean *amplification factors* (along the cross-section) squared (A_f^2).

The *amplification factor* A_f was defined as the ratio between the measured wave heights (or amplitude) at a point to the incoming wave height (or amplitude). The A_f squared represents the increase in wave power compared to the incoming wave power.

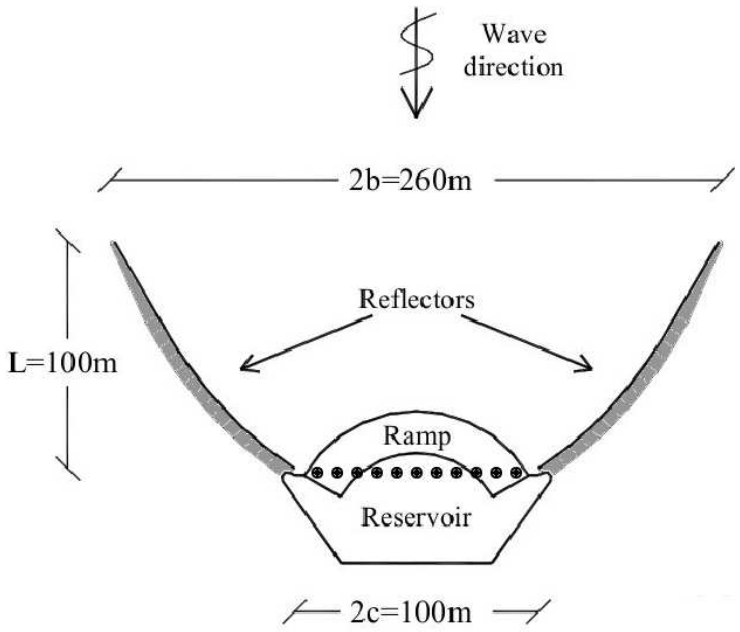

Figure 2.22: Floating wave reflectors of the Wave Dragon *WEC*. Black circles represent the position of 11 wave gauges used to measure surface elevations (Kramer and Frigaard, 2002).

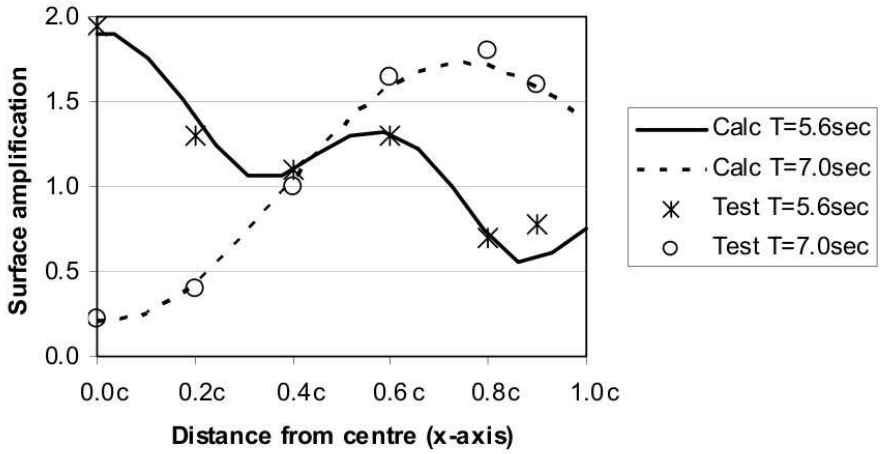

Figure 2.23: Wave Dragon model tests. Surface water amplification at six wave gauges from centre (Kramer and Frigaard, 2002).

The measured amplification factors are presented in Figure 2.23. From this figure it can be seen that the reflectors become more effective with shorter waves. The longer the reflectors, the more power they capture.

What was not presented in Kramer and Frigaard (2002) is the wave between the reflectors. This wave pattern might amplify the wave heights at fixed locations of the cross-section in the study, similarly to the oblique wave pattern from a finite vertical wall illustrated in Figure 2.6. The wave pattern depends on the wave period, as can be seen in Figure 2.23.

Another device with parabolic reflectors is the *OWC* "Mk-1" from Energetech, shown in Figure 2.25. Wave energy is focused under the chamber of an oscillating water column. An air turbine drives a generator.

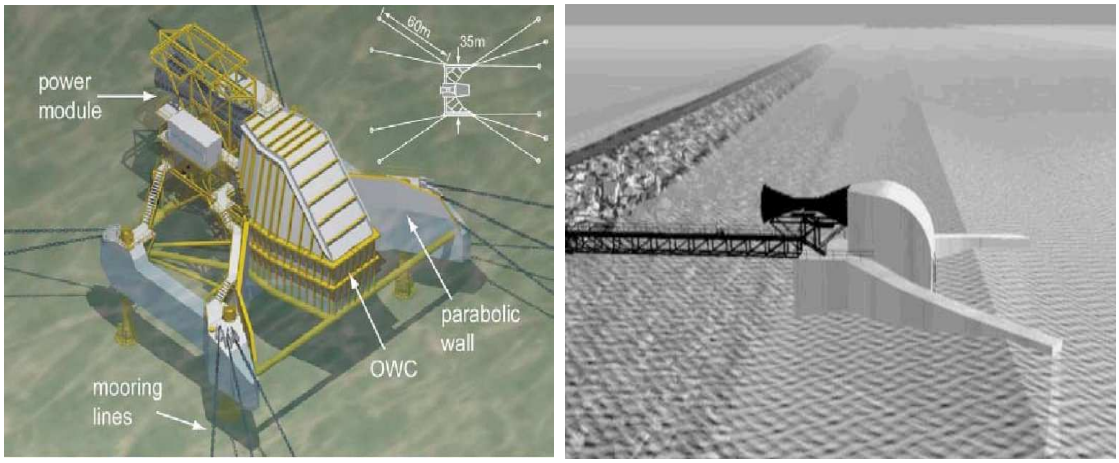

Figure 2.24: Diagrams of the parabolic reflectors on the 500kW oscillating water column "Mk-1" by Oceanlinx (previously Energetech), Australia (Previsic, 2004)

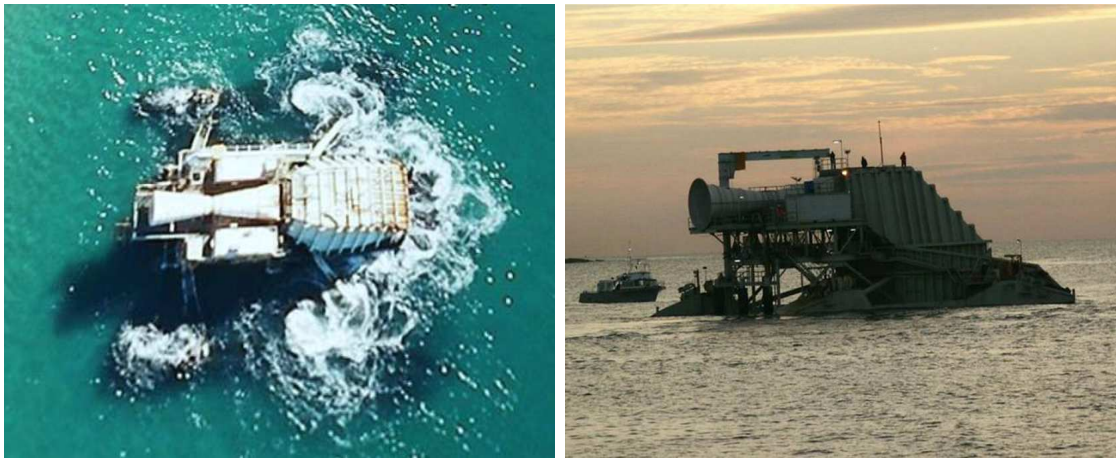

Figure 2.25: *OWC* "Mk-1" by Oceanlinx (previously Energetech), Port Kembla, Australia. (Google Earth, http://www.oceanlinx.com)

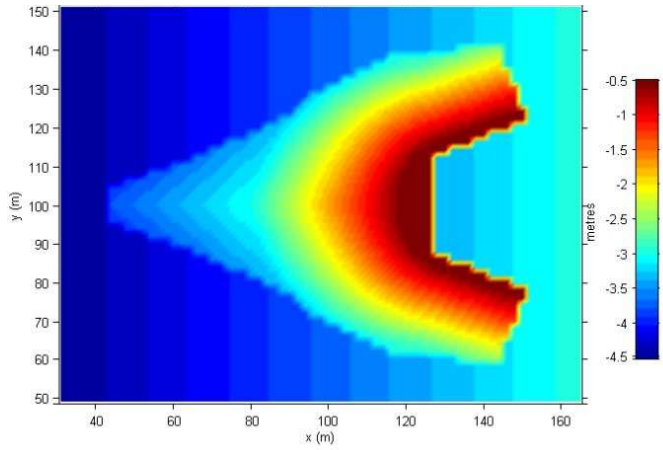

Figure 2.26: Generic design for the Mount Maunganui multi-level surfing reef, New Zealand (Black and Mead, 2009).

2.4.3 Bottom mounds

Bottom mounds are submerged structures that modify the wave height pattern on the lee side of the mound. These underwater mounds have been used primarily for beach protection, but lately also to improve surfing conditions and to enhance wave energy for extraction.

For beach protection, underwater mounds or reef breakwaters induce wave breaking and dissipation by limiting the water depth. These obstacles are linear in plan shape, and prismatic in cross-section. Reef breakwaters transmit but also reflect wave energy.

Artificial surfing reefs are also a type of beach protection structure. These bottom mounds focus the incoming wave energy into an area to increase the wave heights. By doing this, early wave breaking and dissipation occurs further away from the shoreline. The volume and shape of the mound modifies the seabed topography, focusing the wave energy by refraction and shoaling at the lee of the structure. The shape and sizes vary. For instance the artificial reef of Mount Maunganui in New Zealand, illustrated in Figure 2.26, has a v-shape and in plan is about 90 m x 80 m (Black and Mead, 2009).

For wave energy absorption, Wang *et al.* (2002) studied the hydrodynamic performance of an onshore *OWC* on a slope, as shown in Figure 2.27. The investigation was done with a 3D boundary integral method and a physical model with regular waves. It was found that the effect of the approaching slope and water depth at the shoreline are significant on the performance of the *OWC*.

The refraction of waves by the bottom contours is a natural effect that can be used

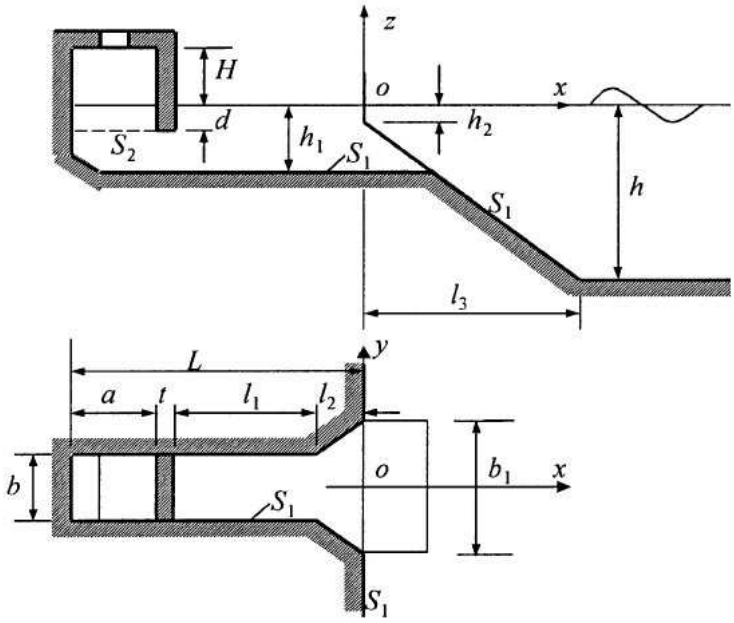

Figure 2.27: Sketch of the *OWC* on an onshore slope by Wang *et al.* (2002).

to select an appropriate nearshore or shoreline site for wave energy conversion.

An underwater mound seaward of an *OWC* was proposed by Gouaud *et al.* (2010) to increase the capture width. The bottom mound in the experiment had an elongated shape in the wave direction, as shown in Figure 2.28. The location of the *OWC* was decided according to the area with higher wave amplification.

A maximum wave amplification factor A_f of 1.6 was found at the lee of the mound, as shown in Figure 2.28, increasing the capture width $\mathcal{L}$ by a factor of 2.5 ($\mathcal{L} \propto A_f^2$). In terms of the relative sizes, the *OWC* width was one eighth of the mound cross-shore direction to benefit from the limited area with amplified wave heights.

This investigation also concluded that shore-based plants should be located in favourable bathymetric conditions, or in ones that can be improved by means of an artificial reef.

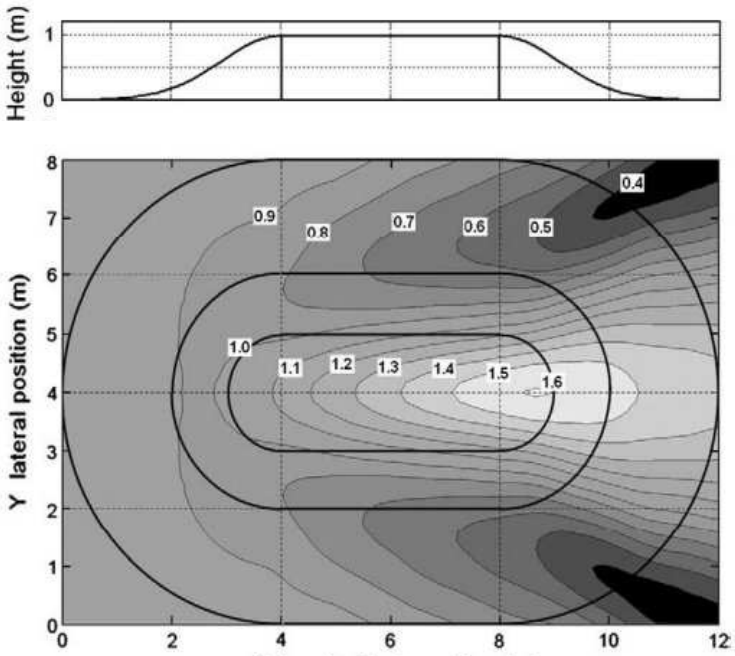

Figure 2.28: Longitudinal section, plan shape and wave amplification factor over an underwater mound after Gouaud *et al.* (2010). In this Figure, waves travel from left to right.

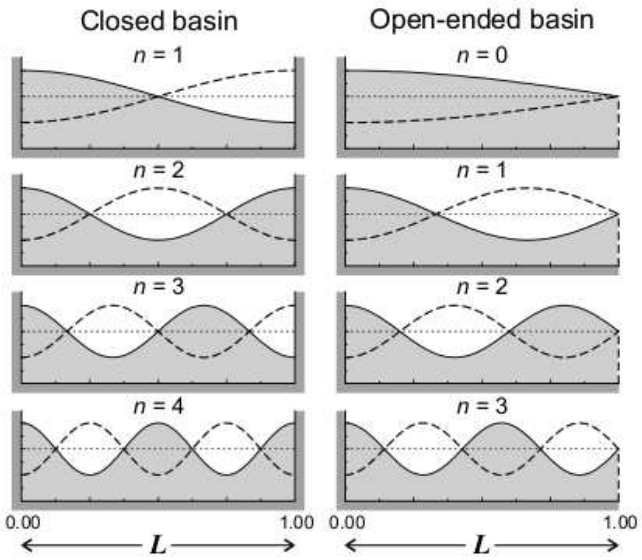

Figure 2.29: Closed and open-ended seiche modes (n) in a rectangular basin with uniform depth. In this figure, L is the length of the basin. Figure from Rabinovich (2010).

2.5 Resonant basins

A resonant basin is a partly enclosed body of water exposed to ocean waves, with the ability to amplify the water surface elevation to maximise wave energy extraction. For instance, a wave absorber with a chamber provided with a submerged entrance defines a basin that can be designed to resonate with the prevailing wave conditions.

This concept is contrary to a "harbour" that, by definition, is a place of refuge or safety for ships, boat and barges. Harbour layouts and coastal defence structures in commercial ports are designed to provide calm waters to maximise the ship-to-shore transfer of products.

Resonant basins for wave energy extraction and harbour oscillations in commercial ports are responses of the same phenomen on resonant oscillations.

2.5.1 Resonant oscillations

Resonant oscillations in a basin is also referred to as harbour resonance, harbour oscillations, surging or seiching (CEM, 2006). As a general term, seiches are long-period standing wave oscillations in enclosed basins that occur when a forcing mechanism, such as tides or winds, matches the natural period of oscillation of the

basin and resonance takes place.

Particularly, harbour oscillation or harbour resonance is a type of seiche that is generated mainly by long waves entering a semi-enclosed basin, like a harbour, and whose mechanism of decay is mainly due to waves being radiated through the harbour entrance (Rabinovich, 2010).

An important property of seiches is that the natural periods of oscillation depend on the basin geometry and water depth, and not on the exciting force. Additionally, harbour resonance has a fundamental mode of oscillation that is absent in enclosed basins, namely the Helmholtz mode, which is also called "pumping mode" or quarter wave oscillation.

The modes of oscillation of an enclosed and open-ended rectangular basin with constant water depth are shown in Figure 2.29. For the enclosed basin, the fundamental mode ($n = 1$) of a harbour with main dimension L_b is half the wave length (L in this figure), and the resonant wave number becomes $k = \pi/L_b$. The general expression for other modes of oscillation is $k = 2\pi/(2L_b/n)$, or simply $k = n\pi/L_b$ for $n = 1, 2, ..$

A similar rule applies for an open basin, but for a quarter wave length. The general expression for the wave number is $k = 2\pi/(4L_b/(2n + 1))$, or simply $k = (2n + 1)\pi/(2L_b)$ for $n = 0, 1, 2...$

Resonant oscillations in basins for wave energy absorption would respond similarly to the exciting force. Instead of long waves, the basin would resonate with relatively larger wave numbers from *seas* and *swells*. Thus, resonating basins for wave energy absorption would be limited in size, depending on wave numbers and modes of oscillation.

2.5.2 Harbour resonance

2.5.2.1 Resonance as a problem

Seiches and harbour resonance have been studied since the 1940s. An early paper by Wilson (1954) reports seiches in Table Bay, South Africa. As shown in Figure 2.30, an antinode was sketched at the entrance of Duncan Basin, this being responsible for further resonance inside the basin.

Researchers have studied harbour oscillations to understand and minimise the amplification of (long) waves. Water surface oscillations in harbours increase ship motions at berth, reducing cargo-handling efficiency, and nodal currents add risk to vessel manoeuvring at the harbour entrance.

The typical periods of harbour oscillations in commercial ports vary between 30 seconds and 10 minutes. One of the essential properties is a relatively low am-

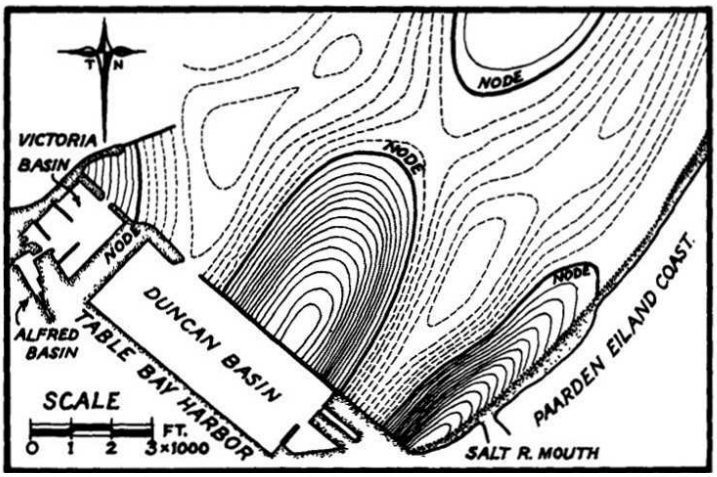

Figure 2.30: Approximate 165 s seiche off Table Bay harbour, after Wilson (1954).

plitude but large horizontal motions (currents).

Similarly, harbour resonance by long waves were extended to study the effect of tsunamis in bays and harbours.

Miles and Munk (1961) were the first to include the radiated waves from the harbour entrance on top of the incoming waves for the solution of harbour resonance in long and narrow harbours. After this work, the literature on harbour resonance became extensive. Some of the research topics are: oscillations in simplified harbour geometries with flat bottoms (Raichlen and Ippen, 1965; Raichlen, 1966); arbitrary shaped harbour theory with flat bottoms (Lee, 1969); effect of bottom discontinuity at harbour entrances (Liu, 1986); harbour oscillations due to tsunamis (Zelt, 1986); resonance in harbours with connecting basins (Lee and Raichlen, 1971; Marcos *et al.*, 2005) and with protruding breakwaters (Mei and Petroni, 1973). More recently, the investigations included the transient response of harbours at resonance (Bellotti, 2007); random sea waves on harbour oscillations (Thompson *et al.*, 1996; Chen and Mei, 2000); transient response of harbours due to long waves (Leppeletier and Raichlen, 1987; Bellotti, 2007); and the effect of bottom slope on harbour resonance (Wang *et al.*, 2011*a*).

Initially the researchers modelled harbours with a flat bottom, straight and vertical boundaries at the harbour and coastline, deep water linear regular waves and simple shaped basins, as shown in Figure 2.31.

The coupling of incoming waves with scattered waves reflected from harbour entrances was studied as a boundary condition for the solution of harbour resonance (Miles and Munk, 1961; Raichlen and Ippen, 1965; Lee, 1969), as resumed in Appendix A.

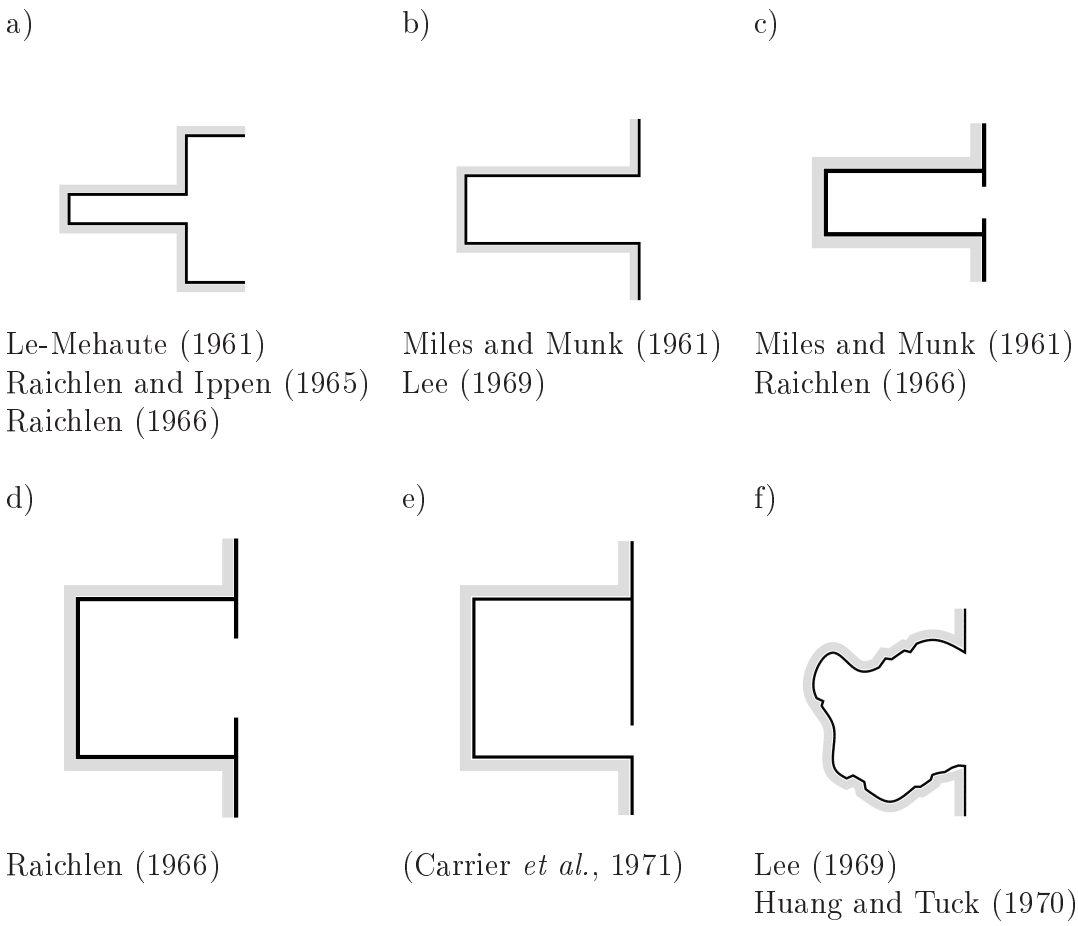

Figure 2.31: Simplified harbour layouts with flat bottom used on harbour resonance studies in the 1960s and early 1970s.

Special attention was given to the open-sea model boundaries to avoid unwanted reflections back into the model and to ensure a Sommerfeld radiation condition, i.e. full dissipation of the waves radiated away from the harbour into the modelled open sea. The results of the work of Ippen and Goda (1963), Raichlen (1966) and Lee (1969) are still valid and referred to in design guidelines for harbour tranquillity, as published in the CEM (2006).

For instance, the arbitrary shaped harbour theory of Lee (1969) solves the wave amplitudes at any position inside the harbour using linear wave theory and given boundary conditions. The main boundary conditions are fully reflective vertical boundaries at the harbour and at the coastline, constant water depth, and that outgoing waves from the harbour mouth decay at an infinite distance from the

harbour (radiation condition). The surface water elevation was modelled as

$$\eta = af(x,y)exp(-i\omega t), \tag{2.5.1}$$

in which a is the wave amplitude of the incident wave, the wave function $f(x,y) = f_i + f_r + f_s$ with f_i the incident wave function, f_r is a reflected wave function considering the harbour closed (fully reflective vertical wall along the shoreline), and f_s is the radiated wave function due to the harbour. The functions f_i and f_r alone describe a standing wave pattern in the absence of the harbour.

To assess the response of a harbour to incident waves, a wave amplification factor is used. As presented by different authors, the amplification factor A_f is the ratio between the amplitude (or wave height) at a fixed point inside the basin, and the amplitude (or wave height) of the incoming wave. In terms of wave energy density, the wave energy density would be modified by a factor of A_f^2 for linear waves, since $\overline{E} \propto a^2$.

The theory and experiments of Lee (1969) and Ippen and Goda (1963) for a fully open and a narrow rectangular basin are shown in Figure 2.32. The amplitude response A_f was calculated as the ratio of the wave amplitude at the center of the back wall (a_b) to the average standing wave amplitude ($2a_i$) at the harbour entrance considering the harbour mouth closed, or

$$A_f = \frac{a_b}{2a_i}. \tag{2.5.2}$$

Physical model tests by Lee (1969) were done with regular waves on a wave tank 4.7 m wide, 9.6 m long and with 25.7 cm of water depth. Wave reflection from the side walls of the wave tank was kept below 20% by means of wire mesh wave absorbers. The model dimensions were 12 cm wide and 31 cm long. According to the author, the difference between the experimental and theoretical values, especially at resonance, can be attributed to viscous dissipation not included in the theory.

For semi-enclosed symmetrical basins, Raichlen (1966) produced amplification factor curves for rectangular harbours at resonance, as shown in Figure 2.33. In this figure, the amplification factor was also defined by equation 2.5.2 at the corner of the back wall of the harbour. The theory of Lee (1969) is a particular case for $l_w/l_B = 0.2$ (harbour width $2b$ is 2 x 2.38 in in Figure 2.32) and $B/l_w = 1$, giving similar theoretical results, with amplification factors of about ~ 8 and ~ 2.5 for the first and second mode of oscillation respectively. From equation 2.5.2, this implies that the amplitude at the corners of the back wall of the harbour is about 16 and five times the incoming wave height respectively.

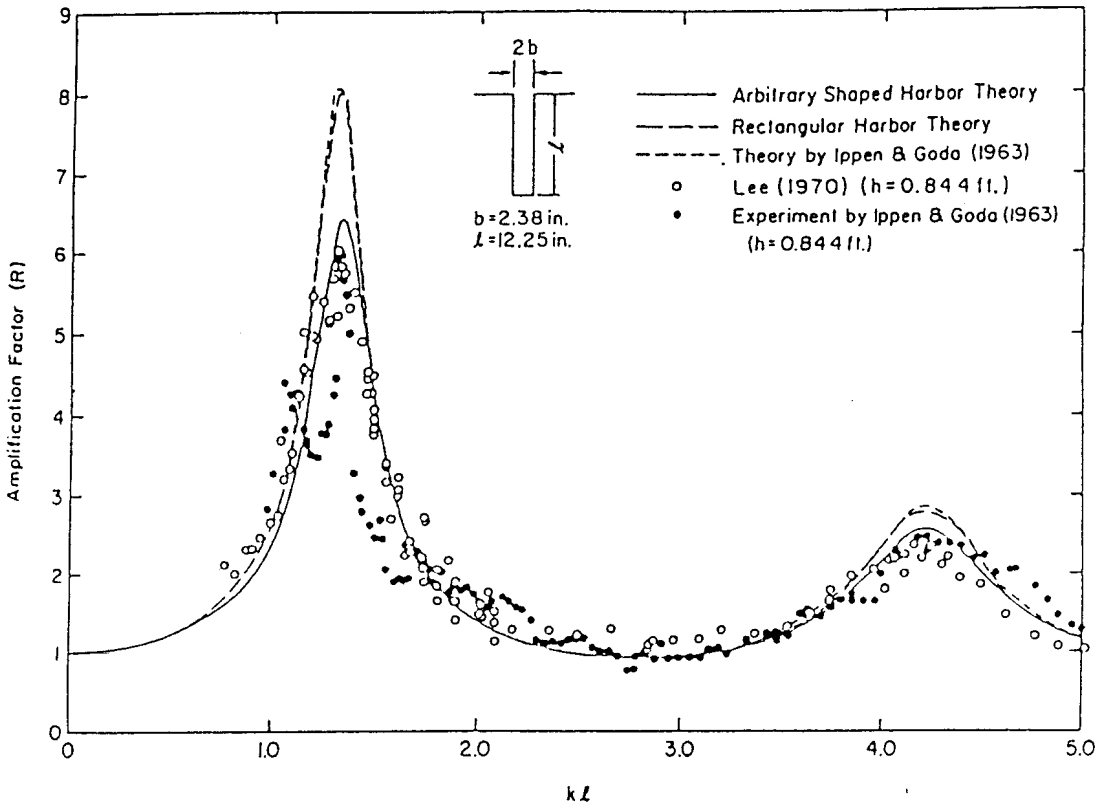

Figure 2.32: Response of a fully open narrow rectangular basin (Lee, 1969).

Also, numerical models have been used to quantify the effect of harbour oscillations. Gierlevsen *et al.* (2001) reported the application of a Boussinesq type of model on the Port of Sines in Portugal. Li (2002) modelled harbour resonance at Pier 400 of the Port of Los Angeles. Kofoed-Hansen *et al.* (2005) modelled a fishing harbour at Torsminde, Denmark, and pier J of the Port of Los Angeles by using a time-domain Boussinesq model.

Recently, Xing (2009) developed a hybrid finite element model that solves the mild slope equation for arbitrary shaped harbours and variable water depth. In this case, wave reflection, refraction and diffraction were included, besides dissipation and flow separation losses at the harbour entrance. The model was validated with the experimental data of (Lee, 1969) and was used to study harbour and bay resonance induced by long waves and tides (Xing *et al.*, 2010).

To assess harbour oscillations of more complicated plan shapes and bathymetries, it is possible to model them in physical or numerical models. Boussinesq-type

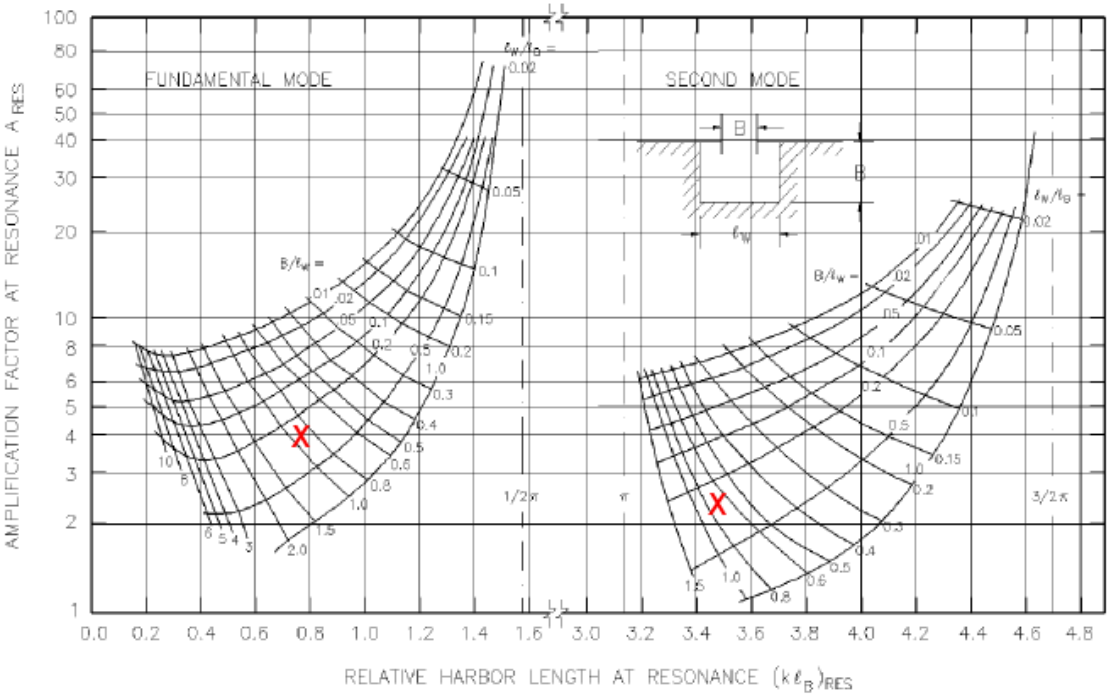

Figure 2.33: Amplification factor at resonance for a symmetrical rectangular harbour (Raichlen, 1966). For a harbour with $l_w/l_b = 0.7$ and $B/l_w = 0.3$, the amplification factors would be 4.3 and 2.3 for the 1^{st} and 2^{nd} mode respectively ("X" in the figure).

numerical models are commonly used to study harbour oscillations considering effects such as reflection, refraction, diffraction and dissipation. Numerical models commercially available includes Mike21-Boussinesq Waves (BW) developed by the Danish Hydraulic Institute, and Pharos by Deltares.

2.5.2.2 Resonators for harbour tranquillity

As a countermeasure for long wave harbour oscillations, resonators for harbour tranquillity were first proposed by Valembois (1953). Resonators are basins located at the access channel of a harbour that induce transversal oscillations. Transverse waves out of phase with the incoming ocean waves produce a node in a standing wave pattern. Ideally, a node at the harbour entrance would reflect the incoming waves and transmit no energy to the basin.

Valembois (1953) demonstrated that an hydraulic resonator in a channel acts as a reflecting structure, but without blocking the channel and passage of ships. This concept is illustrated in Figure 2.34. In Figure 2.34 a), a vertical wall in a channel completely blocks the incoming waves, producing a *standing wave* oscillation with

a) Channel with a wall.

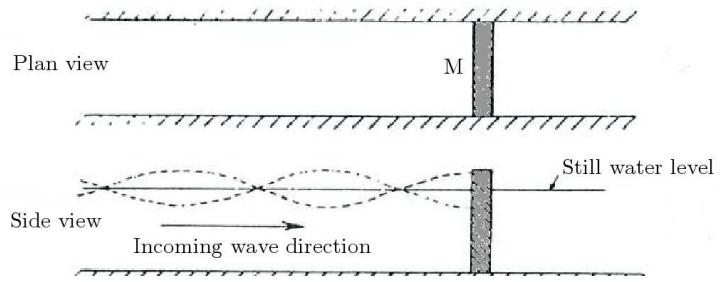

b) Quarter-wave resonator in a channel.

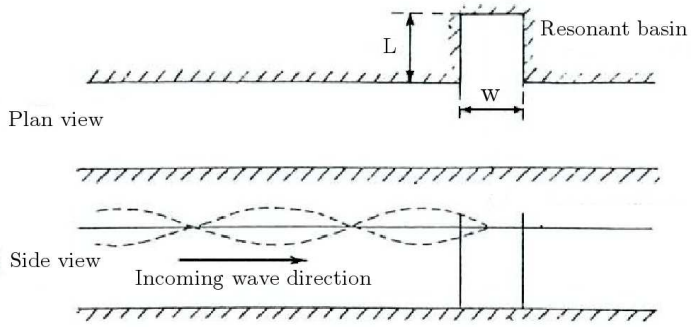

Figure 2.34: Wave reflection a) from a wall and b) by a resonator tuned for the wave frequency, after Valembois (1953).

a *node* at the wall. In Figure 2.34 b), a similar reflection is achieved with a quarter-wave resonator tuned to the wave frequency by inducing a node across the channel on a standing wave pattern, as illustrated in Figure 2.35.

The fundamental concept of Valembois (1953) was tested with regular waves in a standing wave pattern with one and three resonators in a channel, as shown in Figure 2.36. In the figure, the incident waves travel along each channel from right to left. The vertical wall produces a standing wave of amplitude a recorded at the point M at the centre of the wall. The ratio A_f between the amplitude with resonator and the amplitude without resonator at the wall (M) is also shown in the figures as a function of the incoming wave period. It can be seen that the single resonator at resonance reflects the incoming waves almost completely before they reach the wall ($A_f \approx 0$ for $T = 8s$). The drawback is that a single resonator is effective in a narrow frequency band. The effect can be extended for a wider range of wave periods with a battery of resonators, as shown in Figure 2.36 b).

To protect an outer harbour from incident waves, Valembois (1953) proposed a battery of resonators, as shown in Figure 2.37.

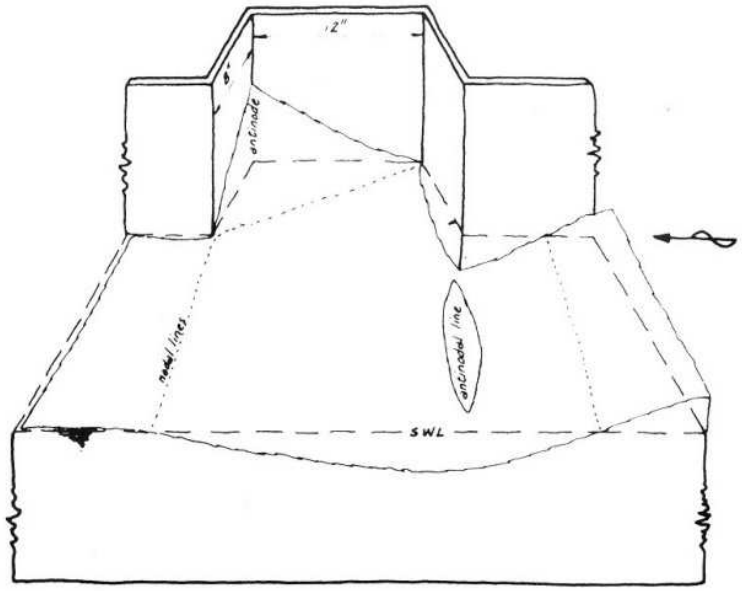

Figure 2.35: First mode of resonance of a resonator (James, 1968). Waves travelling to the left are reflected back by a nodal line across the channel.

a) Single resonator b) Battery of three resonators

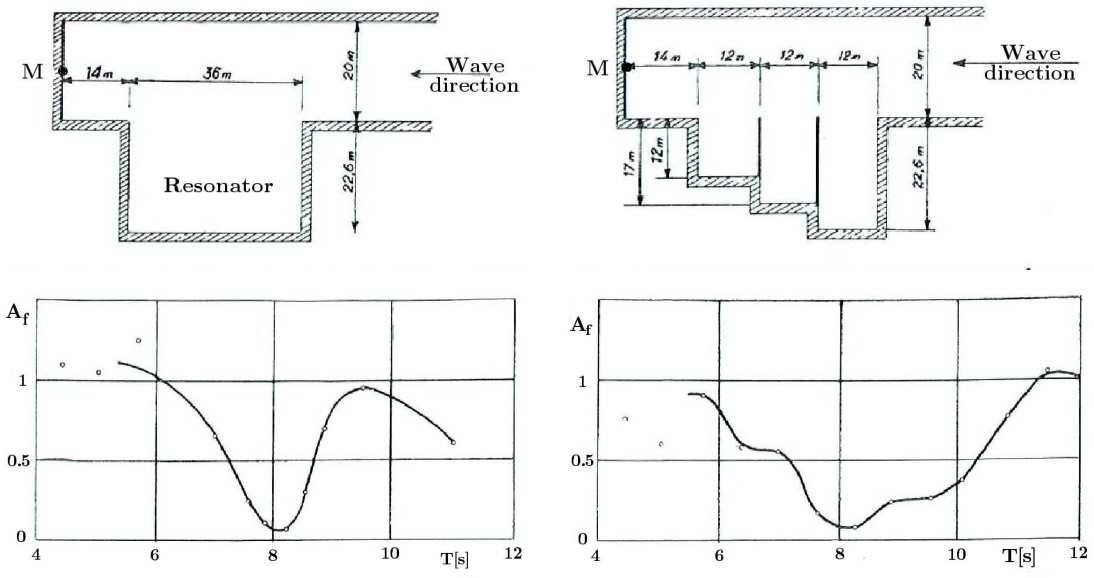

Figure 2.36: Effect of resonator(s) on a standing wave pattern in front of a vertical wall after Valembois (1953). The amplification factor A_f at the wall M is shown as a function of the incoming wave period.

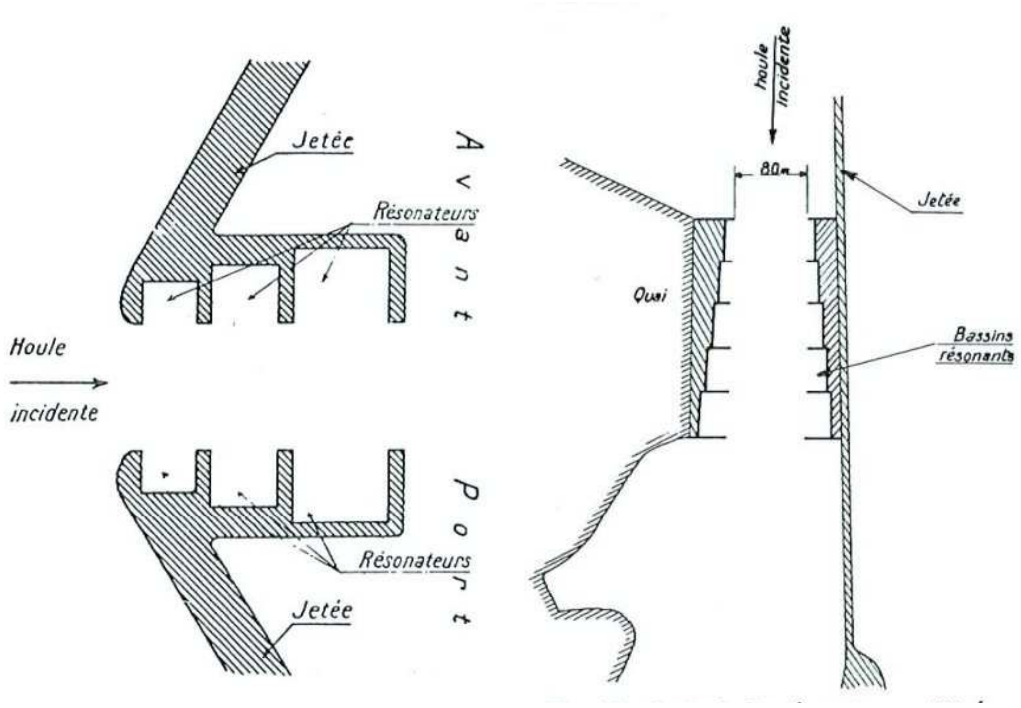

Figure 2.37: Protection of a harbour with a battery of three and five resonators at the harbour entrance channel after Valembois (1953).

Further research on rectangular resonators (James, 1968, 1970, 1971) proved the concept useful for a single frequency, and proposed a widening access channel to be effective for multiple wave numbers. This concept was taken further by the same authors to extract wave energy in the process (Spiers, 1976; James, 1980).

A theoretical study by Wu (1992) verified James's concept of resonators in a narrow channel of no wider than half a wave length. A similar concept was investigated by Twu and Liou (2003) to damp long waves by interconnecting channels. More recently, submerged resonators were studied for wave attenuation (Karambas and Gousidou, 2006).

Another application of resonators is to reduce long waves in a harbour. As a case study, Nakamura (2005) reported the re-analysis of the resonator-like breakwaters of Pier J at the Port of Long Beach, Los Angeles. The port basin and resonator are shown in Figure 2.38. The results of the study reported a 50% reduction in mean wave heights, as shown in Figure 2.39.

The effectiveness of a resonator for incoming swells in breaking and non breaking conditions was proved effective by Nakamura and Latt (2008).

Figure 2.38: Inner basin and resonator of Pier J at the Port of Long Beach, Los Angeles, CA.

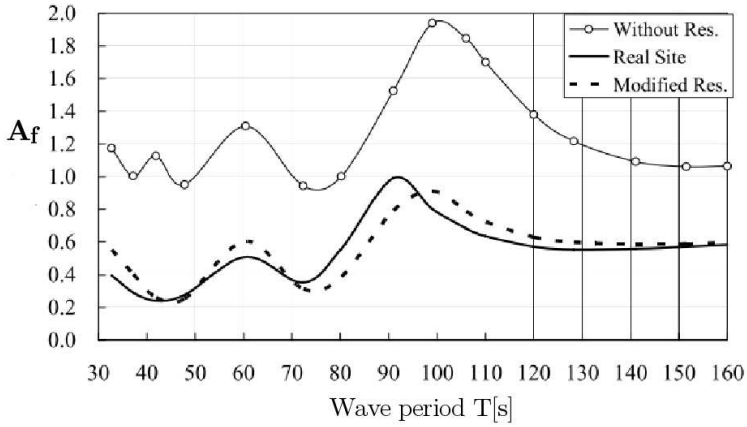

Figure 2.39: Theoretical averaged wave height ratio to incident wave height (A_f) in the inner harbour basin, Pier J at the Port of Long Beach (Nakamura, 2005).

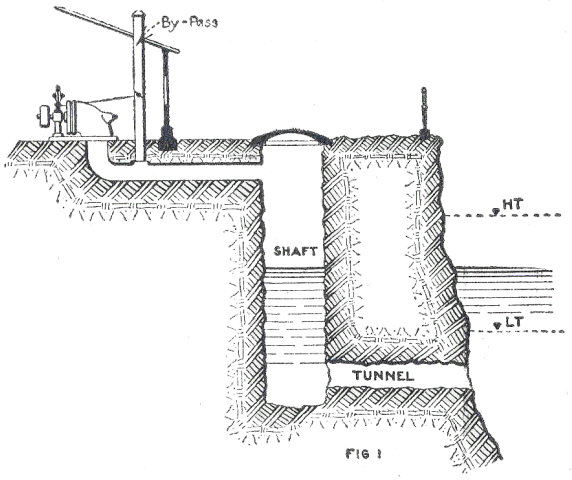

Figure 2.40: Very first wave energy device concept. Mr Bouchaux-Praceique's device in 1920 after Power Magazine, The McGraw Hill Company (Falnes and Hals, 1999).

2.5.3 Resonance in basins for wave energy conversion

An early application of a wave energy absorption device was built around 1910 near Bordeaux in France. A vertical borehole was connected to the sea by a submerged opening, as illustrated in Figure 2.40. The oscillation of the sea water pumped air through a turbine that supplied 1 kW (Falnes and Hals, 1999).

A similar but opposite effect is still utilised to generate waves in hydraulic laboratories. Pneumatic generators can increase or reduce the air pressure inside an enclosed chamber connected to the open water by a submerged opening. If this is done synchronously by the opening and closing of air valves, the oscillation of the water surface inside the chamber generates a wave outside the chamber through the submerged opening.

For optimal wave energy conversion, the chamber of the oscillating water column (OWC) is required to resonate on its Helmholtz or pumping mode. To achieve resonance, the geometry of the chamber and opening are designed to couple with the incoming waves.

Initially a problem, harbour resonance was applied by researchers to wave energy extraction. Evans (1982) investigated the efficiency of a wave energy device within a long and narrow resonant basin (Figure 2.41a).

A specially shaped artificial basin was investigated by Cossalter *et al.* (1982) (Figure 2.41b). The results were promising, but the back wall was required to be shifted to tune the basin for the incoming wave frequencies. The interaction of WEC devices within the volume of water of the basin was not considered, but

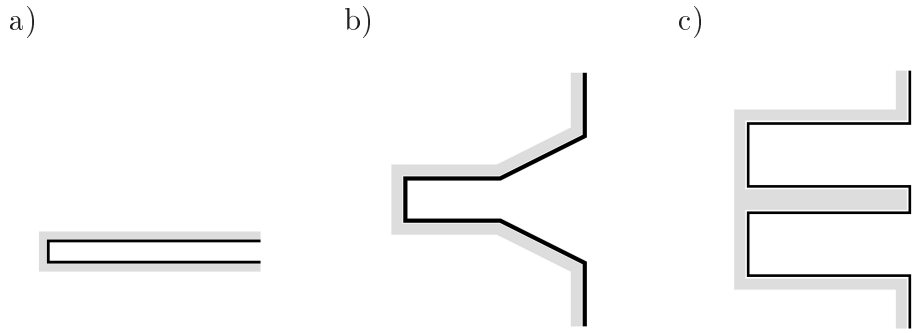

Figure 2.41: Simplified rectangular basin layouts used on selected wave energy capture studies. a) Evans (1982), b) Cossalter *et al.* (1982), Wang *et al.* (2002), c) Malmo and Reitan (1986*a*), McIver and Evans (1988).

recognised as an important effect.

A finite row of basins set into a reflective wall (Figure 2.41c) was investigated by Malmo and Reitan (1986*a*,*b*); McIver and Evans (1988). McIver and Evans (1988) concluded that there is a clear increase in capture width for a group of devices acting together along a reflecting coastline rather than in isolation. Unfortunately, the interaction with waves outside the harbours was not represented.

Projecting side walls on each side of an *OWC* was investigated by Count and Evans (1984). Theoretical results indicated substantial changes in hydrodynamic performance and increased wave energy capture. This increase in capture width was attributed to a "harbour" effect between the side walls.

Ambli *et al.* (1982) also included protruding side walls to improve the resonant conditions of a chamber. The Kvaerner multiresonant *OWC* shown in Figure 2.42 is one early example. From this figure it can be seen that the OWC was built on a cliff with projecting side walls on rock. The effect of the side walls was found to be an improvement on the *OWC* performance for head-on waves (Ambli *et al.*, 1982; Evans, 1982; Count and Evans, 1984). The maximum absorption was found for side wall lengths of the same order of magnitude as the chamber length.

The Limpet *OWC* device (Figure 2.43) also has an external basin. The artificial basin was built due to construction restrictions, since it was not possible to cast the concrete chamber exposed to wave action. A basin was created by a retreat of 17 m inland at 5 m to 7 m water depth, leaving a basin in front of the 21 m wide *OWC* chamber (Whittaker *et al.*, 2002). A drop in performance was reported in Wavegen (2002a), which was due to a combined effect of a shallow approaching seabed and the limited water depth of the basin (Wavegen, 2002b).

Similarly, the *OWC* built in Madras (Figure 2.46) had a cylindrical chamber with

an added complex shape facing the incoming waves to increase power capture (Tseng *et al.*, 2000).

Recently, Tomisawa *et al.* (2008) reported experimental results of the performance of an OWC with projecting side walls.

The latest oscillating water column plant was inaugurated in July 2011 at Mutriku, north of Spain. In this case, 16 *OWCs* were integrated into the bend of a new breakwater. The plan view of the town, harbour and new breakwater are illustrated in Figure 2.47. A sketch of the *OWC* chambers and the plant during construction is shown in Figure 2.48. Wave directionality might play a role in not including projecting side walls from the chamber's openings.

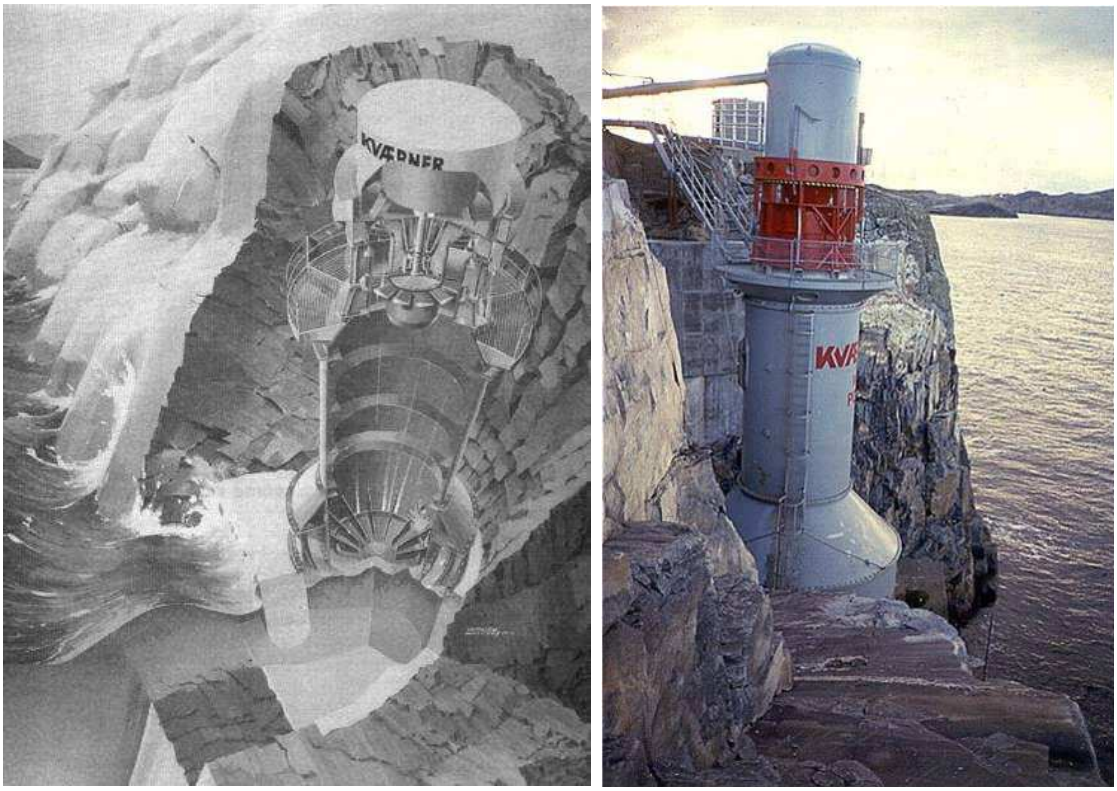

Figure 2.42: The Kvaerner multiresonant *OWC* utilised resonant properties of harbours to improve the efficiency of the wave absorber.

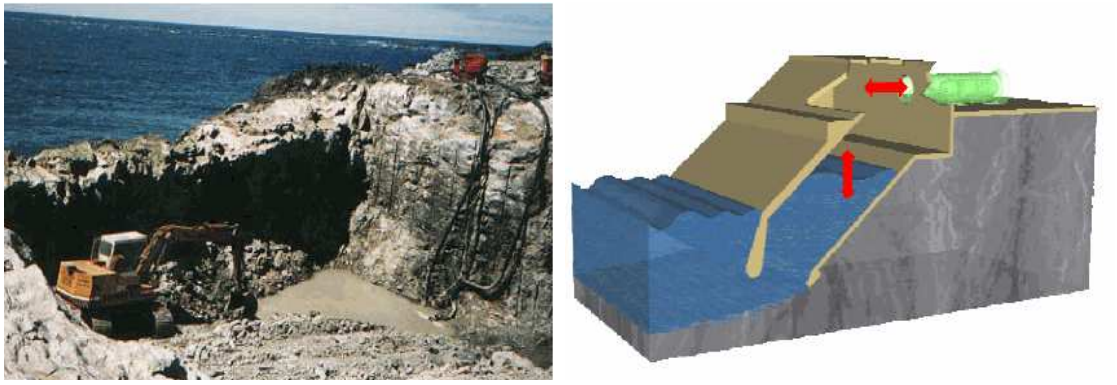

Figure 2.43: 500kW *OWC* Limpet on the Scottish Isle of Islay. Left, artificial basin being excavated during construction (Whittaker *et al.*, 2002). Right, artist's impression.

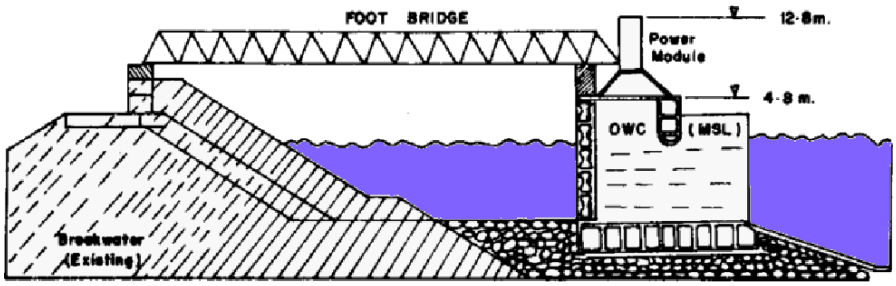

Figure 2.44: Cross-section of a breakwater and on *OWC* wave energy plant. *OWC* designed at the Indian Institute of Technology.

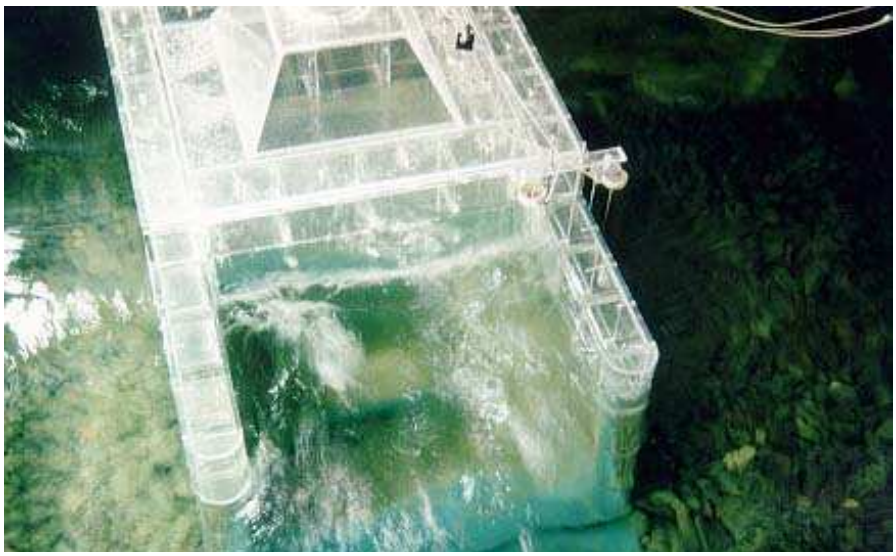

Figure 2.45: Physical model of the *OWC* in Madras, India.

Figure 2.46: Prototype of the *OWC* in Madras, India.

Figure 2.47: Plan view of Mutriku. Town, harbour and new breakwater with an *OWC* integrated into the structure. Image from Google Earth.

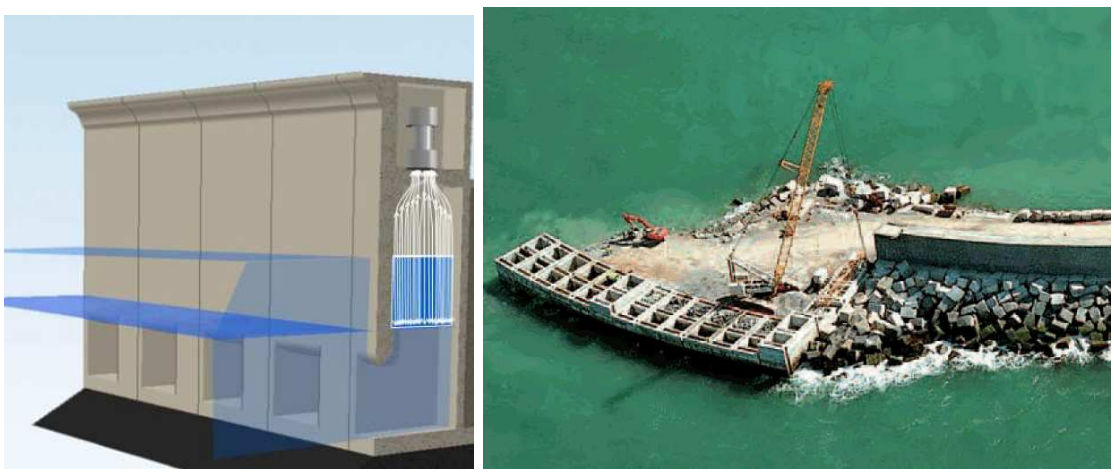

Figure 2.48: Sketch of *OWC* chambers (Arlitt *et al.*, 2007) and Mutriku *OWC* under construction (Torre-Enciso *et al.*, 2009).

2.6 Conclusions

The development of a wave energy basin for wave energy conversion basically can benefit from three areas of research: wave energy conversion devices; resonators; and harbour oscillations. The fundamental property in these research fields is resonance.

Wave energy conversion devices have been classified by their geometry, principle of operation, location and stage of development of the device. All these classifications are centred on the device.

A new and complementary classification is proposed from observing the interaction between the wave converter and the incoming waves. This classification is centred on the resource and has three main groups: *wave interference* devices, *wave collector* devices, and *resonant* devices.

As described in Section 2.3, in order to absorb a wave and convert its energy into useful electrical power it is required to create a new wave. And the new wave must interfere destructively with the incoming waves. Oscillating wave energy converters or point absorbers, which are also classified as *wave interference devices*, are designed to interfere destructively with the incoming waves. In principle this might imply that the performance of a device can be measured by its ability to radiate waves and interfere with the incoming waves. Hence the wave interaction of a floating *WEC* is extremely relevant for device performance.

In contrast, fixed structures like vertical walls, wave reflectors, narrowing channels, bottom mounds and resonant basins are able to increase wave energy density in a specific area. In this thesis this ability of fixed structures is defined as *constructive interference*, an opposite term for the *destructive wave interference* by oscillating bodies defined by Falnes and Budhal (1978). Then, if the radiation pattern of an oscillating *WEC* is relevant for destructive *wave interference* and power capture, scattered waves from fixed structures are also relevant for *constructive wave interference* and the enhancement of wave energy conversion by a *WEC* device.

Resonators, similar to *dynamic reflection* by oscillating bodies, can reflect incoming waves. In the first case a *node* is produced along an arrangement of floating devices. In the second case a nodal line across a channel produces the reflection. This ability of resonators to produce *dynamic reflection* expands the possibilities of fixed structures to be used in wave energy extraction. If a resonator can reflect waves with a nodal line, it might be able to do the opposite with an antinodal line and amplify the wave heights into a basin.

Resonant *WECs*, specifically oscillating water columns, resonate the chamber's surface water level on its Helmholtz mode ("pumping mode") by coupling the flow through the submerged opening with a standing wave outside the chamber's wall.

The addition of side walls to the chamber's opening increases the device's performance by a "harbour" effect and the reduction of lateral scattering of reflected waves.

Longer side walls, which are able to produce a quarter-wave length oscillation in front of an oscillating water column chamber, have not been implemented successfully for increasing capture width. In the specific case of the *OWC* Limpet at Isley, poor performance was reported to be a consequence of limited water depths, which induce wave breaking and non-linear waves.

Resonating basins with at least one nodal line inside the basin have not been proposed for wave energy conversion. This resonant basin would be larger in size, in the order of and limited by a few quarter-wave lengths.

To assess harbour oscillations of more complicated plan shapes and bathymetries, is possible to use a physical or numerical model. Boussinesq type of numerical models are commonly used to model harbour oscillations when considering effects such as reflection, refraction, diffraction and dissipation.

Physical experiments and numerical model results are available for long wave harbour resonance and provide guidance on amplification factors for simple shaped harbours with a flat bottom, symmetric entrances and fully reflective coastlines. These amplification factors are provided at the back wall of the harbour for head-on incident waves. Theoretical amplification factors (A_f) for rectangular harbours at resonance are promising for wave energy extraction within a resonant basin, but vary with the relative basin length and entrance widths.

It can be concluded that significant efforts have been made to enhance wave energy for extraction. *Wave interference* devices, *wave collector* devices and *wave resonance* devices have been proposed and prototypes have been built.

In a similar line of investigation, the development of a wave energy basin to enhance wave energy conversion is promising. The concept should consider the interaction of the basin with the incoming waves and make use of the research on and properties of the devices already classified. According to this, a resonant basin with a wide entrance is preferred for increasing the capture width and the incoming wave energy flux. The challenge is how to produce constructive interference between outgoing waves from the harbour mouth and incoming waves.

Chapter 3

Methodology

3.1 Introduction

The objective of this research was to determine whether a special basin with a specific geometry open to the sea can increase the local wave energy density, and whether it is feasible to be used to maximize wave energy extraction.

From the literature review presented in Chapter 2, it was concluded that the concept of a wave energy basin must meet three criteria. Firstly, the basin must resonate. Secondly, it should have a wide entrance to increase capture width. And finally, the basin entrance should produce constructive interference between outgoing waves from the basin mouth and incoming waves.

A resonant basin can be designed following the principles of harbour oscillation, and also from other fields of research not covered in this thesis such as acoustics and mechanical vibrations that deal with similar physical problems.

On the other hand, there is a compromise required between a wide entrance and a resonant basin. Due to this, in this thesis a basin is considered that resonates not only along the basin, but also resonates in the cross-basin direction. Resonant waves in the cross direction would be reinforced by waves resonating along the basin. Wave energy in the cross direction would reflect wave energy between the parallel side walls of the basin. Wave energy density would be enhanced and be available for extraction, for instance by *OWCs* located along the side walls. The basin would dissipate energy primarily through the basin entrance. Naturally there are other mechanisms of dissipation, such as bottom friction, walls roughness and turbulence by flow separation at the entrance.

An asymmetrical entrance is considered to stimulate a cross-wave pattern and wave energy capture inside the basin.

The concept of the basin considers a simple square shape with a flat bottom and

an asymmetrical entrance. The flat bottom is chosen to simplify and isolate the resonant behaviour from other wave interactions. Additionally, deep water waves are considered for linear wave theory to remain valid for this investigation. To generalise the results and avoid bottom wave interactions, in this thesis a vertical edge coastline was selected. This is similar to the models of harbour oscillation reviewed.

Physical and numerical modelling techniques were used to investigate the resonant basin. In both cases, the modelled area included a large extension outside the basin, since it was concluded in Chapter 2 that the wave interaction outside the basin entrance is relevant for the study.

Physical modelling imposes limitations. Firstly, it limits the scale of the model. Traditional harbour models are tested with shallow water waves. On the contrary, deep water waves were required in this study. Consequently the length scale needs to be large and wave heights small to produce linear waves of small amplitude.

Numerical model testing of a deep resonant basin is also not common. Resonant oscillations in harbours are modelled with Boussinesq type models, but in shallower depths. Again, deep water waves require special attention. Similar to resonant harbour studies, a Boussinesq type model was selected in this thesis.

In both cases, the physical and the numerical model tests are aimed at obtaining wave energy densities inside the basin. Regular waves were chosen to better observe wave patterns.

3.2 Layout of proposed resonant basin

From Chapter 2, it was evident that a number of wave effects might be used in isolation or combination to enhance wave energy density. For a basin at the coastline, the combined effects of *constructive interference*, *wave collection* and a *resonant basin* are proposed.

The proposed basin is sketched in Figure 3.1. The asymmetric entrance is intended to induce cross-waves inside the basin. The basin width dimension, w, will provide a half wave oscillator with a nodal line on its centre.

The basin sketched in Figure 3.1 has the dimensions shown in Table 3.1. The model was scaled to 1:200, following the Froude number scale law. Hence the time scale N_T is related to the length scale $N_L = 200$ by the relation $N_T = \sqrt{N_L}$. The proposed prototype basin width is three times wider than the *OWC* Limpet. In addition, the model size is similar to the harbour modelled by Lee (1969).

The model of the rectangular-shaped basin had internal dimensions 425 mm long

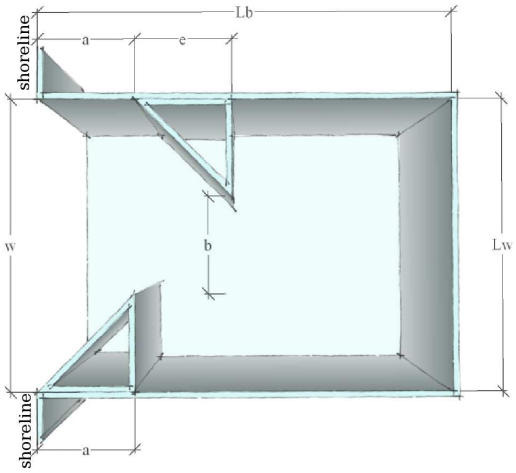

Figure 3.1: Basin model parameters.

Table 3.1: Resonant basin model and prototype dimensions as from Figure 3.1.

Basin geometric dimensions		Model[mm]	Prototype[m]
Width at basin entrance	w	300	60
Basin length	L_b	425	85
Width at basin back wall	L_w	300	60
Breakwater offset from shoreline	a	100	20
Entrance gap	b	100	20
Offset between breakwaters	e	100	20
Water depth	d	245	49

and 300 mm wide. At the harbour entrance, two breakwaters, each 100 mm long, leave a gap of 100 mm at the centre of the harbour entrance. To achieve the asymmetric entrance, the two breakwaters were placed with an offset of 100 mm. In order to keep the harbour mouth as open as possible for power capture, and to reduce the reflection of waves, the breakwaters had a triangular shape, in plan similar to Cossalter *et al.* (1982) and Wang *et al.* (2002).

3.3 Physical model experiments

A physical model was built on a quasi-3D wave tank available at the CSIR. The objective of the model was to produce basin resonance. Hence, special attention was given to minimise resonance of the wave tank due to the model characteristics and layout.

The proposed model had a highly reflective coastline and a basin near or at res-

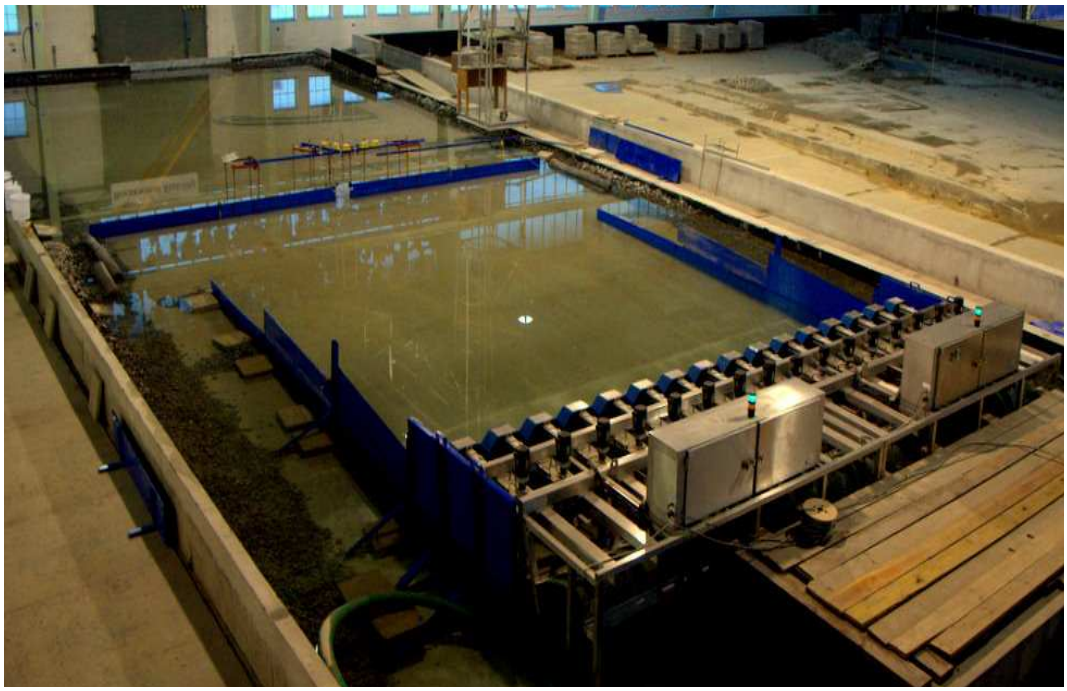

Figure 3.2: View of the quasi-3D wave basin, 12 m wide and 32 m long. Wave makers at the bottom right confined by wave guides.

onance. A vertical edge coastline parallel to the wave makers would reflect most of the wave energy back to the wave maker. The superposition of waves reflected from the shoreline and radiated from the harbour would impose a complex wave pattern in front of the wave makers. This is relevant since the water surface elevation along the paddles is used as input data to correct the generated waves by a dynamic wave absorption system. The dynamic wave absorption system is used to avoid a fictitious build-up of wave energy in the wave tank by the return waves.

Regular and small-amplitude waves were used in the experiments for better visualisation and understanding of wave patterns.

The wave tank layout, on the other hand, makes it a quasi-3D wave basin. Wave makers located on a narrow side of the basin (Figure 3.2) were fitted with wave guides that prevented lateral dissipation of the wave energy from the reflected and radiated waves.

For these reasons, qualitative trial tests were performed first to test the wave tank in a highly reflective condition, and then to finalise the methodology and scope of the physical modelling.

In this section, the wave tank, the basin model and the experimental equipment

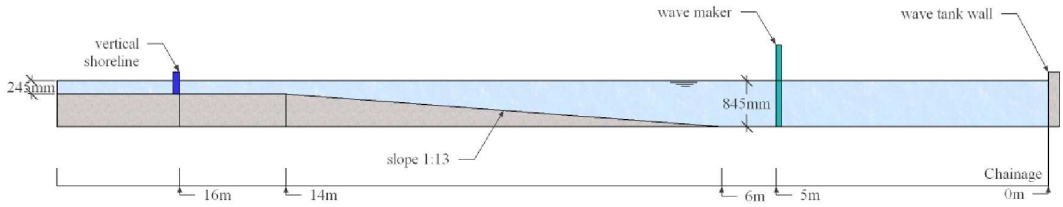

Figure 3.3: Profile of wave tank bottom. Paddles of the wave maker at chainage 5 m, modelled shoreline at chainage 16 m.

are described. The results of trial tests of the wave tank with a vertical wall as a coastline are shown in Section 3.3.5, and the modelling limitations are presented in Section 3.5.

3.3.1 Wave tank

The wave tank used in the experiments was 12 meters wide, 32 m long, and 1 m deep at the deeper end. A general view of the tank section is shown in Figure 3.2. The maximum water depth was 845 mm, with a free board of 205 mm.

The bottom profile of the wave tank is shown in Figure 3.3. It is flat for the first 6 m of the deeper side of the basin. At chainage 6 m, a 1:13 slope starts up to chainage 14 m. From chainage 14 m onwards there is a gentle slope of 1:400, which continues up to chainage 17 m, where the bottom start changing for an existing previous model. The wave maker paddles on standby position are located at chainage 5 m.

For the experiments, the bottom profile of the wave basin was kept unchanged and the model shoreline was positioned at chainage 16 m, parallel and 11 m from the paddles of the wave maker.

The total length of the wave tank was reduced by the position of the modelled shoreline, as seen in Figure 3.4 and Figure 3.5. The shoreline used in the model was a vertical wall made of four plywood panels, 20 mm thick, 0.4 m wide and 2 m long, extending for about 8 m but leaving a 300 mm gap at the centre of the basin to attach the resonant basin model.

3.3.2 Wave makers, wave guides and wave absorption

The piston-type wave maker used in the experiments was arranged in a block of 16 units each of 0.5 m width, allowing wave fronts of 8 m long. The paddle's home position was in chainage 5 m, as shown in Figure 3.4. This allowed enough space for a wave absorption system behind the paddles. The waves generated behind the

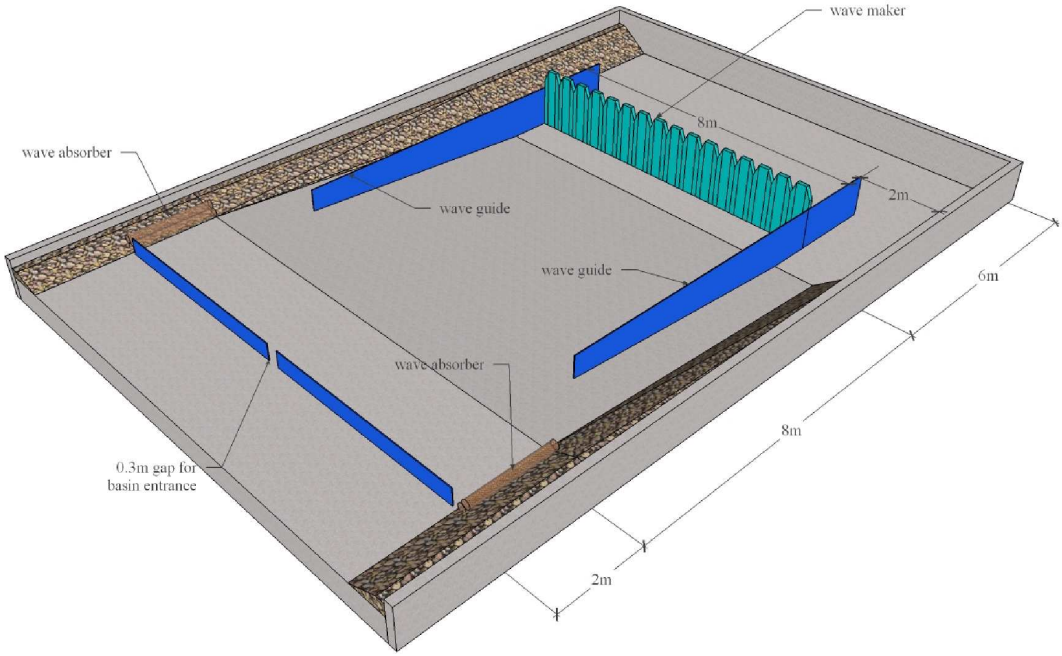

Figure 3.4: Sketch and general dimensions of the wave tank.

Figure 3.5: Quasi-3D wave basin. On the right, the wave maker units and wave guides. On the left, the vertical shoreline and basin model.

Figure 3.6: Wave absorbers: gravel slope and wire rolls.

paddles were absorbed by a thick sponge on a slope, which is the standard setup of the HR Wallingford piston-type paddle system.

Steel plates were used as wave guides at both ends of the wave maker block of units (Figures 3.4 and 3.5). This was to channel the waves along the tank. Both wave guides, 2 m apart from the side wall of the tank, were used to avoid 3D effects generated at the side of the wave makers. These effects include wave dissipation by eddies and crossed waves generated by the diffracted waves from the paddle.

Wave guides were extended from the wave maker to chainage 12.2 m, as shown in Figure 3.5, to reduce both wave attenuation and the generation of cross waves. In the absence of wave guides, wave attenuation can be expected due to the increase in length of the generated wave fronts, from 8 m at the wave maker to 12 m of the full wave tank width. Also, without wave guides, cross waves can be generated by wave reflection from the vertical side walls of the wave tank.

Between the end of the wave guides and the model shoreline, a gap of 3.8 m long between chainage 12.2 m and 16 m was left to absorb cross waves diffracted from the end of the wave guides, and radiated waves from the modelled basin. Existing 40 mm crushed stones were kept in position on a slope. Extra wire rolls were placed in front of the rock slope for extra wave attenuation, as shown in Figures 3.4 and 3.6.

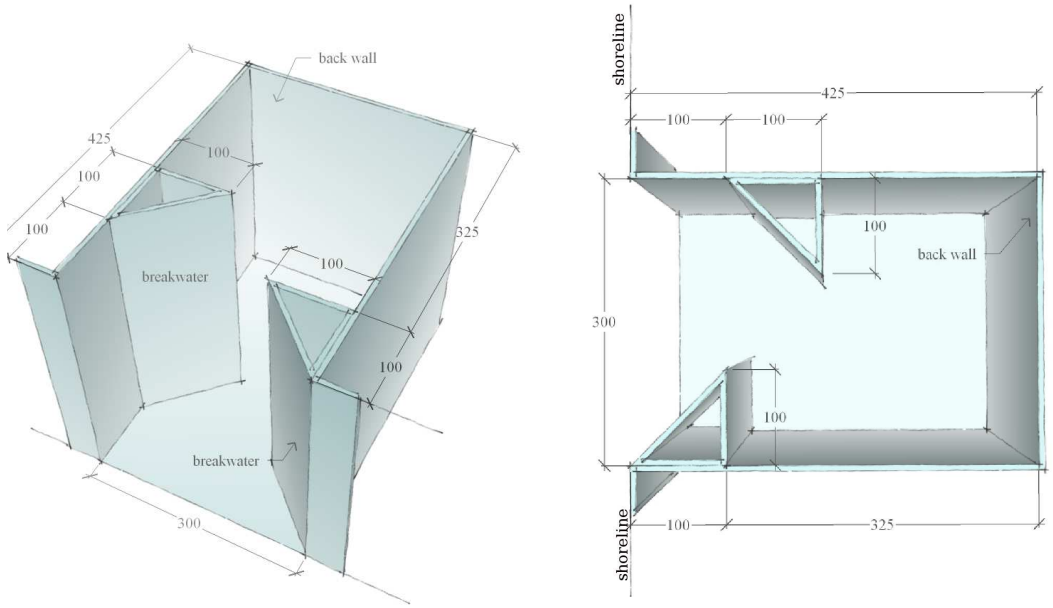

Figure 3.7: Artist's impression of the model.

3.3.3 Model of the resonant basin

The model was built of perspex, 6 mm thick, with individual side walls assembled in place. At the edges of the basin entrance, on its assembly with the plywood panels, an indent was left to fit a perspex panel, also 6 mm thick, close the harbour entrance.

The final lengths of the internal basin excluding the entrance seaward of the breakwaters were 325 mm on the longer side wall and 225 mm on the shorter side wall. The harbour width was kept constant at 300 m.

3.3.4 Measurements of wave conditions

Water surface elevations were measured with calibrated capacitive wave gauges at five locations, and data were recorded and post-processed with the GEDAP package (Generalized Experiment Control and Data Acquisition Package, Miles (1997)) currently used at the CSIR hydraulic laboratory.

Capacitance wave probes consist of twin copper-isolated wires of 0.5 mm outer diameter and about 8 mm apart, stretched along a support as shown in Figure 3.8. The insulated sensing wires make it possible to place many sensors in the water with minimum interference between them. The measured output voltages, which have a linear response to water levels, are connected to an amplifier and

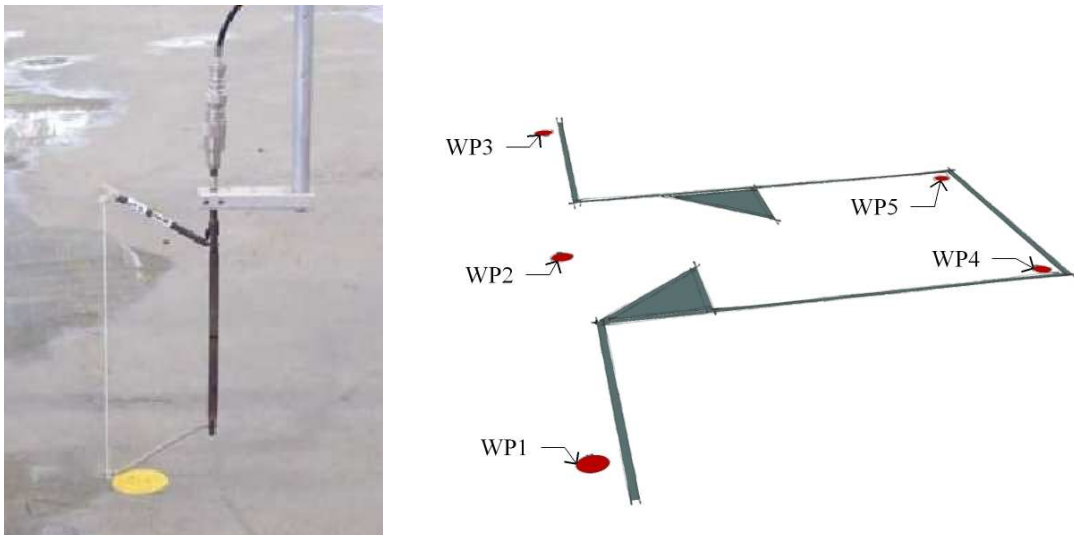

Figure 3.8: A capacitance wave probe (Van der Molen *et al.*, 2010) and location of wave probes WP-1 to WP-5 in the model.

can be calibrated to corresponding water levels. This type of wave probe has an accuracy of about ±0.5 mm (Van der Molen *et al.*, 2010).

Calibration and data acquisition were performed using the software NDAC that is a module of the GEDAP package. Sampling frequency was set to 20 Hz and wave parameters were calculated for a prescribed time window.

The location of five wave probes in the model is as shown in Figure 3.8. Wave probes WP1, WP2 and WP3 were located parallel to the shoreline and between 10 mm to 20 mm from the wall. Wave probes WP4 and WP5 were located inside the harbour, about 10 mm from the back wall and 10 mm from the side walls. The basin model and wave gauges are shown in Figure 3.9

Two amplification factors were determined inside the basin following the procedure of Lee (1969). Similarly to this reference, the amplification factor A_f was calculated as the ratio between the time average of wave heights at a point inside the basin and to the time average of wave heights at the three wave probes outside the harbour, but with the basin closed. Then the amplification factor for the wave probes WP4 and WP5 is then,

$$A_{fi} = \frac{\overline{H_{(WP)_i}}}{\frac{1}{3}\Sigma_{j=1}^{j=3}\overline{H_{(WP)_j}}} \tag{3.3.1}$$

The subindex i identifies the position of the wave probe (i = 4,5 for WP4 and WP5 respectively) and $H_{(WP)_i}$ the average wave height from the measured records

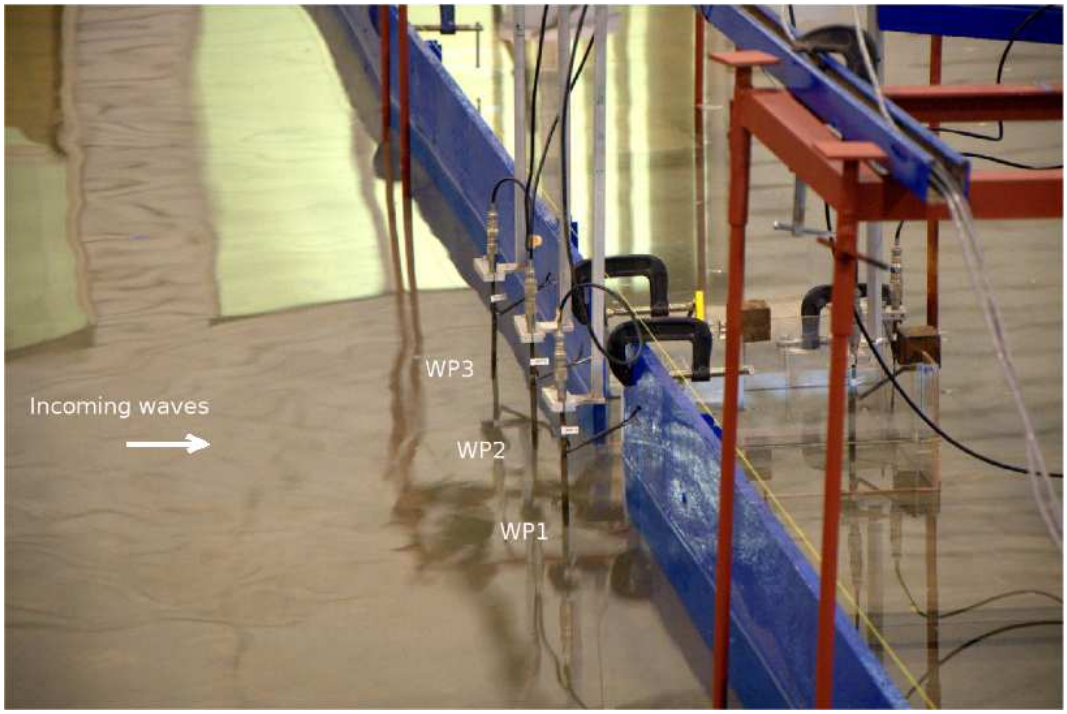

a) Lateral view of the wave tank, vertical shoreline (blue) and WP1 to WP3.

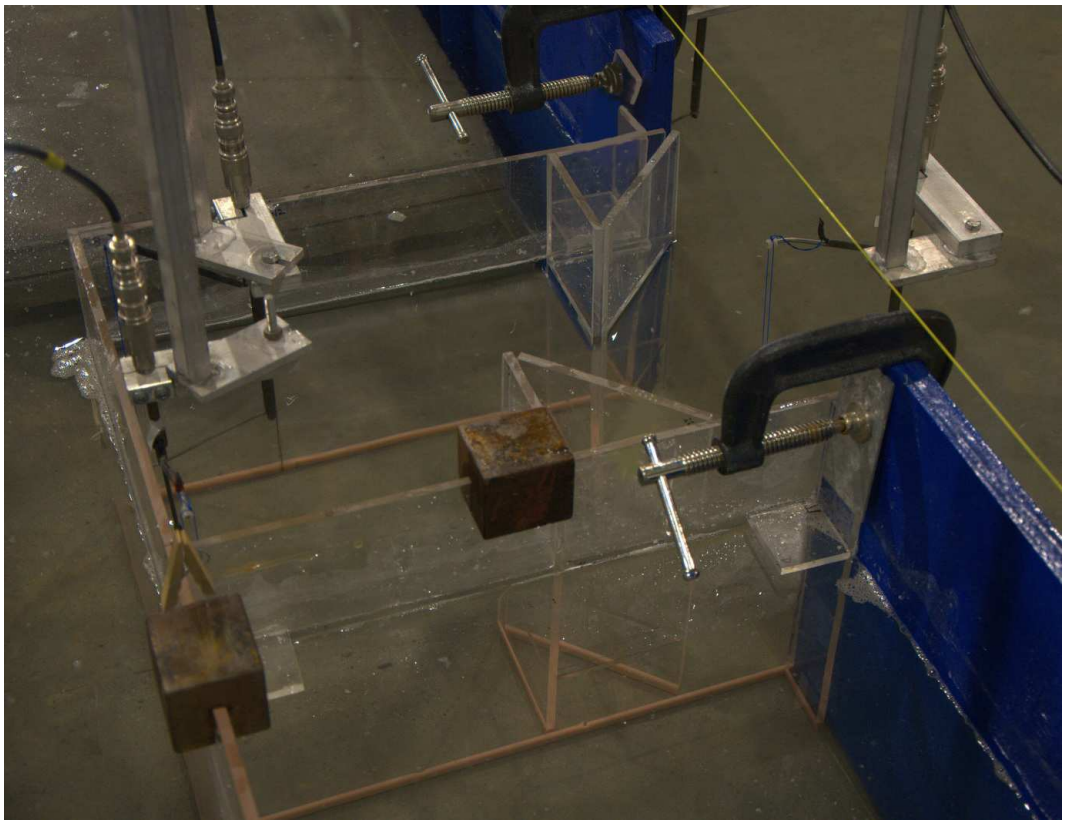

b) View of the basin and wave probes WP2, WP4 and WP5.

Figure 3.9: Arrangement and support of wave probes. a) Harbour model in place at the centre. b) Wave probes WP1, WP2 and WP3 in front of the harbour and parallel to the coastline.

at wave probe i.

3.3.5 Trial tests

In this particular model setup, the model of the basin was required to be tested at or near to resonance, so it was envisaged that the resonant basin might couple with the wave tank. To minimise this effect, wave absorbers were placed on a section of the side walls as described in Section 3.3.2. Besides this, trial tests were required to verify the response of the wave tank with wave guides, and the generation of waves with dynamic wave absorption. With dynamic wave absorption activated, two effects were detected soon after waves reflected from the shoreline reached the wave maker.

Firstly, cross-wave energy build up in the wave tank is a model effect to be avoided. For the frequency tested, namely 1.6 Hz, the 600 mm wave length is close to the 500 mm paddle width, paddle wave probe separation, and resonance condition of the wave tank. Cross-wave resonant conditions were observed with antinodes at the centre and edges of the individual paddles, as shown in Figure 3.10.

Secondly, and with the harbour entrance open, reflected waves from the vertical shoreline and the basin produced a time-average s-shape alignment on the wave-maker paddles, as shown in Figure 3.11. This s-shape was centred on the 3rd and 4th paddle from the basin centre line (11th and 12th paddle from the far side of the observer in Figure 3.11).

From this resultant time average s-shape alignment it can be inferred that the combined reflected and radiated wave heights of the model were not only at a different phase, but also higher at this point. This fact was not clear to the naked eye due to the small wave heights, but rather to the wave gauges fixed at the paddle's front faces.

It can be proposed that these higher wave heights were an effect of the asymmetric basin entrance. Unfortunately no further investigations were carried out to further explain this effect, due to the fact that the wave maker had to be stopped due to cross-wave energy build up.

Without dynamic wave absorption the response of the wave tank was as expected. Waves kept bouncing between the vertical shoreline and the paddles of the wave maker. This reflective and resonant response of the wave tank can be seen in Figure 3.12. This figure illustrates the water surface elevations outside the harbour, at WP1, for wave maker run durations of 50 s, 100 s and 360 s.

Waves generated for 50 s were reflected back from the shoreline to the wave maker, and then reflected back again to the model. The short duration of the test did not

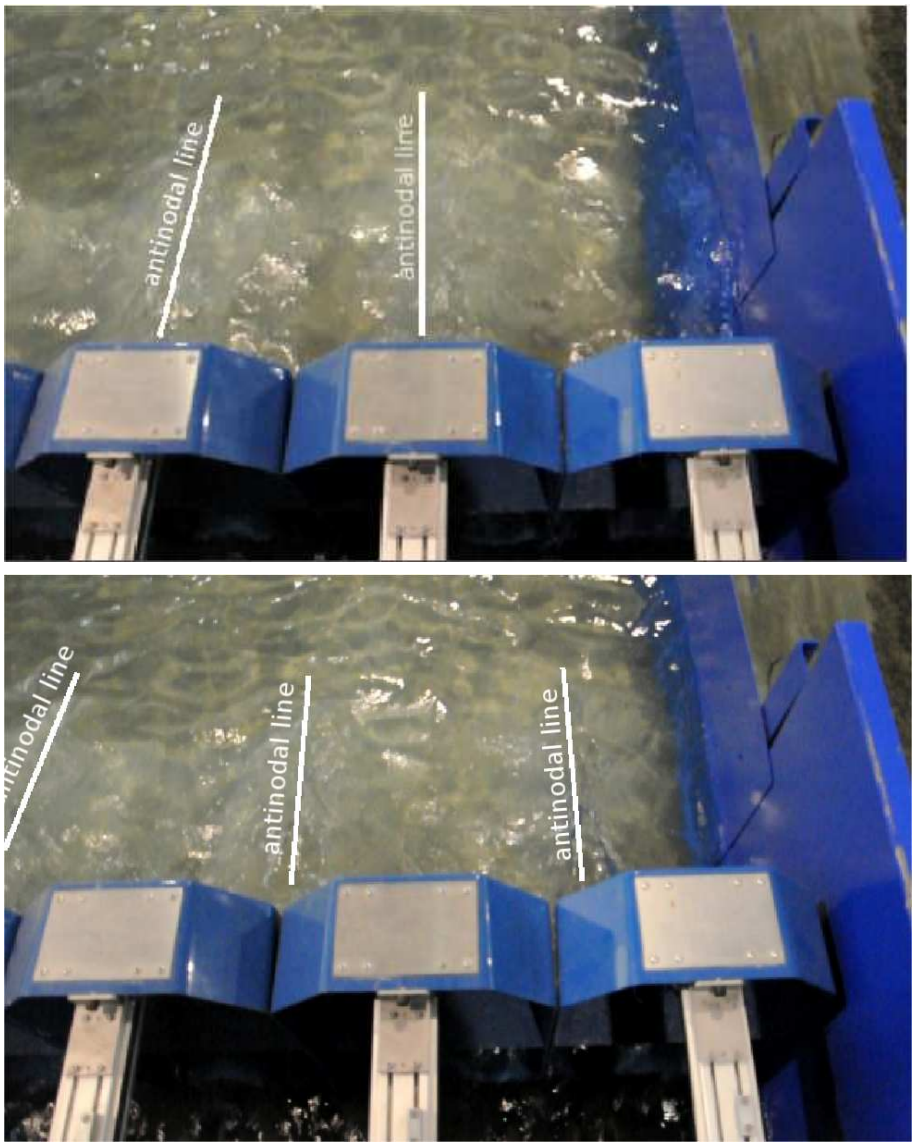

Figure 3.10: Nodes and antinodes of standing waves across the wave basin. Top: antinodes near the centre of the paddles. Below: antinodes near the sides of the paddles.

Figure 3.11: Left: paddles acquire an s-shape with dynamic wave absorption. Right: paddles aligned while working without dynamic wave absorption.

allow superposition of waves at WP1, as shown in Figure 3.12a. In this figure, the generated wave train was recorded at the shoreline wall twice, as two individual wave trains.

In contrast, by generating waves for 100 s there is an overlap of waves, which limits the duration of the tests. Re-reflected waves from the wave maker add unwanted wave energy. In Figure 3.12b, waves are amplified after 75 s of record, leaving about 40 s or 64 undisturbed waves for this frequency.

Finally, waves were generated and recorded for 360 s. As illustrated in Figure 3.12c, the superposition of the generated and reflected regular waves produced amplified wave heights depending on their phase.

Due to these unforeseen model effects it was decided to deactivate the dynamic wave absorption system for the tests series, with the penalty of having to shorten the duration of the tests.

The behaviour of the wave tank with regular waves was typically as shown in Figure 3.13. A standing wave pattern was formed progressively from the shoreline and towards the wave makers. The radiated waves from the harbour entrance were observed as shown in Figure 3.13 (bottom).

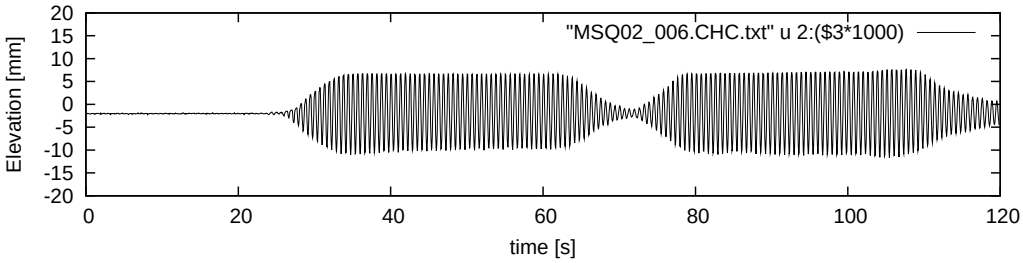

a) Wave makers running for 50 s.

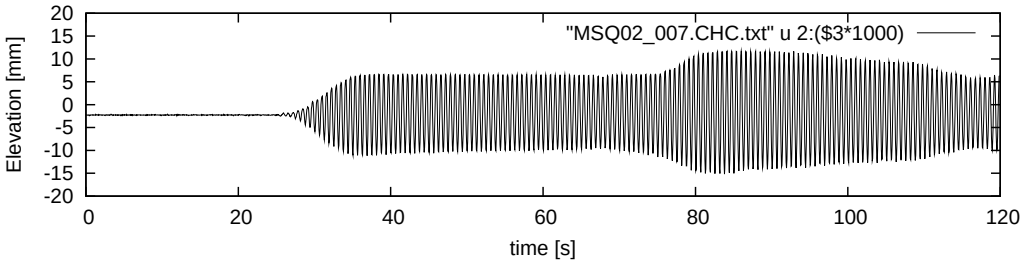

b) Wave makers running for 100 s.

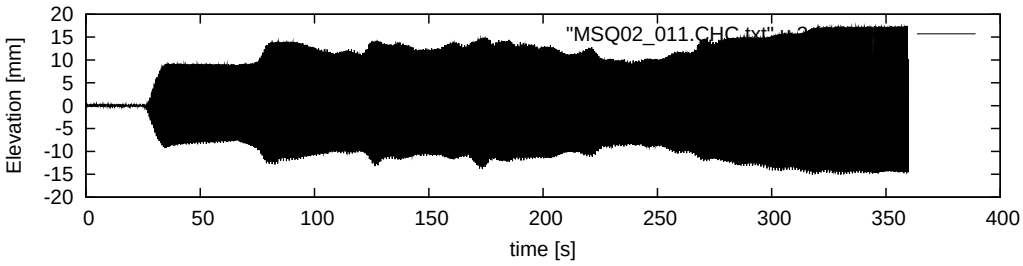

c) Wave makers running for 360 s.

Figure 3.12: Water surface elevation at WP1 with wave maker active for different durations and without dynamic wave absorption.

Figure 3.13: Standing waves from reflection at the coastline (top) and radiated waves from the basin entrance (bottom).

3.4 Numerical modelling

The same basin geometry that was built for the physical model experiments was modelled numerically with some variations.

Regular small amplitude waves were used in all the runs to better visualise wave effects. The frequency range was selected to excite the basin on its first and second mode of oscillation in the transversal basin direction. This was for prototype wave periods of between 8 s and 14 s.

Perfect reflection at the shoreline and basin walls was considered to simplify the model.

The selected numerical model was Mike 21, developed by the DHI, specifically with its Boussinesq Waves (BW) module. This model was available at the University of Stellenbosch and is one of the state-of-the-art tools to model basin resonance.

The model setup is presented in Section 3.4.1, and the model output parameters are described in Section 3.4.2.

3.4.1 Model setup

The numerical model setup was designed to include the interaction between the incoming progressive waves and the reflected and radiated waves from the vertical shoreline and harbour respectively. Small-amplitude waves were required, as well as good absorption at the seaward boundaries.

The regular mesh was defined as a 400 x 800 square grid of cells of 5 m in size. With this mesh the prototype domain dimensions were 2000 m long in the x direction (onshore) and 4000 m wide in the y direction (alongshore). The shoreline was located at grid line $x = 300$ and the basin was located midpoint of the shoreline.

The spacing resolution of $\Delta x = 5m$ allowed 20 points per wave length L for the shortest period to be modelled of 8 s. The recommended maximum value is 10 m to 14 m ($\Delta x \leq L/n$, $n \in [7 - 10]$, DHI (2009)).

The time step was chosen to be 0.2 s using enhanced Boussinesq equations to include deep-water terms ($0.22 < h_{max}/L_0 < 0.5$). Accordingly, the linear dispersion factor was set up to $1/B = 0.0476$. With this configuration, the maximum Courant number as calculated with the model setup planner tool was 0.89.

Regular and uni-directional wave fronts of $H_{mo} = 0.5m$ were generated parallel to the offshore boundary by means of an internal wave generation line extended along the model domain, as shown in Figure 3.15. The selected wave height combined with a fully reflective coastline will provide a standing wave of 1.0 m. Between the internal generation line and the offshore boundary, a sponge layer was included to

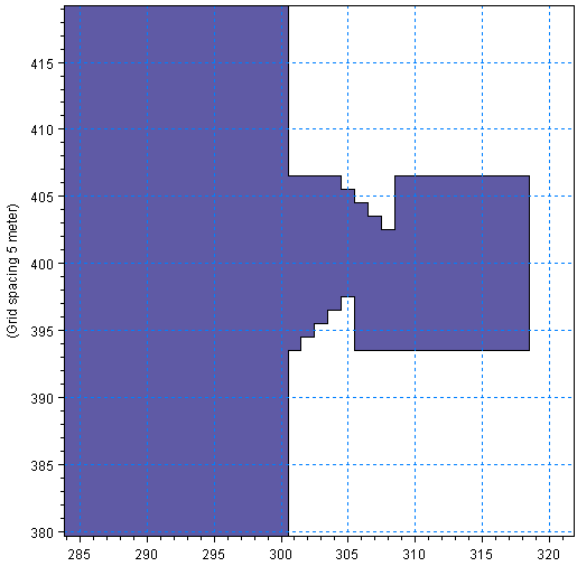

Figure 3.14: Harbour layout.

absorb wave energy from waves leaving the model domain.

Additionally, two *sponge layers* were placed at both sides of the open sea area to absorb reflected and radiated waves from the resonant basin (Figure 3.15).

The *sponge layers* were used as numerical wave absorbers to provide a suitable boundary condition in the open sea region. To be effective, sponge layer thickness should be in the order of one to two times the wave length corresponding to the most energetic waves, or at least 20 lines wide for typical short-wave studies (DHI, 2009). For the model, 30 lines were chosen ($N_{Sponge} = 30$) with a prototype sponge thickness of 150 m. Selected sponge parameters were a = 8 and r = 0.75 in the expression $C_{sponge} = a^{r^{i-1}}$ i = 1, N_{Sponge}.

A single porosity layer was placed at the shoreline and along the basin walls for numerical stability. A highly reflective boundary was used with a porosity value of $n = 1$. This translates to a reflection coefficient C_r of one.

3.4.2 Output parameters

The output parameters from the model were basically water surface elevations η, and wave energy flux.

The storage of energy in a wave is the wave energy density or the specific wave energy in units of Joules per square metre. In small-amplitude waves it is half potential and half kinetic energy.

The instantaneous potential wave energy in a column of water of height $d + \eta$ and

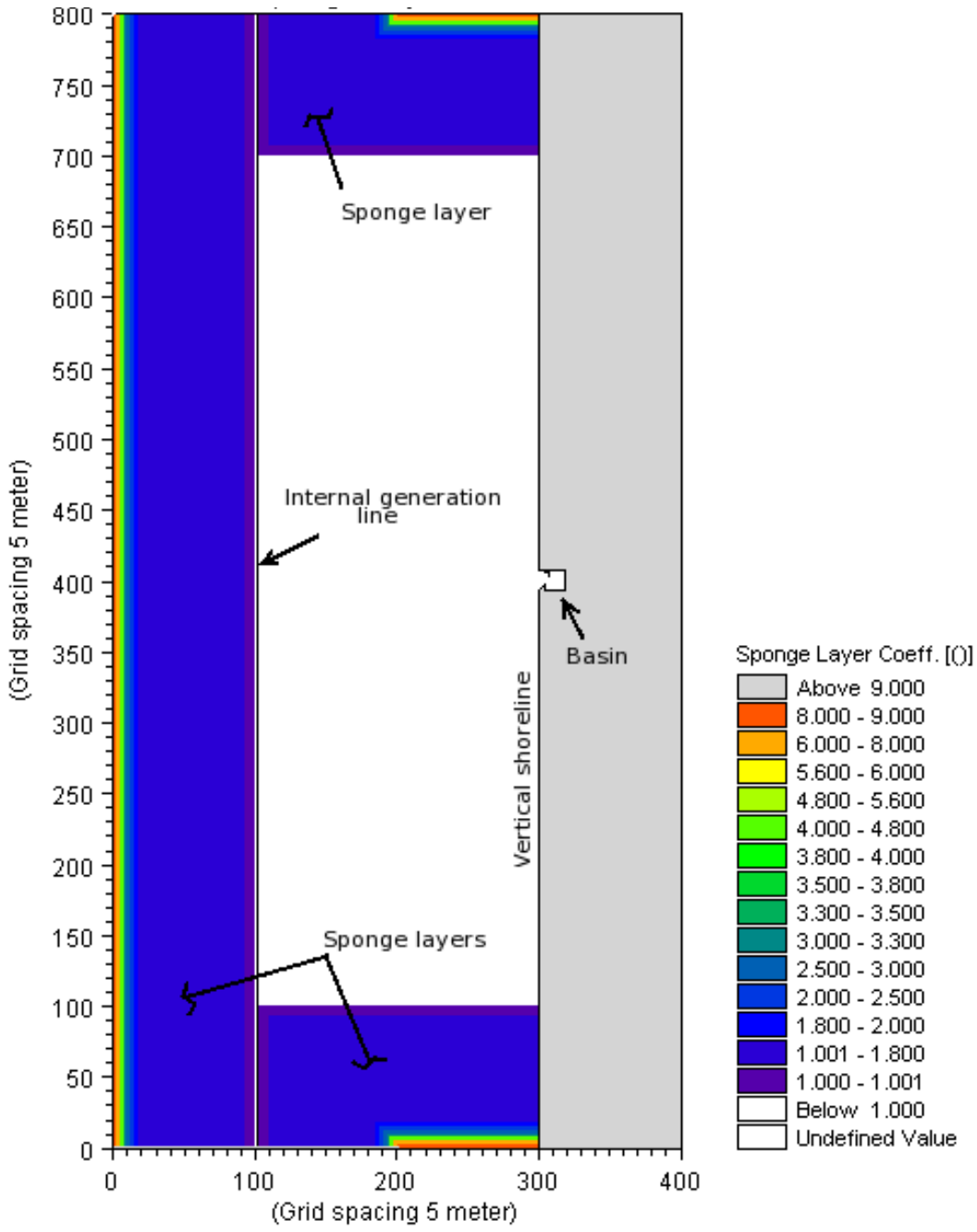

Figure 3.15: Model layout and sponge layers. The internal generation line was set at $x = 102$.

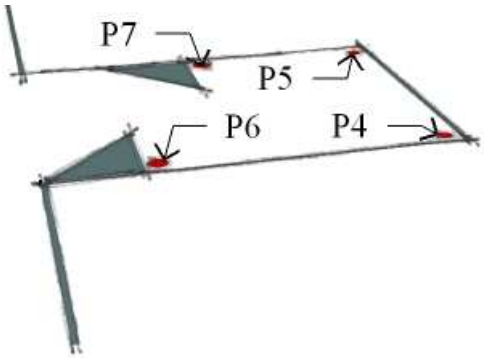

Figure 3.16: Identification and location of points inside the basin for the extraction of water surface elevation (η).

unit plan section is $E_p = \rho g(d+\eta)^2/2$. The first term, $\rho g d^2/2$, is the hydrostatic potential energy and $\rho g d\eta$ vanishes in the average on small-amplitude or sinusoidal waves (Falnes, 2002). Hence the average potential wave energy density is $\overline{E_p} = \rho g\overline{\eta^2}/2$. The over bar line implies average in time. This equation simplifies to $\overline{E_p} = \rho g a^2/4$ for small-amplitude waves of amplitude a.

Since the potential wave energy is half the total wave energy, the total average energy stored per unit horizontal surface area is

$$\overline{E} = \rho g\overline{\eta^2}\Big[\frac{J}{m^2}\Big], \tag{3.4.1}$$

or $\overline{E} = \rho g a^2/2$ for small-amplitude waves, with the over line implying average in time.

Equation 3.4.1 was used to calculate the average wave energy density available in the corners of the basin (points P4 to P7 in Figure 3.16). In addition, the average wave energy density was calculated at the North, East and South basin side walls as defined in Figure 3.17, and inside a region of the basin as illustrated in the grey area in Figure 3.17.

The energy transport by waves, also called wave energy flux or wave power F, is the rate of energy that it is transmitted forward by a wave per unit of time. In the literature the wave energy flux F is also represented by the letters P or J. In terms of volumetric fluxes,

$$F = \rho g\Big(P+Q\Big)\Big[\frac{W}{m}\Big], \tag{3.4.2}$$

in which P and Q are the volumetric fluxes in the x and y directions respectively, in units of $m^3/m/s$. The energy fluxes were extracted to investigate the impact of

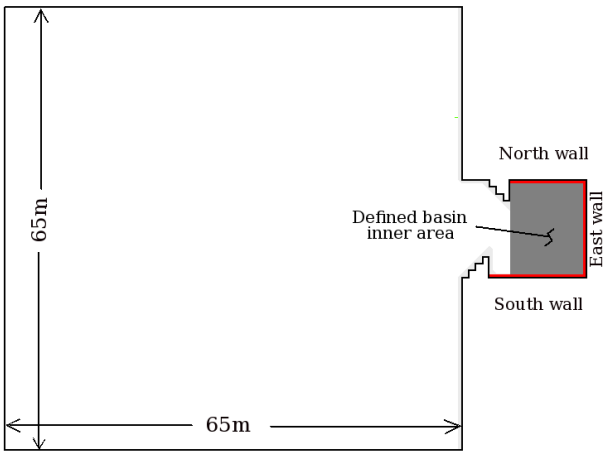

Figure 3.17: Model area for the extraction of water surface elevation η and wave energy fluxes.

the asymmetric entrance on the transverse flux (Q).

The test series is presented in Table 3.2 in terms of prototype wave period T and wave number k, and model frequency f.

Finally, amplification factors A_f were calculated using equation 2.5.2, $A_f = \frac{a_b}{2a_i}$, with a_b the average wave amplitude on selected points and a_i the incoming wave amplitude.

Table 3.2: Numerical model test series

Prototype		Model 1:200	Prototype		Model 1:200
T [s]	k	f [Hz]	T [s]	k	f [Hz]
6.0	0.112	2.36	9.3	0.047	1.52
6.5	0.095	2.17	9.4	0.046	1.50
7.0	0.082	2.02	9.5	0.045	1.49
7.5	0.072	1.88	10.0	0.041	1.41
8.0	0.063	1.77	11.0	0.035	1.28
8.5	0.051	1.66	12.0	0.030	1.17
8.8	0.052	1.60	13.0	0.027	1.08
8.9	0.051	1.59	14.0	0.024	1.01
9.0	0.050	1.57	15.0	0.022	0.94
9.1	0.049	1.55	16.0	0.020	0.88
9.2	0.048	1.53			

3.5 Limitations

The proposed methodology was intended to simplify the reality and gain better insight into a complex three-dimensional problem. A simple shaped resonant basin was selected between many options, and tested with a similar methodology as for harbour response studies with long waves. This was considered acceptable since a resonant basin for wave energy density enhancement is an unconventional concept in coastal and port engineering.

One of the main limitations of the proposed methodology is that wave energy losses inside the basin are not integrated into the models. Absorption of power by a wave energy device is not considered. Radiated waves from absorbers might modify this capacity. Similarly, dissipation at the harbour boundaries is considered only in the physical model. Hence the results are only indicatives of potential wave energy storage inside the basin.

The assumption of regular small-amplitude waves is another limitation of the methodology. To model these waves it is required to use a very deep basin. The basin is in the order of seven times deeper than artificial basins built for wave energy absorption, and about three times deeper than a deep-water artificial harbour. It therefore becomes a limitation in terms of constructibility as it is. Further studies considering non-linear waves are required to model the basin in shallower water depths.

The experiments present further limitations in terms of boundary conditions and type of measurement devices. In the physical model the wave maker with dynamic absorption deactivated and wave guides does not provide a radiation condition on those boundaries. As a consequence, the duration of the tests is limited. Besides, the paddles of the wave maker move as a unit. Therefore the basin behaves like a wide 2D flume. On the other hand, the measurement of surface elevations is at single points. Three-dimensional measurements were possible only with the numerical model.

All the above practical limitations provide values that must be used with caution, even though they provide trends, behaviours, and insight into the modeller and the reader. These results are valuable for lateral thinking and awareness of the problems to be solved in the future.

Chapter 4

Presentation and discussion of results

This chapter presents the results of physical and numerical model experiments. Additional information is presented in the Appendixes. Selected measured water surface oscillations from the physical model are shown in Appendix B, and plots from the numerical modelling are illustrated in Appendix C.

4.1 Results from physical model experiments

The very first results were observed during the trial tests presented in Section 3.3.5. Additionally, visual inspection of the oscillations in the basin were helpful to understand the patterns inside the resonant basin.

Test series included frequencies from 1 to 2 Hz with a $\Delta f = 0.2Hz$. In prototype scale, this represents wave periods from 7 s to 14 s.

Water surface elevations were measured at wave probes WP1, WP2, WP3, WP4 and WP5 (Figure 4.1). Measured oscillations are presented in Appendix B. From these measurements only the first tens of seconds were used to calculate wave heights (Hs). This was done to avoid post-processing re-reflected waves, as shown in Section 3.3.5. By visual inspection of the recorded time series, in the order of 50 s of record, depending on wave celerity, were used and post-processed with the software GDAP.

The processed results for Hs at wave probes WP1, WP2 and WP3 are shown in Figure 4.2. Measurements were taken with the basin closed to record the undisturbed wave heights outside the basin, i.e. the superposition of incoming and reflected waves. These measurements were used to calculate the amplification factors A_f. As described in Section 3.3.4, the amplification was calculated as the

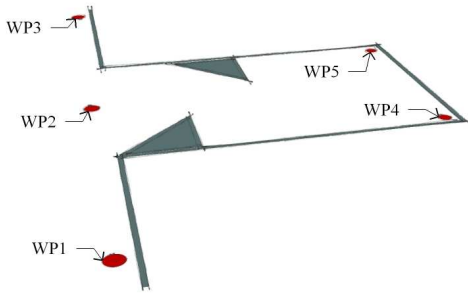

Figure 4.1: Wave probe location (repetition of Figure 3.8).

ratio between the average wave amplitude (or wave height) at a point inside the basin, and the average wave amplitude (or wave height) outside the basin with its entrance closed. Figures are presented with prototype wave periods.

All the test series were repeated once, hence the average wave height values $\overline{Hs}$ were calculated using records from three wave probes and six values.

Processed results for $\overline{Hs}$ at wave probes WP4 and WP5 are shown in Figure 4.3. Similarly, wave heights are presented against prototype wave periods. Average wave heights were calculated from the two records per wave period.

Finally, calculated amplification factors for WP4 and WP5 are illustrated in Figure 4.4 and shown in Table 4.1.

Table 4.1: Measured wave heights and calculated amplification factor (A_f) for wave probes WP4 and WP5 (Figures 4.2, 4.3 and 4.4). [1] Wave heights are averages of WP1, WP2 and WP3.

f[Hz]	$T[s]$	$\overline{Hs}$[m]	$\overline{Hs}$[m]		A_f	
	[s]	Basin closed [1]	WP4	WP5	WP4	WP5
		(Figure 4.2)	(Figure 4.3)		(Figure 4.4)	
1.0	14.1	0.027	0.025	0.021	0.91	0.77
1.2	11.8	0.019	0.015	0.012	0.80	0.61
1.4	10.1	0.015	0.019	0.011	1.21	0.69
1.6	8.8	0.015	0.025	0.016	1.68	1.1
1.8	7.9	0.012	0.004	0.021	0.28	1.73
2.0	7.1	0.011	0.011	0.007	1.03	0.61

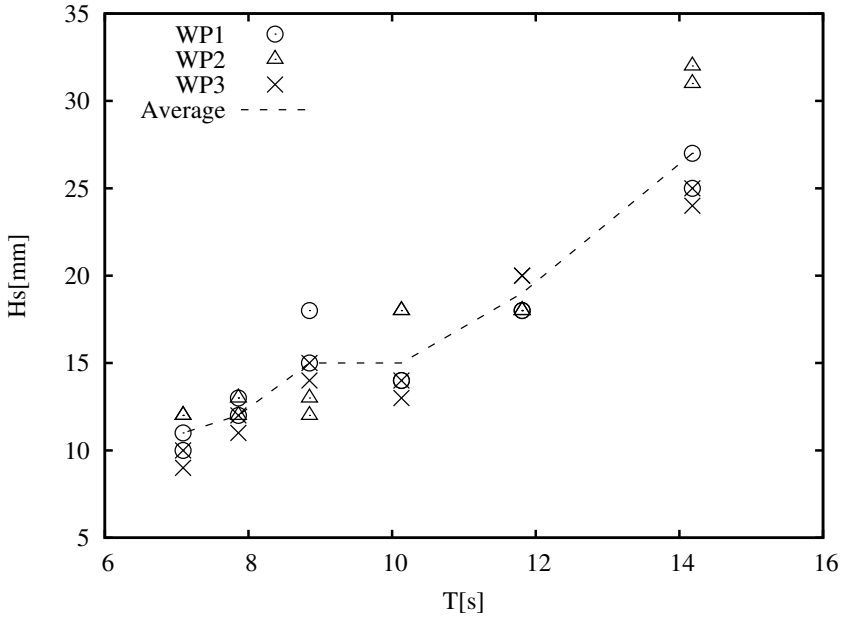

Figure 4.2: Measured wave heights and average values at WP1, WP2 and WP3 with harbour closed.

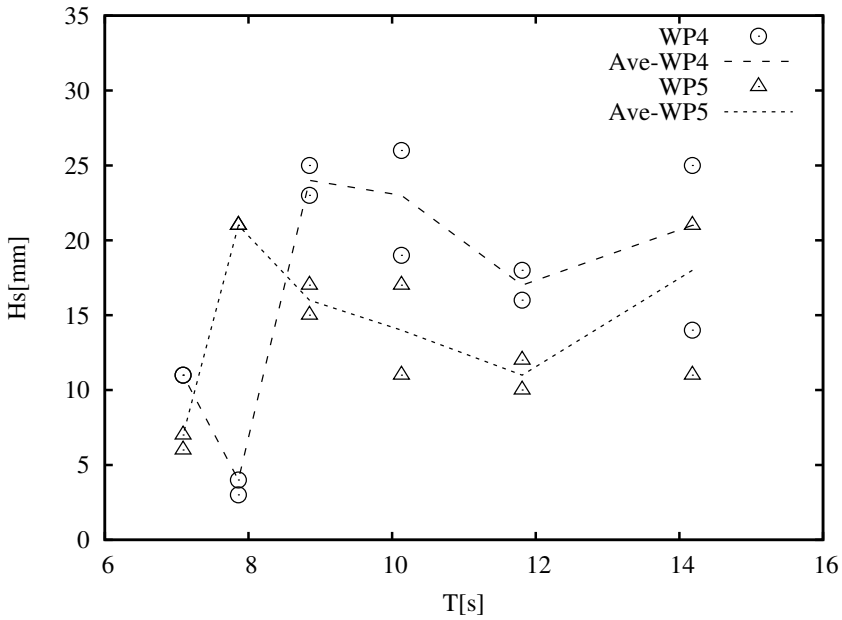

Figure 4.3: Measured wave heights at WP4 and WP5.

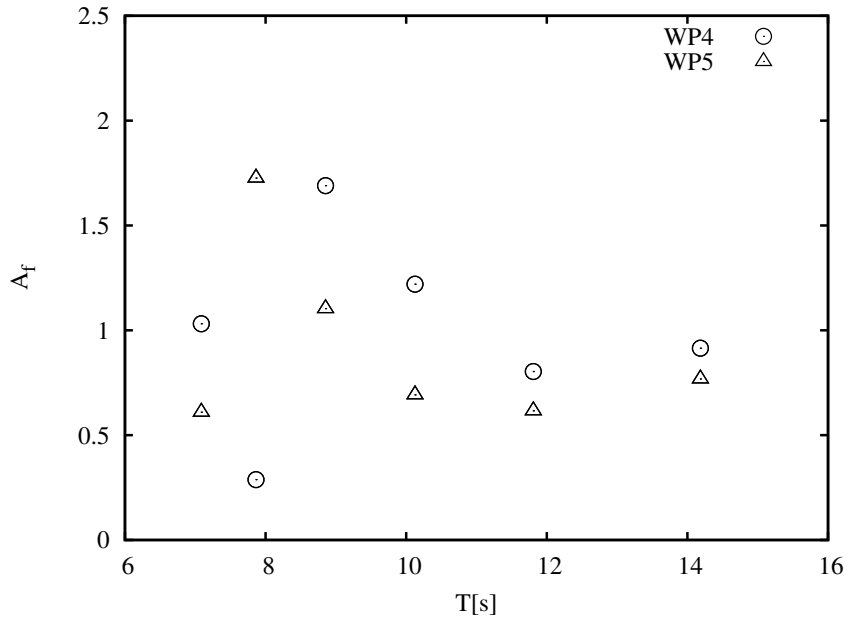

Figure 4.4: Calculated amplification factors at WP4 and WP5.

4.2 Results from numerical modelling

Numerical model runs were considered for 21 wave periods, from 6 s to 16 s at prototype scale, as shown in Table 3.2. This compares with the six wave periods from 7 s to 14 s used in the physical model.

Water surface elevations were extracted from the area defined in Figure 3.17, the basin inner area, basin walls and basin corners to calculate wave energy densities. Additionally, wave energy fluxes were extracted from the larger area defined in Figure 3.17

Extracted water surface oscillations $\eta(x, y, t)$ were post-processed with a script to calculate average wave heights, variance of the surface elevation, and wave energy density $\overline{E}$ (equation 3.4.1). Amplification factors A_f and wave energy density $\overline{E}$ were calculated at: the corners of the resonant basin, as previously shown in Figure 3.16; at the three boundary walls, North, East and South; and at the basin inner area.

The calculated amplification factors A_f on the basin corners are shown in Figures 4.5, 4.6 and 4.7. Points P5 and P7 define the "North" wall. Points P4 and P5 define the limits of the "East" wall, and points P4 and P6 define the "South" wall.

Average wave energy density along the "North", "East" and "South" walls is illus-

trated in Figures 4.8, 4.9 and 4.10 respectively.

For comparison purposes, the average wave energy density at the basin inner area was included in all three figures as a dotted line. The average wave energy density of the incoming waves, $\overline{E} = \rho g a_i^2/2 = 1.257[kJ/m^2]$ with $a_i = 0.5m$, is also shown in the figures as a horizontal dashed line. Hence, wave energy density above this line is considered an increase with respect to the incoming waves.

Plots of water surface elevation and fluxes (P,Q) for selected wave periods between 6 s and 16 s are shown in Figures 4.11 to 4.19. Additional plots for all periods simulated are presented in Appendix C.

Finally, the results are also shown in tabular form for the calculated amplification factor A_f and average wave energy density $\overline{E}$. The calculated amplification factors for points P4 to P7 are presented in Table 4.2. Wave length L and wave number k are also included. Calculated wave energy densities for the "North", "East" and "South" basin walls are presented in Table 4.3. Wave length L and average wave energy at the basin inner area $\overline{E_{basin}}$ are also included.

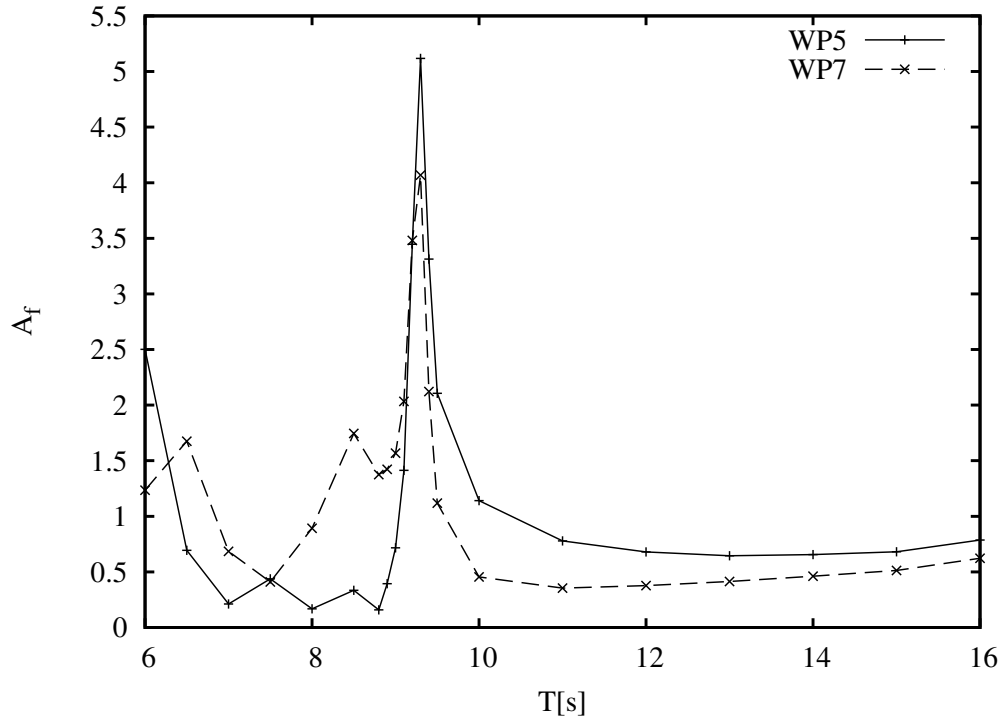

Figure 4.5: Amplification factors, Points P5 and P7, limits of the "North" wall.

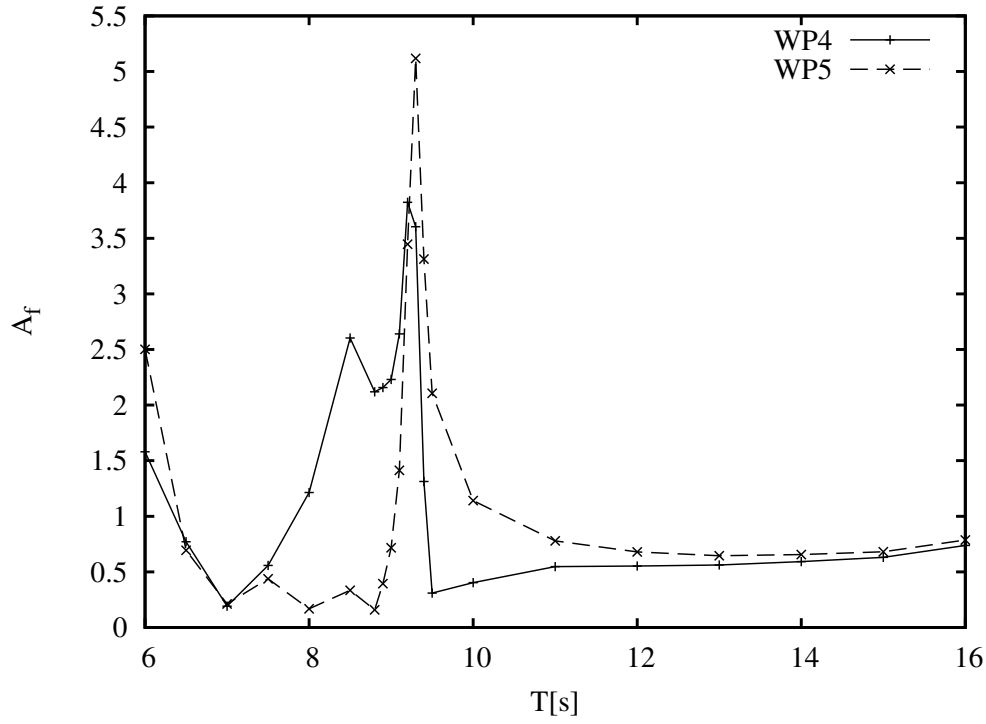

Figure 4.6: Amplification factors, Points P4 and P5, limits of the "East" wall.

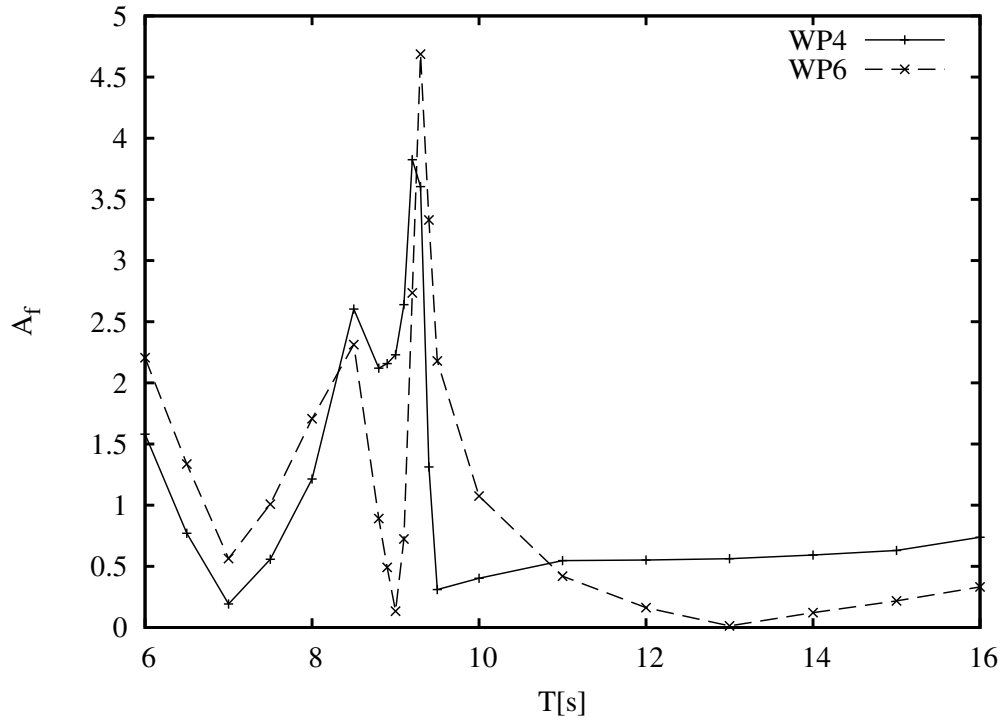

Figure 4.7: Amplification factors, Points P4 and P6, limits of the "South" wall.

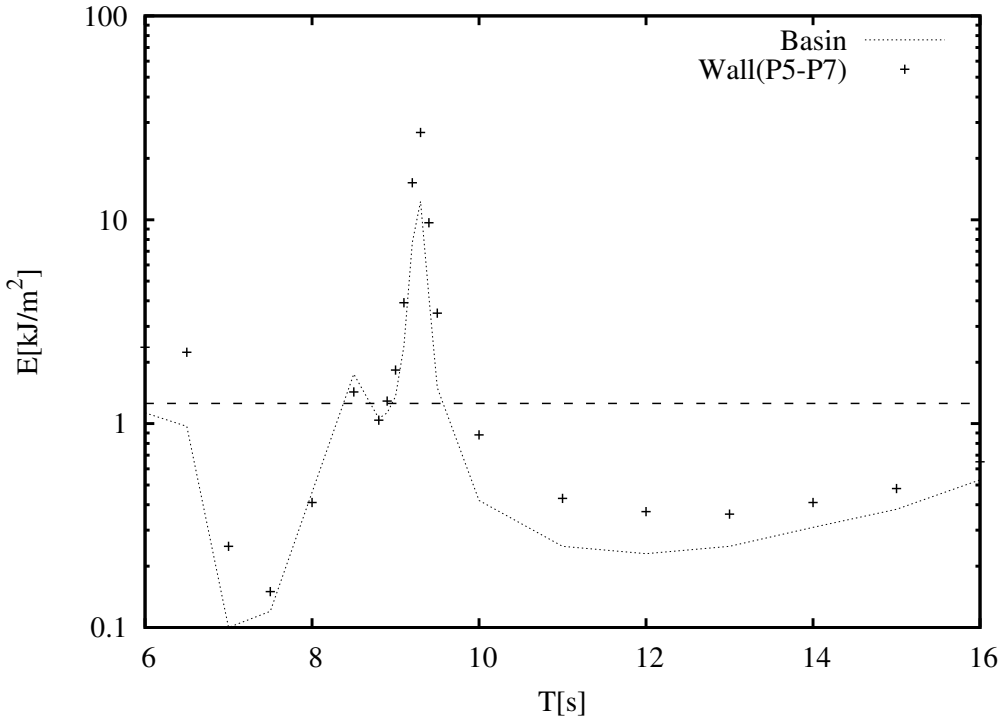

Figure 4.8: Wave energy density at the "North" wall (Figure 3.16).

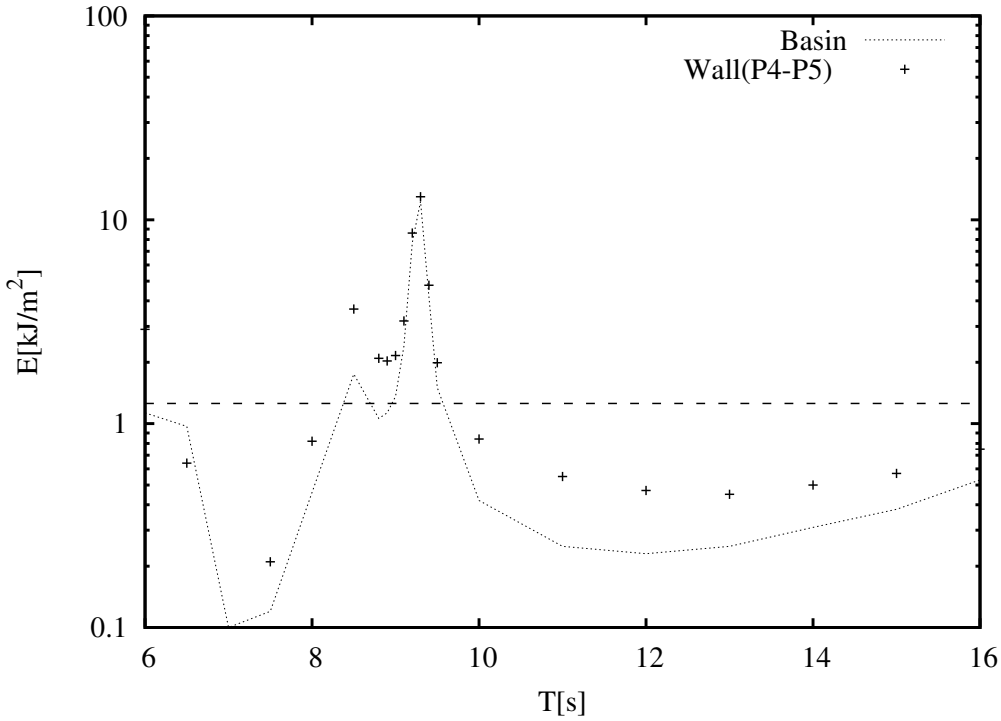

Figure 4.9: Wave energy density at the "East" wall (Figure 3.16).

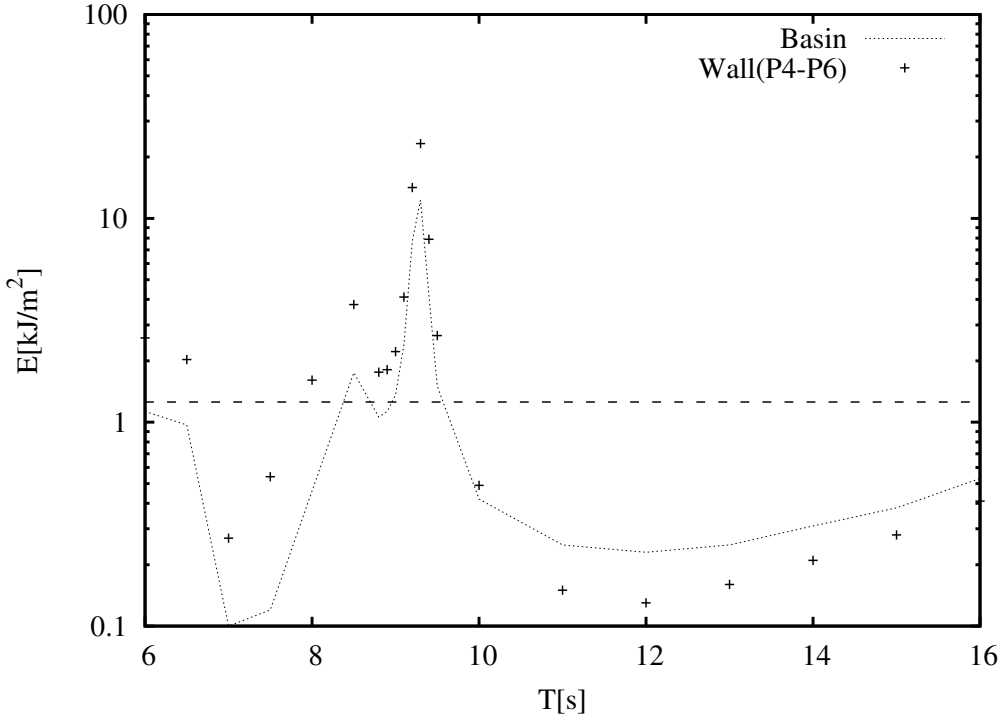

Figure 4.10: Wave energy density at the "South" wall (Figure 3.16).

Table 4.2: Tabular results of average amplification factors at points P4 to P7.

T[s]	L[m]	k	P7	P5	P6	P4
6	56.2	0.1117	1.2	**2.5**	2.2	**1.5**
6.5	65.9	0.0952	1.6	0.6	1.3	0.7
7	76.4	0.0821	0.6	0.2	0.5	0.1
7.5	87.6	0.0716	0.4	0.4	1.0	0.5
8	99.5	0.0631	0.8	0.1	1.7	1.2
8.5	111.9	0.0561	1.7	0.3	2.3	2.6
8.8	119.6	0.0525	1.3	0.1	0.8	2.1
8.9	122.2	0.0514	1.4	0.3	0.4	2.1
9	124.8	0.0503	1.5	0.7	0.1	2.2
9.1	127.4	0.0493	2.0	1.4	0.7	2.6
9.2	130.0	0.0483	3.4	3.4	2.7	**3.8**
9.3	132.6	0.0473	4.0	**5.1**	4.6	3.6
9.4	135.3	0.0464	2.1	3.3	3.3	1.3
9.5	137.9	0.0455	1.1	2.1	2.1	0.3
10	151.2	0.0415	0.4	1.1	1.0	0.4
11	178.1	0.0352	0.3	0.7	0.4	0.5
12	204.8	0.0306	0.3	0.6	0.1	0.5
13	231.1	0.0271	0.4	0.6	0.0	0.5
14	257.1	0.0244	0.4	0.6	0.1	0.5
15	282.6	0.0222	0.5	0.6	0.2	0.6
16	307.8	0.0204	0.6	0.7	0.3	0.7

a) Surface elevations (η).

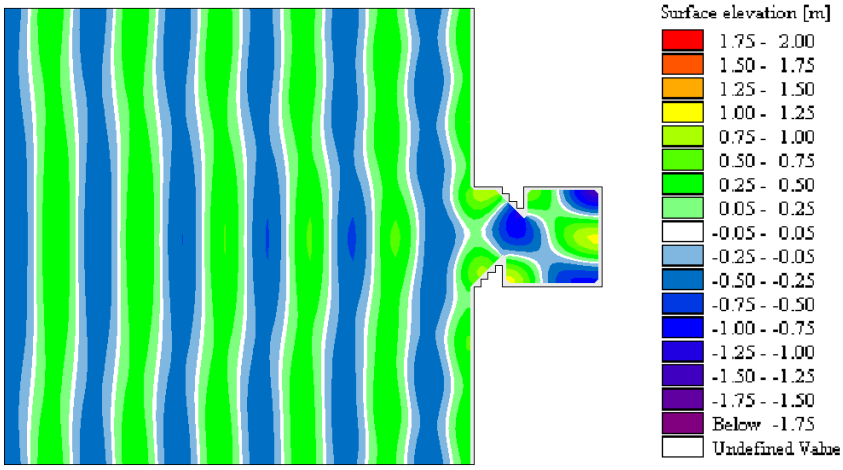

b) Flux (P).

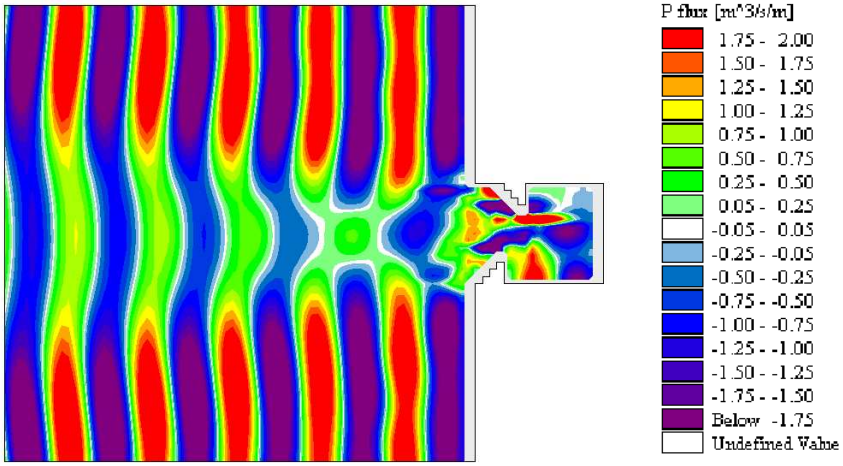

c) Flux (Q).

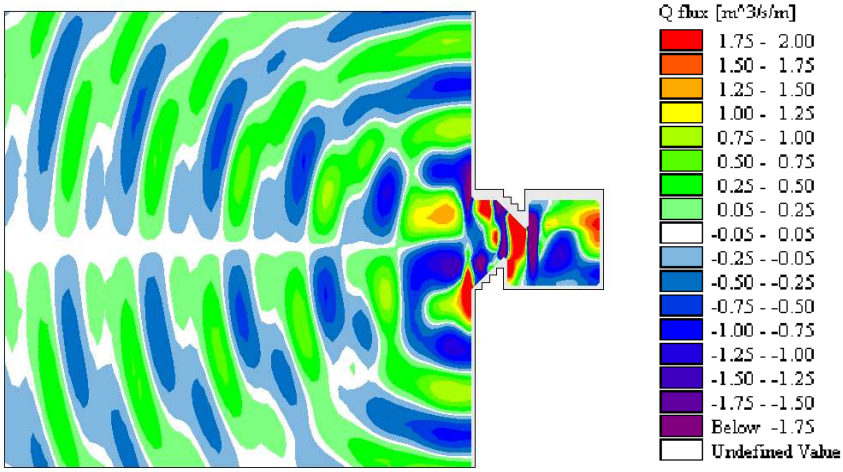

Figure 4.11: Snapshot for $T = 6.0s$ at maximum displacement of surface elevation η inside the basin.

a) Surface elevations (η).

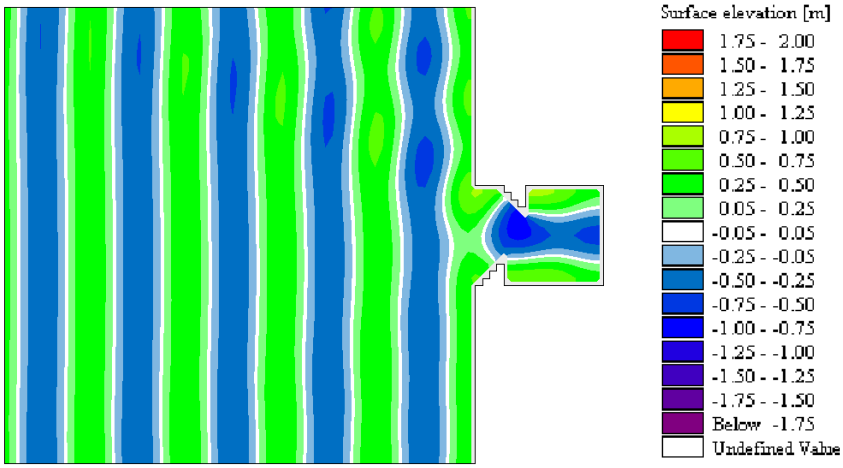

b) Flux (P).

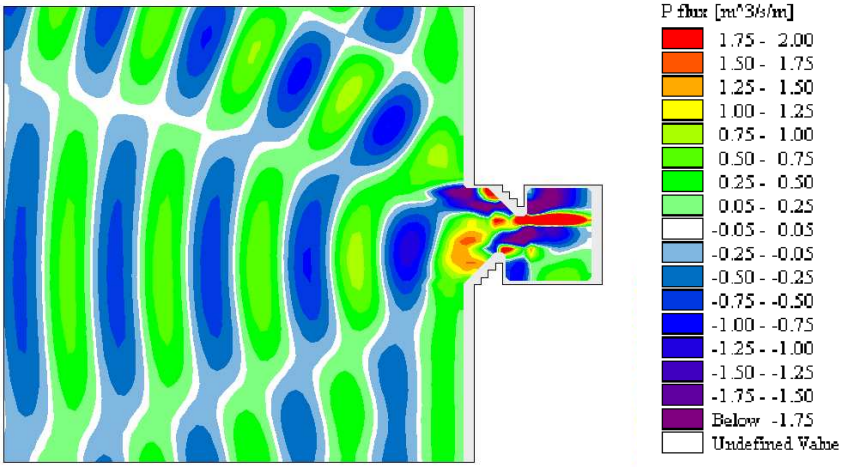

c) Flux (Q).

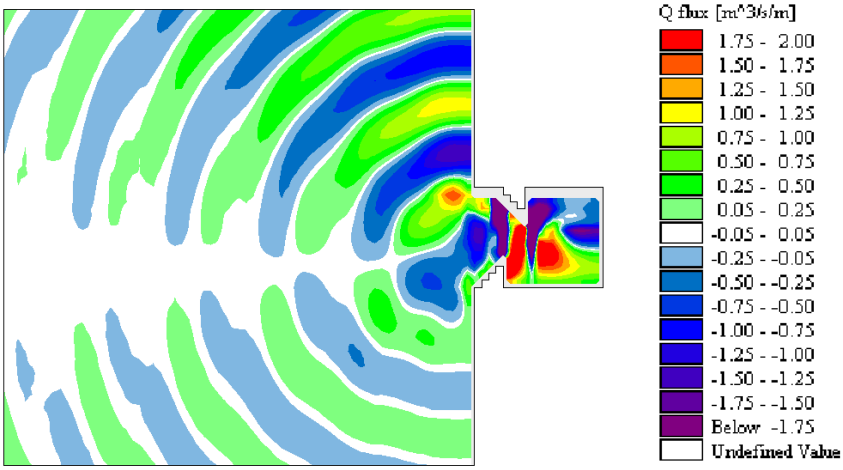

Figure 4.12: Snapshot for $T = 6.5s$ at maximum displacement of surface elevation η inside the basin.

a) Surface elevations (η).

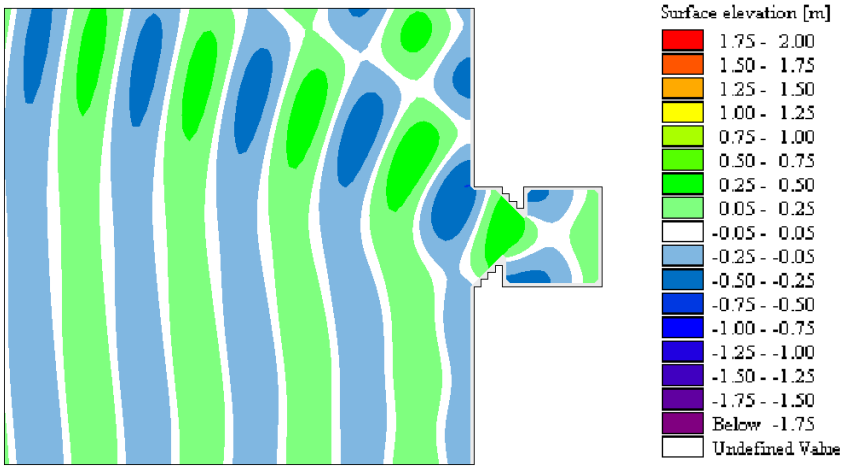

b) Flux (P).

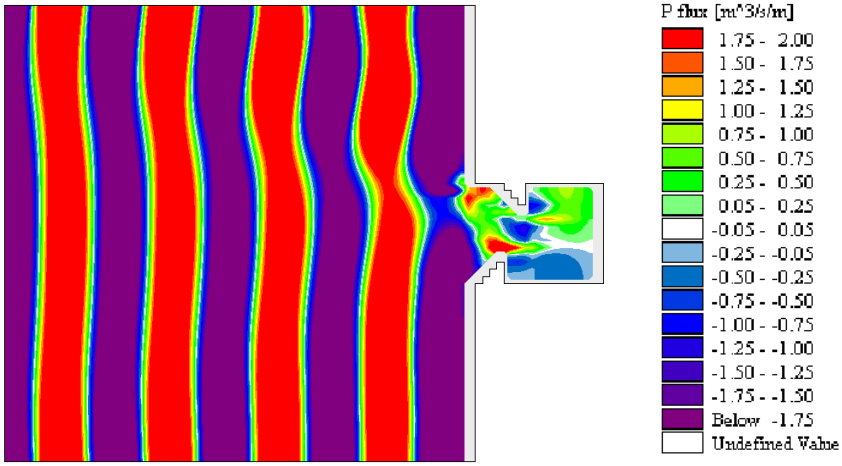

c) Flux (Q).

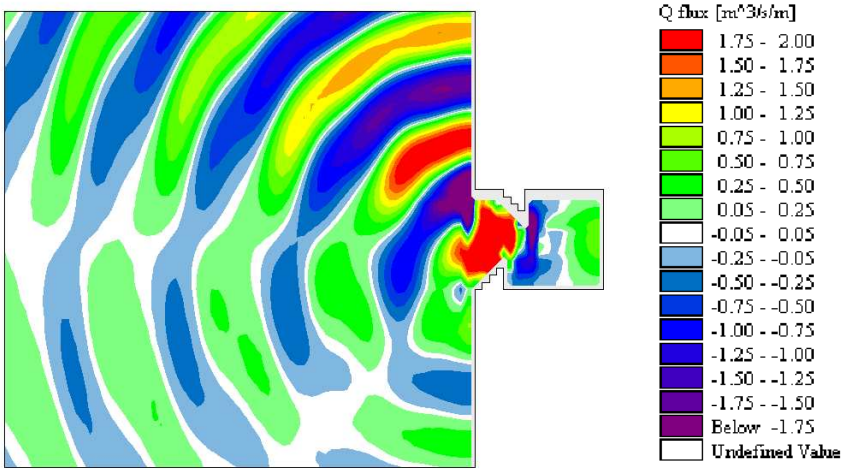

Figure 4.13: Snapshot for $T = 7.0s$ at maximum displacement of surface elevation η inside the basin.

a) Surface elevations (η).

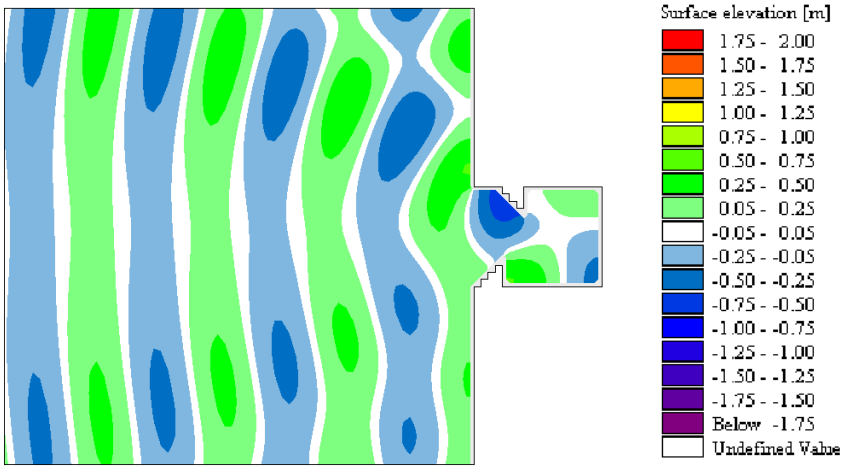

b) Flux (P).

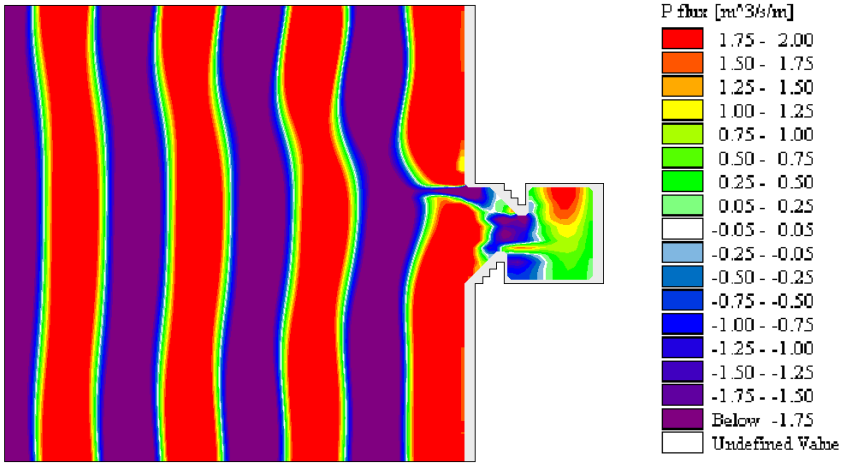

c) Flux (Q).

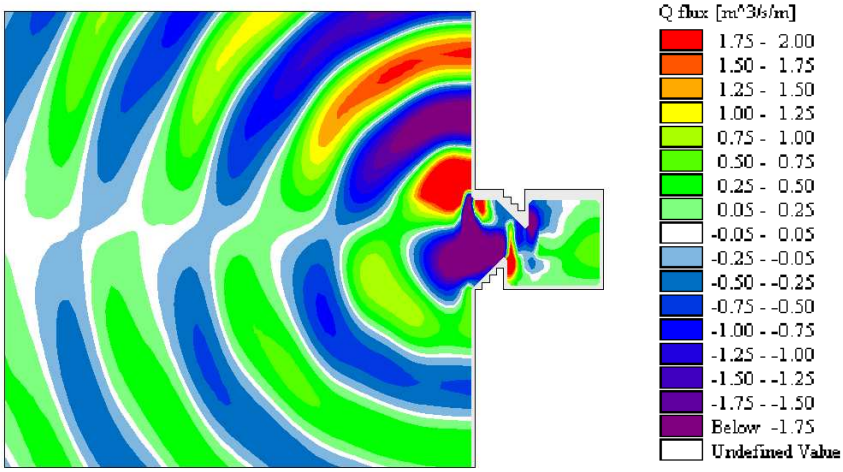

Figure 4.14: Snapshot for $T = 7.5s$ at maximum displacement of surface elevation η inside the basin.

a) Surface elevations (η).

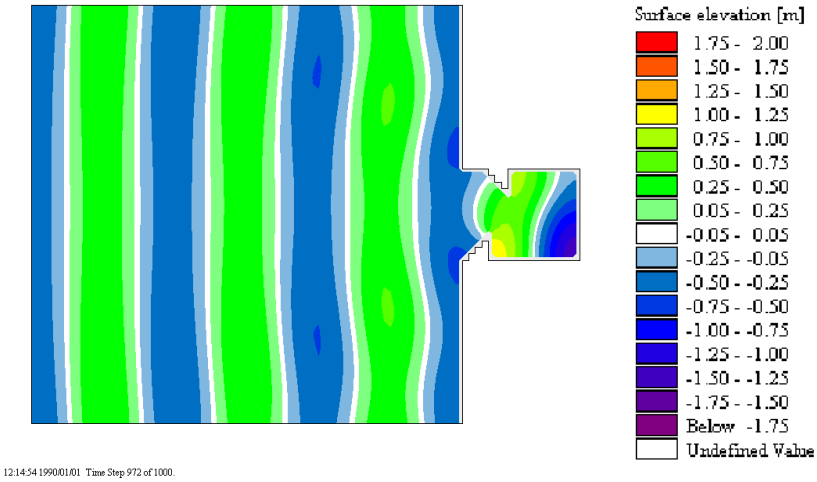

b) Flux (P).

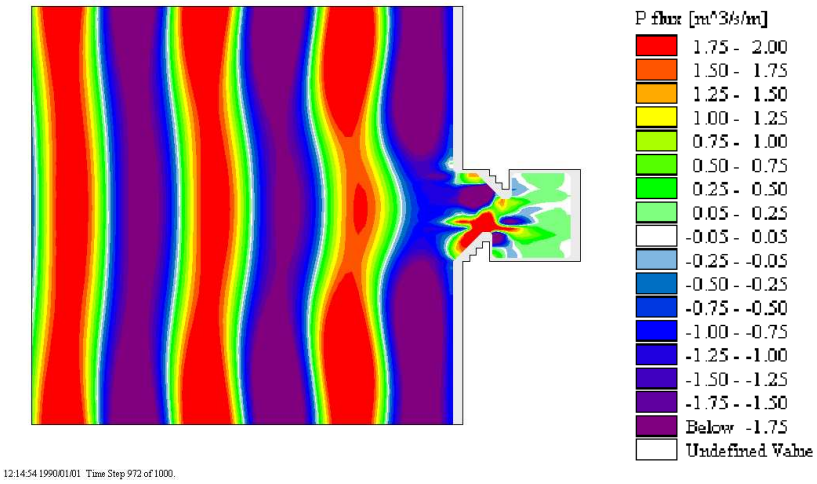

c) Flux (Q).

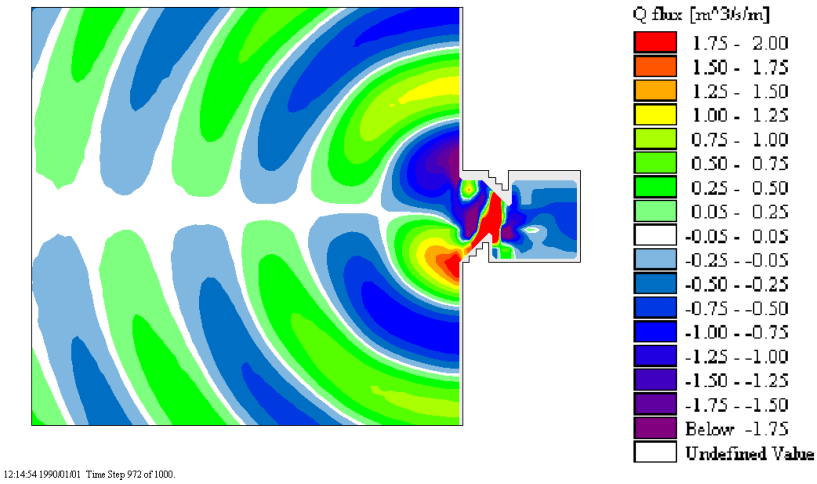

Figure 4.15: Snapshot for $T = 8.5s$ at maximum displacement of surface elevation η inside the basin.

a) Surface elevations (η).

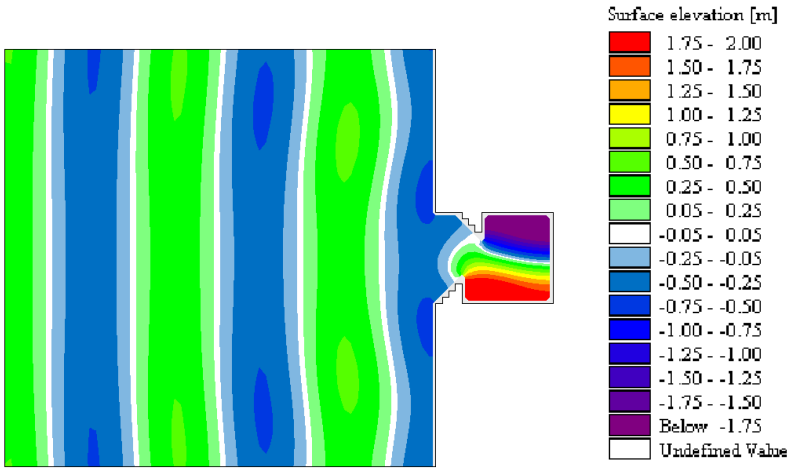

b) Flux (P).

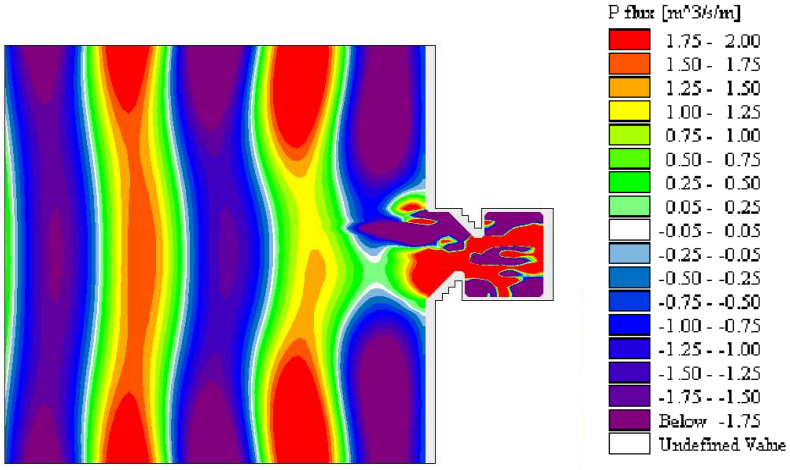

c) Flux (Q).

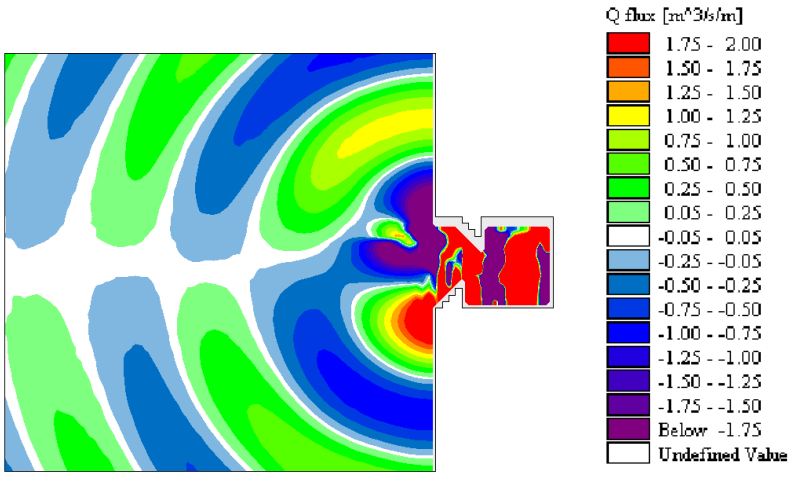

Figure 4.16: Snapshot for $T = 9.3s$ at maximum displacement of surface elevation η inside the basin.

a) Surface elevations (η).

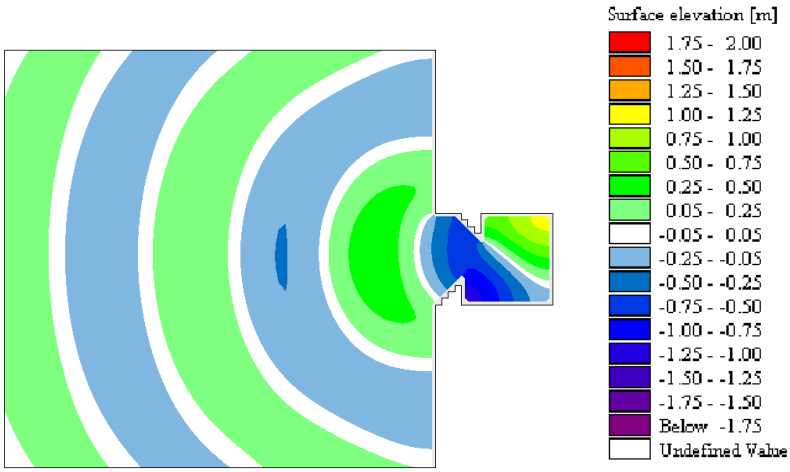

b) Flux (P).

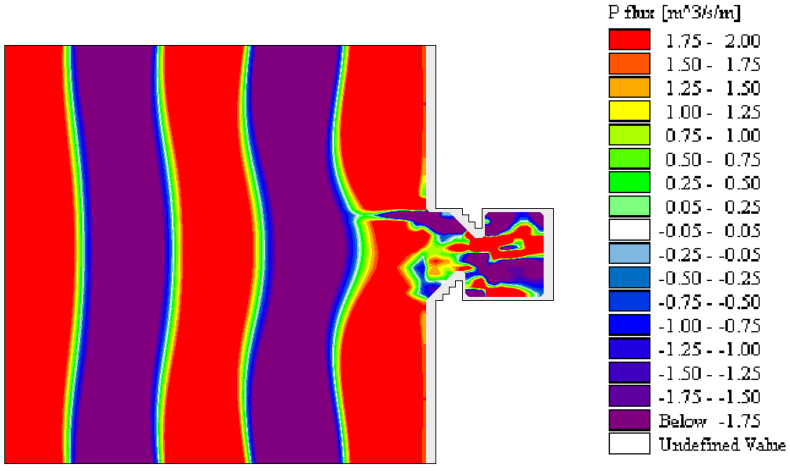

c) Flux (Q).

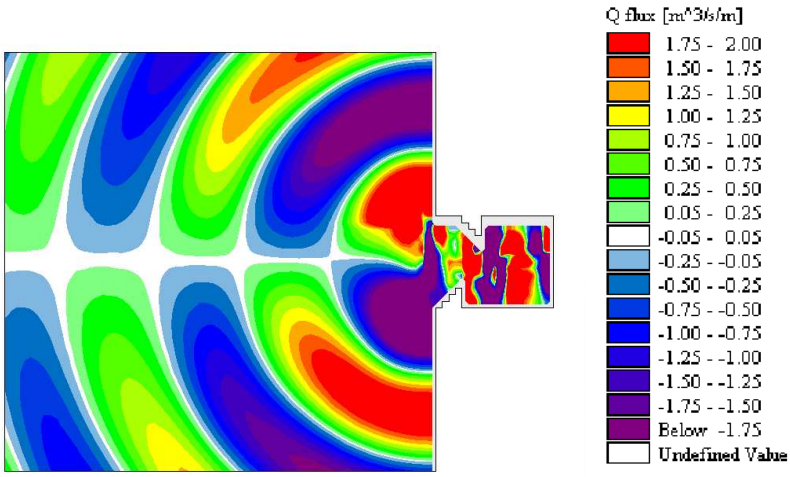

Figure 4.17: Snapshot for $T = 9.5s$ at maximum displacement of surface elevation η inside the basin.

a) Surface elevations (η).

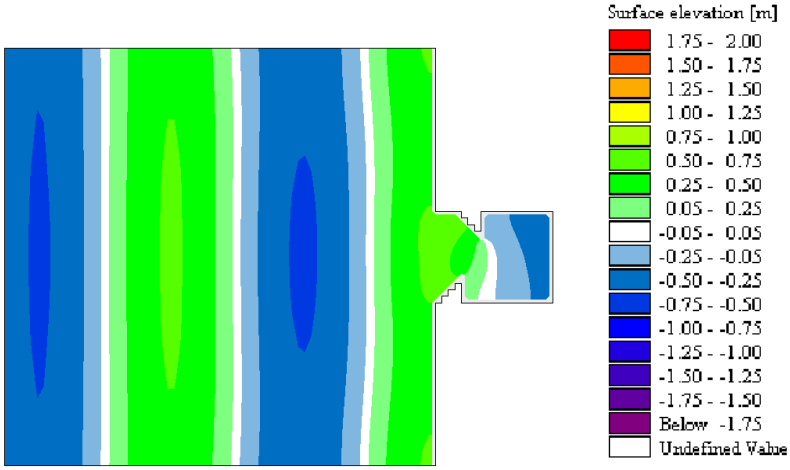

b) Flux (P).

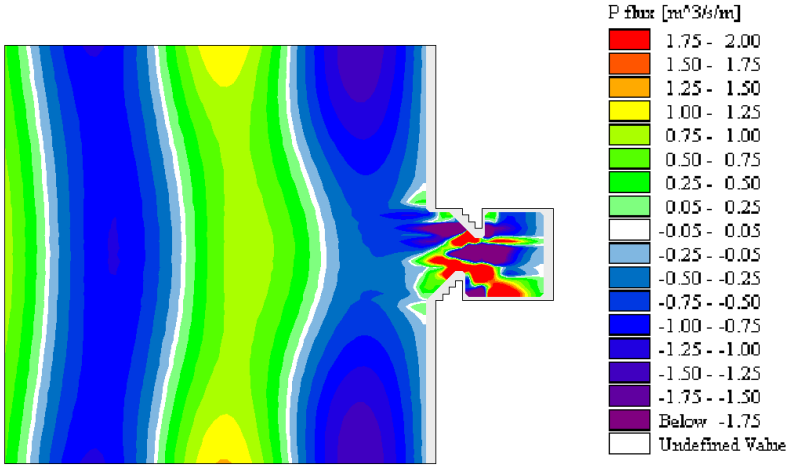

c) Flux (Q).

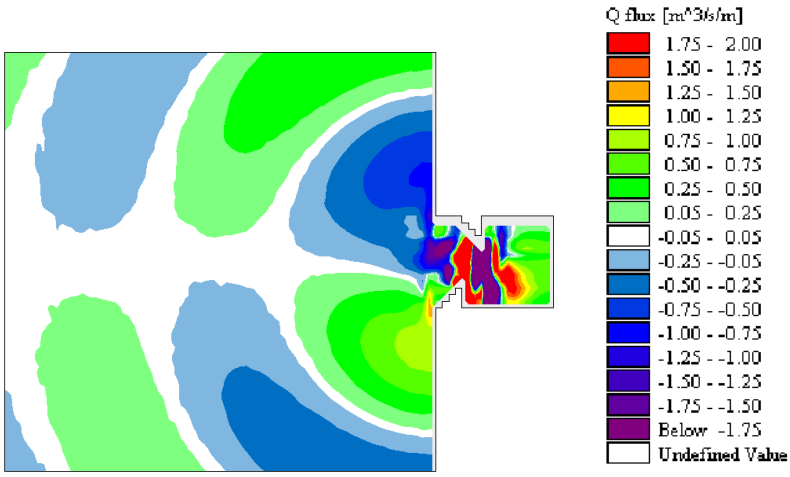

Figure 4.18: Snapshot for $T = 12.0s$ at maximum displacement of surface elevation η inside the basin.

a) Surface elevations (η).

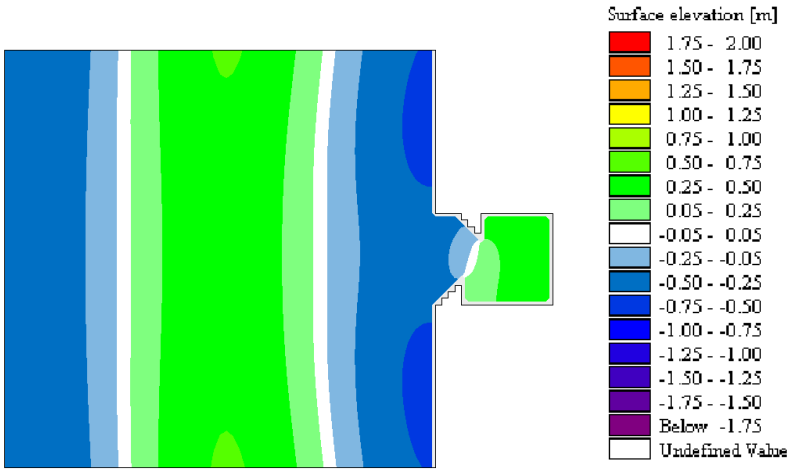

b) Flux (P).

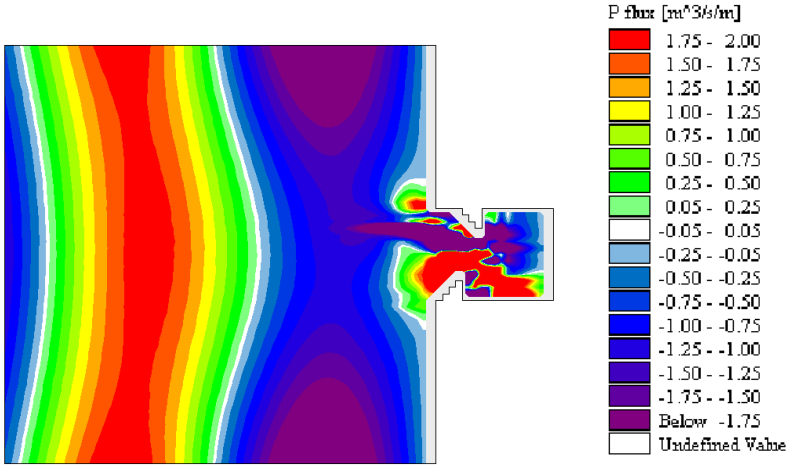

c) Flux (Q).

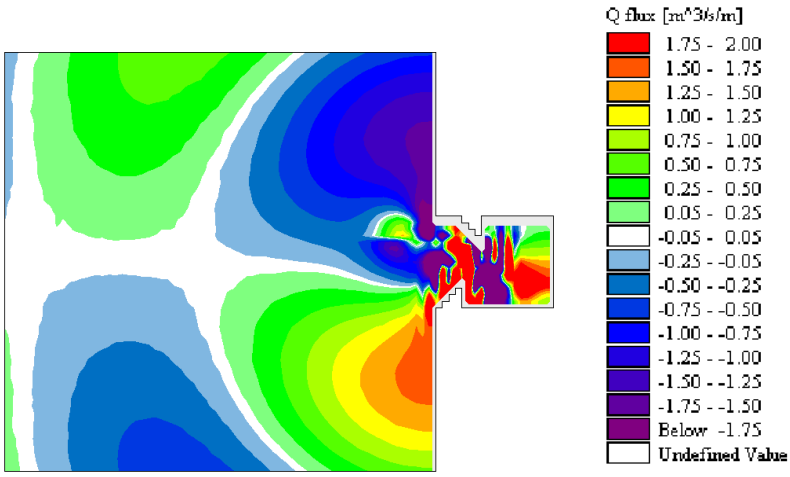

Figure 4.19: Snapshot for $T = 16.0s$ at maximum displacement of surface elevation η inside the basin.

Table 4.3: Tabular results of average wave energy density presented in Figures 4.8, 4.9 and 4.10 in units of $[kJ/m^2]$.

T[s]	L[m]	$\overline{E_{basin}}$	"North" Wall $\overline{P5-P7}$	"South" Wall $\overline{P4-P6}$	"East" Wall $\overline{P4-P5}$
6	56.2	1.13	2.37	2.59	2.90
6.5	66.0	0.97	2.24	2.03	0.64
7	76.5	0.10	0.25	0.27	0.09
7.5	87.7	0.12	0.15	0.54	0.21
8	99.6	0.46	0.41	1.61	0.82
8.5	112.0	1.75	1.43	3.78	3.65
8.8	119.6	1.06	1.04	1.76	2.09
8.9	122.2	1.13	1.29	1.81	2.03
9	124.8	1.36	1.83	2.22	2.16
9.1	127.4	2.40	3.92	4.11	3.19
9.2	130.1	7.73	15.19	14.16	8.60
9.3	132.7	12.29	26.78	23.27	12.98
9.4	135.3	4.19	9.66	7.89	4.77
9.5	138.0	1.50	3.48	2.66	1.99
10	151.3	0.42	0.88	0.49	0.84
11	178.1	0.25	0.43	0.15	0.55
12	204.8	0.23	0.37	0.13	0.47
13	231.2	0.25	0.36	0.16	0.45
14	257.1	0.31	0.41	0.21	0.50
15	282.6	0.38	0.48	0.28	0.57
16	307.8	0.53	0.65	0.41	0.75

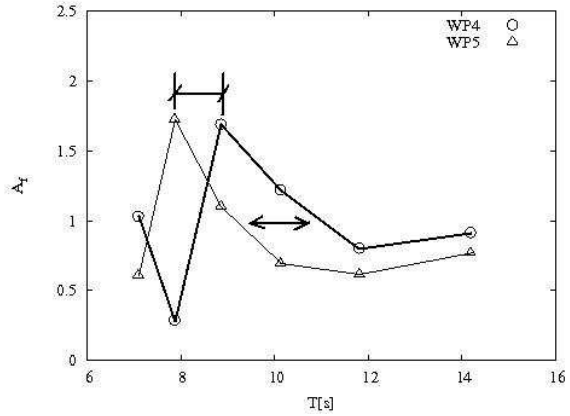

Figure 4.20: Amplification factors shifted in wave period for WP4 and WP5.

4.3 Discussion of results

In this section the results obtained from the physical and numerical models are analysed and discussed.

The results for the physical model were limited to measurements of surface oscillations at two locations inside the basin. These locations were selected to record the maximum variation of surface elevation at the back wall of the basin. The results presented in Figure 4.4 and Table 4.1 show a shift in wave period between both locations.
The maximums and minimum values, as well as the whole curves, are shifted horizontally (in wave period) in about $1s$ as shown in Figure 4.20. A difference of $0.8s$, for instance waves with periods of $8s$ and $8.8s$ in water depths of 50m, have a difference in wave length of 20 m (wave lengths of 100 m and 120 m respectively).

This difference matches the length difference of 20m between the "North" and "South" walls, which are 45 m and 65 m long respectively. Moreover, the shortest wall ("North") is related to the shortest wave length at the peak A_f (WP5 at $7.9s$). The longest wall ('South") is related to the longest wave length at the peak A_f (WP4 at $8.8s$). This may indicate that the asymmetric entrance can control the shifting in wave period of the amplification factor at the back wall corners.

The results for the numerical model at the back wall or "East" wall are illustrated in Figure 4.6. From this plot, amplification factors at P4 are shifted slightly to the lower periods when compared with P5. This is on the opposite direction from the physical results in Figure 4.20.

In addition, the wave period range in which $A_f > 1$ is wider for P4 when compared

with P5. Hence, Point 4 is more suitable than Point 5 for wave energy extraction if a wider period range for operation is required.

The results for the physical and numerical models can be compared at the back wall, between Points WP4-P4 and WP5-P5 respectively. If the amplification factors are compared at specific periods, the results for the two models differ. Amplification factors near the peak enhancement at the corners of the back wall are shown in Table 4.4.

Table 4.4: Amplification factors from physical and numerical models at the corners of the back wall. $^{(1)}$: result for $T = 8s$, $^{(2)}$: result for $T = 10s$..

T[s]	A_f physical and (numerical) model			
	WP4	(P4)	WP5	(P5)
7.9	0.28	$(1.2)^{(1)}$	1.73	$(0.1)^{(1)}$
8.8	1.68	(2.1)	1.10	(0.1)
10.1	1.21	$(0.4)^{(2)}$	0.69	$(1.1)^{(2)}$

From this table it can be seen that the results do not present a correlation at the period range of interest. If all the data points are plotted in the same graph, as in Figure 4.21, a better correlation would be obtained if the data points are shifted horizontally, as shown in the same figures.

A horizontal shift of WP4 data points to the left in Figure 4.21 requires that the wave period needs to be shorter for a given calculated A_f. This is not physically possible, since the wave period of the incoming waves does not change. What can change is the resonant conditions inside the basin. In the physical model, longer waves were enhanced. This shift in period, or resonant wave lengths, may then be attributed to a slight difference in size between the physical and numerical models. A physical (numerical) model that is slightly larger (shorter) when compared to the numerical (physical) model would enhance longer (shorter) wave lengths and produce this horizontal shift.

In contrast, point WP5 is shifted in the opposite direction in Figure 4.21. In this case the physical (numerical) model dimension that is driving the resonant modes must be shorter (larger) when compared to the numerical (physical) model to produce this horizontal shift.

A difference in size between the physical and numerical models is not strictly possible, since both models were built and designed to be compared. Slight variations in length are possible due to construction tolerances, but this should not be relevant. On the other hand, it is not strictly the basin size that is the end parameter for harbour resonance. It is the resonant length induced by the basin entrance.

The harbour entrance effect, as described by Miles and Munk (1961), produces a shift of the nodal line seaward basin entrance. As a result, from this reference it can be deduced that the enhanced quarter wave length is in the order of 10% to 30% longer than the basin length, depending on the width of the entrance gap.

The numerical model probably is not modelling the hydrodynamics at the basin entrance properly, but this is not conclusive. Further studies would be required to confirm this or establish another reason for this shift.

It is concluded that the shifts in wave period observed and described in Figure 4.21 can be produced by a difference in location of the nodal line at the basin entrance. Moreover, since the entrance is asymmetric, the nodal line is a curve that adopts different curvatures, which can enhance or decrease the amplification factor in one or the other back wall corner as described later in this section.

From the results for the numerical model (Figure 4.6 and Table 4.2), the maximum amplification factors obtained at the back wall are $A_{f(P5)} = 5.1$ and $A_{f(P4)} = 3.8$ for the first mode of oscillation (n = 1, m = 1) at $T \sim 9.3s$. This result averages 4.45, similar to the theoretical $A_f = 4.3$ (Figure 2.33, n = 1).

For the second mode of oscillation (n = 2, m = 2), $A_{f(P5)} = 2.5$ and $A_{f(P4)} = 1.5$ at $T \sim 6s$. This results in an average of 2.0, also very similar to the theoretical $A_f = 2.3$ (Figure 2.33, n = 2).

These values are only indicative of the basin response, since they do not include losses by wall roughness. Unfortunately, due to the wave period shift between physical and numerical model results, a comparison of the maximum values is not possible. In spite of this, amplification factors obtained from the physical model, which include losses, indicate amplification factors above 1.5, which is considered attractive for wave energy conversion.

The average wave energy density in the inner area of the basin is presented in Figure 4.8 by a dotted line (and repeated in Figures 4.9 and 4.10). It can be seen that there is an increase in wave energy density in this area for periods between 8.5 s and 9.5 s. In contrast, the wave energy is reduced at higher and lower periods (7 s to 8 s and 10 s to 16 s). Hence there is a narrow band of about $1s$ in which wave energy storage is increased by basin resonance.

Along the basin walls (Figures 4.8, 4.9 and 4.10), the response at the shorter "East" and "North" walls is similar, but with higher A_f for the longer periods when compared with the basin. The response of the "East" wall is as expected, since waves with longer periods would enhance wave heights at the back wall and decrease the amplification towards the basin entrance.

For better insight into the resonant modes, further results were obtained by visual inspection of the surface elevation plots presented in Figures 4.11 to 4.19. With the

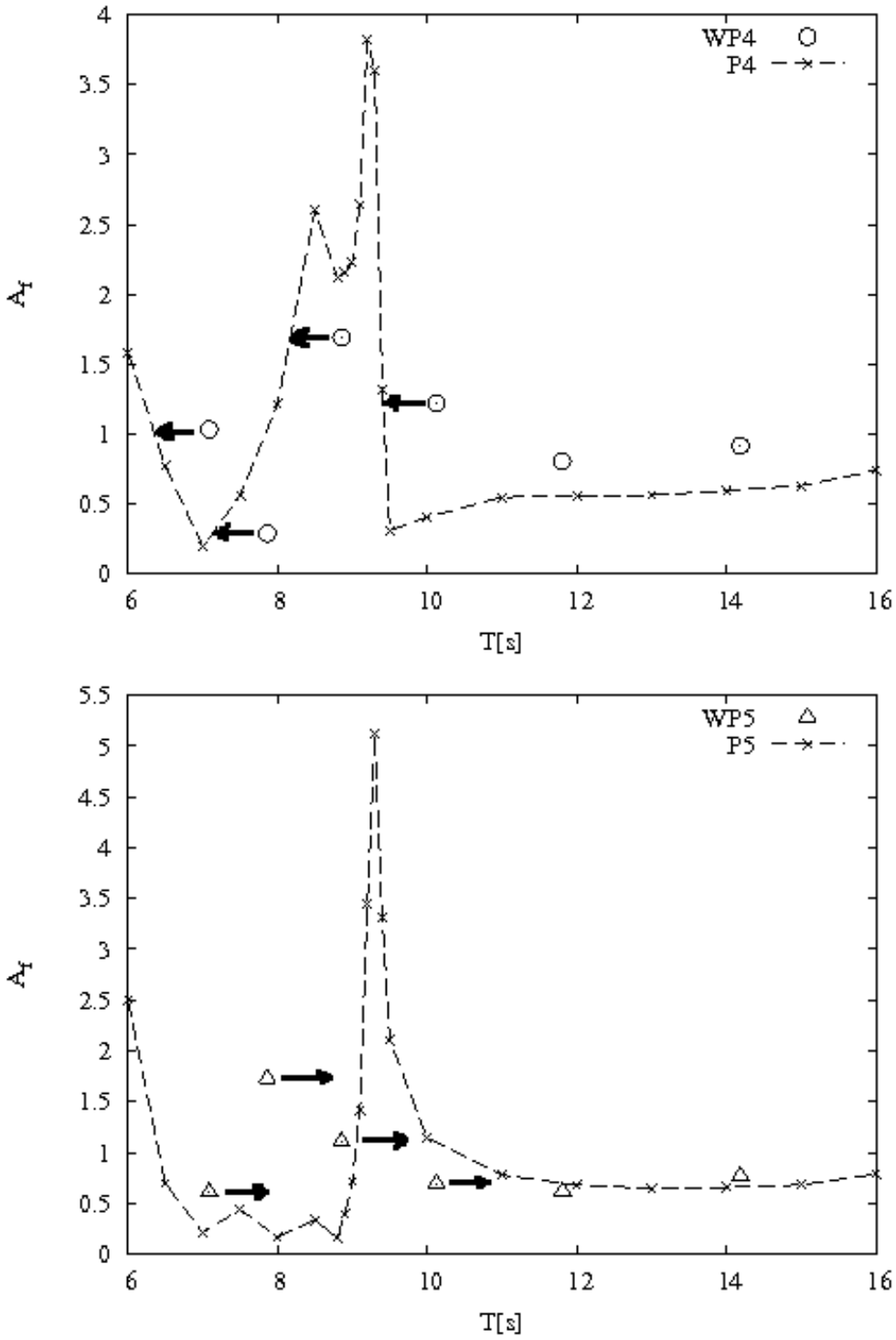

Figure 4.21: Comparison of amplification factors (A_f) at points 4 and 5 between physical and numerical (dashed lines) models.

help of these images, the resonant modes of oscillation along (n) and across (m) the basin were included in Table 4.5, together with the average wave energy densities at the basin inner area and basin side walls. It must be remembered that the wave energy density of the undisturbed incoming waves is $\overline{E} = \rho g a_i^2/2 = 1.257[kJ/m^2]$ with $a_i = 0.5m$.

Table 4.5: Mode of oscillation and wave energy density at the basin inner area and at the walls. $^{(1)}$: Diagonal nodal line.

	mode of oscillation			Wave energy density $[kJ/m^2]$			
T[s]	n	m	L [m]	$\overline{E}_{basin}$	"North" wall	"East" wall	"South" wall
6	2	2	56.2	1.13	2.37	2.9	2.59
7	$2^{(1)}$	$2^{(1)}$	76.5	0.1	0.25	0.09	0.27
8.5	2	0	112	1.75	1.43	3.65	3.78
9.3	1	1	132.7	12.29	26.78	12.98	23.27
9.5	2	$1^{(1)}$	138	1.5	3.48	1.99	2.66
12	1	0	204.8	0.23	0.37	0.47	0.13
16	1	0	307.8	0.53	0.65	0.75	0.41

From Table 4.5, and also from Figures 4.8, 4.9 and 4.10, it can be observed that wave energy density is decreased at the walls and at the basin inner area for wave periods from 7 s to 8 s. This is due to diagonal nodal lines (Figure 4.13) that reduces the overall wave energy density in the basin.

The area outside the basin provides additional information. In Figure 4.13 it can be observed that for $T = 7s$ there is a clear asymmetry of the scattering of surface elevations (η) and wave energy fluxes P and Q. Characteristic patterns of P-fluxes for wave periods that result in higher wave energy densities inside the basin, $T = 6.0$, $T = 8.5$ and $T = 9.3s$, are regrouped in Figure 4.22. It can be observed that there is a reduction in the instant wave energy flux in front of the basin entrance when compared with the flux reflected from the shoreline.

On the other hand, Q-fluxes for wave periods that result in lower wave energy densities inside the basin, $T = 6.5s$, $T = 7.0s$ and $T = 7.5s$, are regrouped in Figure 4.23. In these cases, the flux is asymmetric in the direction of the shoreline.

From these last plots it is confirmed that the wave energy fluxes in the area near the basin are relevant to enhance wave energy density, in a similar way to wave energy extraction by wave energy converters.

For maximum wave energy enhancement inside a resonant basin, outgoing waves from the basin entrance should interfere destructively with the incoming P-flux. This takes place under resonant conditions by radiated waves from the harbour

with a different phase.

In addition, Q-flux should be symmetric to the main resonant axis of the basin. If it is not, diagonal oscillations would reduce the wave energy density inside the basin.

Finally, it can be concluded that the proposed wave energy basin does enhance wave energy density for a specific wave period range. From the results for the physical model, a maximum amplification factor of 1.7 increases wave energy density by a factor of 2.9.
The asymmetric entrance does the job to induce cross-waves. This can be used to enhance wave heights on a preferred side wall.

a) P-flux for $T = 6s$.

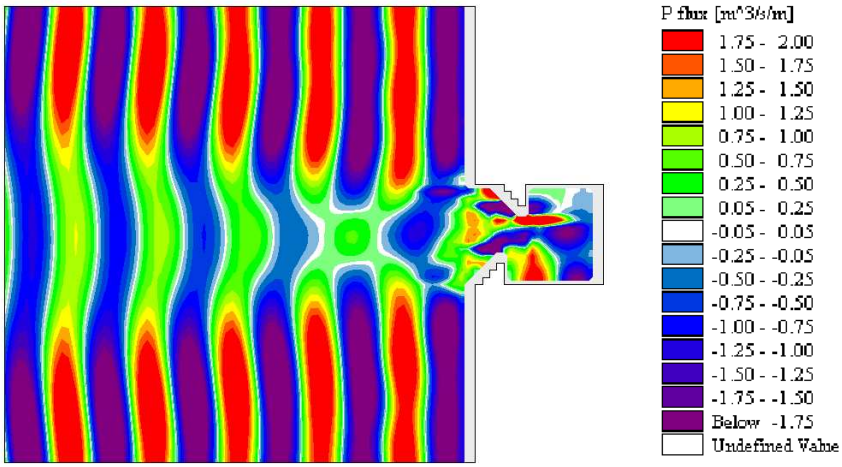

b) P-flux for $T = 8.5s$.

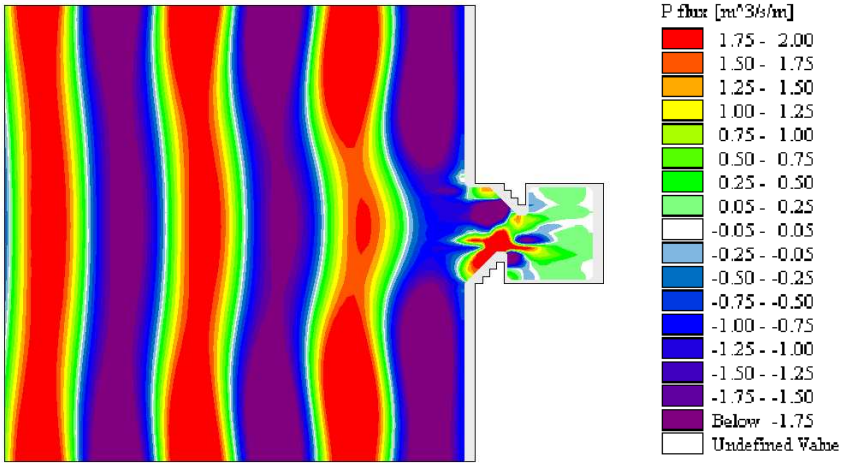

c) P-flux for $T = 9.3s$.

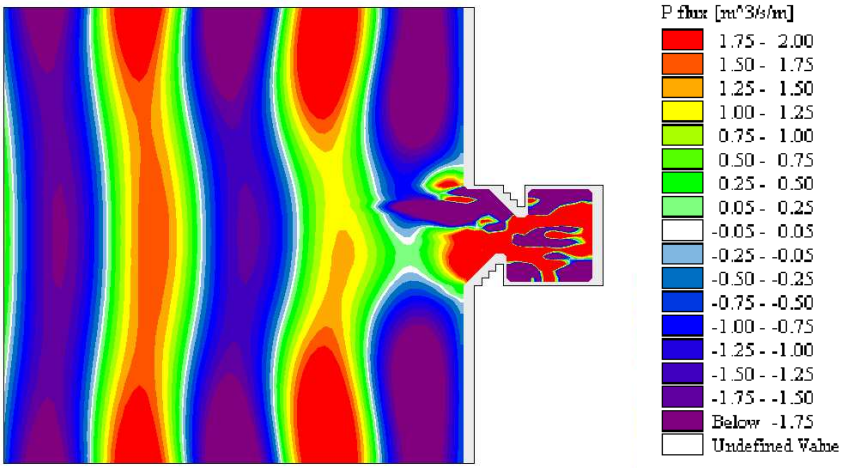

Figure 4.22: Snapshots of P-flux. Cases at peak amplification factors.

a) Q-flux for $T = 6.5s$.

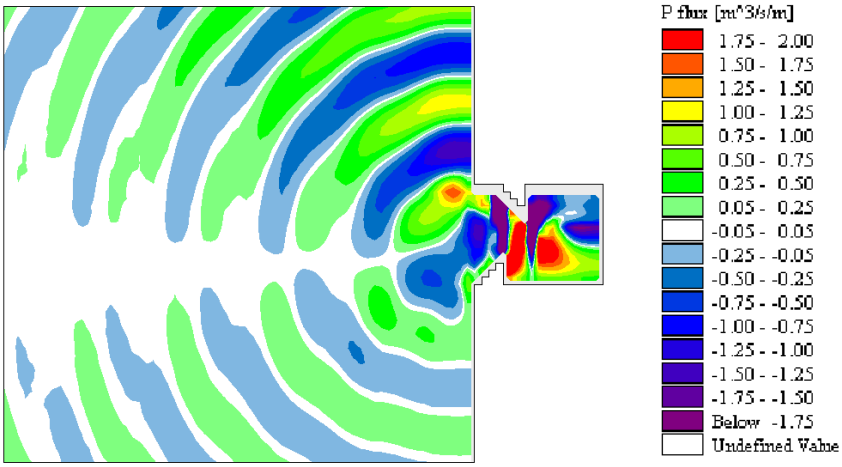

b) Q-flux for $T = 7.0s$.

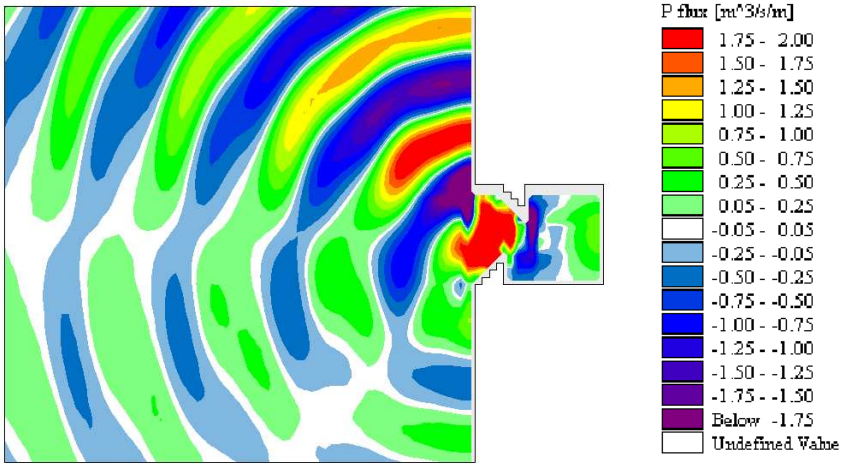

c) Q-flux for $T = 7.5s$.

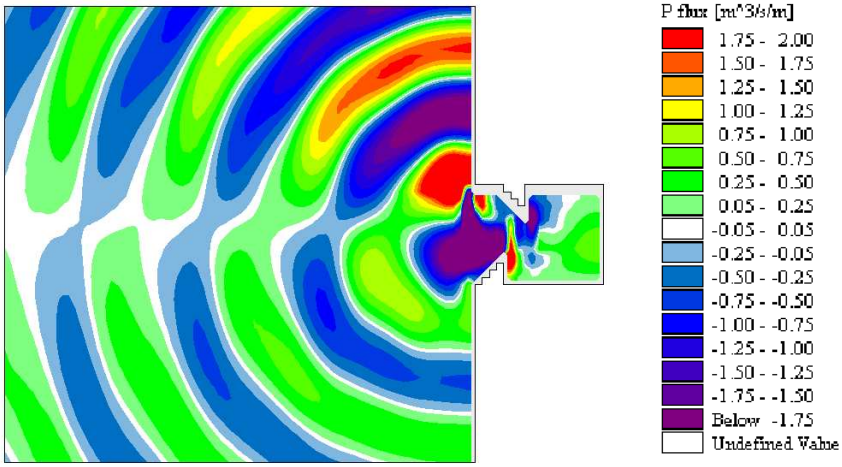

Figure 4.23: Snapshots of Q-flux. Cases of low amplification factors.

Chapter 5

Conclusions

The conversion of wave energy to useful electricity is a technical challenge that requires the expertise of multiple disciplines. Coastal (ocean) engineering is one of them, providing support on resource assessment and the design of temporary or permanent infrastructure in the marine environment.

In terms of resource assessment, suitable locations with higher wave energy densities can be investigated and proposed, or the resource can be modified to optimise wave energy density and availability.

From the literature review (Chapter 2) it can be observed that significant efforts, investigations and designs have been made to increase the wave energy density before conversion to electricity. Designs have included wave reflectors, funnelling channels, protruding walls and bottom mounds.

The principle is that a good wave energy converter has to interfere destructively with the incoming waves. Fixed structures interfere constructively. Hence it is clear that the interaction between the wave energy device, the coastline, and the incoming waves is of primary importance for wave energy conversion.

A new classification of devices is proposed on the basis of the interaction of *WECs* with the resource: *wave interference devices*, *wave collector devices* and *wave resonance devices*. This classification can be used to better understand the wave conditions that can be used to improve the performance of a *WEC*.

A resonant basin with a simple layout and an asymmetric entrance was proposed in Chapter 3 and tested in a physical and numerical model. The basin entrance with a "V" shape provided a wave front of the same width as the basin. The narrow entrance gap produces a trapping effect. The asymmetric entrance was seen to turn waves and induce resonance in the cross direction.

The principle of enhancing wave energy density in the proposed resonant basin has been shown to perform well, but only within a limited wave period range.

From the results of physical and numerical models (Chapter 4), the first conclusion is that the asymmetric entrance is able to induce cross-waves. A clear longitudinal (n = 1,2) and a transverse (m = 1,2) resonant oscillation were present when a maximum amplification factor was reached.

A second result is that the proposed basin has a useful resonant response for a period range of one second. Out of this band, the basin becomes counterproductive by reducing the wave energy density.

Fixed structures can be seen as constructive wave energy collectors. The response of a resonant basin with opposite parallel walls, as the one tested in this thesis, is limited in bandwidth. To increase the bandwidth it would be required to shift the side walls and tune the basin to the wave conditions. A different basin layout including side walls at an angle different from 90 degrees may also work.

Wave energy extraction from the basin was not included in the scope of this thesis, but it is recognised that this is a relevant issue that can lead to further and even more promising studies. The interaction of waves reflected from fixed structures and radiated from wave energy devices could be used to enhance wave energy for conversion. For instance a *WEC* device such an oscillating water column may be used to induce cross-waves inside the resonant basin instead of using fixed asymmetric breakwaters.

Appendices

Appendix A

Analytical expressions

A.1 Coupling of plane waves with scattered waves from a harbour entrance

Lee (1969) worked on a Boundary Element Method that satisfies the Helmoltz equation and solves Laplace's velocity potential. It was assumed that outside the harbour the water surface elevation η is of the form $\eta = a_i f(x,y)e^{-i\omega t}$. The wave function $f(x,y) = (f_i + f_r + f_s)$ was defined by f_i incident, f_r reflected, and f_s scattered wave functions. The other parameters, a_i and $e^{i\omega t}$, are the incoming wave amplitude and a time factor respectively. The wave function $f(x,y)$ had to satisfy the Helmoltz equation,

$$\frac{\partial^2 f}{\partial x^2} + \frac{\partial^2 f}{\partial y^2} + k^2 f = 0 \tag{A.1.1}$$

with the boundary conditions

$$\frac{\partial f}{\partial n} = 0 \quad \text{at the shoreline} \tag{A.1.2}$$

$$\frac{\partial f}{\partial n} = \frac{\partial f_h}{\partial n} \quad \text{at the basin entrance} \tag{A.1.3}$$

$$\lim_{x,y\to\infty} f = f_i + f_r \quad \text{radiation condition,} \tag{A.1.4}$$

where n is a vector normal to the slope. Outside the harbour, Lee (1969) used a Hankel function, $H_0^{(1)}(kr)$, which satisfies the radiation condition at infinity. The outgoing scattered wave function f_s can be approximated by the equation A.1.5 with a, k and ω the amplitude, wave number and phase of the oscillation respectively. As a property, f_s approaches zero at infinity ($kr \to \infty$), as shown in Figure A.1. Using this expression, the scattering of a point-source oscillation can be defined by equation A.1.6

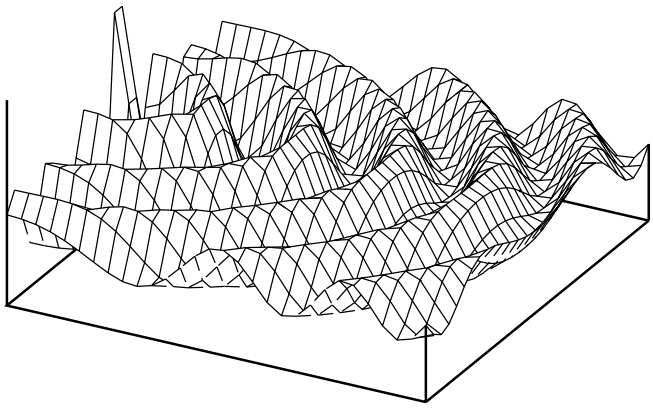

Figure A.1: Wave scattering from a point source (equation A.1.6).

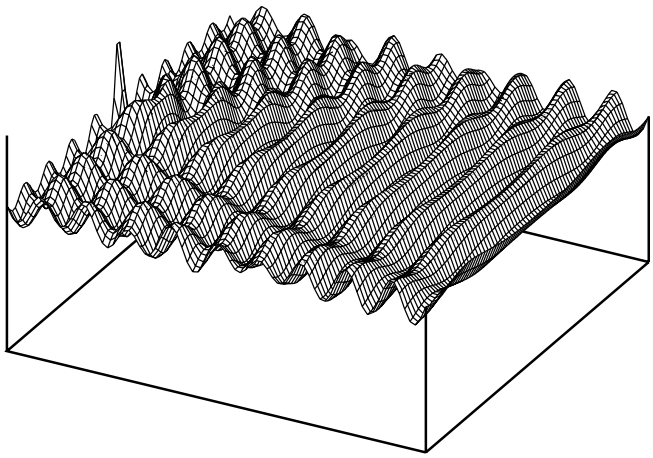

Figure A.2: Coupling of plane waves with scattered waves from a harbour entrance f(x,y).

$$f_s = H_0^{(1)}(kr) \sim \sqrt{\frac{2}{\pi(kr)}} e^{i(kr-\frac{\pi}{4})} \tag{A.1.5}$$

$$\eta_s = aH_0^{(1)}(kr)e^{-i\omega t} \sim a\sqrt{\frac{2}{\pi(kr)}} e^{i(kr-\omega t-\frac{\pi}{4})} \tag{A.1.6}$$

Appendix B

Physical model measurements

B.1 Physical model test series

Table B.1: Physical model test series

Test	h	f	Notes
MSQ 02 001	256	1.5	Wave probes (WPs) at the centre of the walls
MSQ 02 002	256	1.5	WPs relocated to the corners of the basin
MSQ 02 003	256	1.0	
MSQ 02 004	256	1.6	
MSQ 02 005	256	1.6	Repetition of MSQ02 004
MSQ 02 006	256	1.6	Wave maker (WM) running for 50 s
MSQ 02 007	256	1.6	WM running for 100 s
MSQ 02 008	256	1.6	WM running for 15 s
MSQ 02 009	256	1.6	WM running for 30 s
MSQ 02 010	256	1.6	WM running for 40 s
MSQ 02 011	256	1.6	WM running for 360 s, WP1 to WP3 moved closer to the wall, <20 mm
MSQ 02 012			bye
MSQ 02 013	245	1.0	WM running for 360 s, recording (REC) for 600 s
MSQ 02 014	245	1.2	WM running for 360 s, REC for 600 s
MSQ 02 015	245	1.4	
MSQ 02 016	245	1.6	
MSQ 02 017	245	1.8	WMs running for 500 s, REC for 600 s
MSQ 02 018	245	2.0	
MSQ 02 019	245	1.0	
MSQ 02 020	245	1.0	
MSQ 02 021	245	1.2	
MSQ 02 022	245	1.4	
MSQ 02 023	245	1.6	
MSQ 02 024	245	1.8	
MSQ 02 025	245	2.0	
MWL 03 001	245	1.0	
MWL 03 002	245	1.2	
MWL 03 003	245	1.4	
MWL 03 004	245	1.6	
MWL 03 005	245	1.8	
MWL 03 006	245	2.0	
MWL 03 007	245	1.0	
MWL 03 008	245	1.2	
MWL 03 009	245	1.4	
MWL 03 010	245	1.6	
MWL 03 011	245	1.8	
MWL 03 012	245	2.0	
MSQ 03 001	30	0.9	
MSQ 03 002	30	0.9	
MSQ 03 003	30	0.9	
MSQ 03 001	30	1.7	

B.2 Input signal for the paddles of the wave maker

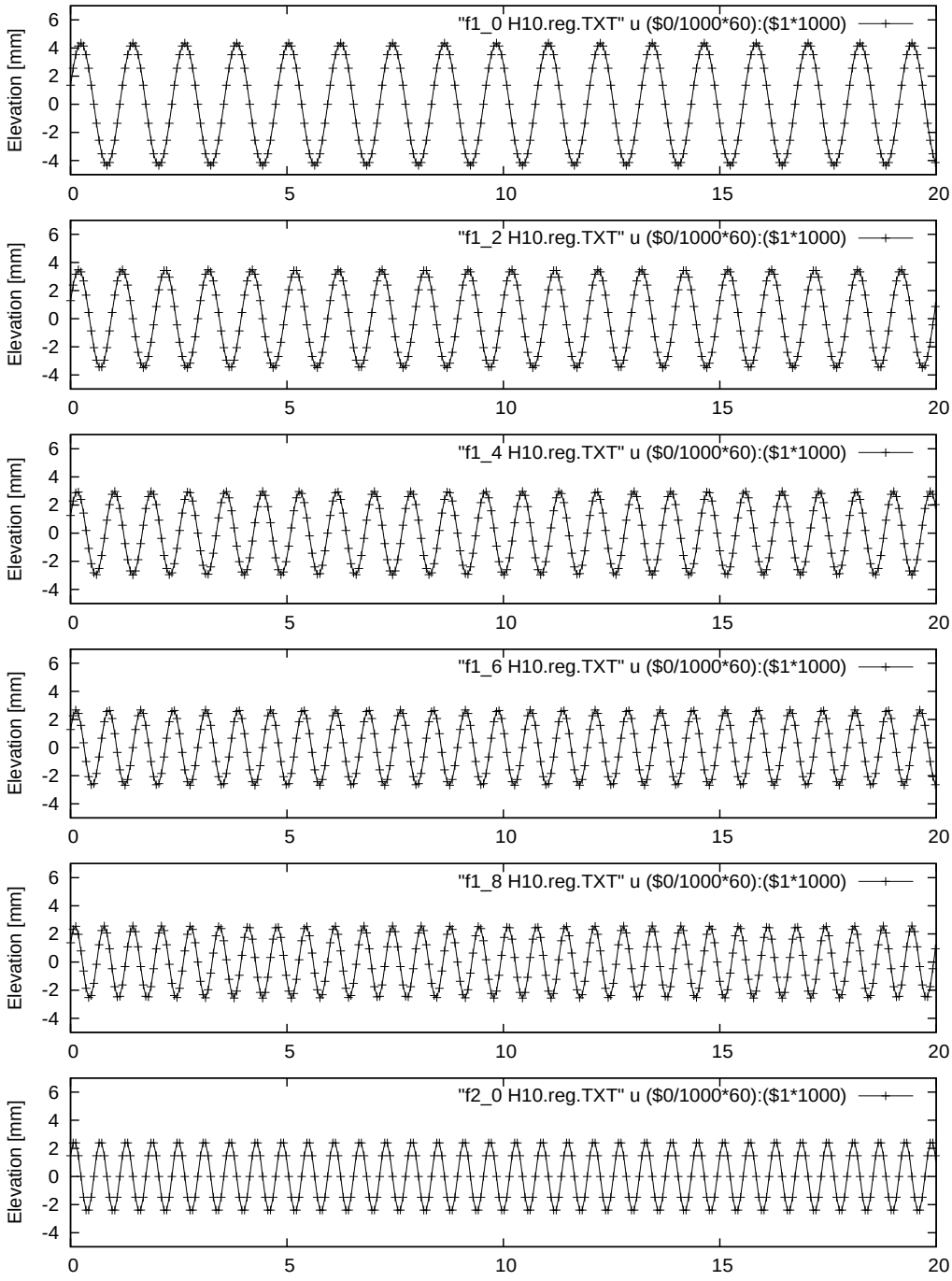

Figure B.1: Wave maker paddle displacements in [mm] for different frequencies. From top to bottom: 1Hz, 1.2Hz, 1.4Hz, 1.6Hz, 1.8Hz, and 2.0Hz.

B.3 Measured water surface elevations with the basin open

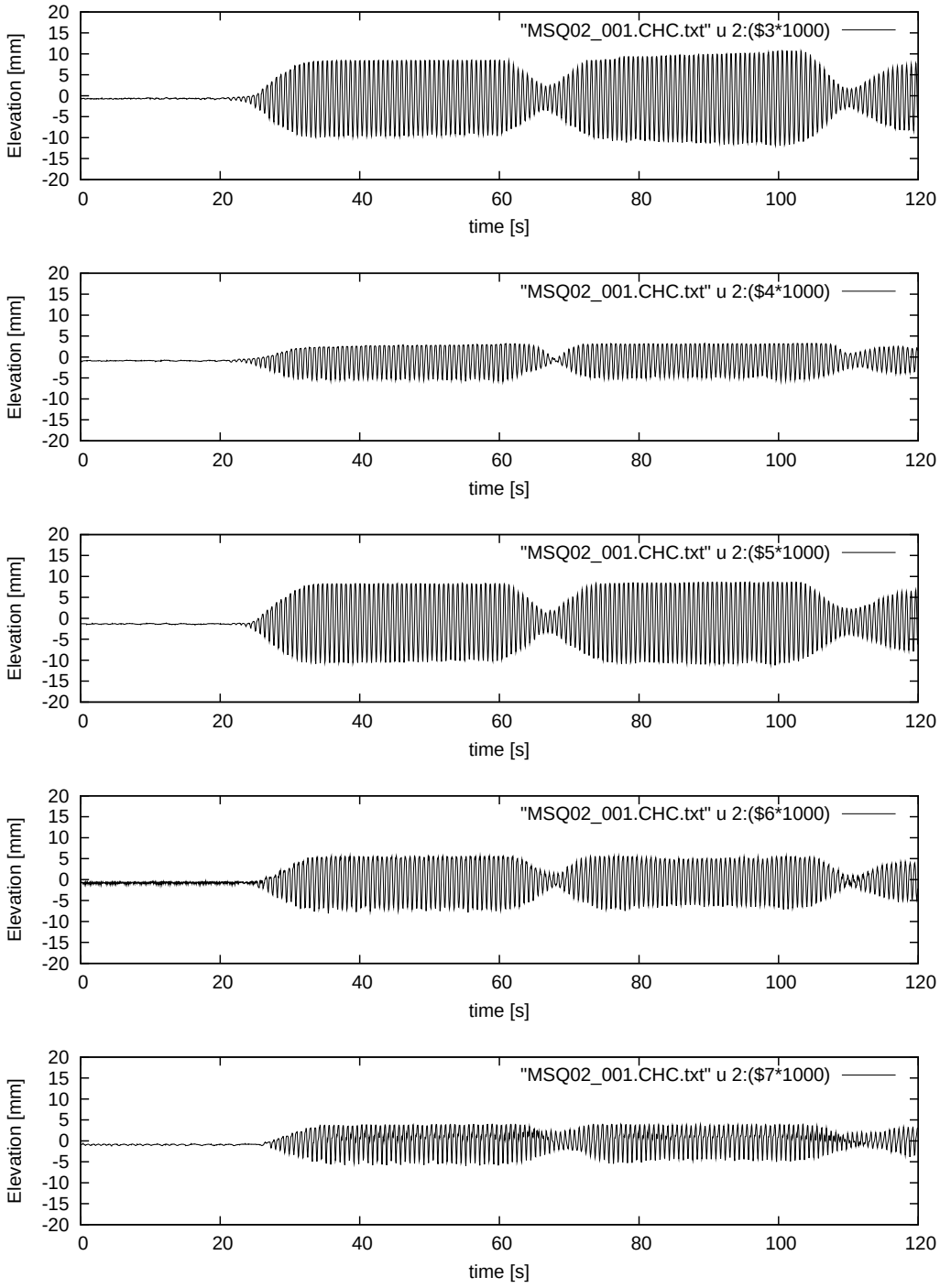

Figure B.2: Test run with f = 1.5 Hz: wave probes at the centre of the walls (MSQ02 001). From top to bottom, wave probes WP1 to WP5.

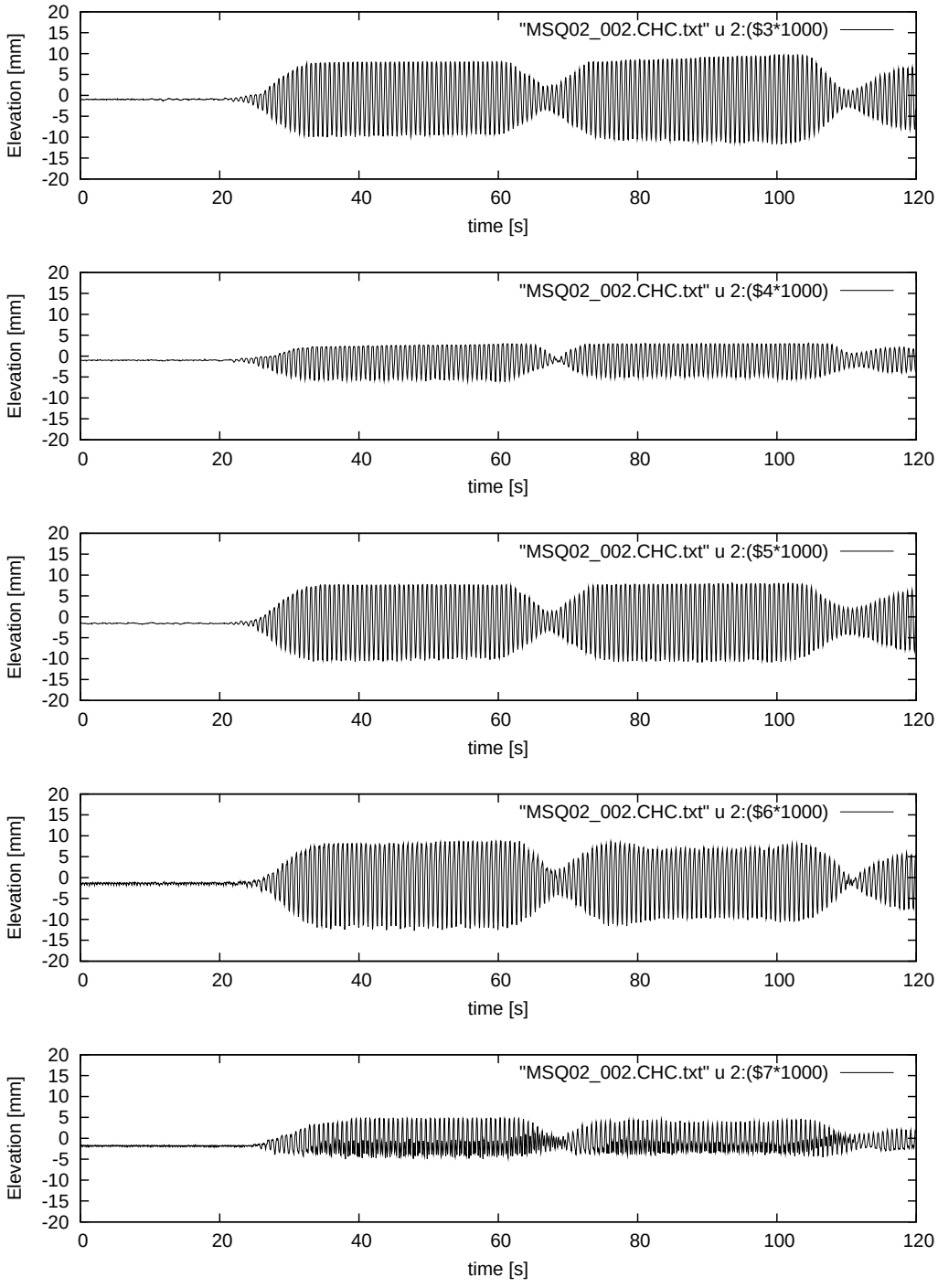

Figure B.3: Test run with f = 1.5H z (MSQ02 002). From top to bottom, wave probes WP1 to WP5.

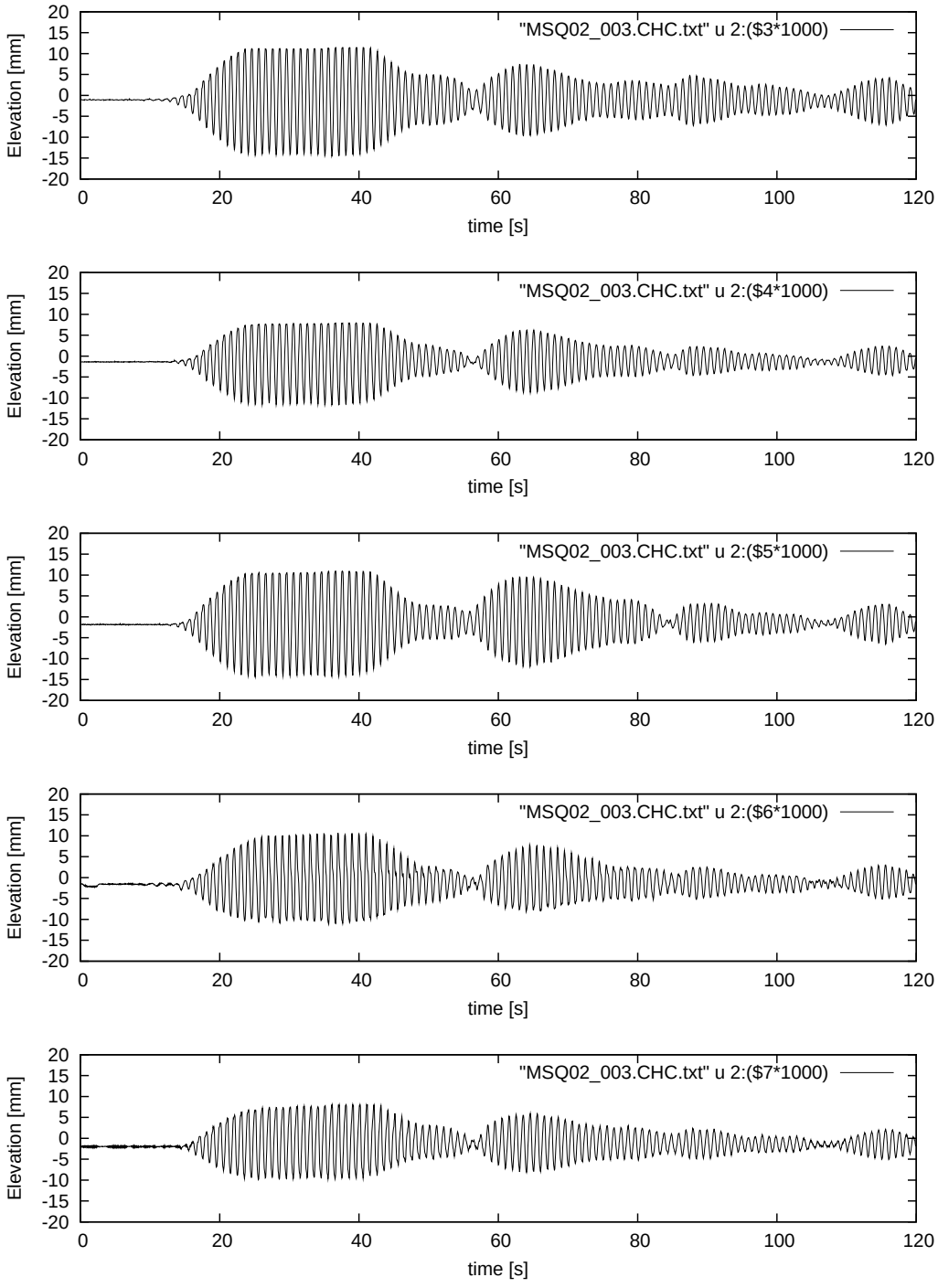

Figure B.4: Test run with f = 1.0 Hz (MSQ02 003). From top to bottom, wave probes WP1 to WP5.

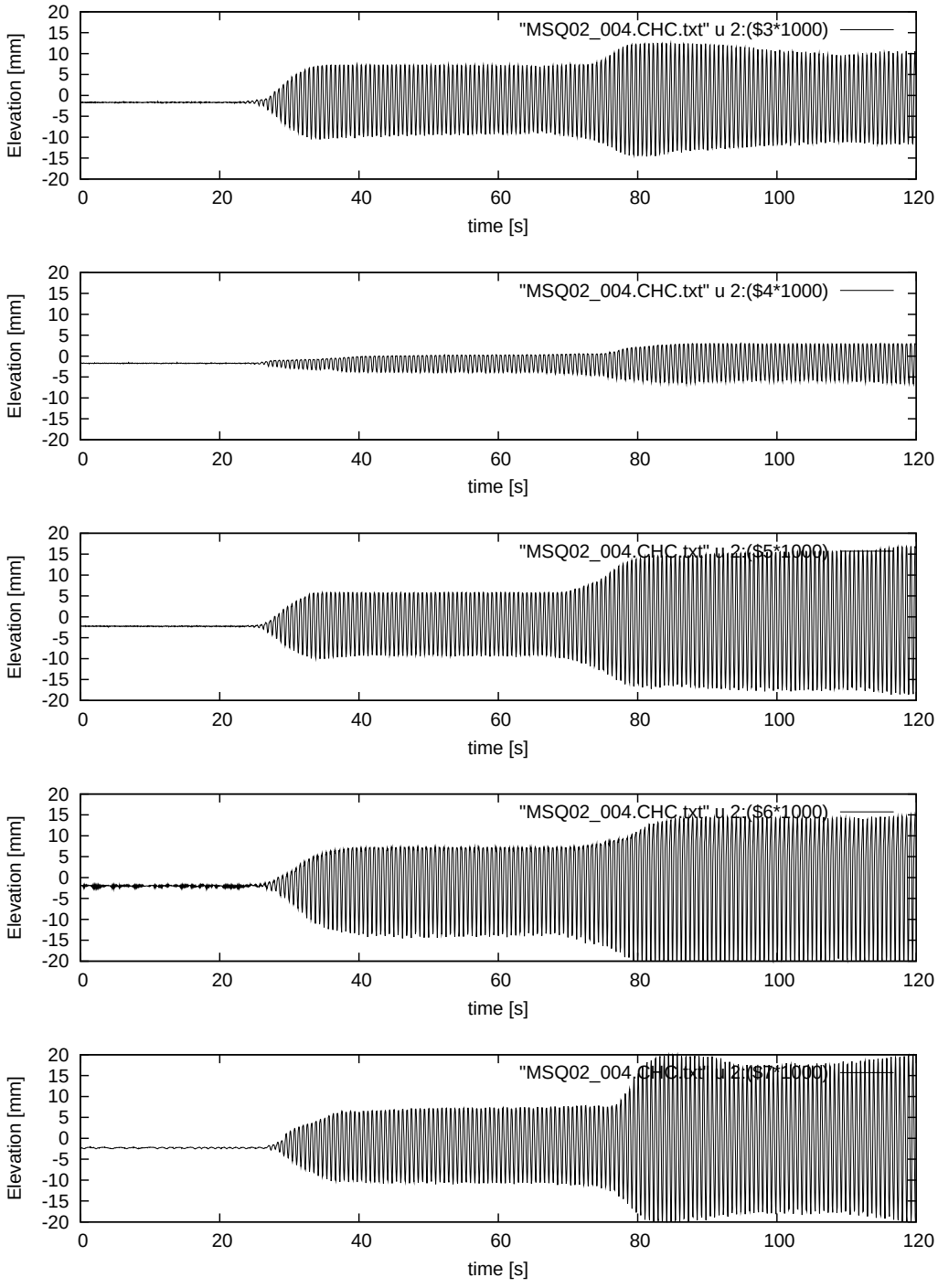

Figure B.5: Test run with f = 1.6 Hz (MSQ02 004). From top to bottom, wave probes WP1 to WP5.

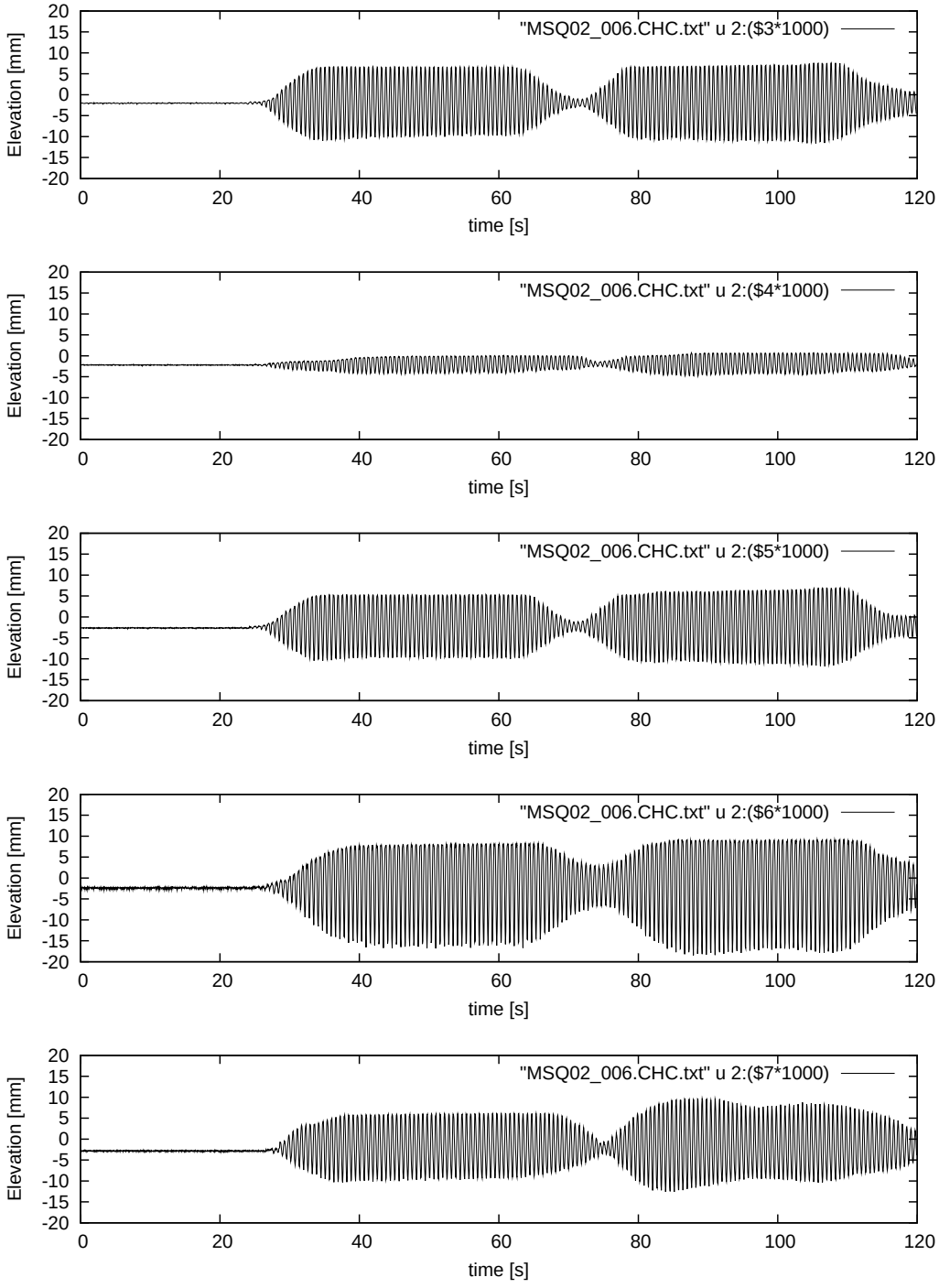

Figure B.6: Test run with f = 1.6 Hz. Wave maker running for 50 s (MSQ02 006). From top to bottom, wave probes WP1 to WP5.

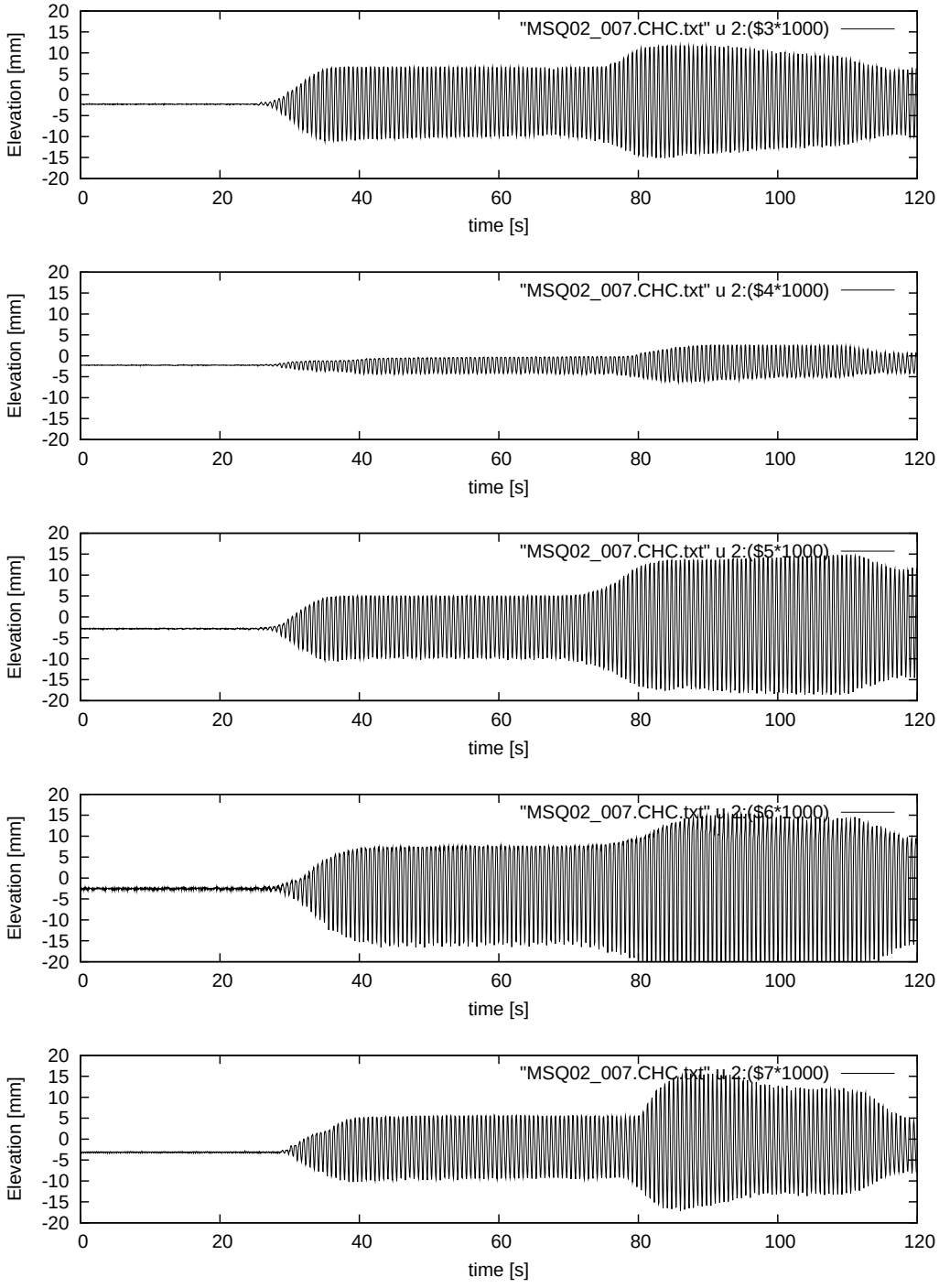

Figure B.7: Test run with f = 1.6 Hz. Wave maker running for 100 s (MSQ02 007). From top to bottom, wave probes WP1 to WP5.

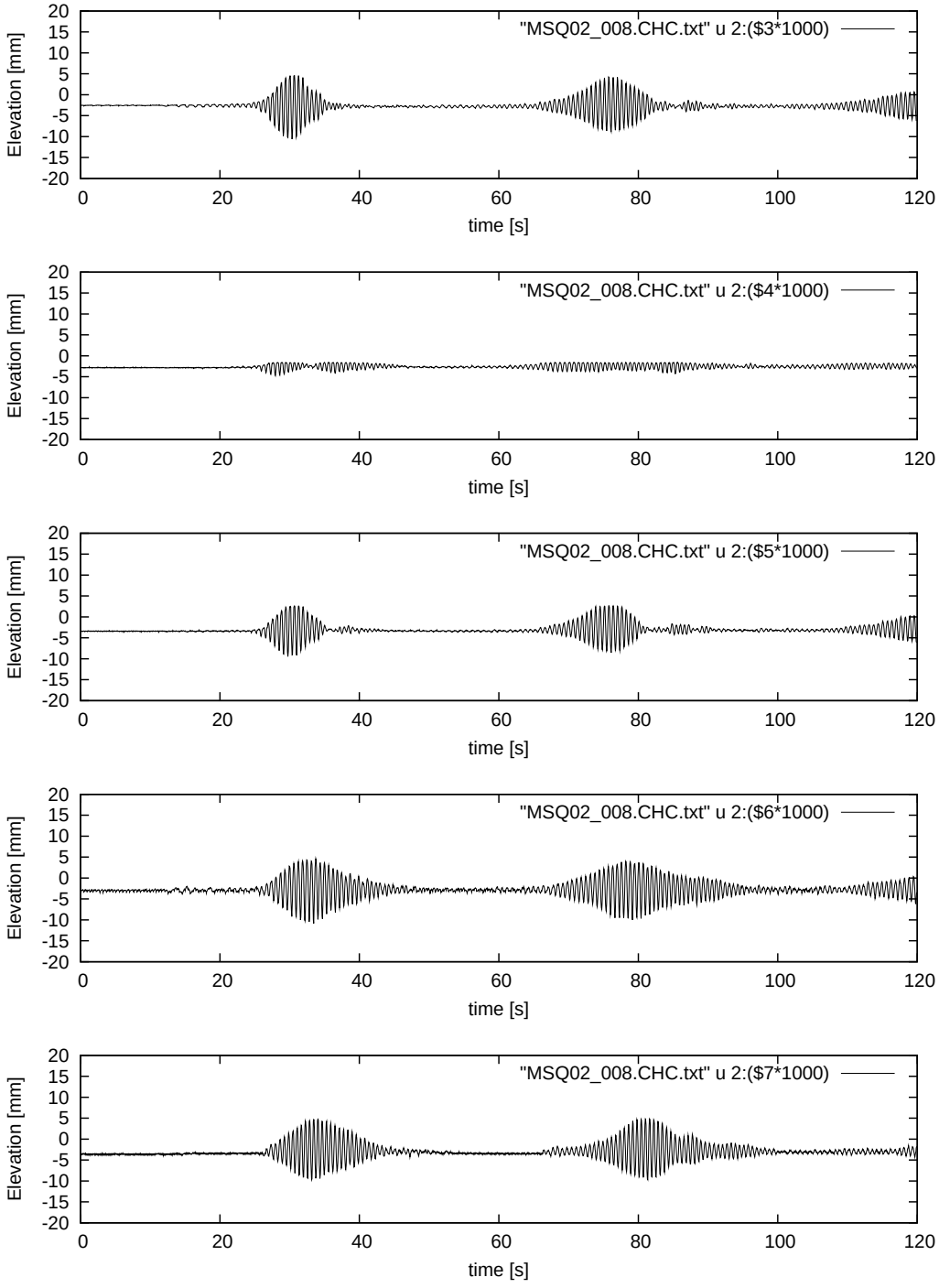

Figure B.8: Test run with f = 1.6 Hz. Wave maker running for 15 s (MSQ02 008). From top to bottom, wave probes WP1 to WP5.

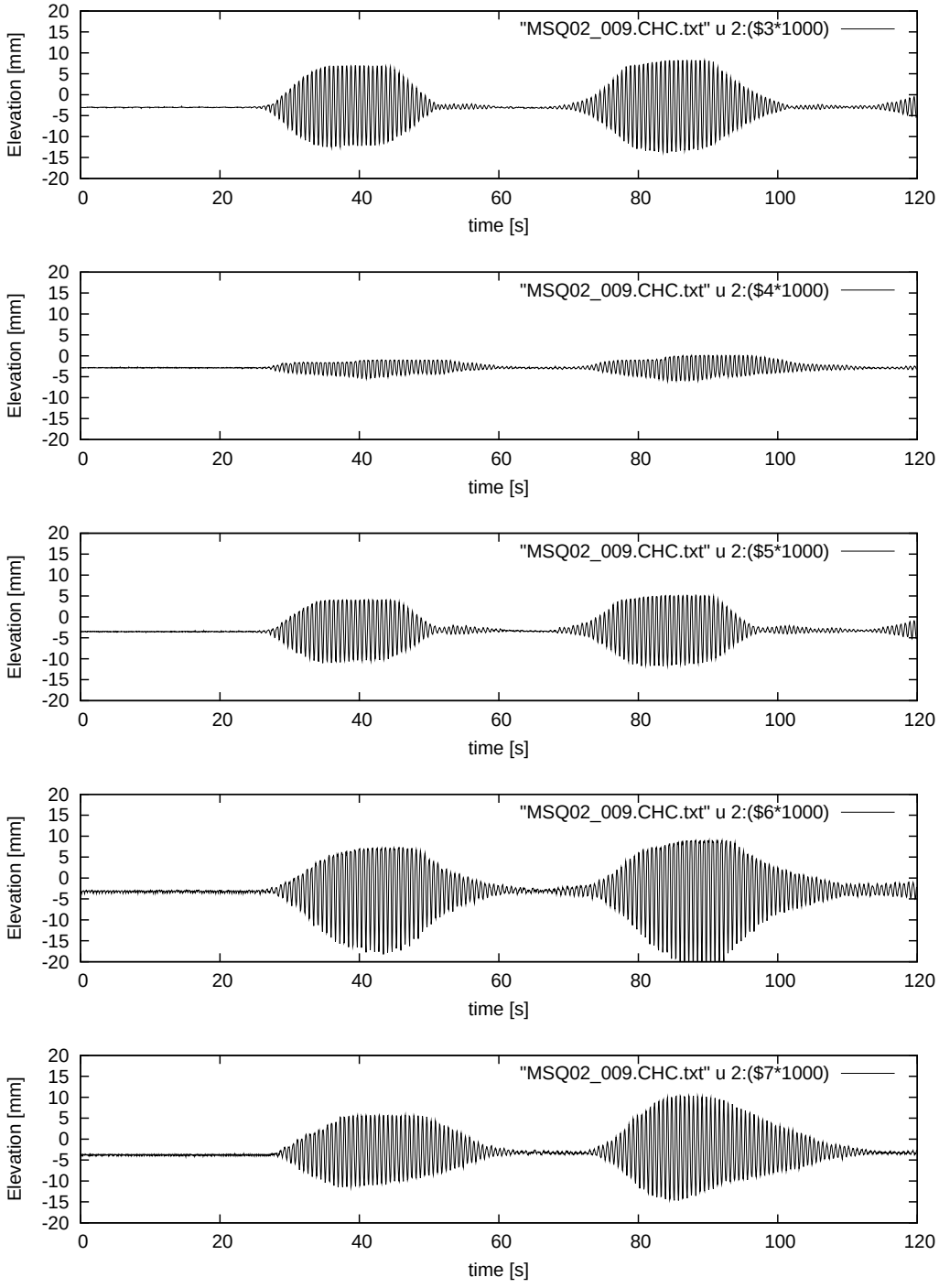

Figure B.9: Test run with f = 1.6 Hz. Wave maker running for 30 s (MSQ02 009). From top to bottom, wave probes WP1 to WP5.

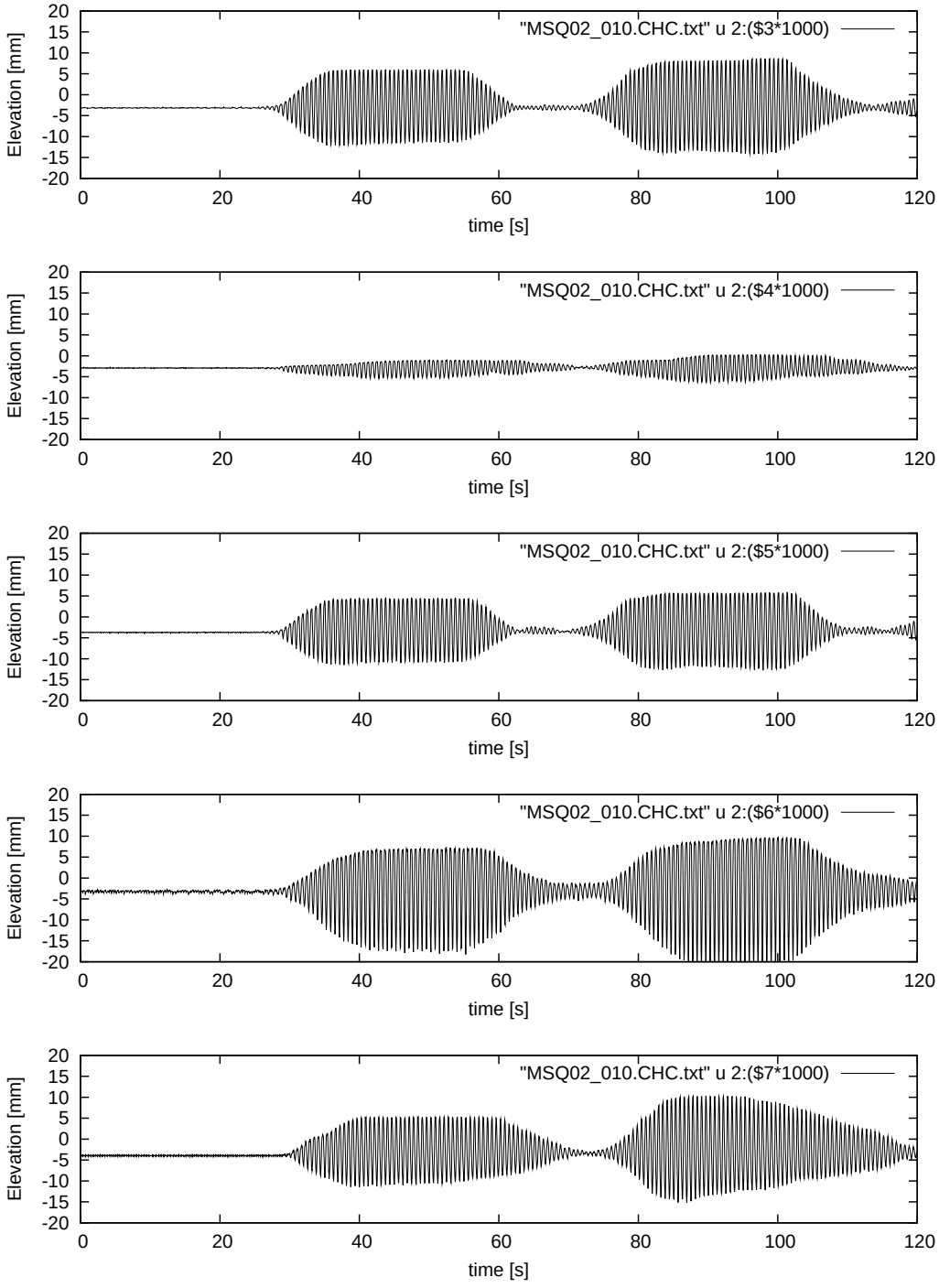

Figure B.10: Test run with f = 1.6 Hz. Wave maker running for 40 s (MSQ02 010). From top to bottom, wave probes WP1 to WP5.

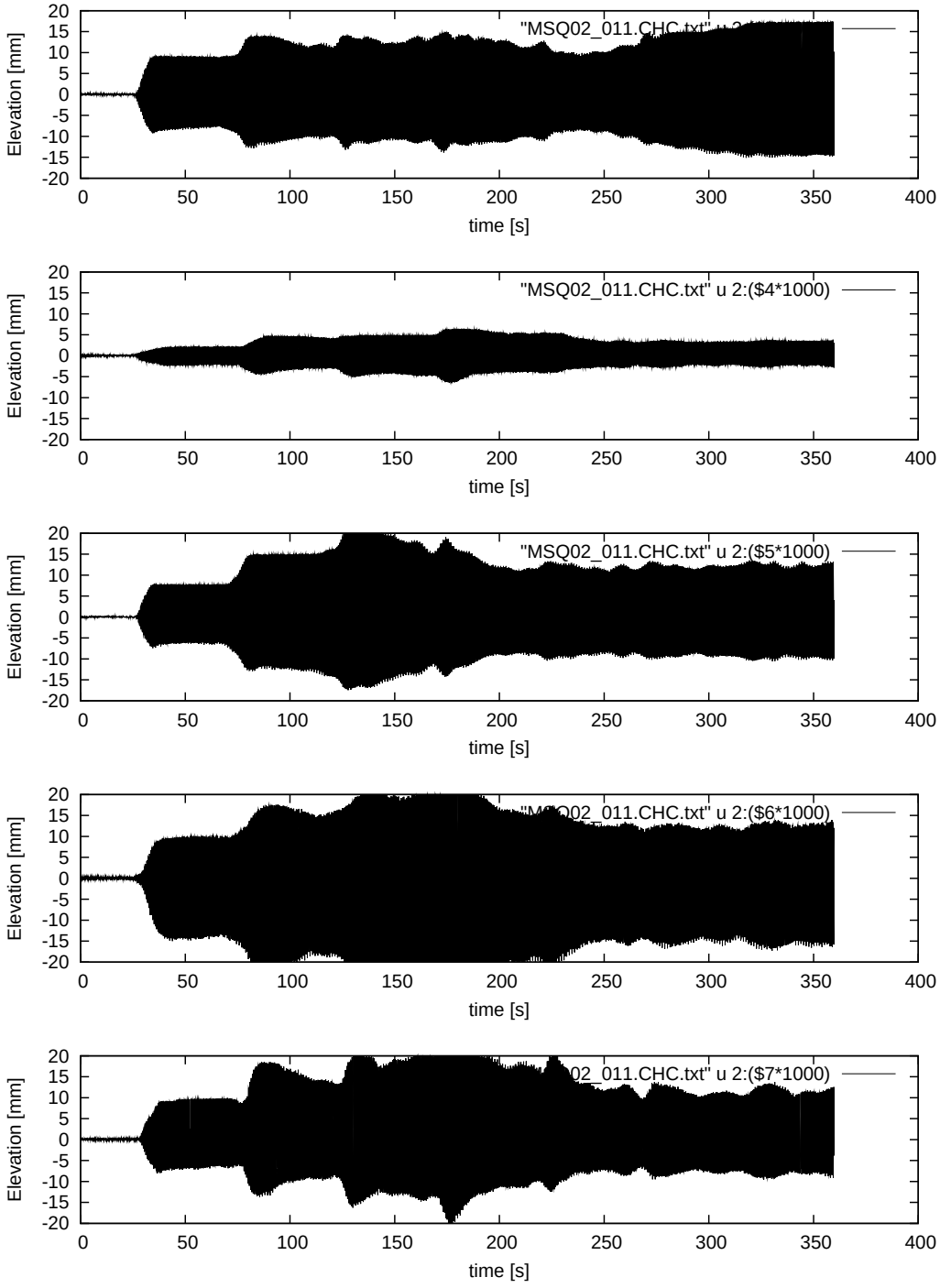

Figure B.11: Test run with f = 1.6 Hz. Wave maker running for 360 s, and WPs moved closer to the wall, $<$ 20 mm (MSQ02 011). From top to bottom, wave probes WP1 to WP5.

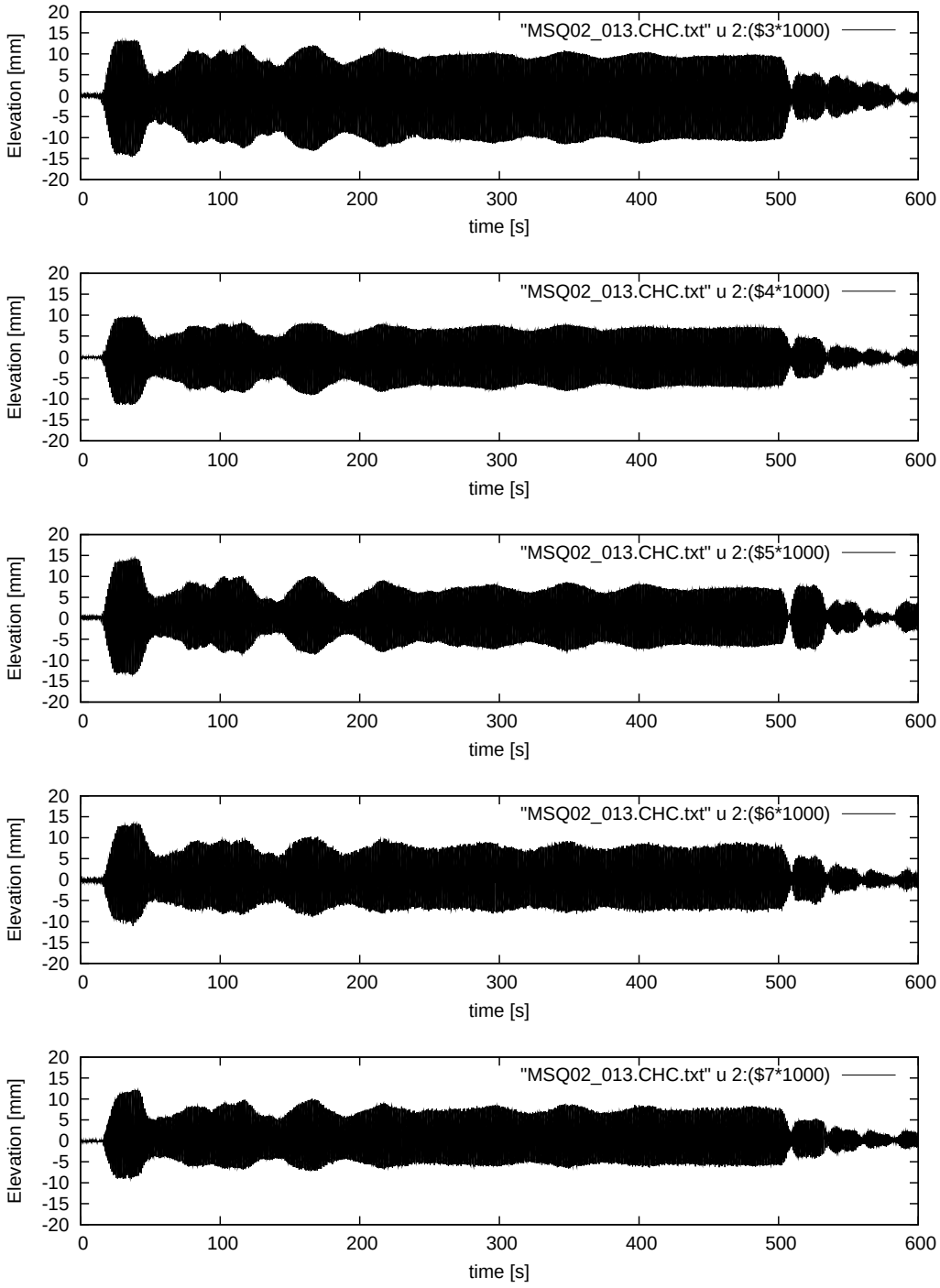

Figure B.12: Test run with f = 1.0 Hz, d = 245 mm. Wave maker running for 360 s (MSQ02 013). From top to bottom, wave probes WP1 to WP5.

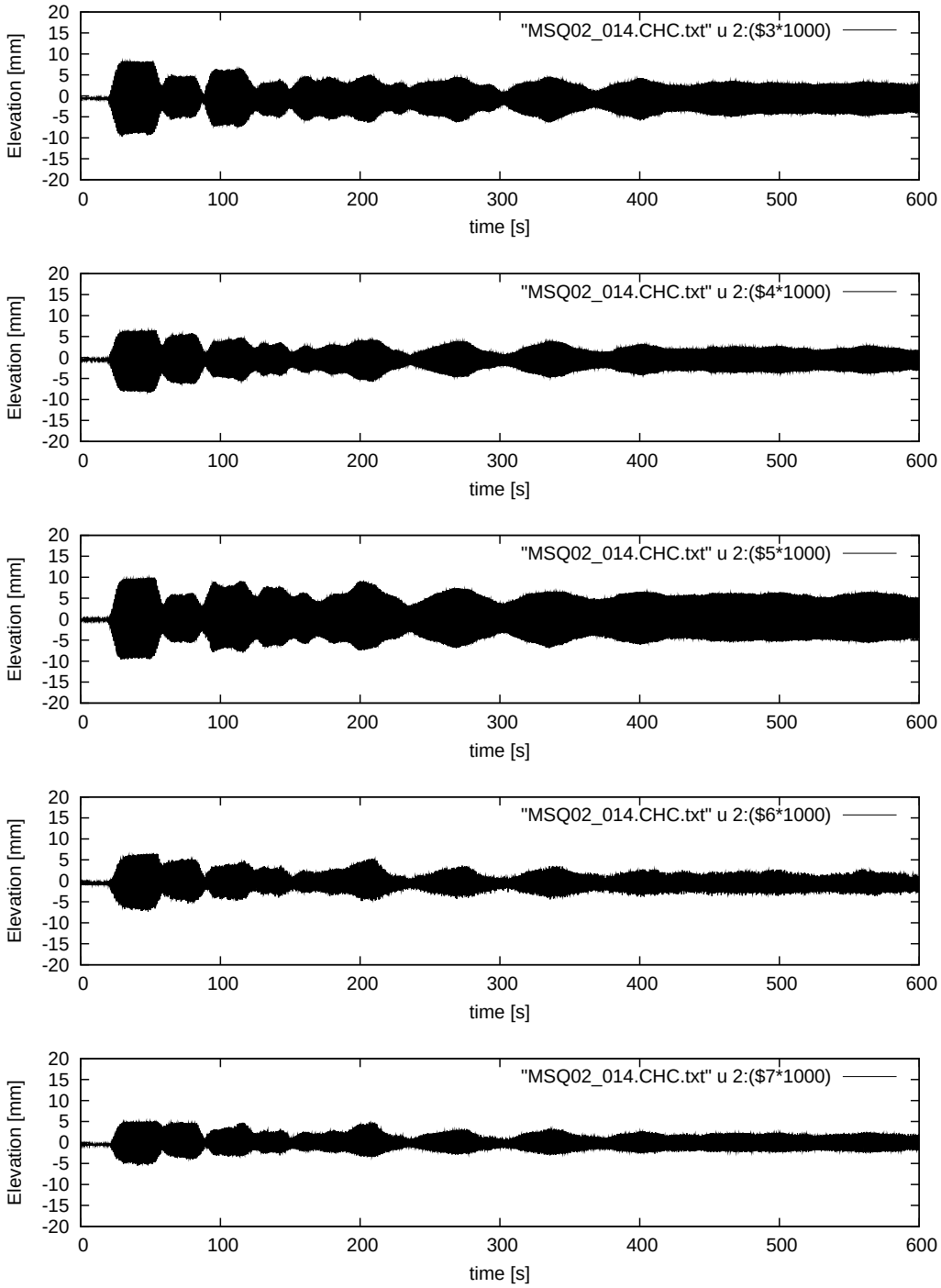

Figure B.13: Production run with f = 1.2 Hz, d = 245 mm. Wave maker running for 360 s (MSQ02 014). From top to bottom, wave probes WP1 to WP5.

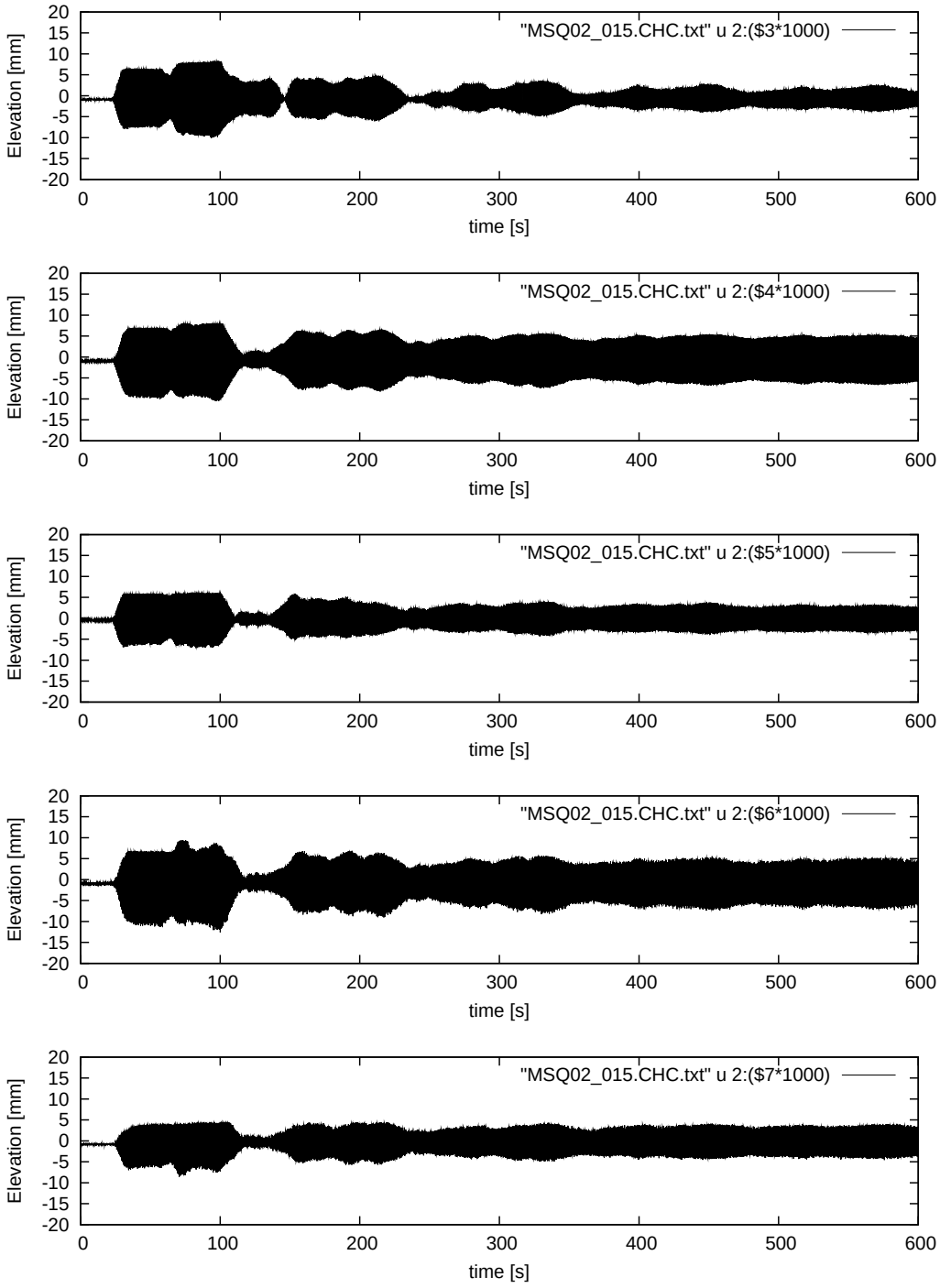

Figure B.14: Production run with f = 1.4 Hz, d = 245 mm. Wave maker running for 360 s (MSQ02 015). From top to bottom, wave probes WP1 to WP5.

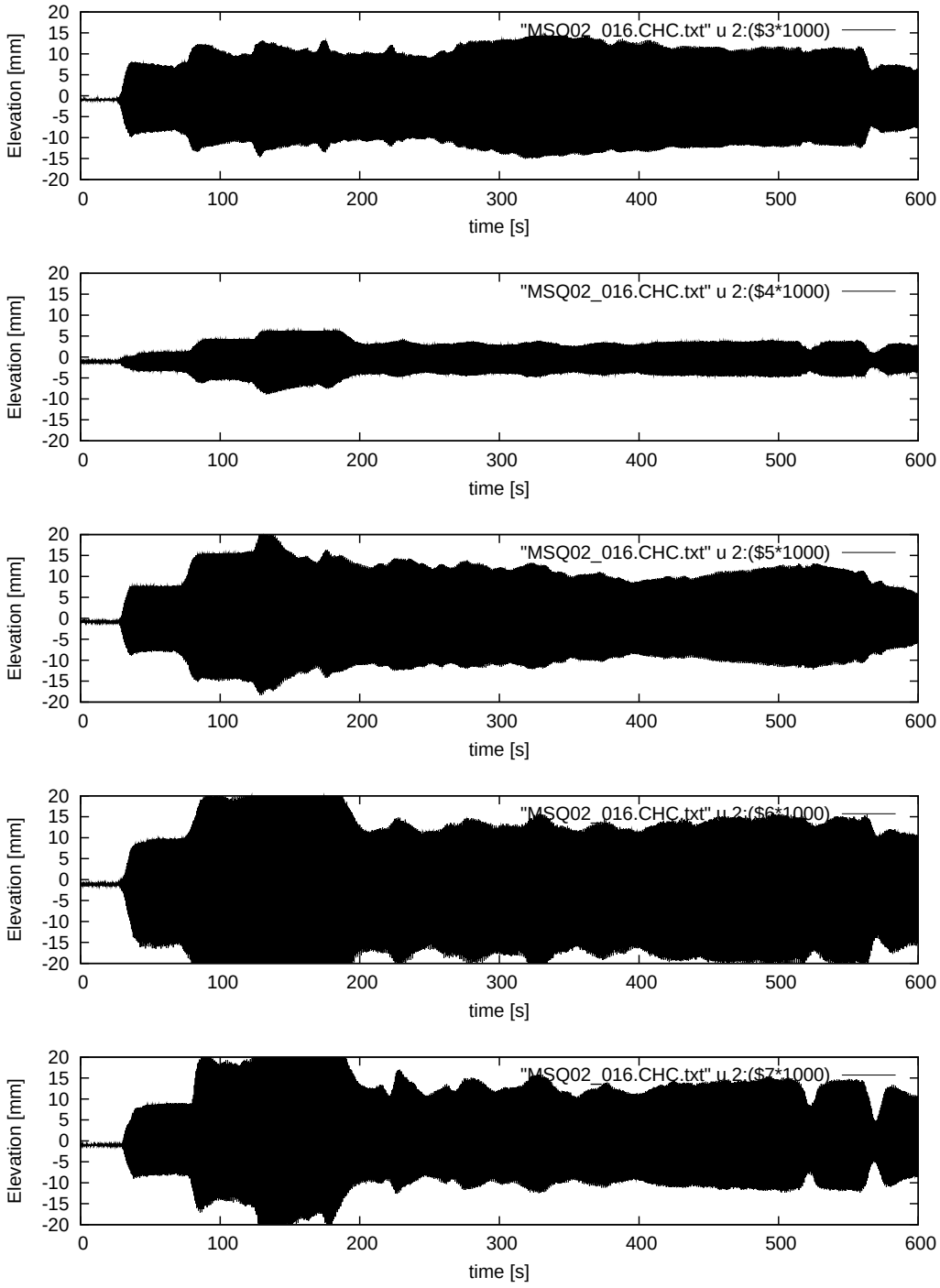

Figure B.15: Production run with f = 1.6 Hz, d = 245 mm. Wave maker running for 360 s (MSQ02 016). From top to bottom, wave probes WP1 to WP5.

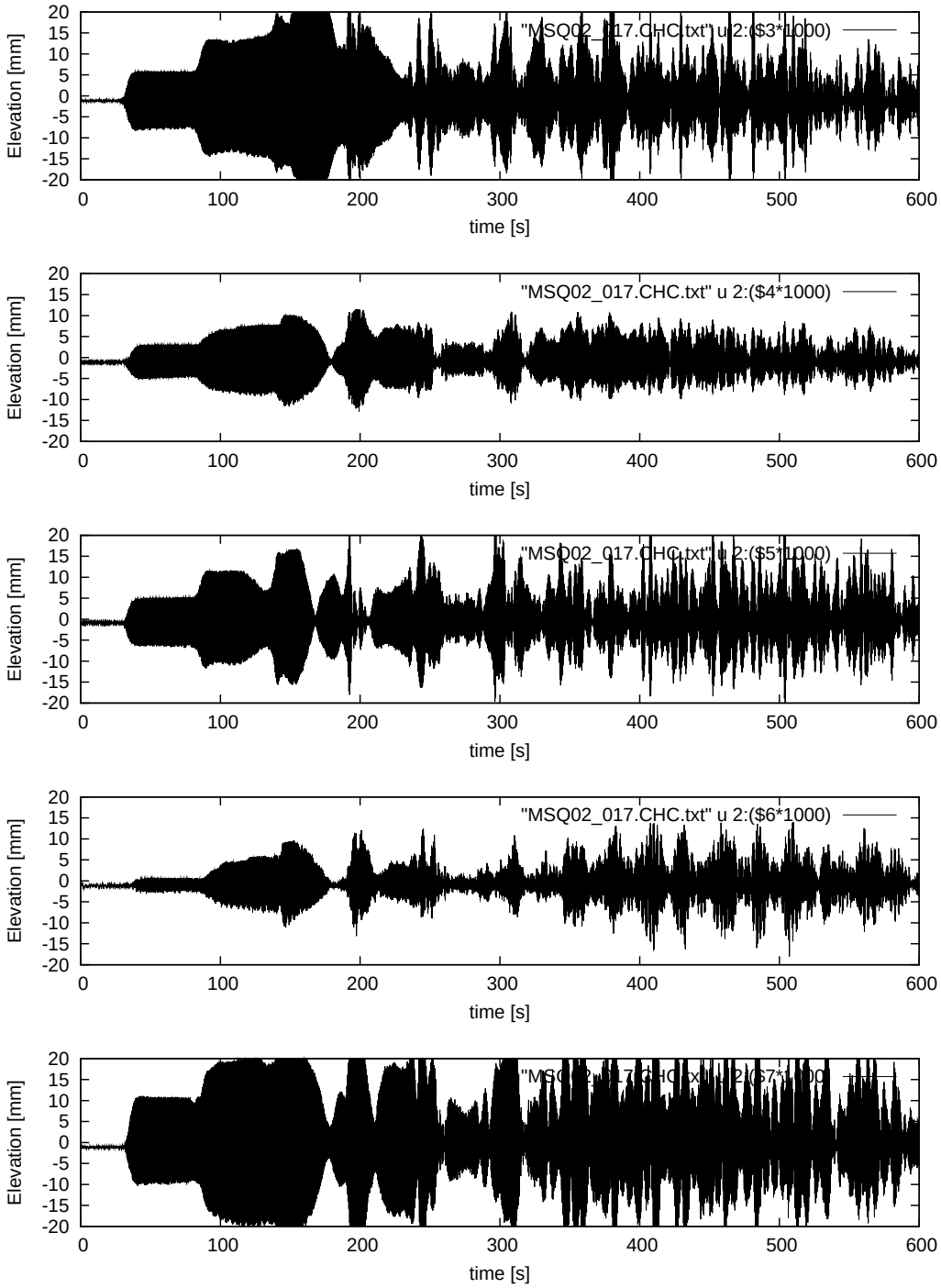

Figure B.16: Production run with f = 1.8 Hz, d = 245 mm. Wave maker running for 360 s (MSQ02 017). From top to bottom, wave probes WP1 to WP5.

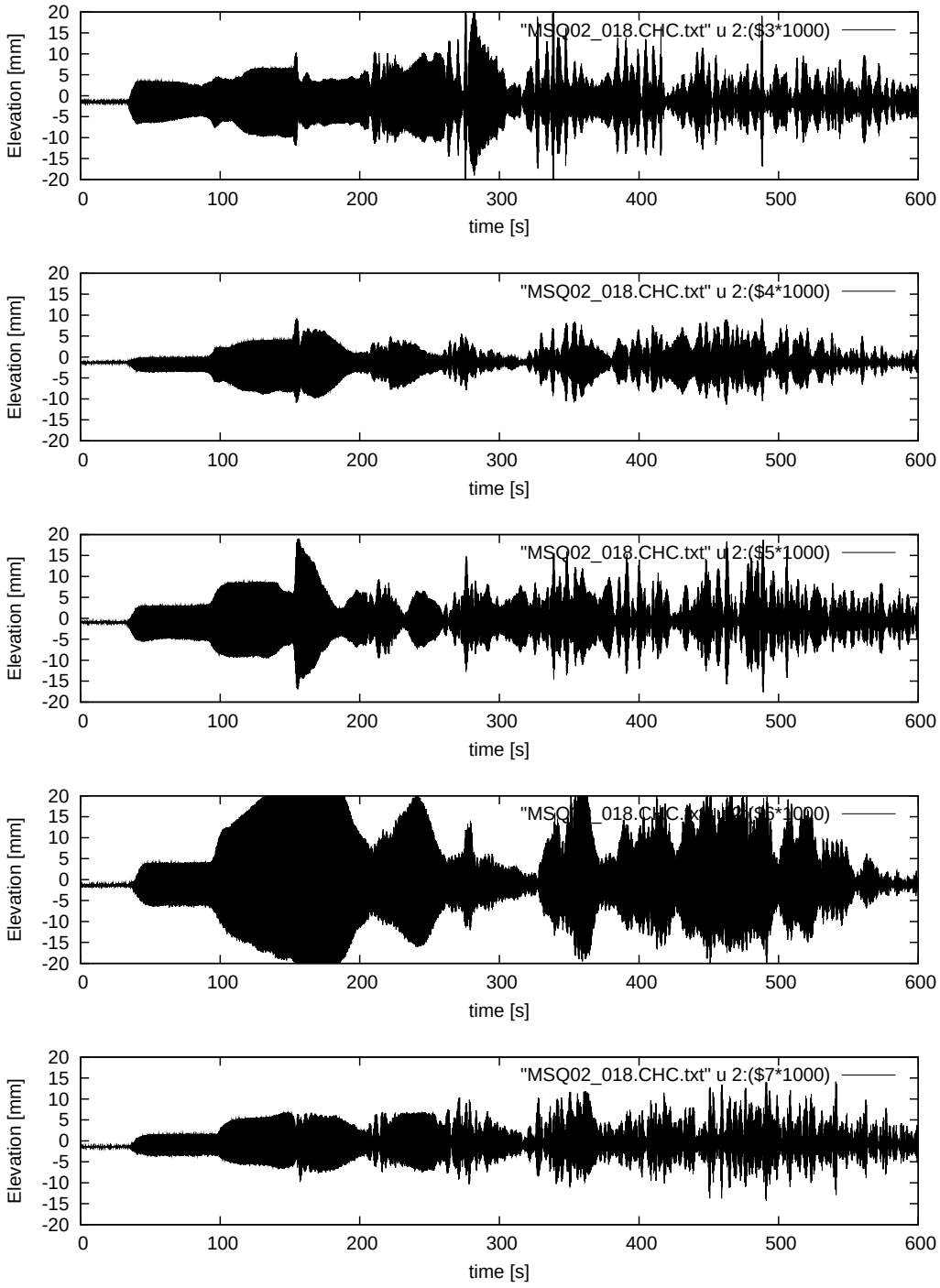

Figure B.17: Production run with f = 2.0 Hz, d = 245 mm. Wave maker running for 360 s (MSQ02 018). From top to bottom, wave probes WP1 to WP5.

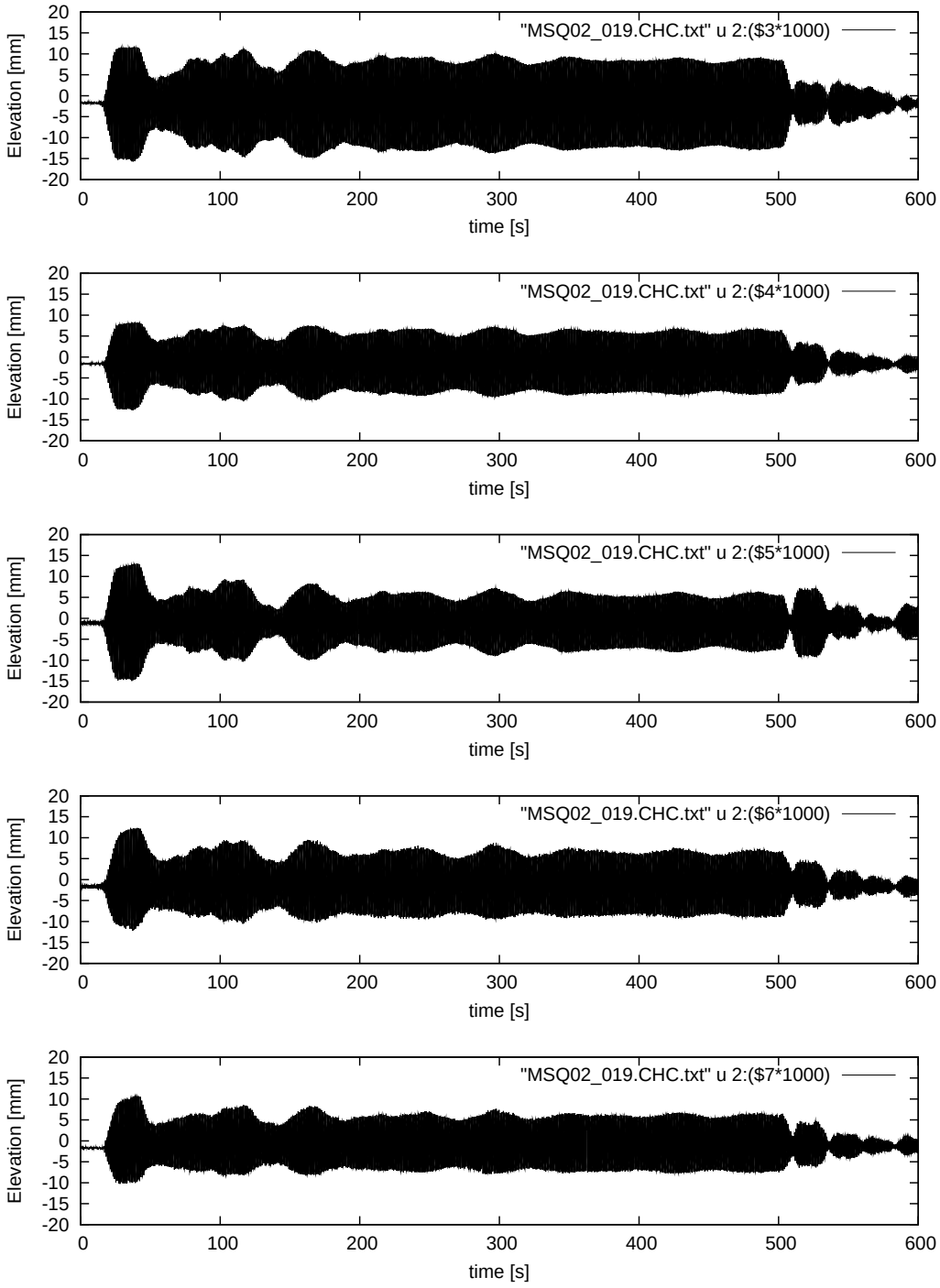

Figure B.18: Production run with f = 1.0 Hz, d = 245 mm. Wave maker running for 360 s (MSQ02 019). From top to bottom, wave probes WP1 to WP5.

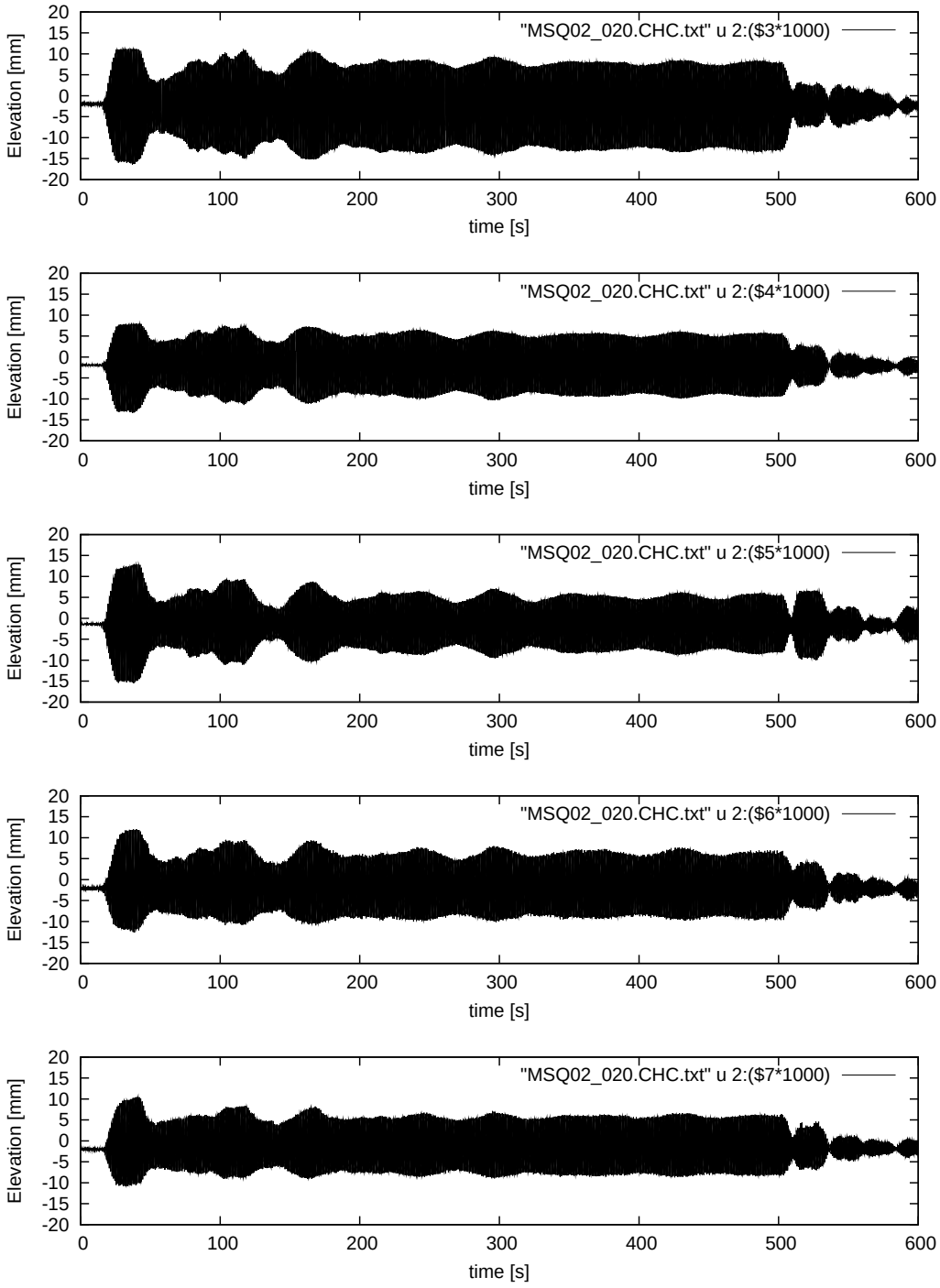

Figure B.19: Production run with f = 1.0 Hz, d = 245 mm. Wave maker running for 360 s (MSQ02 020). From top to bottom, wave probes WP1 to WP5.

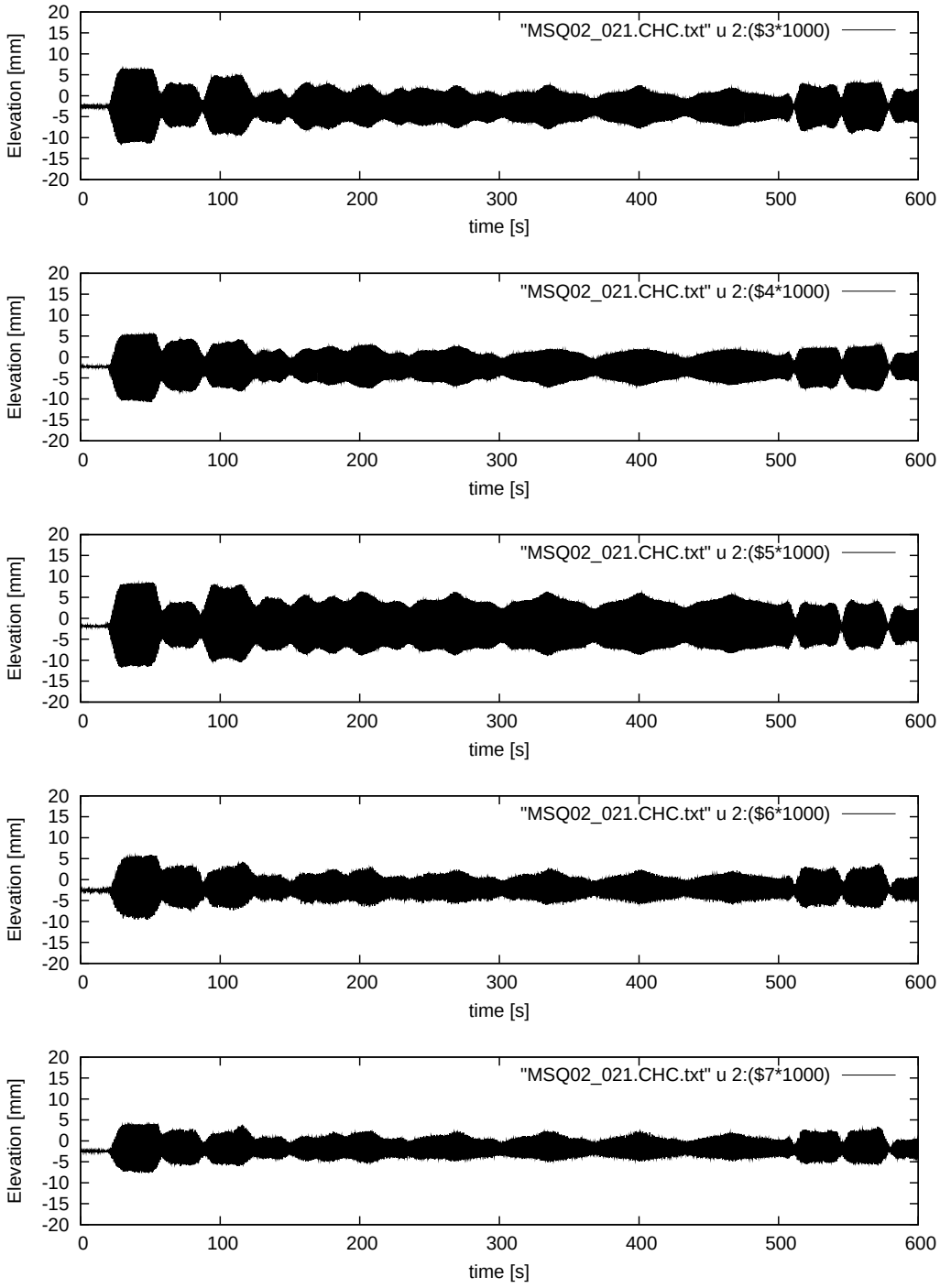

Figure B.20: Production run with f = 1.2 Hz, d = 245 mm. Wave maker running for 360 s (MSQ02 021). From top to bottom, wave probes WP1 to WP5.

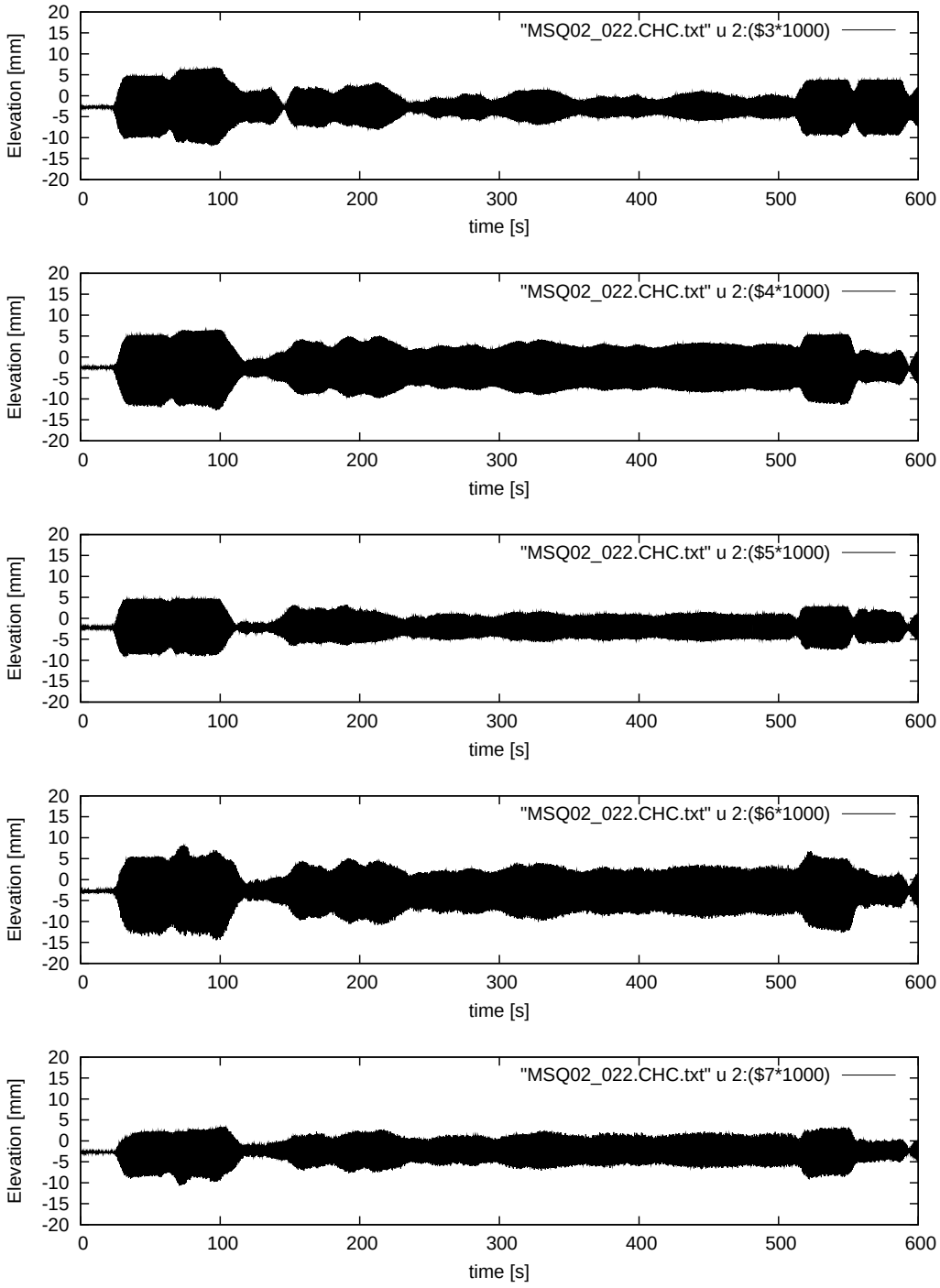

Figure B.21: Production run with f = 1.4 Hz, d = 245 mm. Wave maker running for 360 s (MSQ02 022). From top to bottom, wave probes WP1 to WP5.

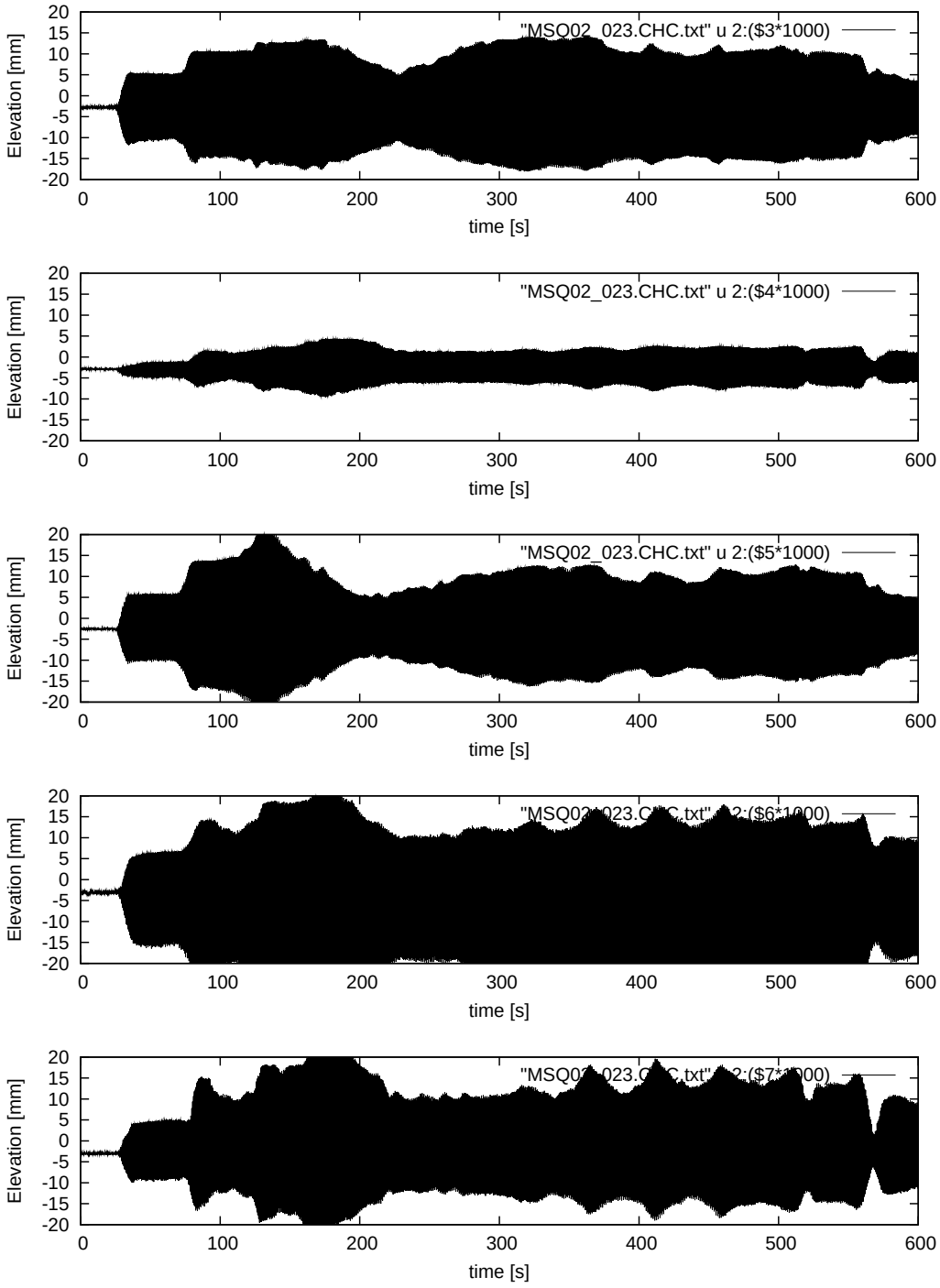

Figure B.22: Production run with f = 1.6 Hz, d = 245 mm. Wave maker running for 360 s (MSQ02 023). From top to bottom, wave probes WP1 to WP5.

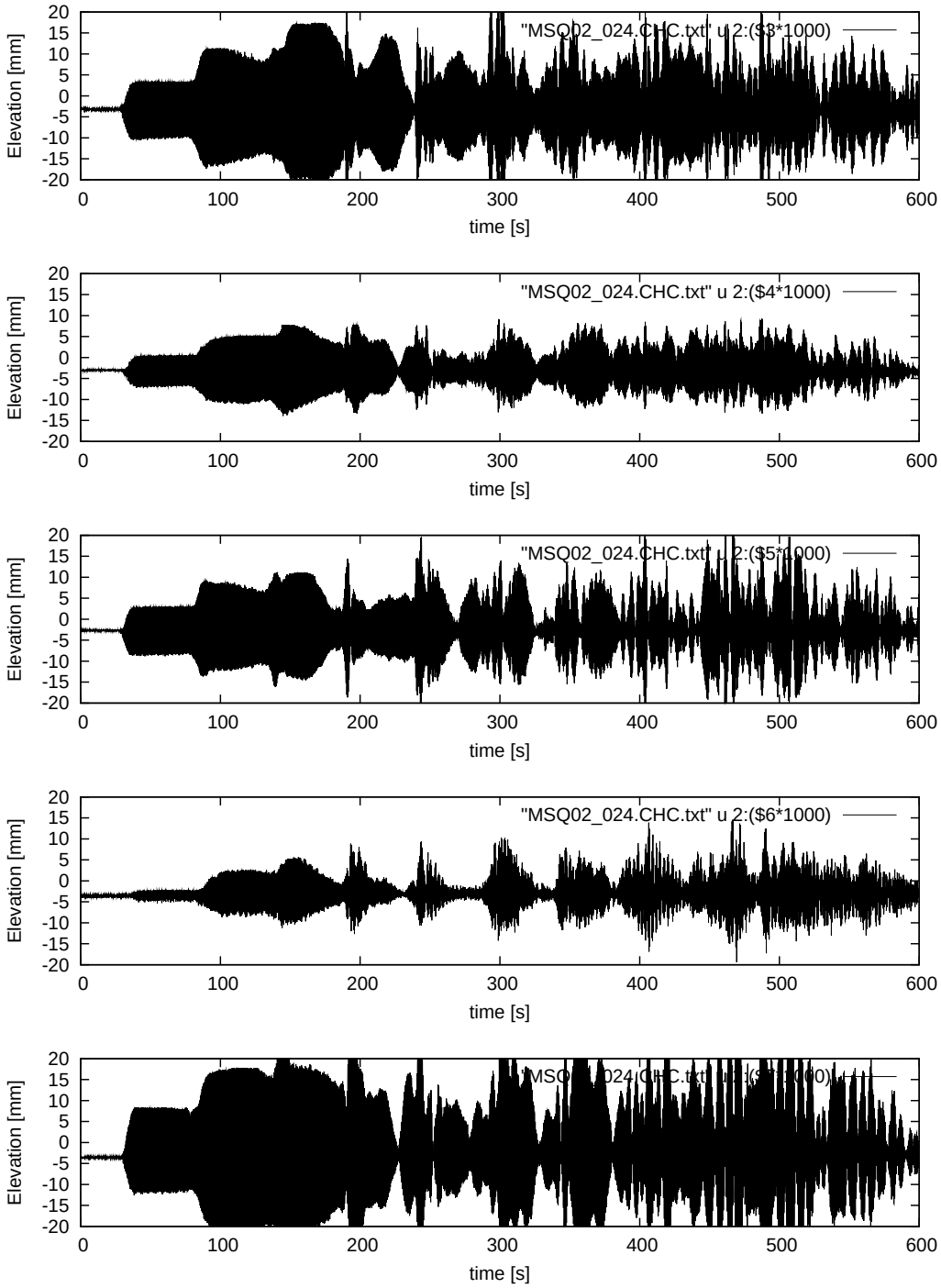

Figure B.23: Production run with f = 1.8 Hz, d = 245 mm. Wave maker running for 360 s (MSQ02 024). From top to bottom, wave probes WP1 to WP5.

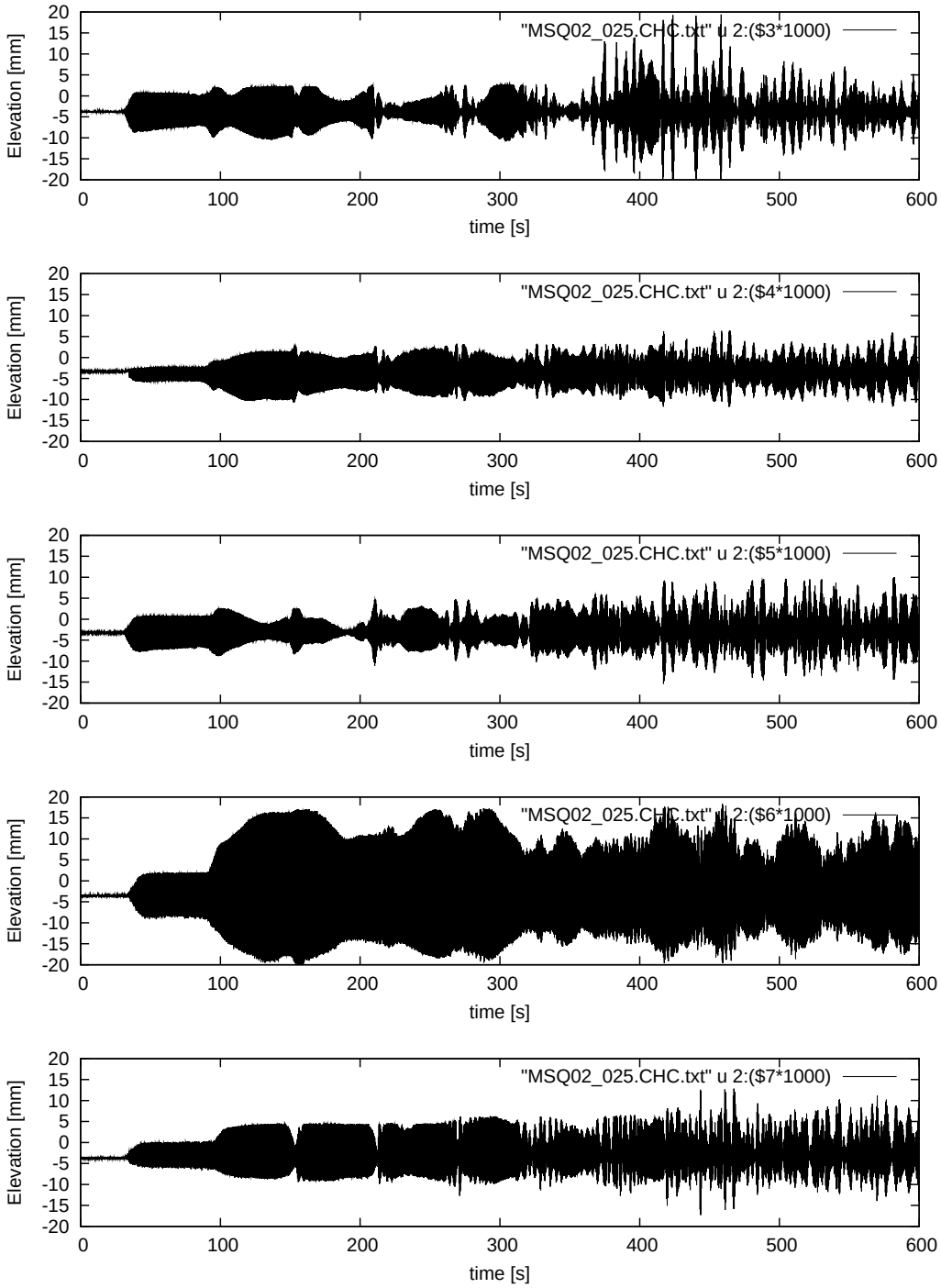

Figure B.24: Production run with f = 2.0 Hz, d = 245 mm. Wave maker running for 360 s (MSQ02 025). From top to bottom, wave probes WP1 to WP5.

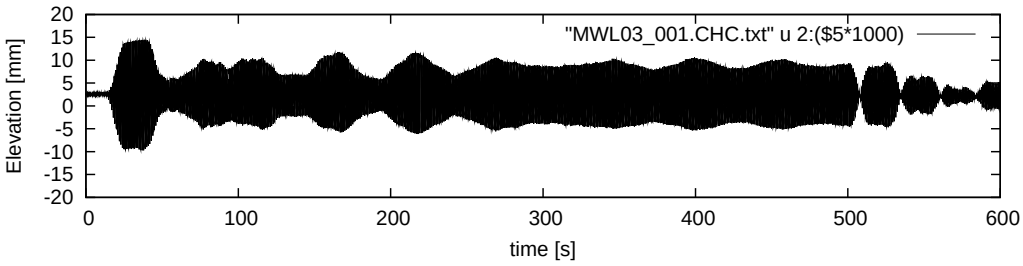

Figure B.25: Production run, basin closed, f = 1.0Hz (MWL03 001). From top to bottom, wave probes WP1 to WP3.

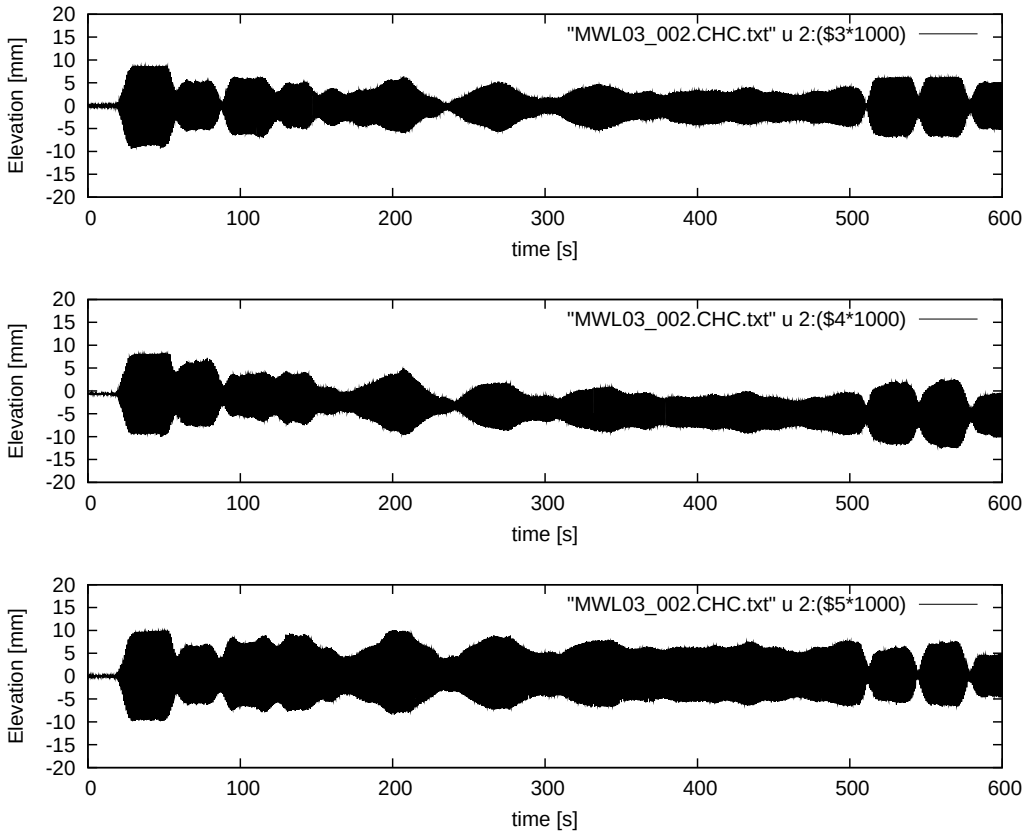

Figure B.26: Production run, basin closed, f = 1.2 Hz (MWL03 002). From top to bottom, wave probes WP1 to WP3.

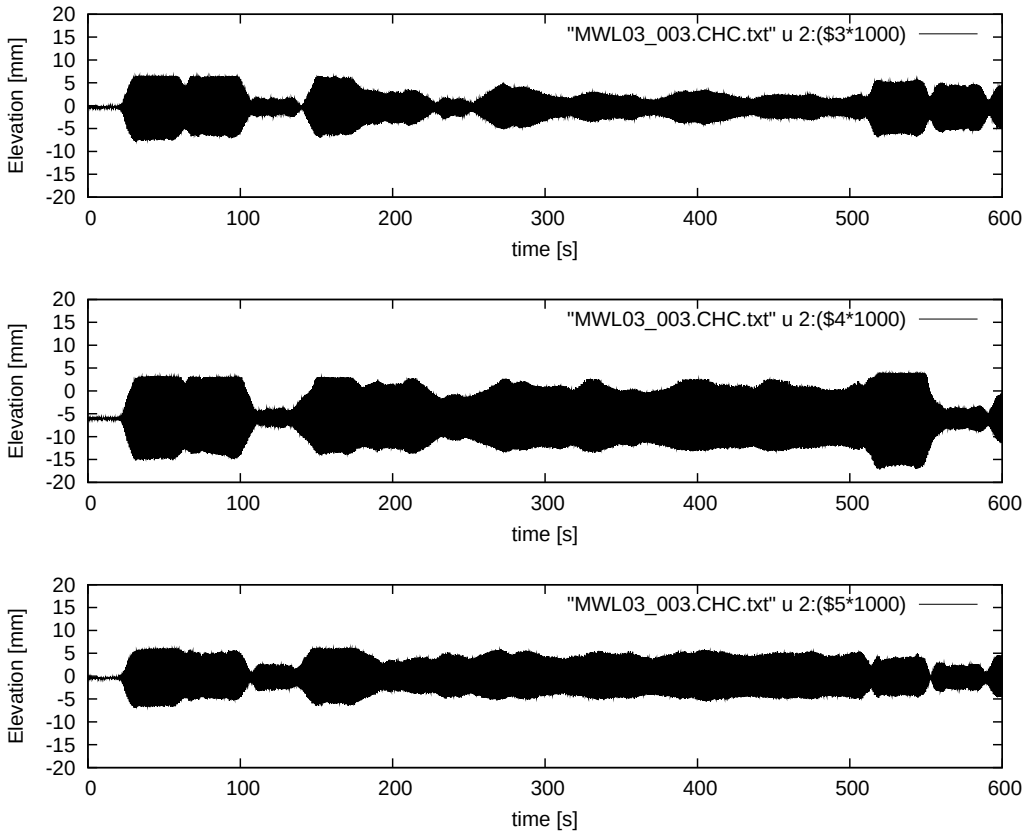

Figure B.27: Production run, basin closed, f = 1.4 Hz (MWL03 003). From top to bottom, wave probes WP1 to WP3.

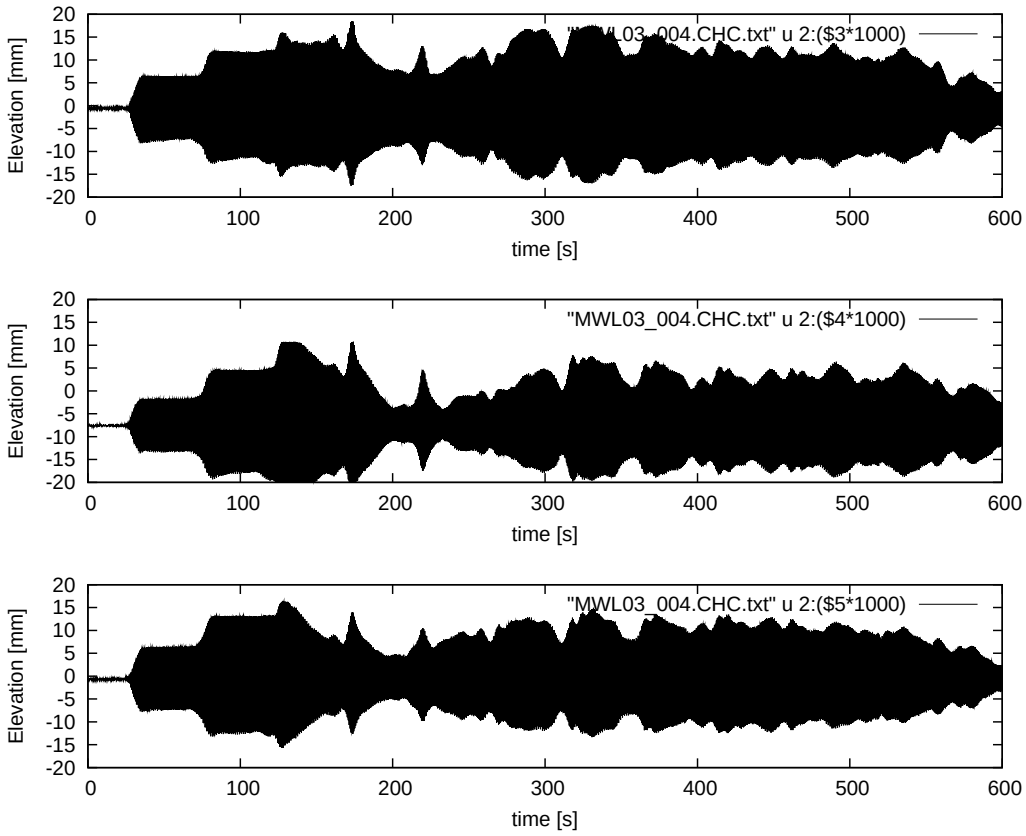

Figure B.28: Production run, basin closed, f = 1.6 Hz (MWL03 004). From top to bottom, wave probes WP1 to WP3.

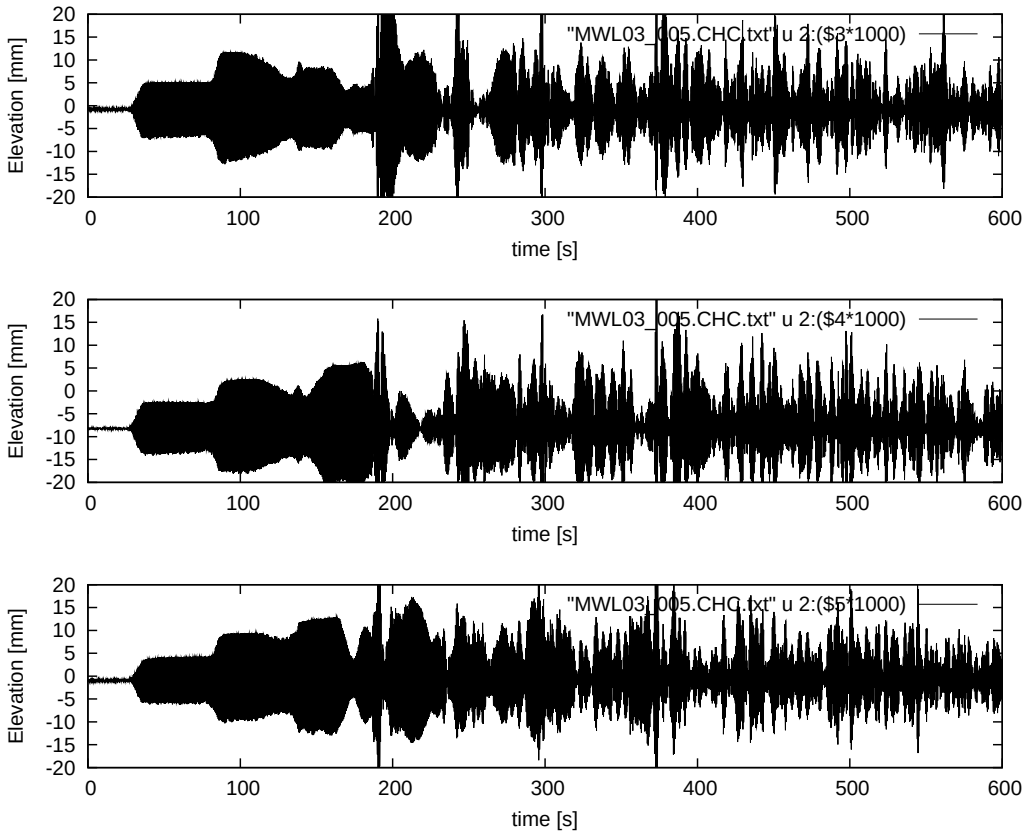

Figure B.29: Production run, basin closed, f = 1.8 Hz (MWL03 005). From top to bottom, wave probes WP1 to WP3.

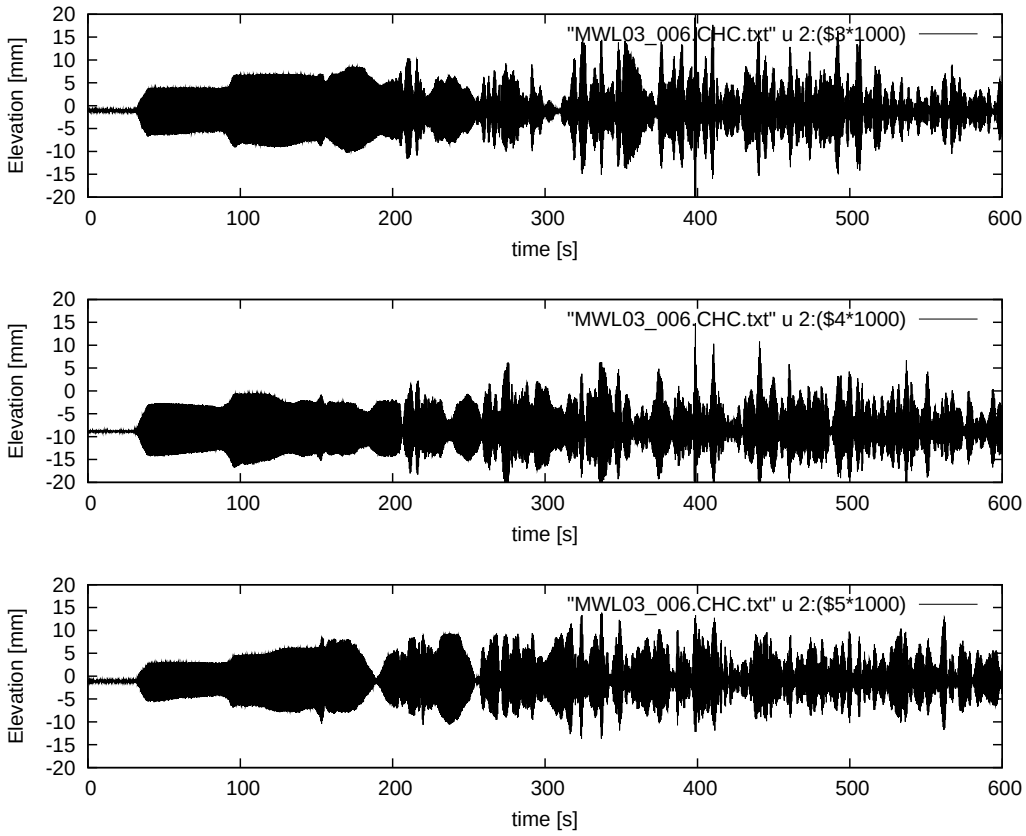

Figure B.30: Production run, basin closed, f = 2.0 Hz (MWL03 006). From top to bottom, wave probes WP1 to WP3.

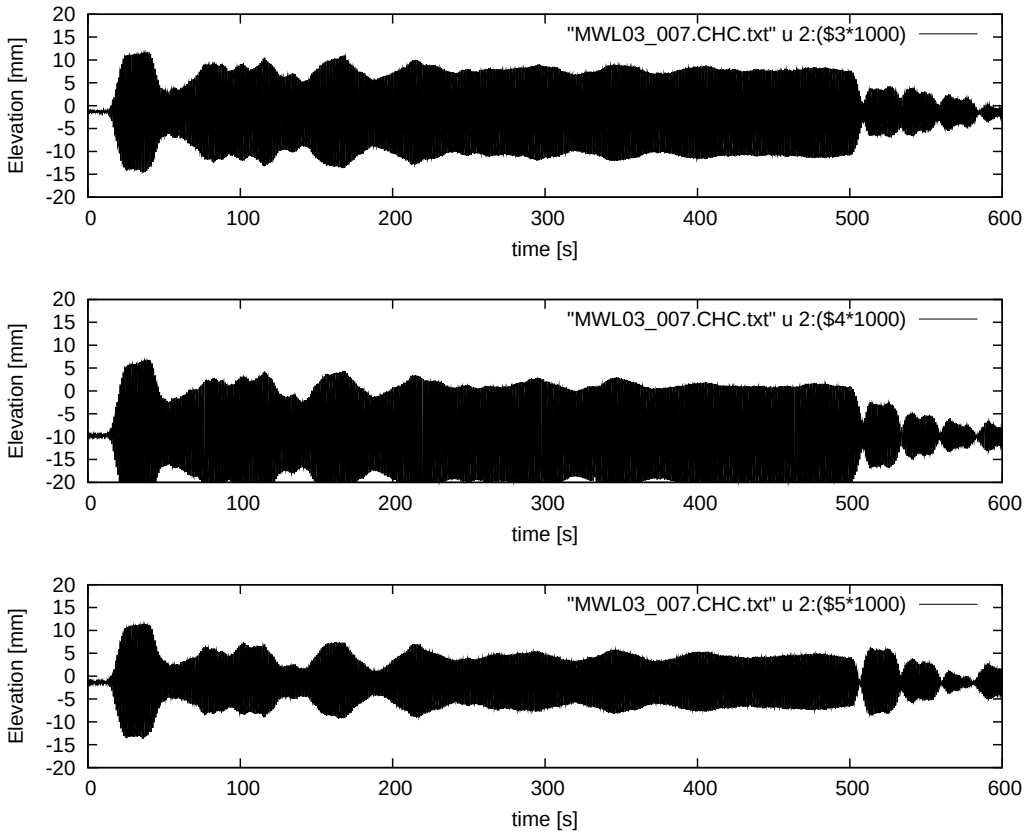

Figure B.31: Production run, basin closed, f = 1.0 Hz (MWL03 007). From top to bottom, wave probes WP1 to WP3.

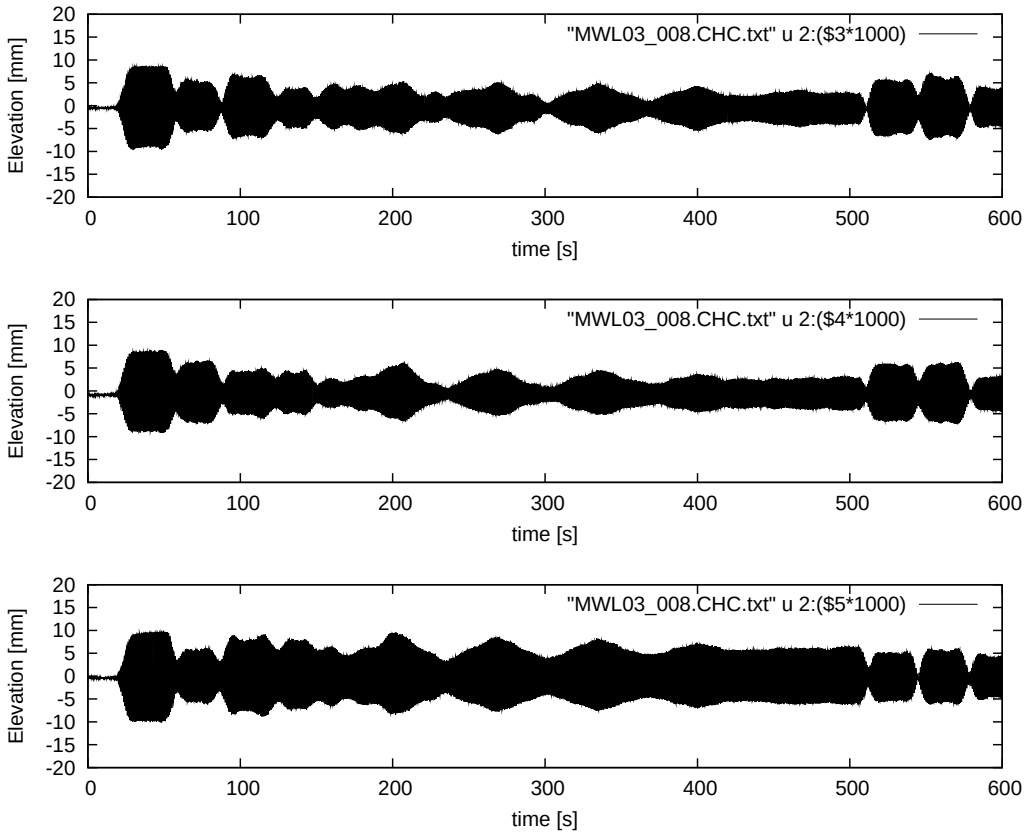

Figure B.32: Production run, basin closed, f = 1.2 Hz (MWL03 008). From top to bottom, wave probes WP1 to WP3.

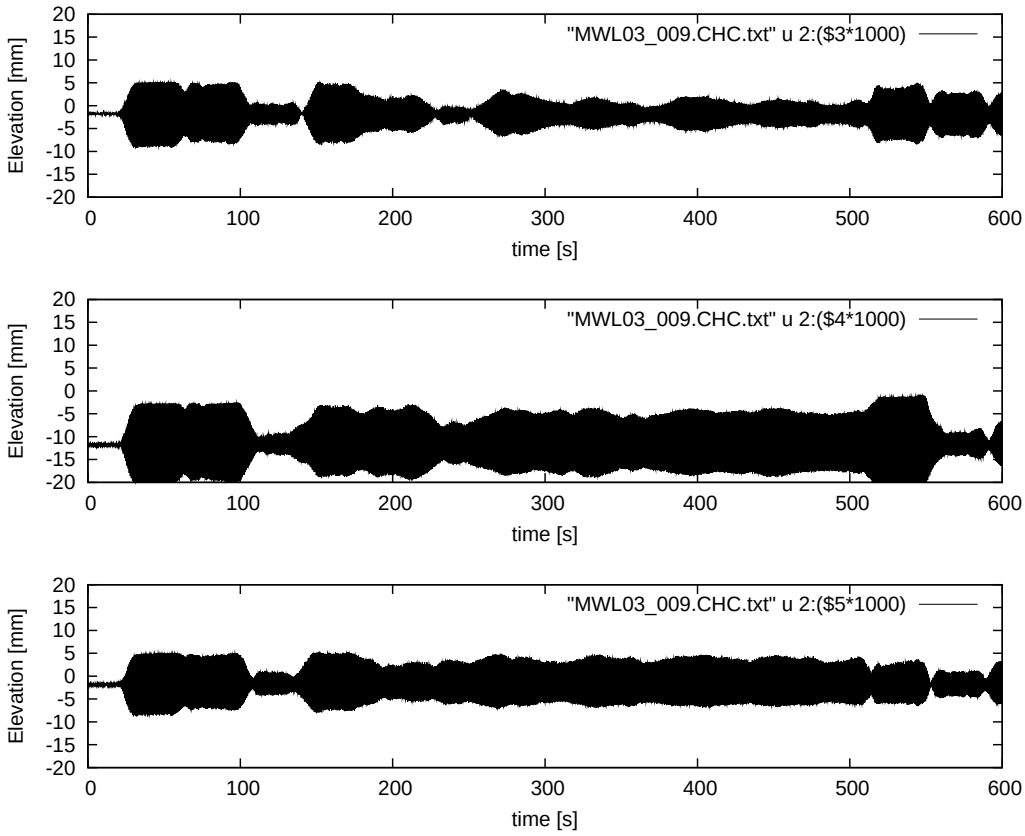

Figure B.33: Production run, basin closed, f = 1.4 Hz (MWL03 009). From top to bottom, wave probes WP1 to WP3.

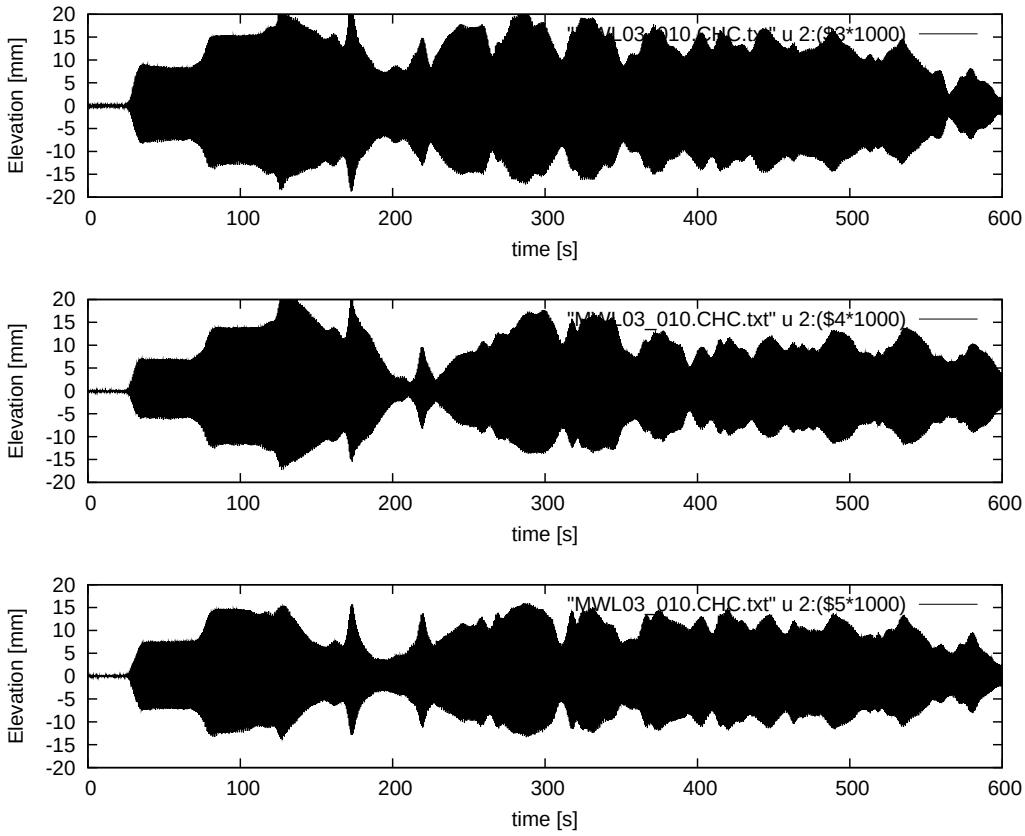

Figure B.34: Production run, basin closed, f = 1.6 Hz (MWL03 010). From top to bottom, wave probes WP1 to WP3.

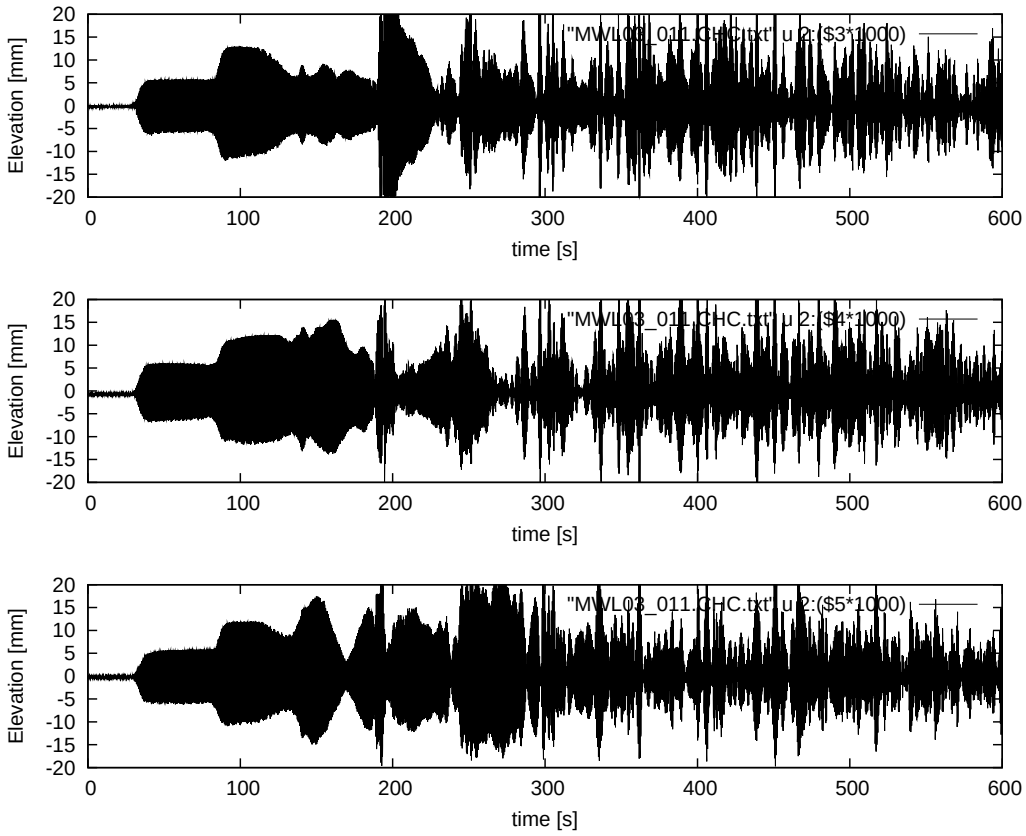

Figure B.35: Production run, basin closed, f = 1.8 Hz (MWL03 011). From top to bottom, wave probes WP1 to WP3.

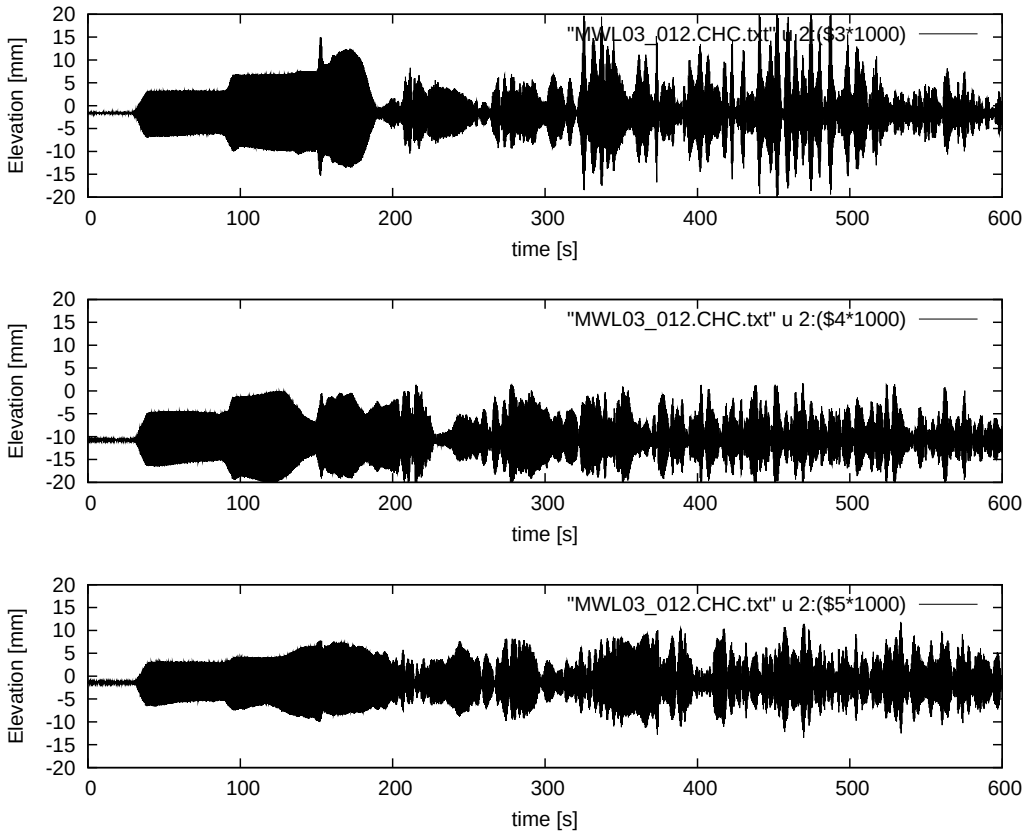

Figure B.36: Production run, basin closed, f = 2.0 Hz (MWL03 012). From top to bottom, wave probes WP1 to WP3.

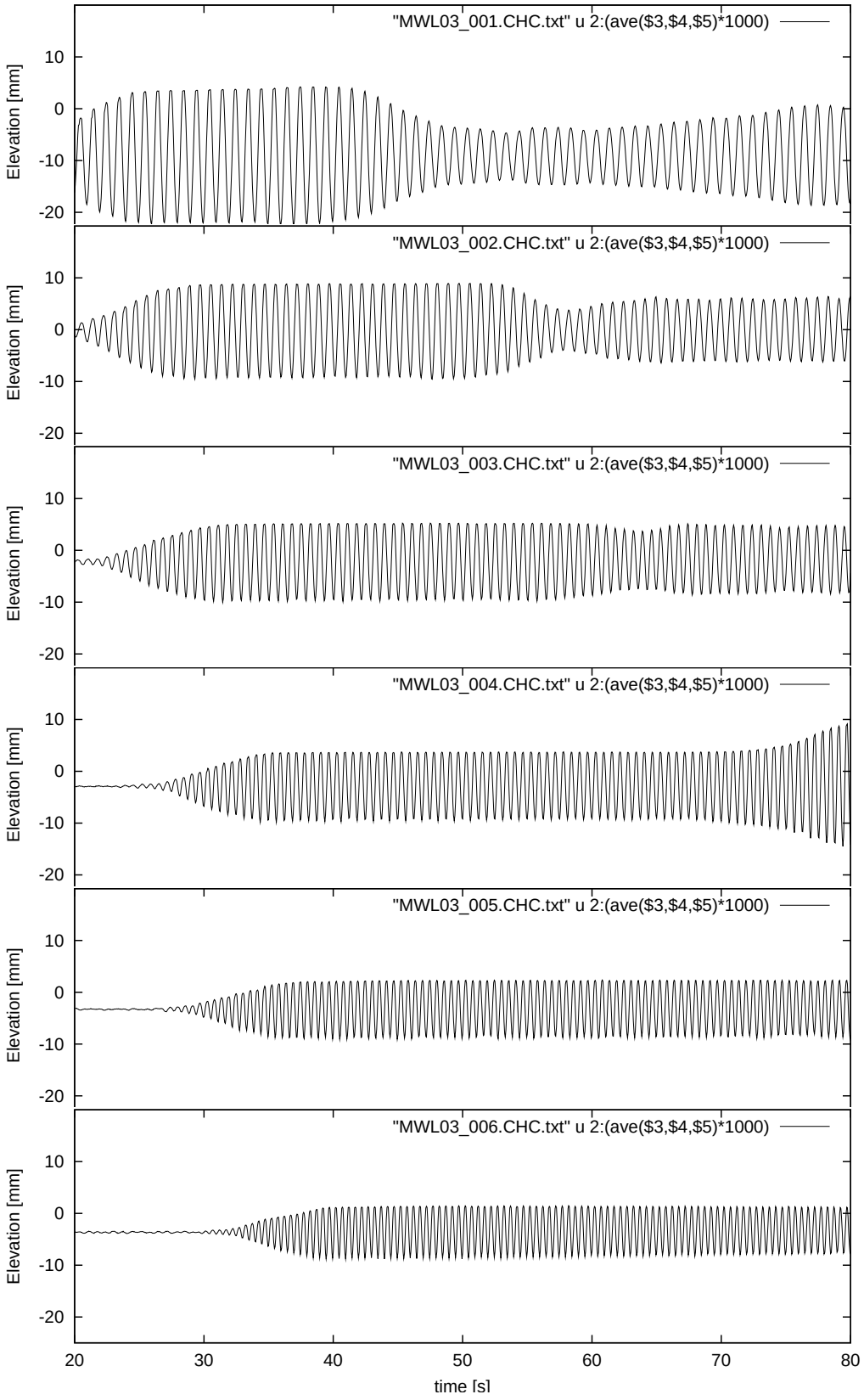

Figure B.37: Average water surface oscillations (three probes), test series no. 1. From top to bottom: 1.0 Hz, 1,2 Hz, 1,4 Hz, 1.6 Hz, 1.8 Hz and 2.0 Hz (MWL03 001-006).

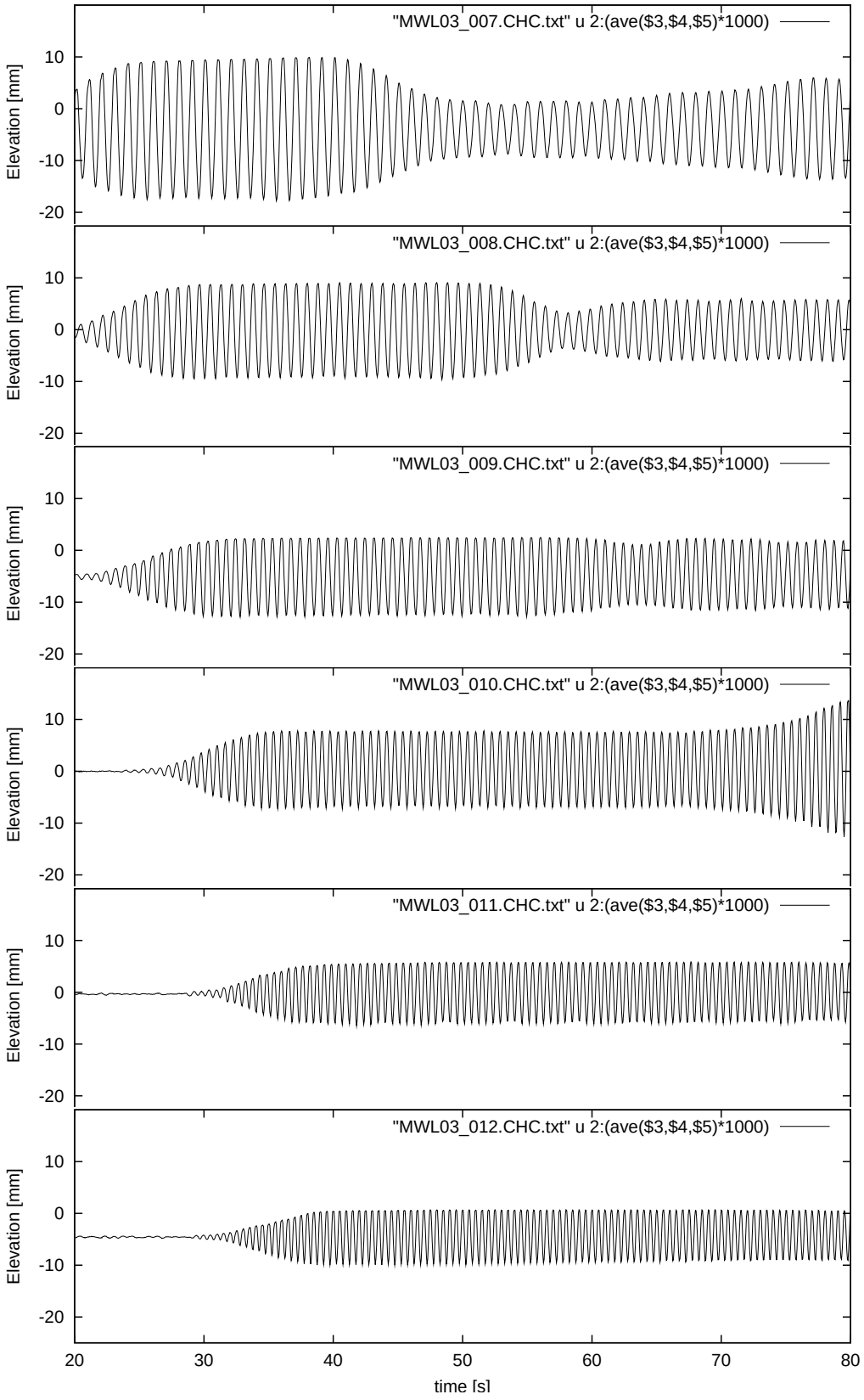

Figure B.38: Average water surface oscillations (three probes), test series no. 2. From top to bottom: 1.0 Hz, 1,2 Hz, 1,4 Hz, 1.6 Hz, 1.8 Hz and 2.0 Hz (MWL03 007-012).

Appendix C

Numerical model results

C.1 Plots of surface elevations

a) η for two opposite phases.

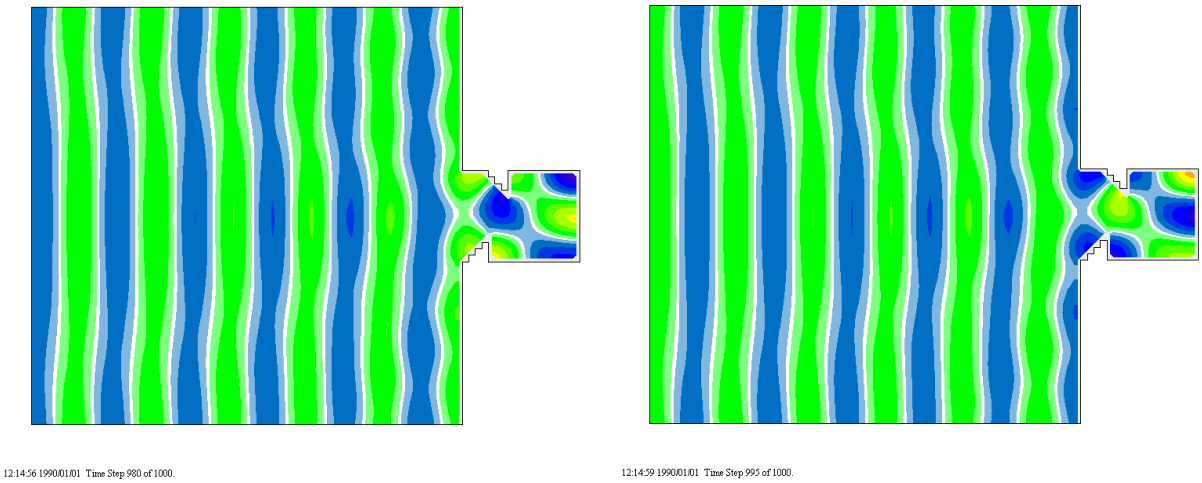

b) P for two opposite phases.

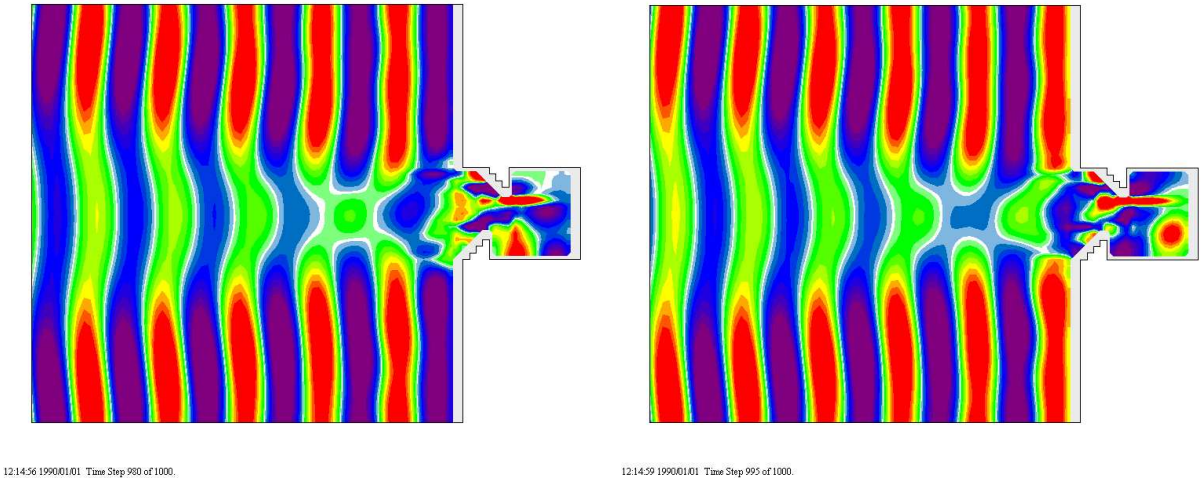

c) Q for two opposite phases.

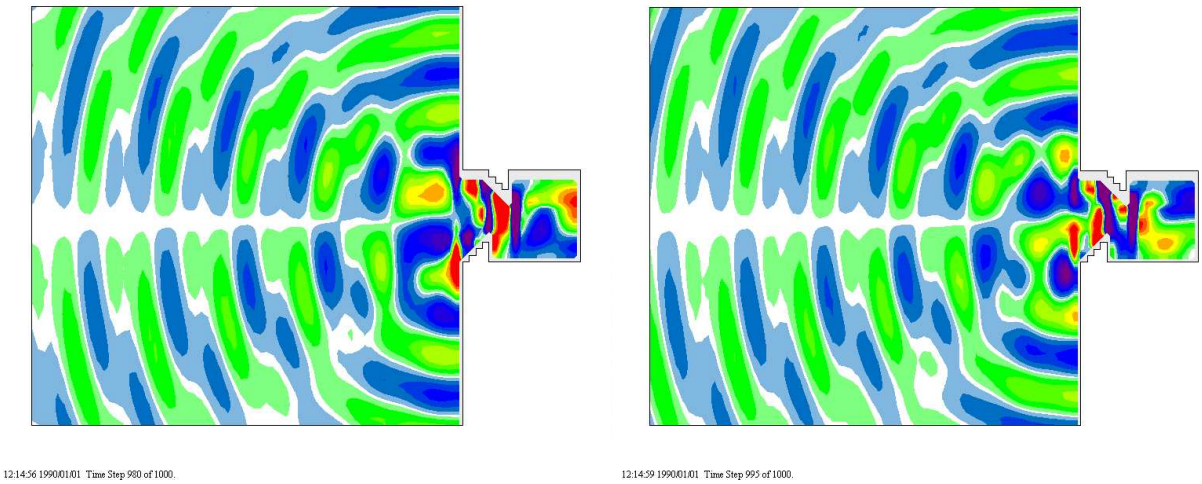

Figure C.1: Surface elevation η, flux P, flux Q for $T = 6.0s$ and two opposite phases.

a) η for two opposite phases.

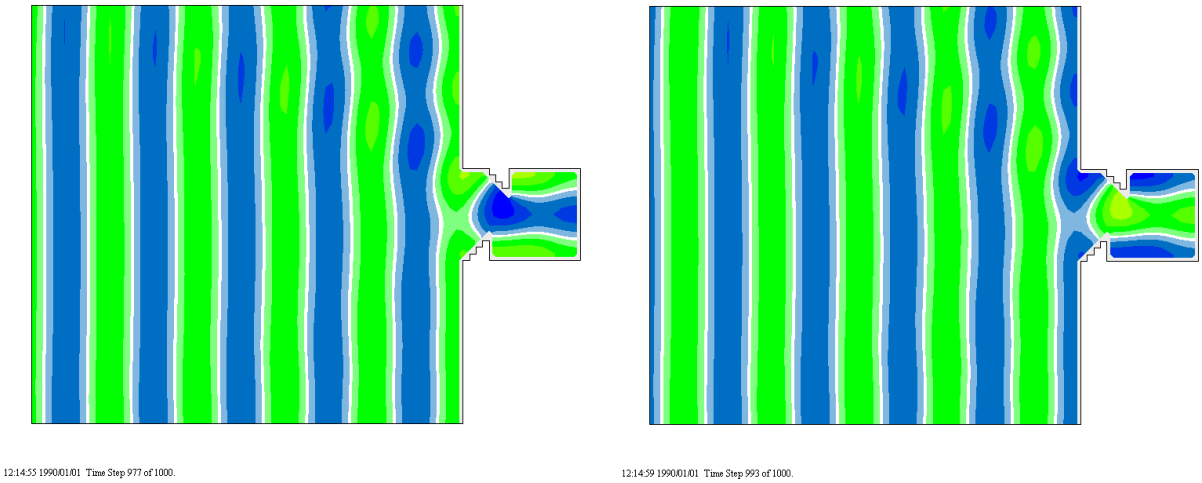

b) P for two opposite phases.

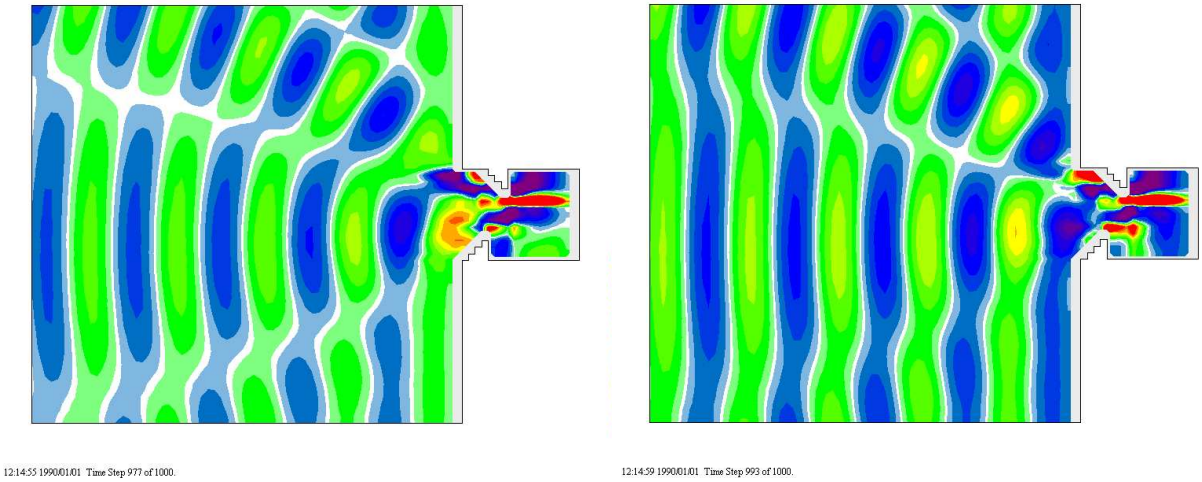

c) Q for two opposite phases.

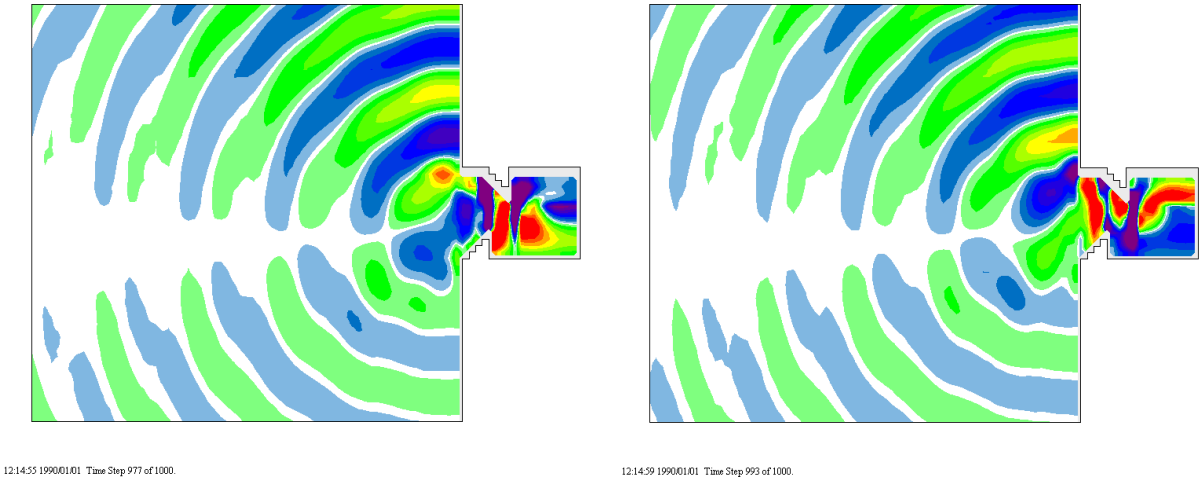

Figure C.2: Surface elevation η, flux P, flux Q for $T = 6.5s$.

a) η for two opposite phases.

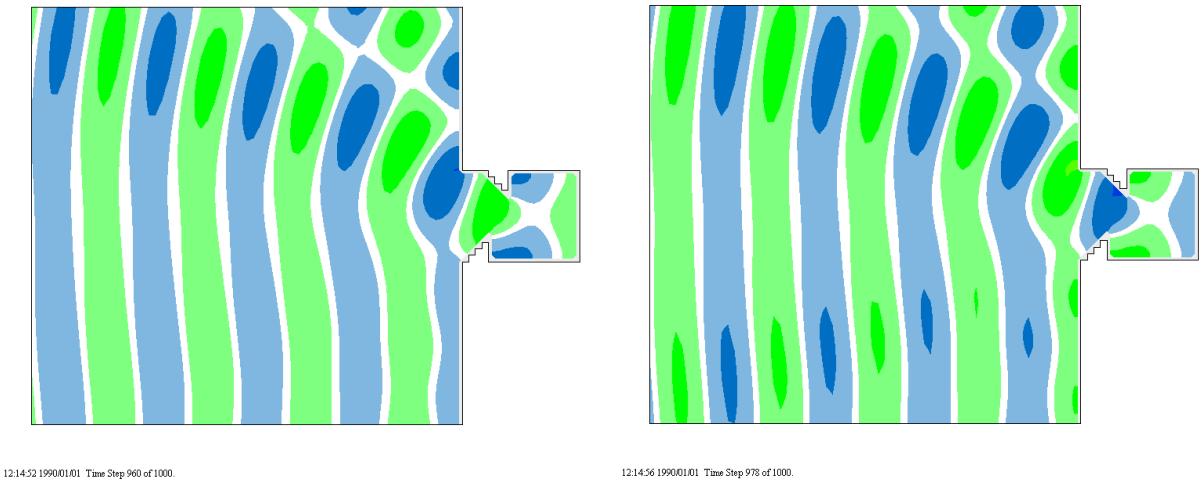

b) P for two opposite phases.

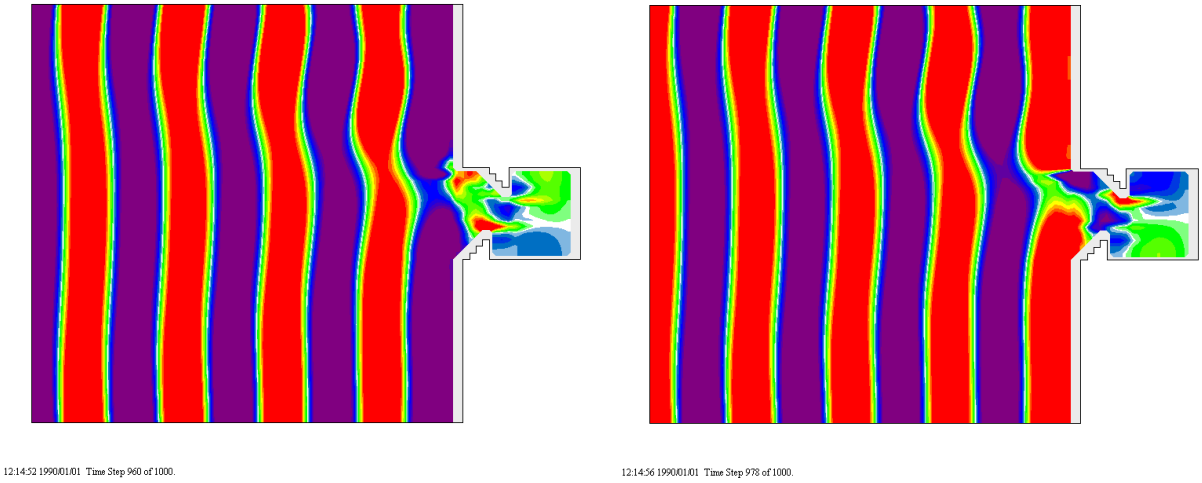

c) Q for two opposite phases.

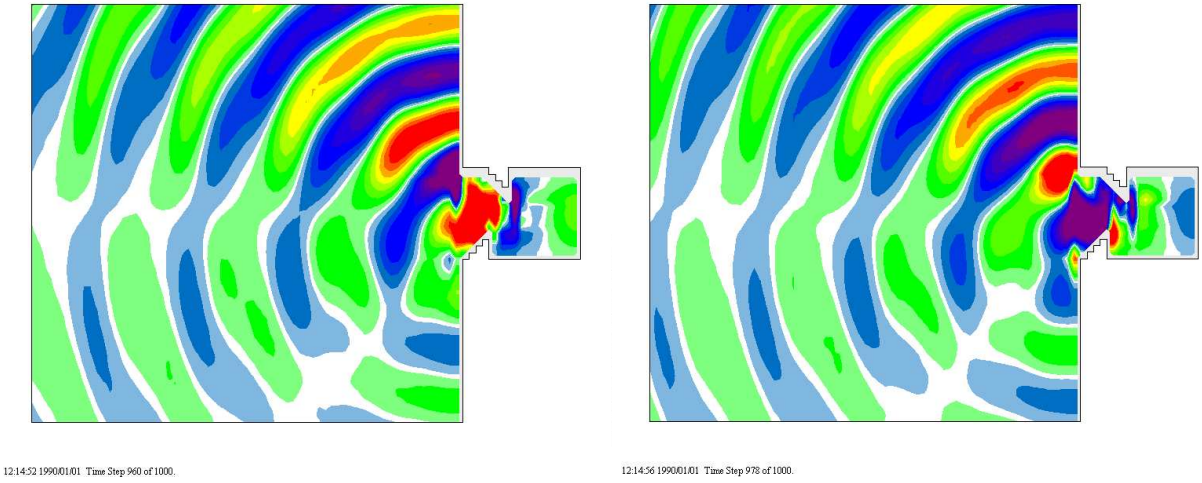

Figure C.3: Surface elevation η, flux P, flux Q for $T = 7.0s$.

a) η for two opposite phases.

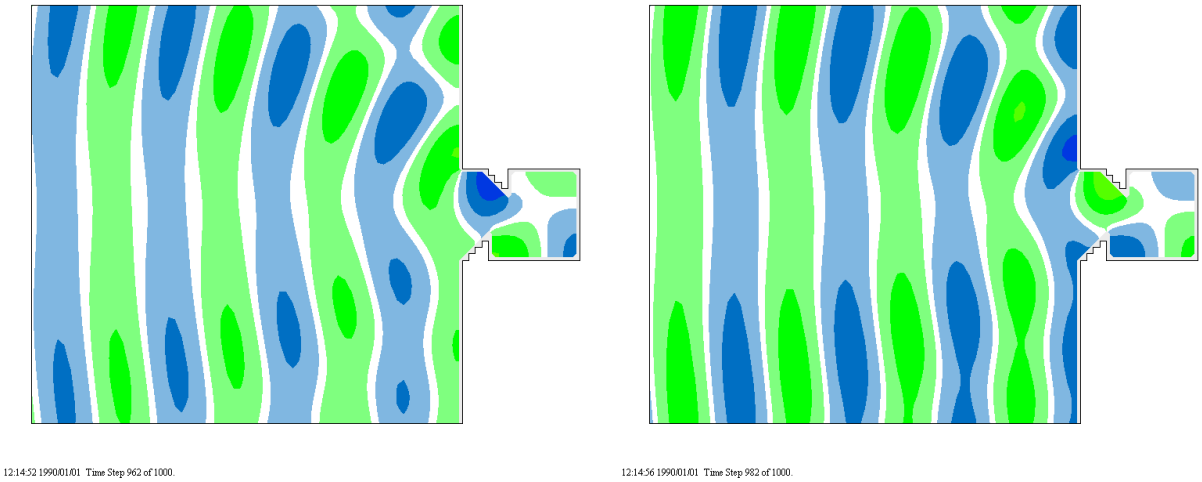

b) P for two opposite phases.

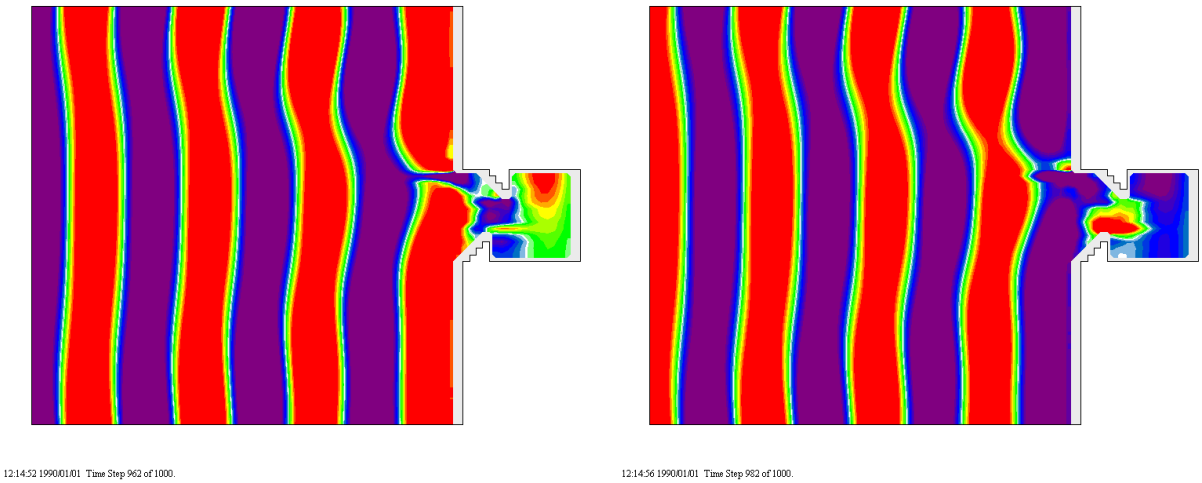

c) Q for two opposite phases.

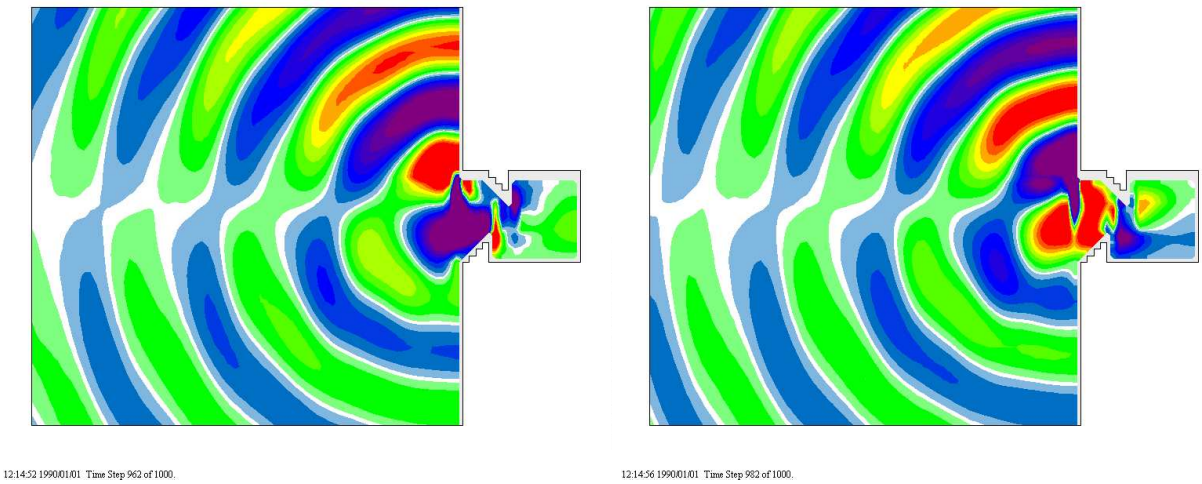

Figure C.4: Surface elevation η, flux P, flux Q for $T = 7.5s$.

a) η for two opposite phases.

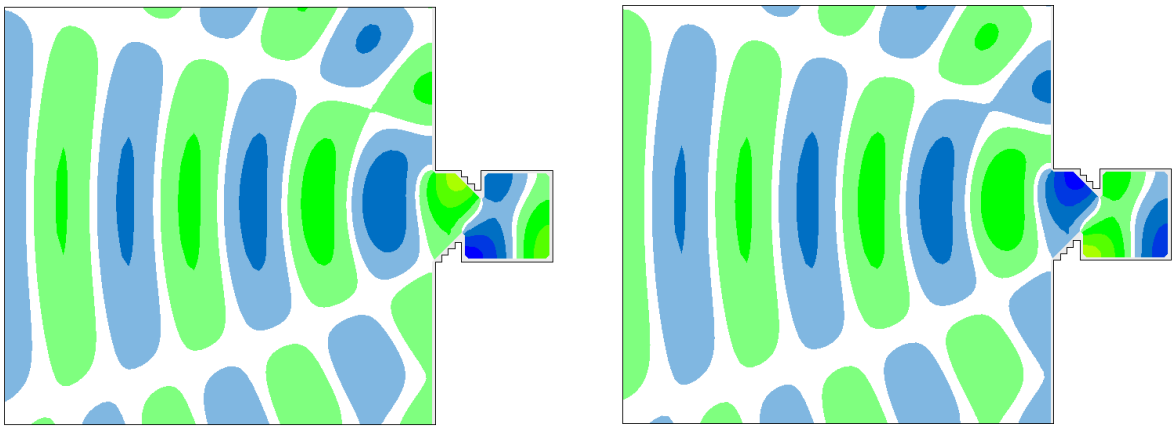

b) P for two opposite phases.

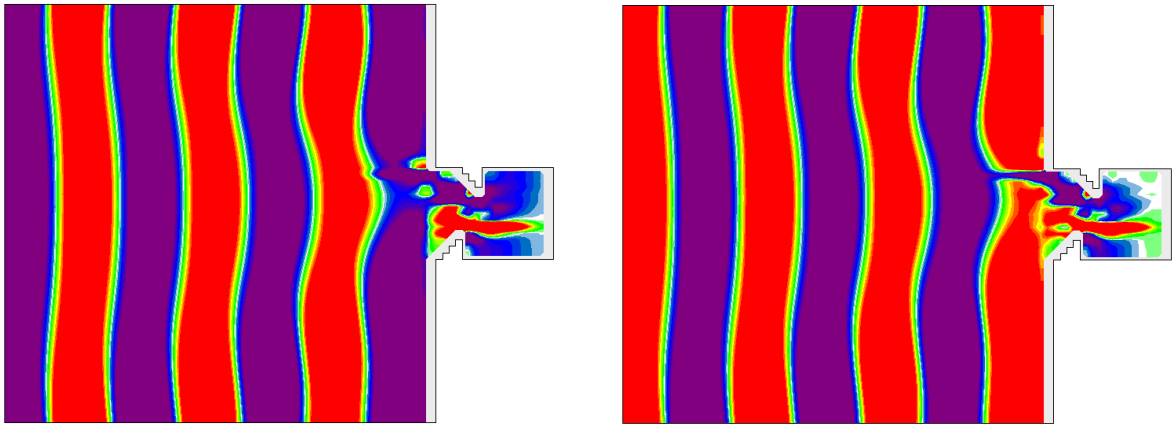

c) Q for two opposite phases.

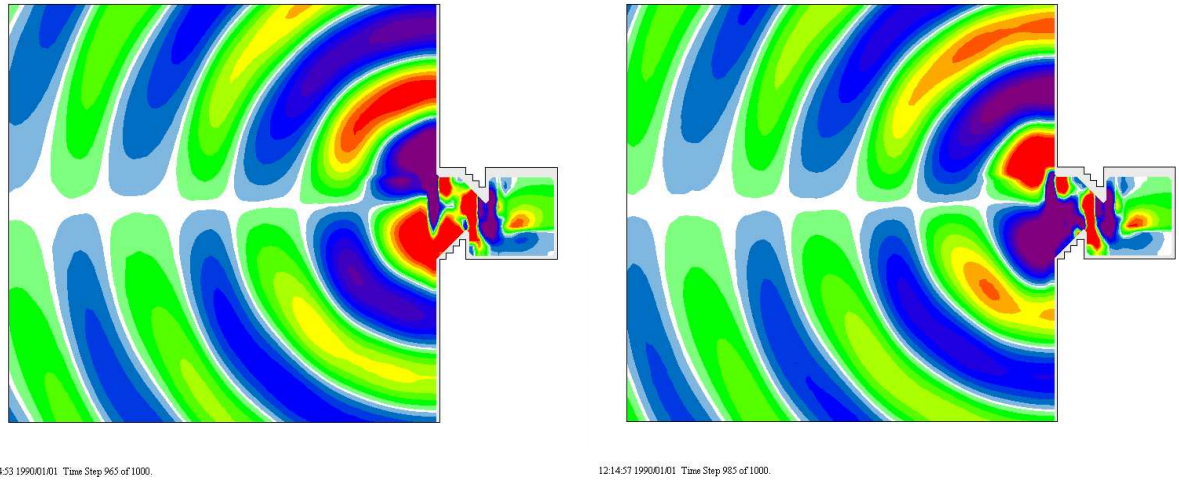

Figure C.5: Surface elevation η, flux P, flux Q for $T = 8.0s$.

a) η for two opposite phases.

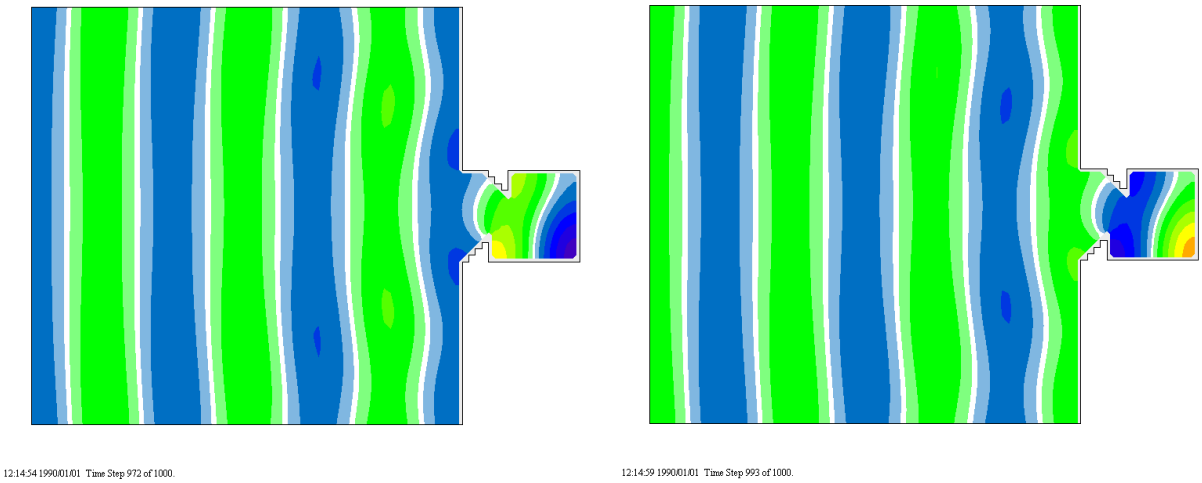

b) P for two opposite phases.

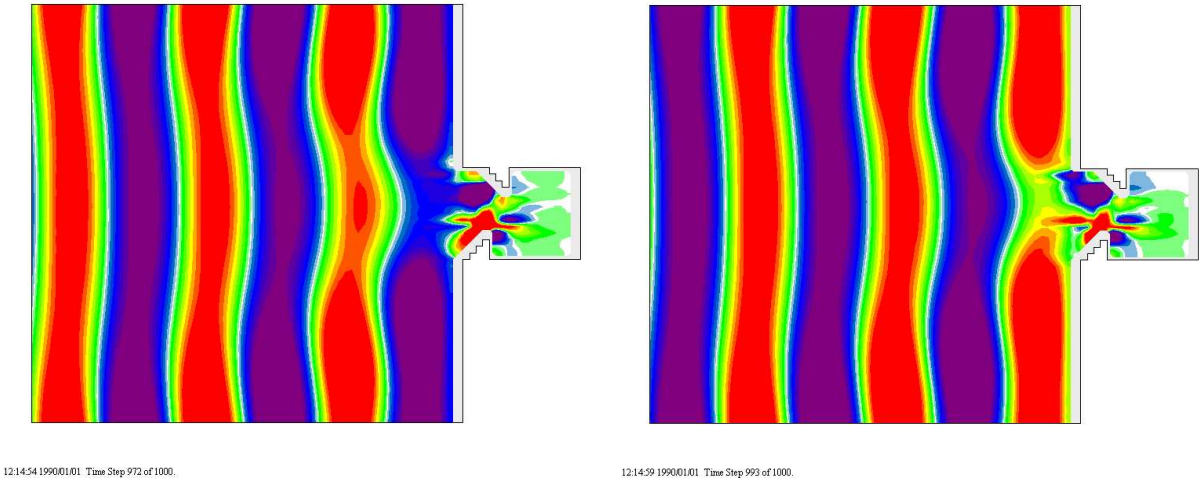

c) Q for two opposite phases.

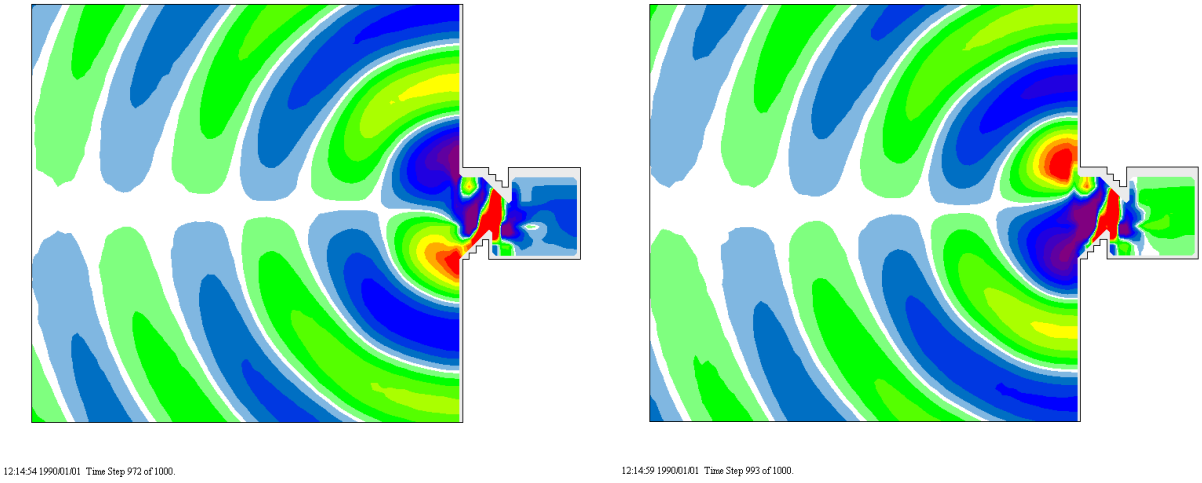

Figure C.6: Surface elevation η, flux P, flux Q for $T = 8.5s$.

a) η for two opposite phases.

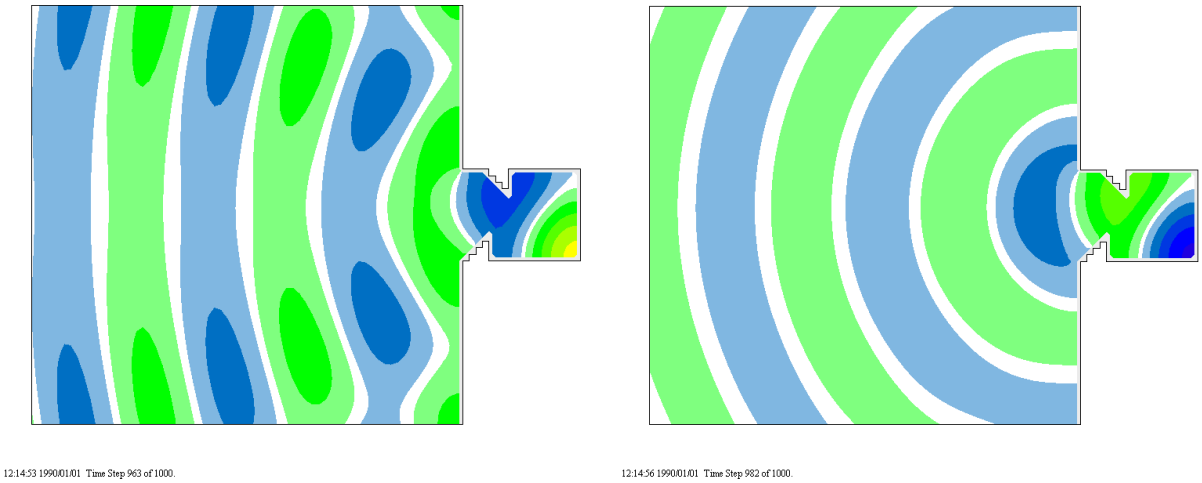

b) P for two opposite phases.

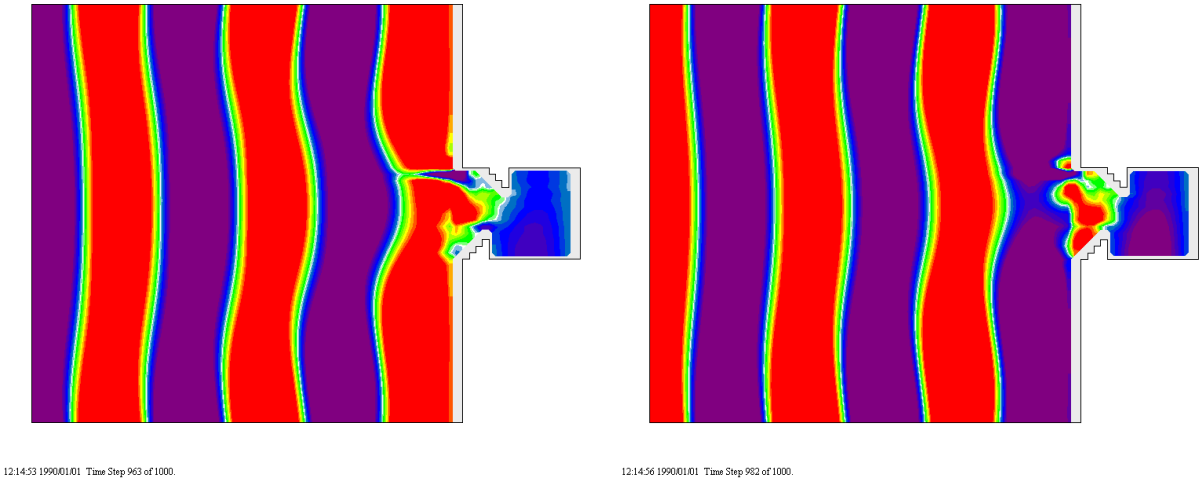

c) Q for two opposite phases.

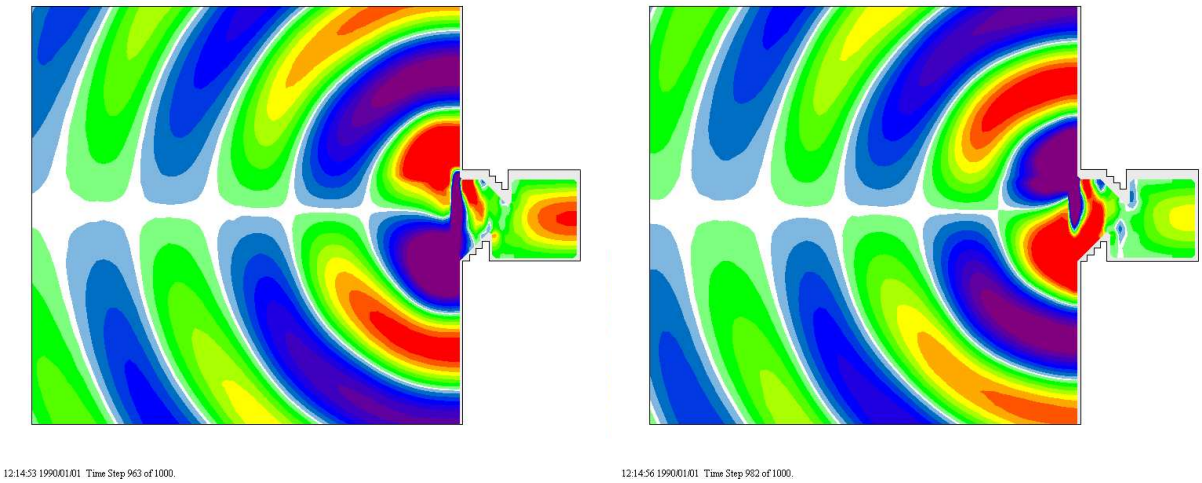

Figure C.7: Surface elevation η, flux P, flux Q for $T = 8.8s$.

a) η for two opposite phases.

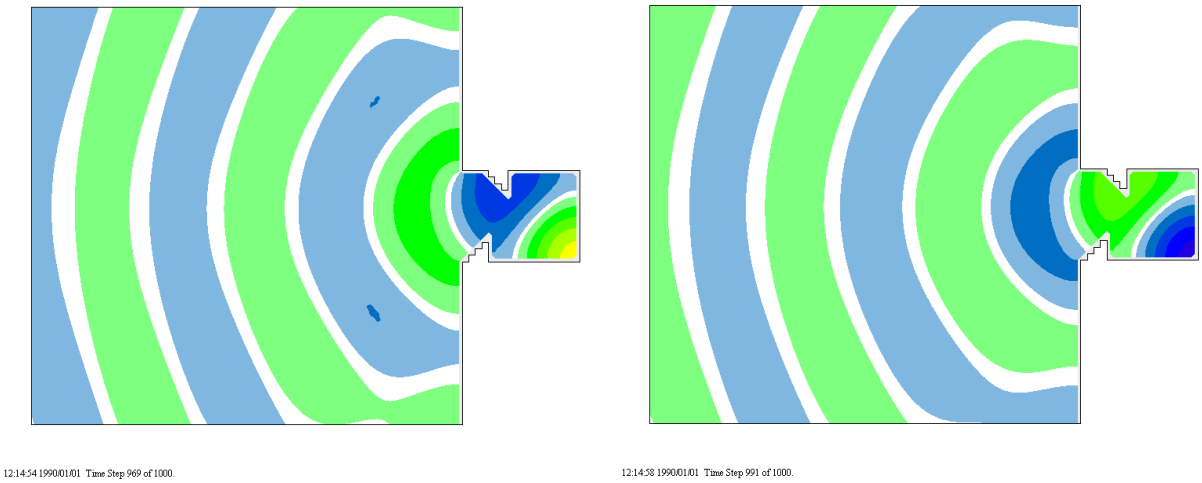

b) P for two opposite phases.

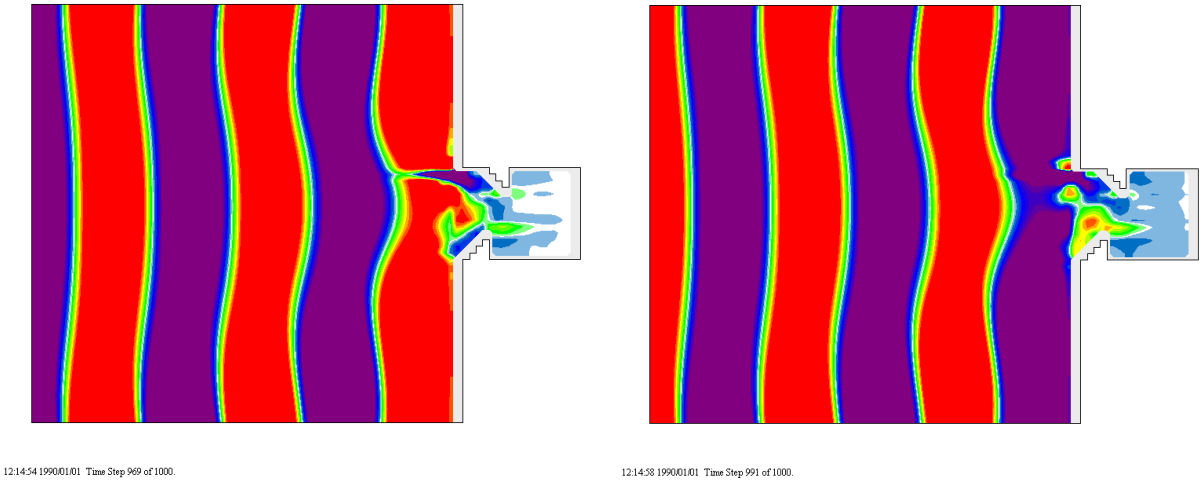

c) Q for two opposite phases.

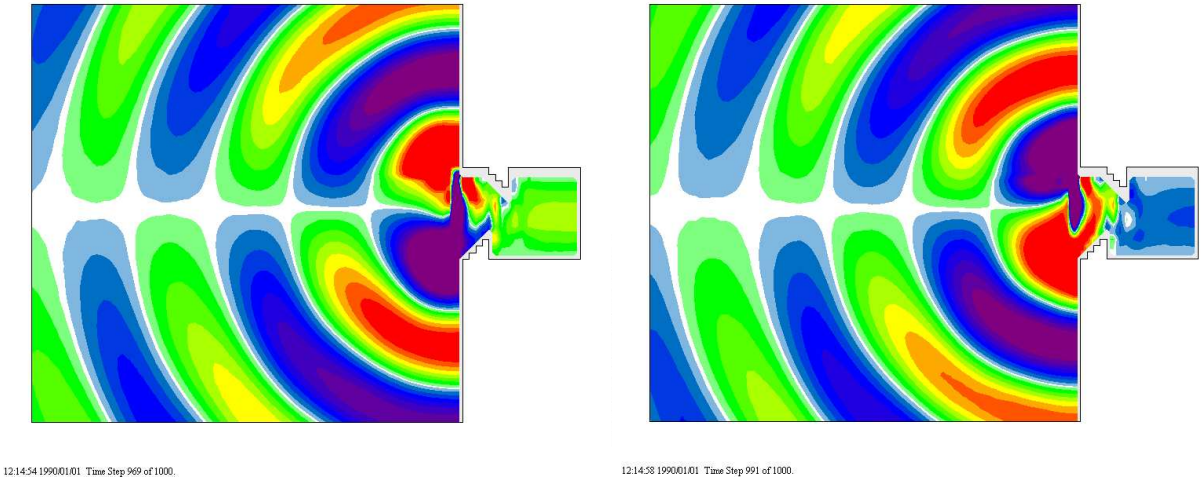

Figure C.8: Surface elevation η, flux P, flux Q for $T = 8.9s$.

a) η for two opposite phases.

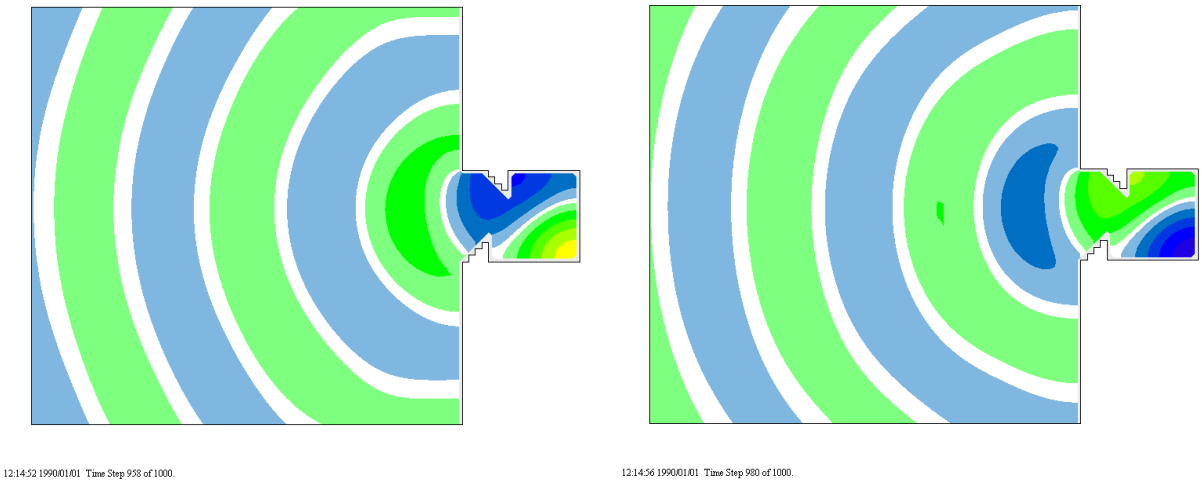

b) P for two opposite phases.

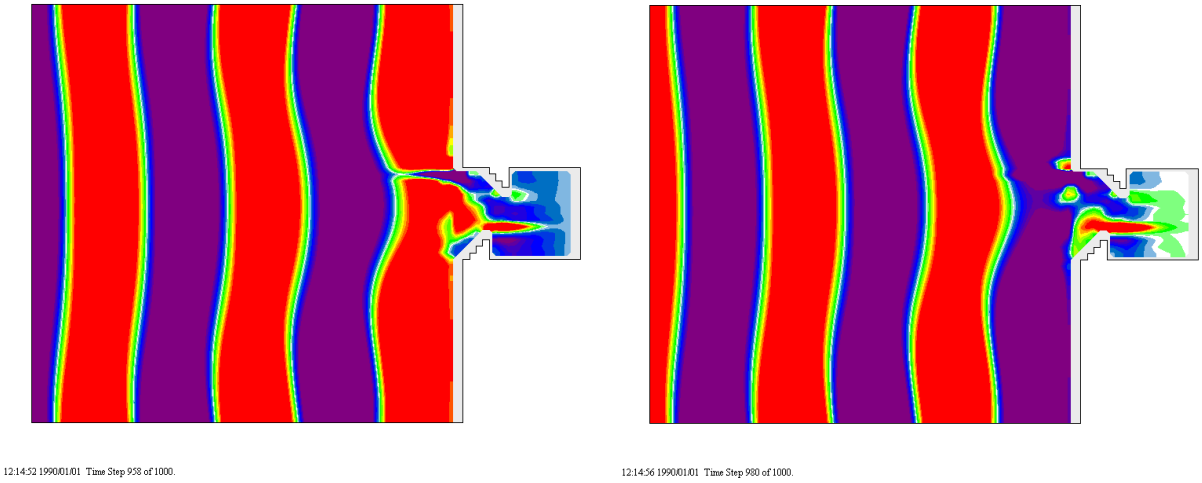

c) Q for two opposite phases.

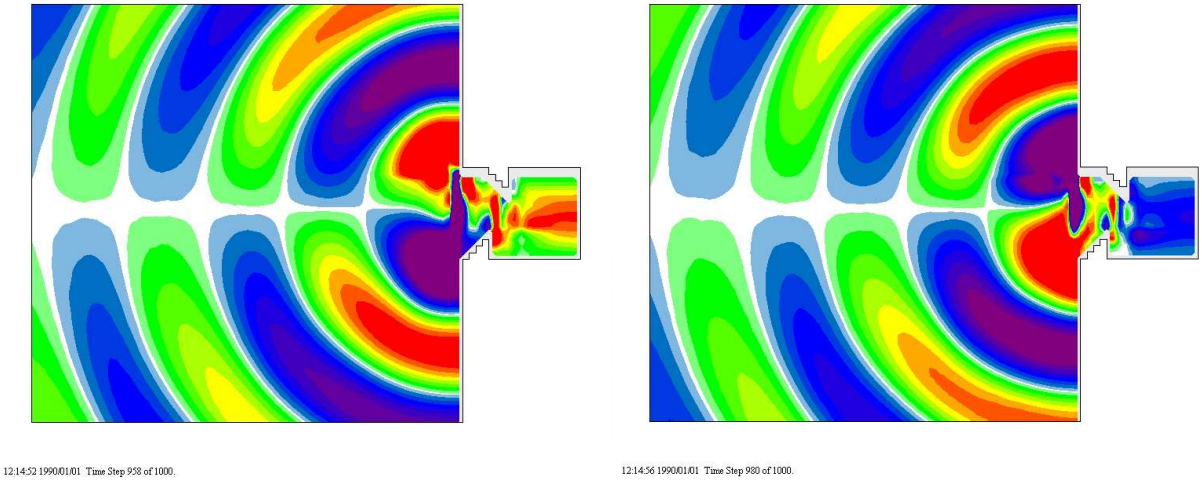

Figure C.9: Surface elevation η, flux P, flux Q for $T = 9.0s$.

a) η for two opposite phases.

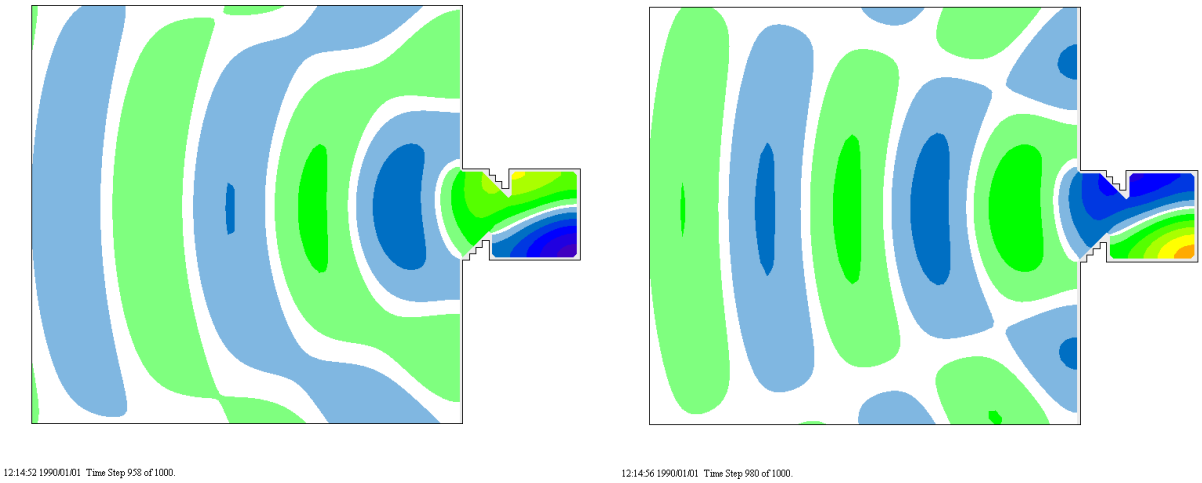

b) P for two opposite phases.

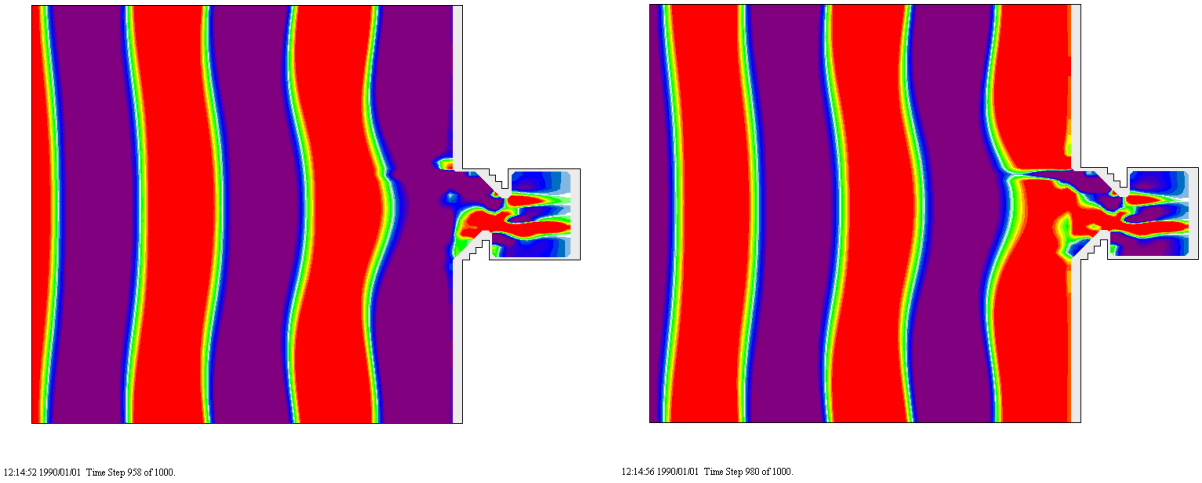

c) Q for two opposite phases.

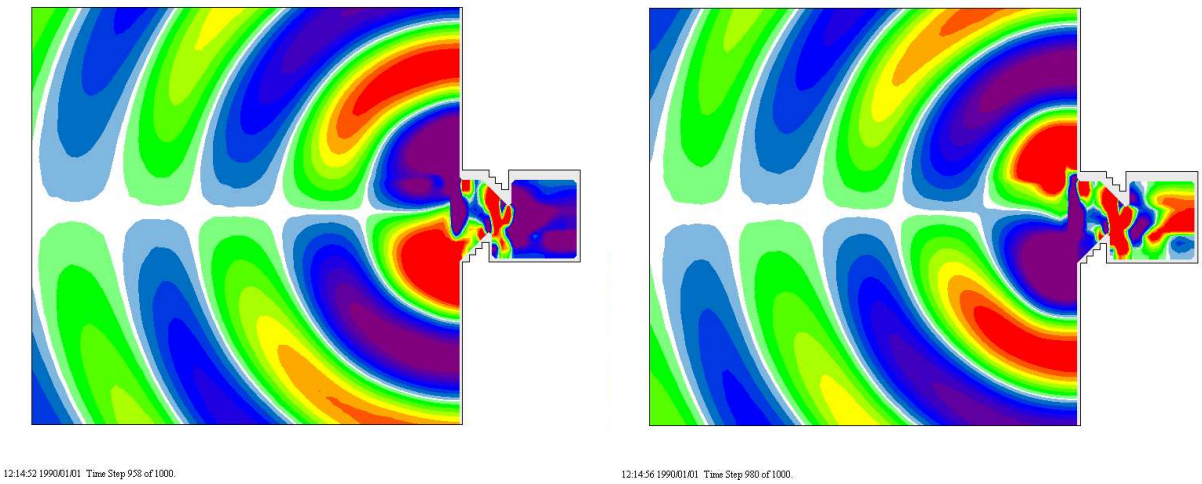

Figure C.10: Surface elevation η, flux P, flux Q for $T = 9.1s$.

a) η for two opposite phases.

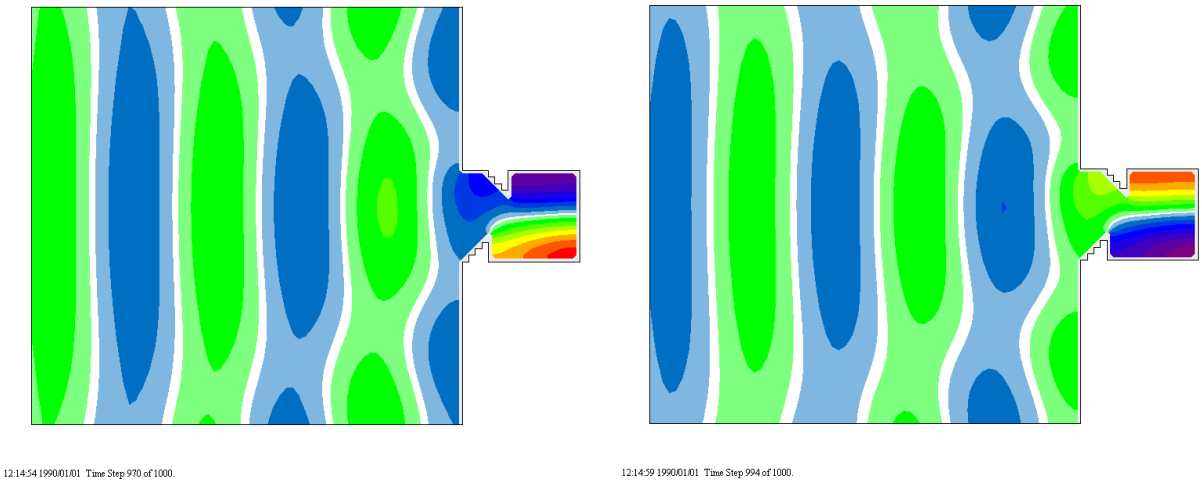

b) P for two opposite phases.

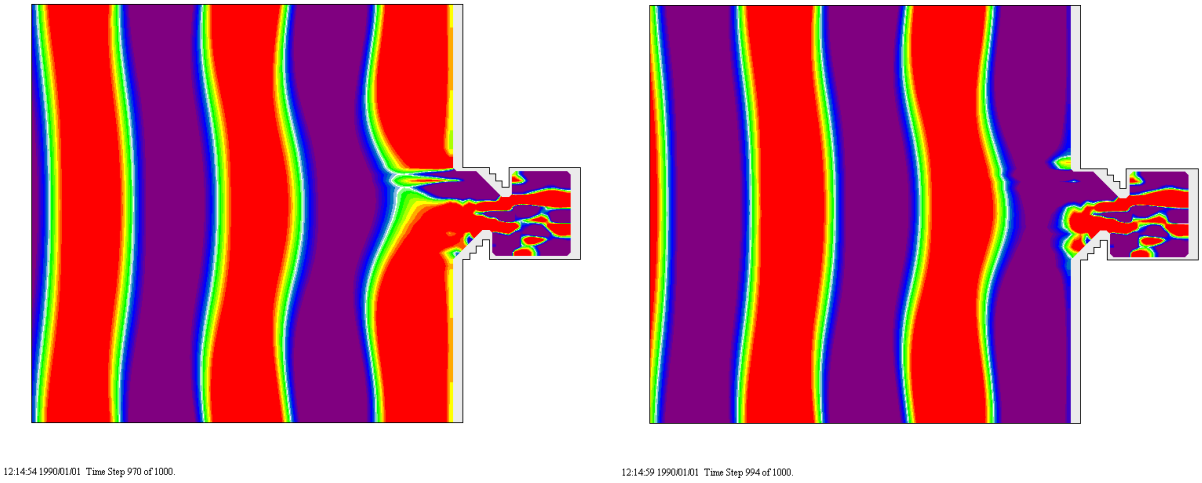

c) Q for two opposite phases.

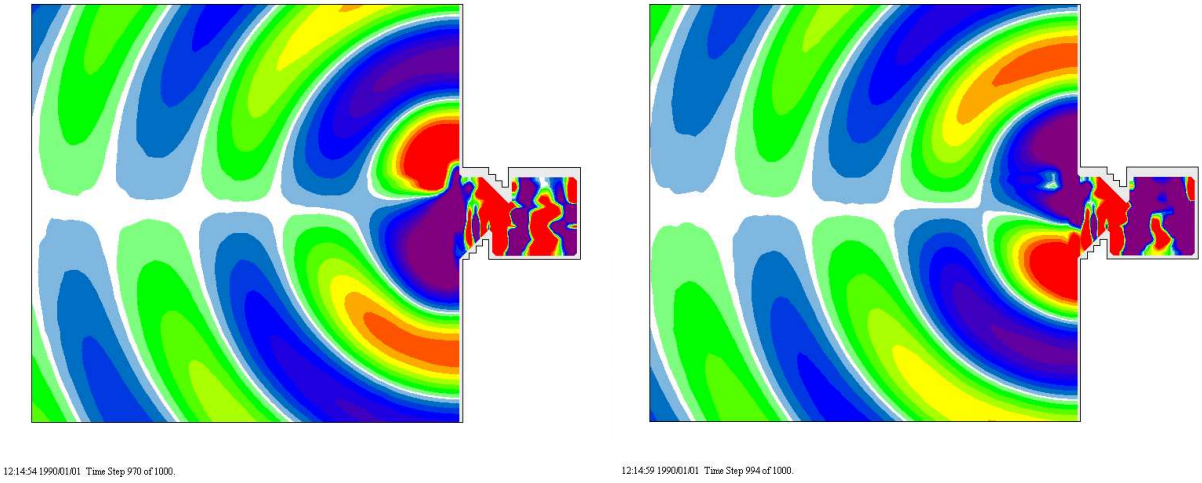

Figure C.11: Surface elevation η, flux P, flux Q for $T = 9.2s$.

a) η for two opposite phases.

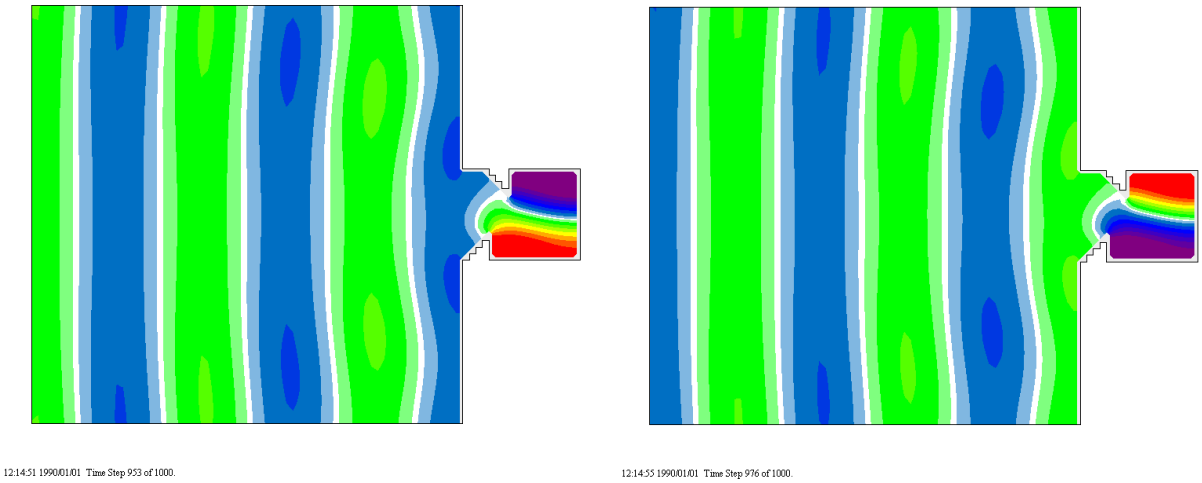

b) P for two opposite phases.

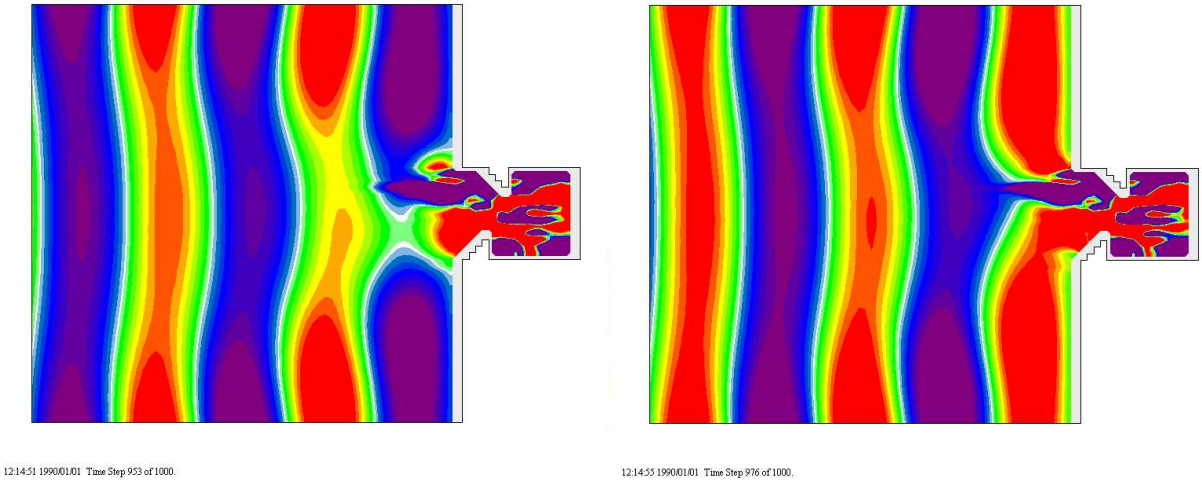

c) Q for two opposite phases.

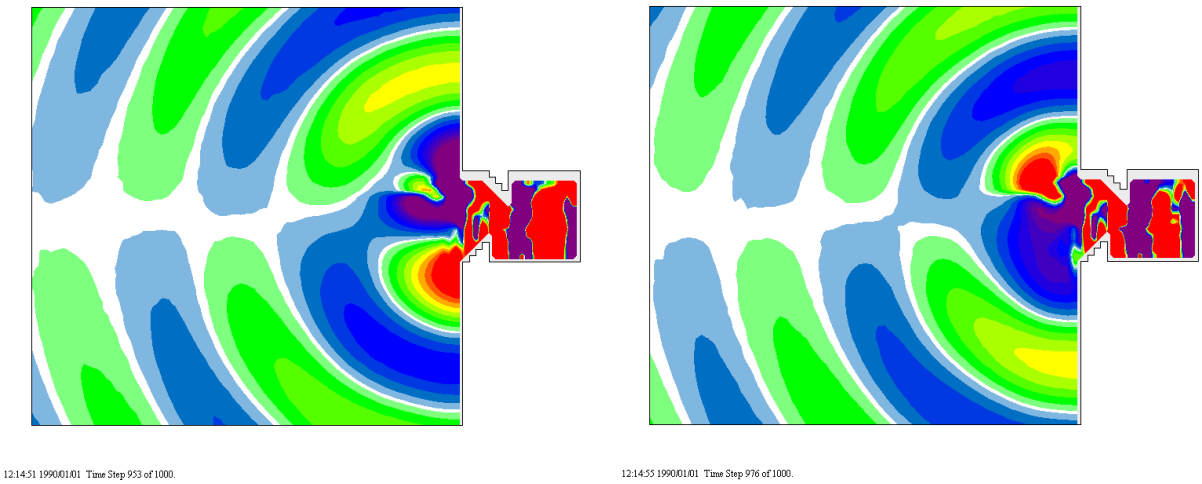

Figure C.12: Surface elevation η, flux P, flux Q for $T = 9.3s$.

a) η for two opposite phases.

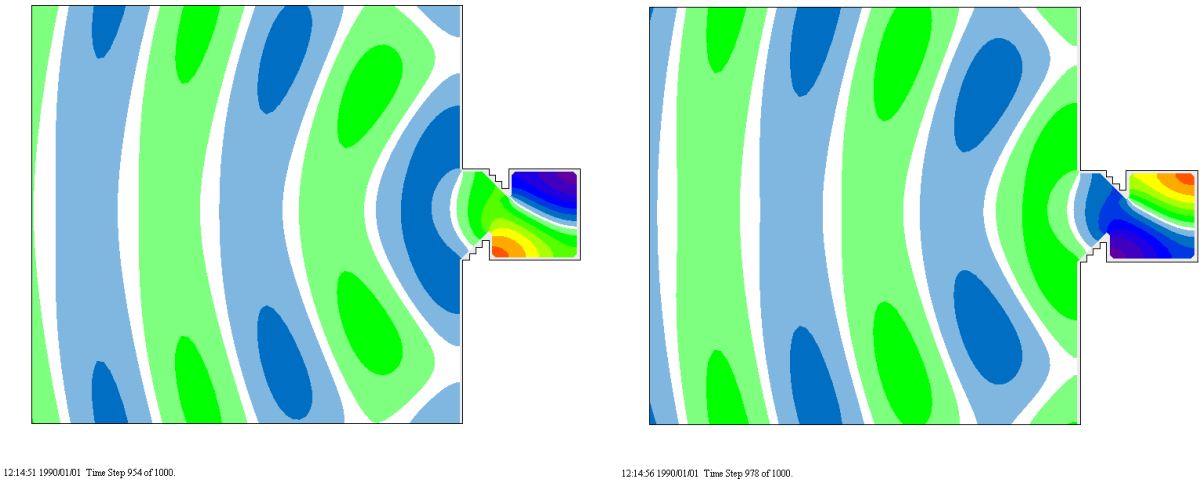

b) P for two opposite phases.

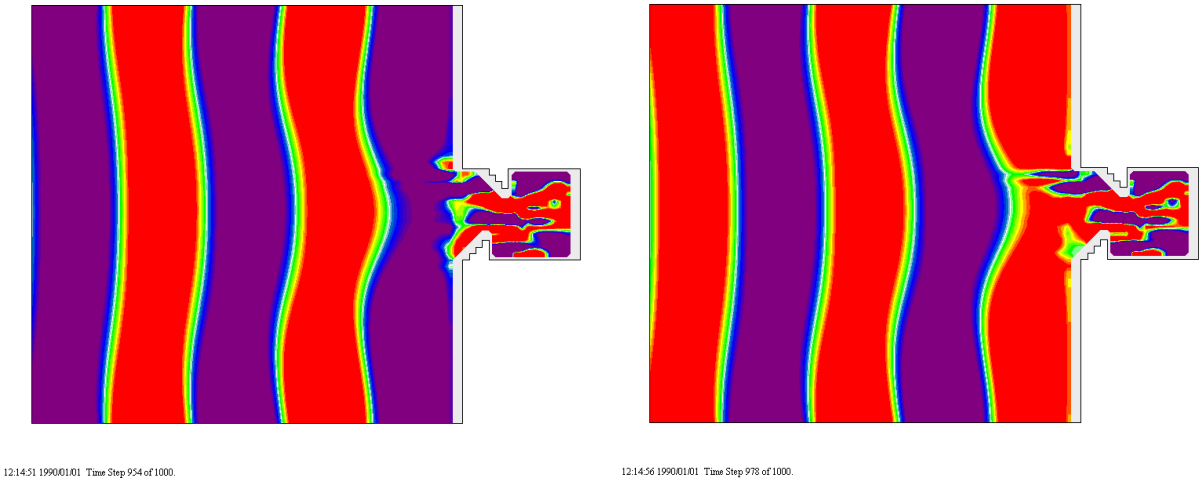

c) Q for two opposite phases.

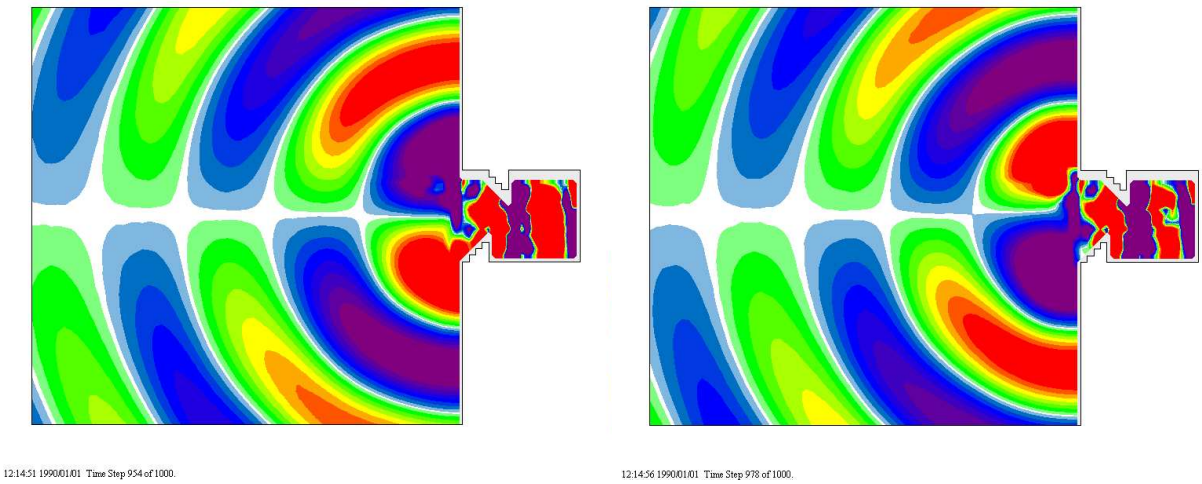

Figure C.13: Surface elevation η, flux P, flux Q for $T = 9.4s$.

a) η for two opposite phases.

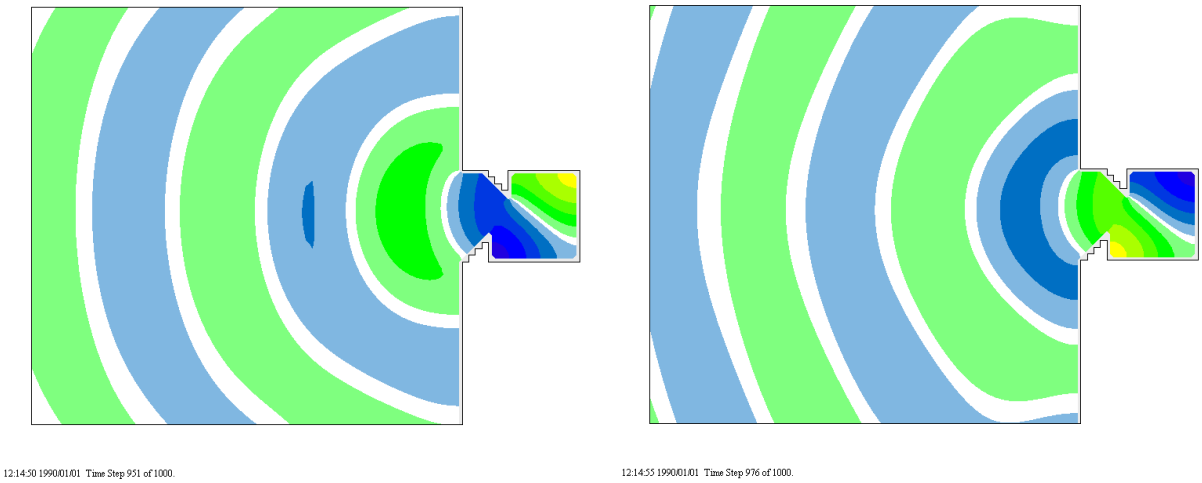

b) P for two opposite phases.

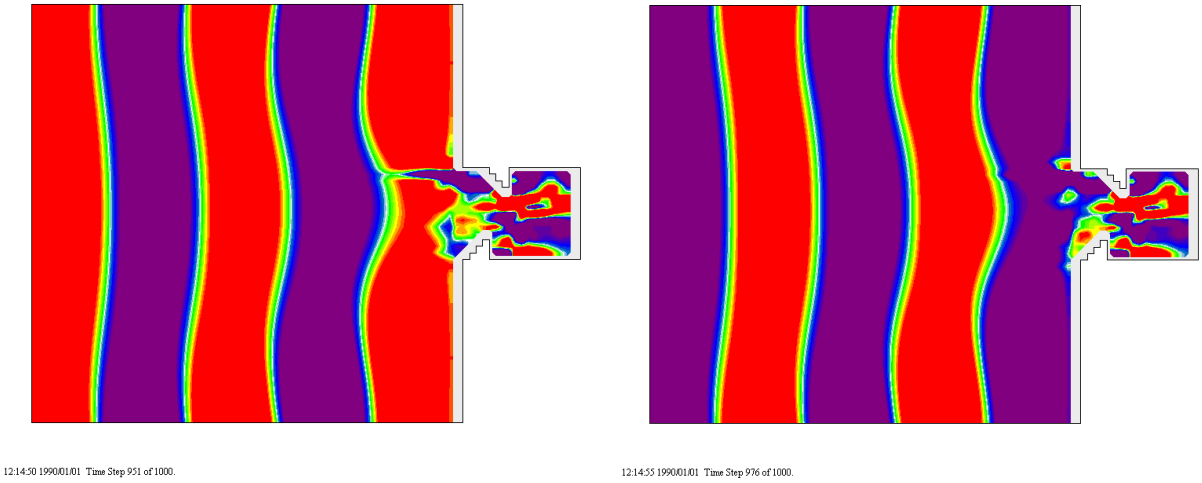

c) Q for two opposite phases.

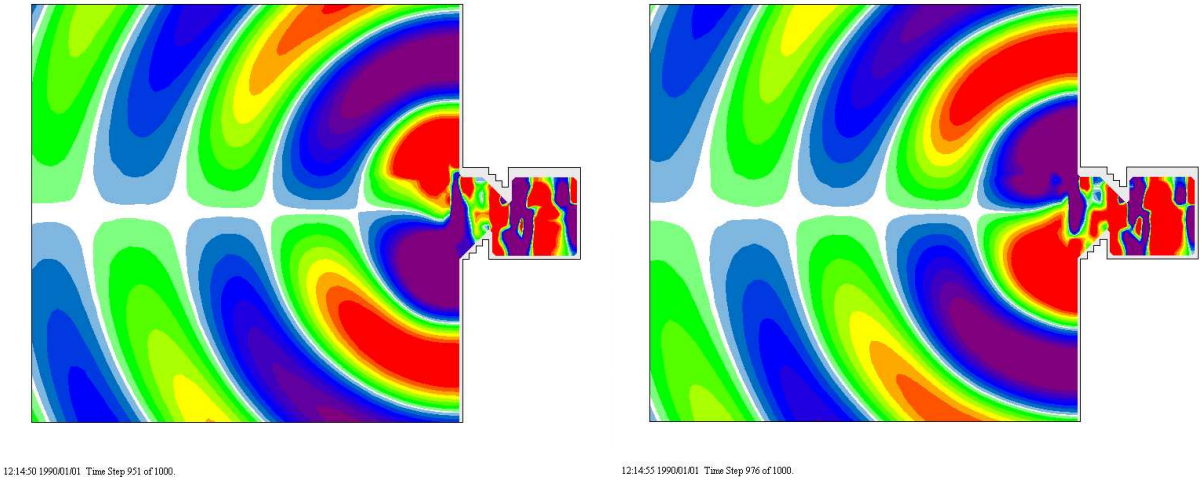

Figure C.14: Surface elevation η, flux P, flux Q for $T = 9.5s$.

a) η for two opposite phases.

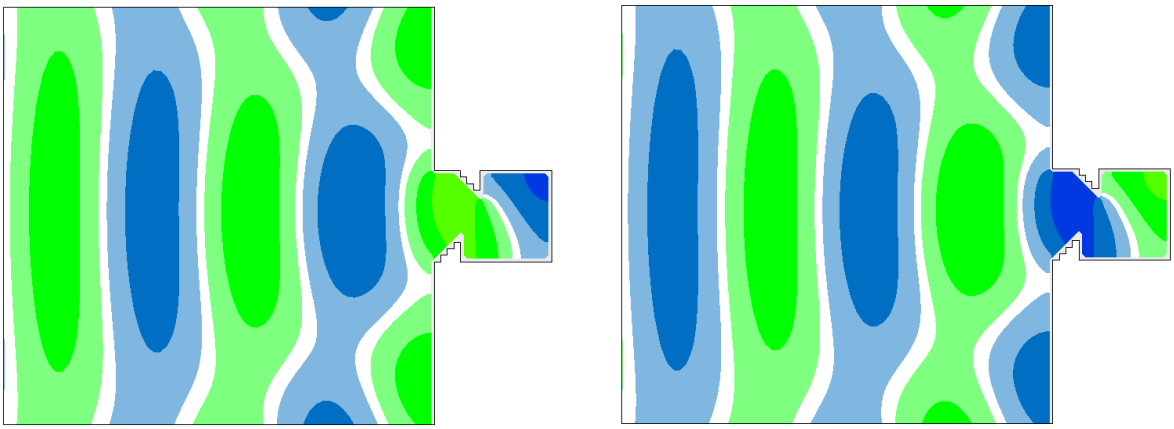

b) P for two opposite phases.

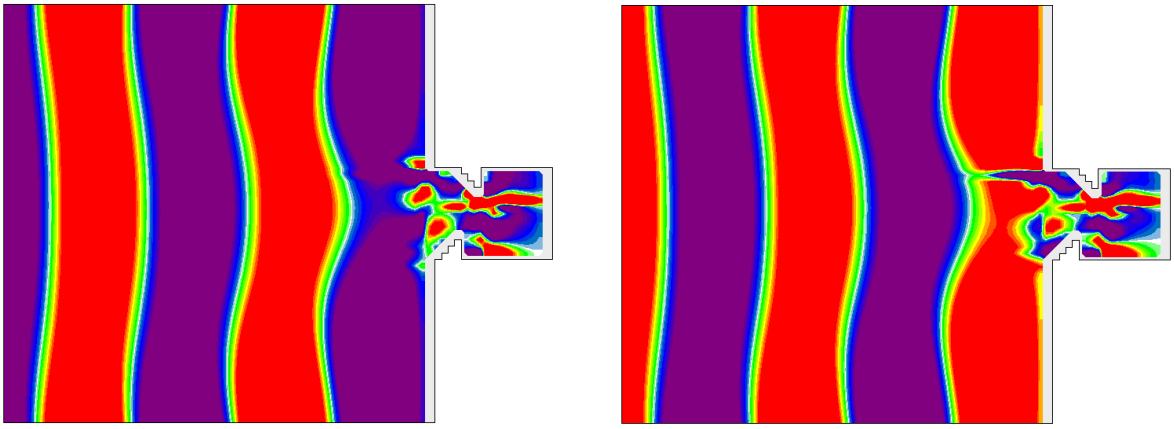

c) Q for two opposite phases.

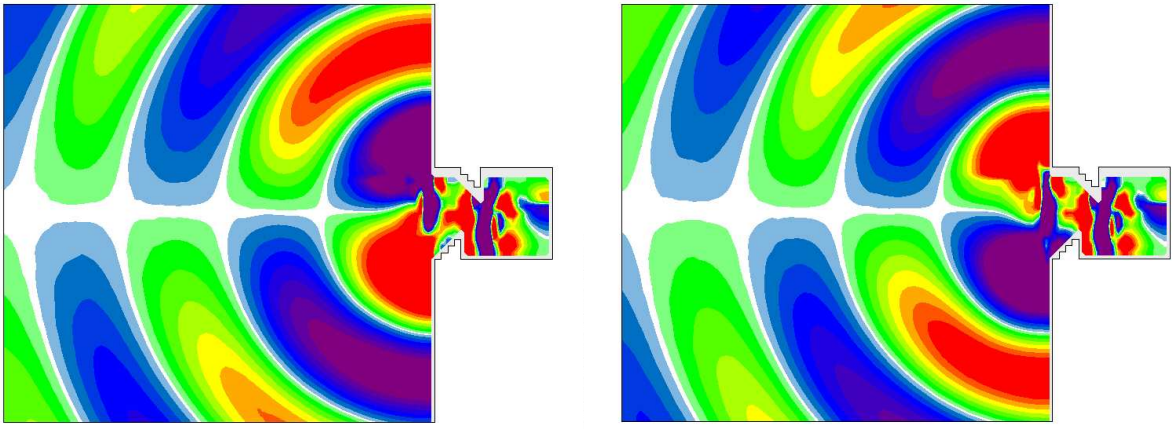

Figure C.15: Surface elevation η, flux P, flux Q for $T = 10.0s$.

a) η for two opposite phases.

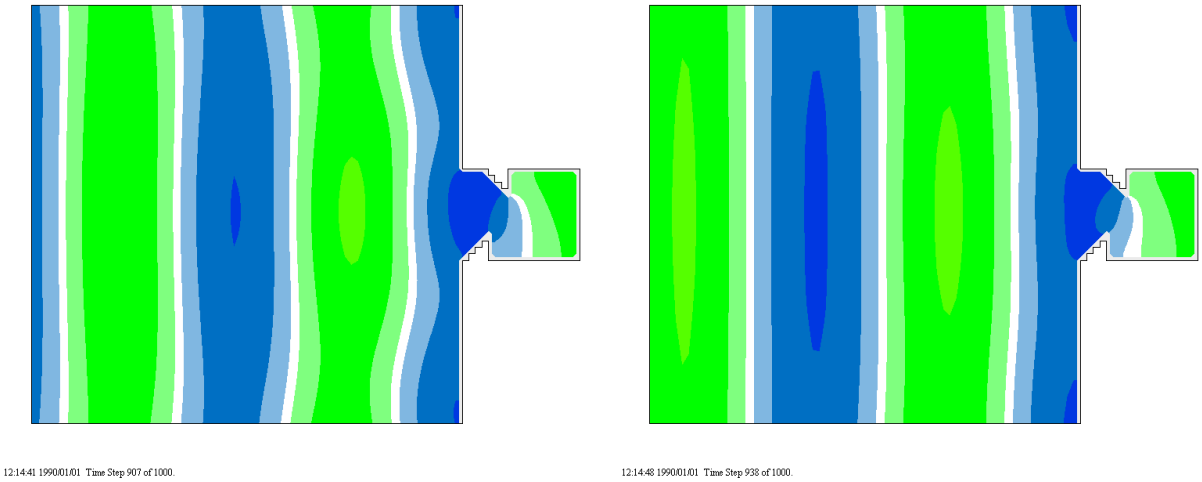

b) P for two opposite phases.

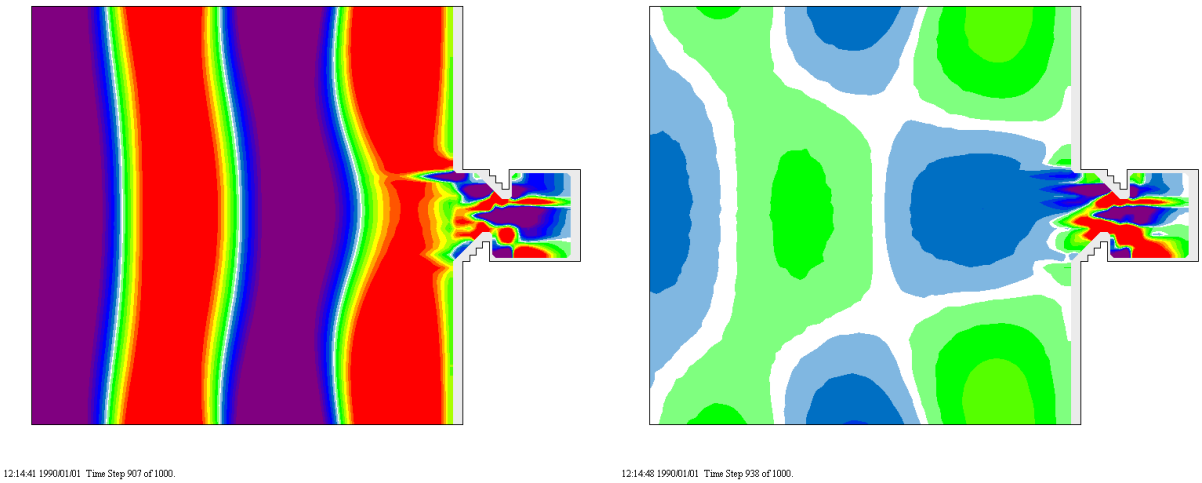

c) Q for two opposite phases.

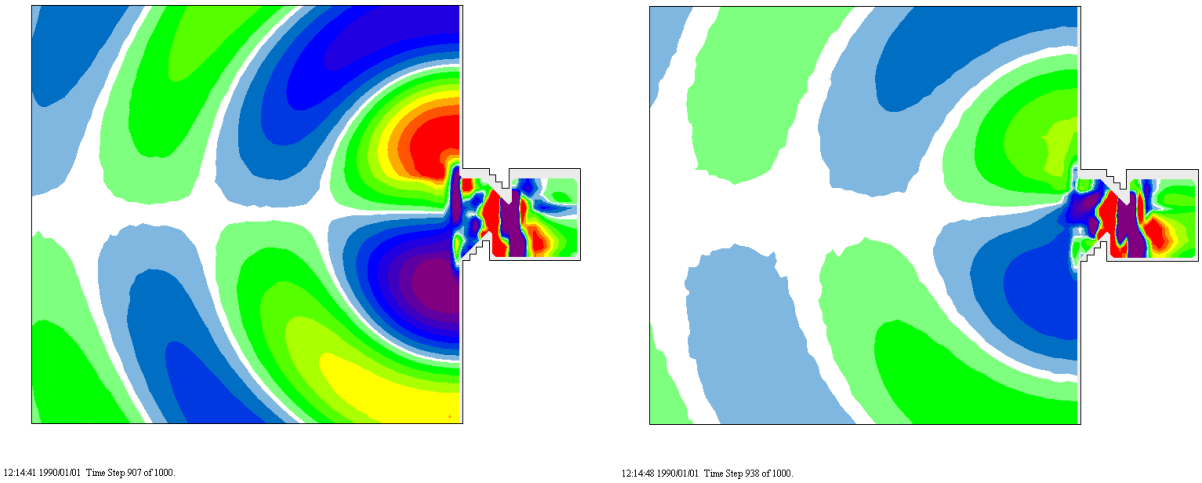

Figure C.16: Surface elevation η, flux P, flux Q for $T = 11.0s$.

a) η for two opposite phases.

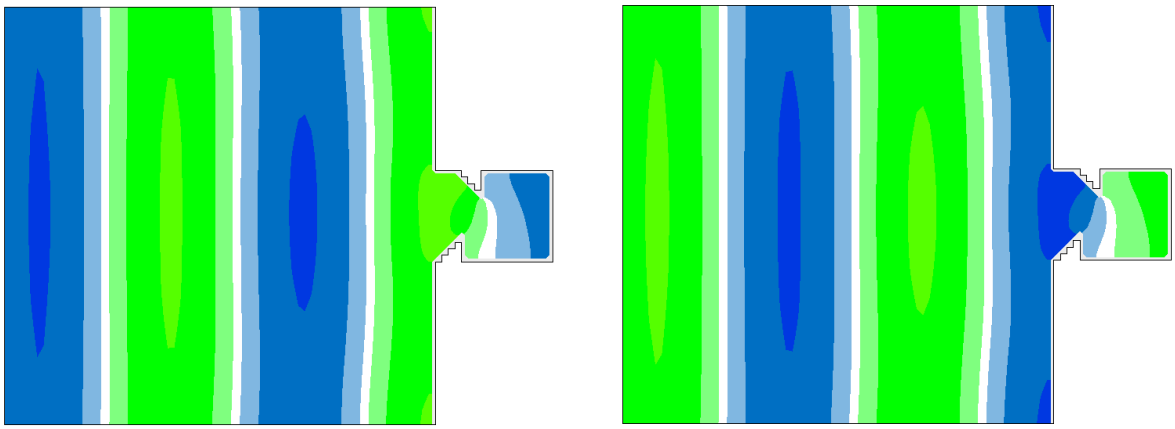

b) P for two opposite phases.

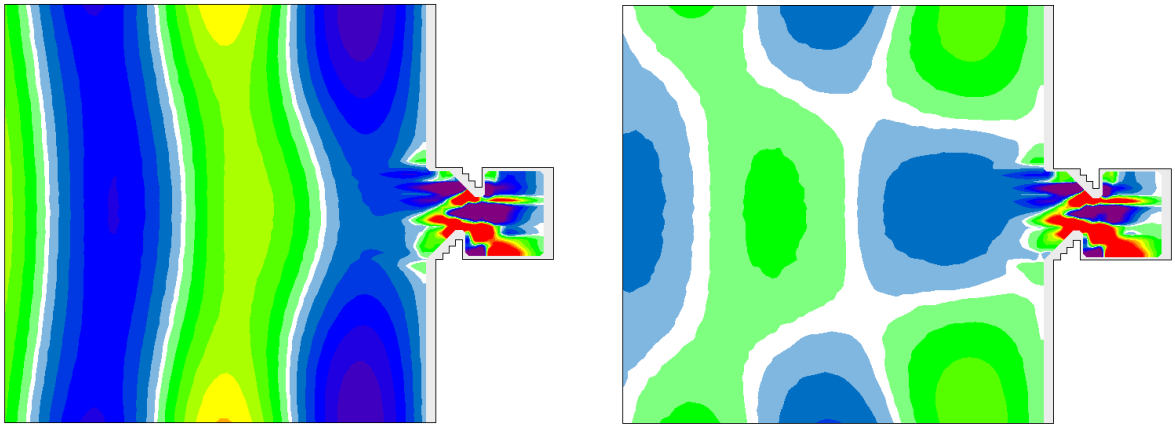

c) Q for two opposite phases.

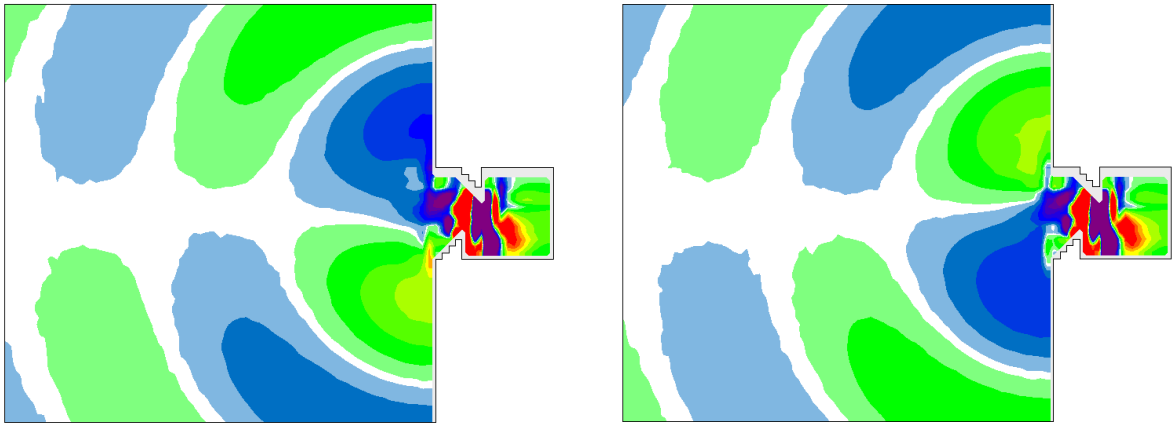

Figure C.17: Surface elevation η, flux P, flux Q for $T = 12.0s$.

a) η for two opposite phases.

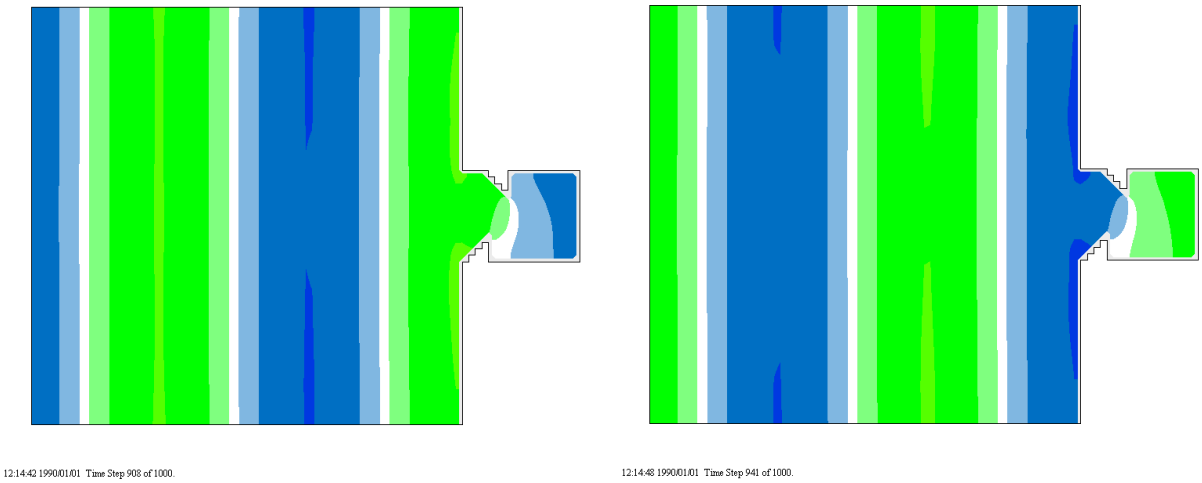

b) P for two opposite phases.

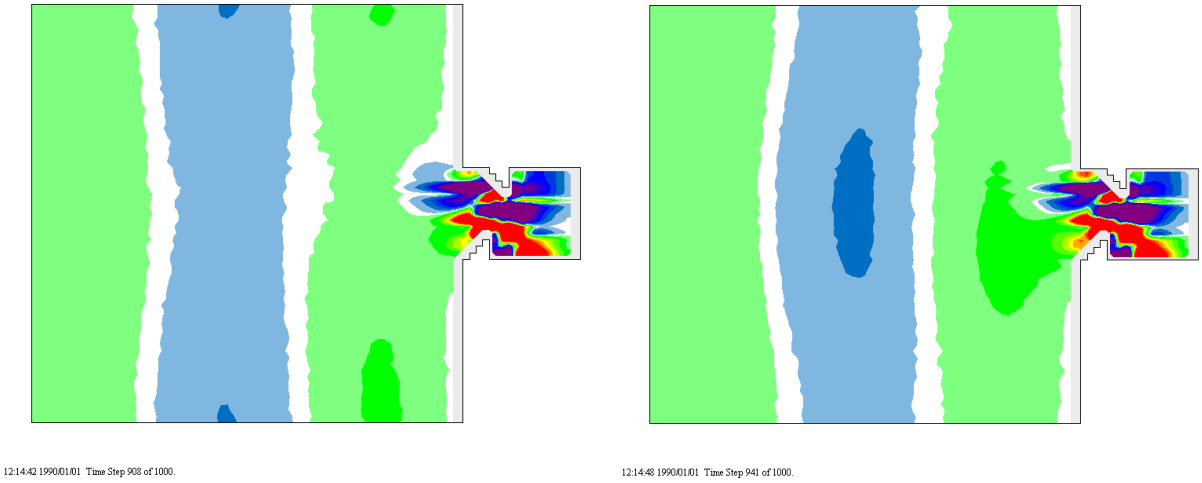

c) Q for two opposite phases.

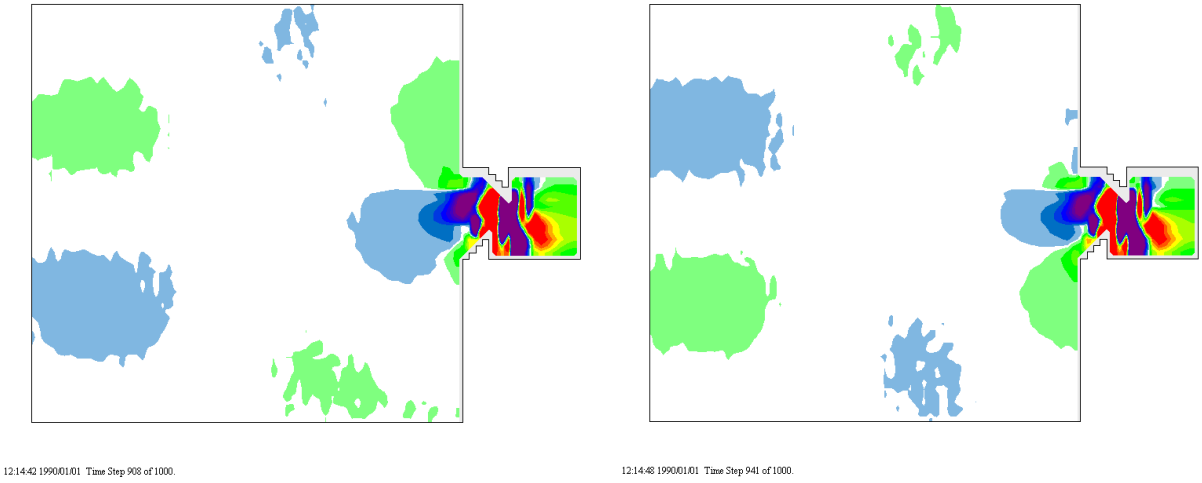

Figure C.18: Surface elevation η, flux P, flux Q for $T = 13.0s$.

a) η for two opposite phases.

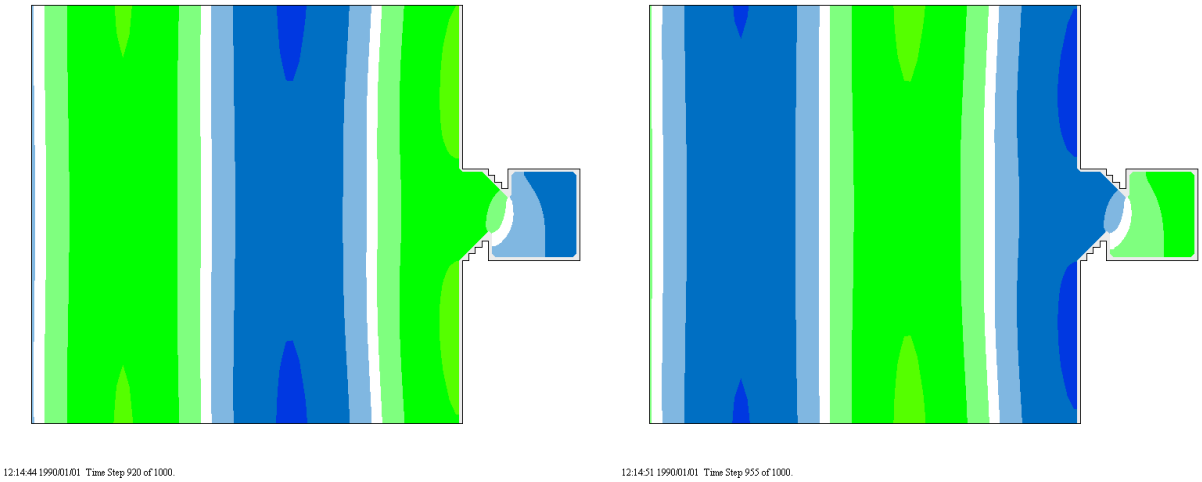

b) P for two opposite phases.

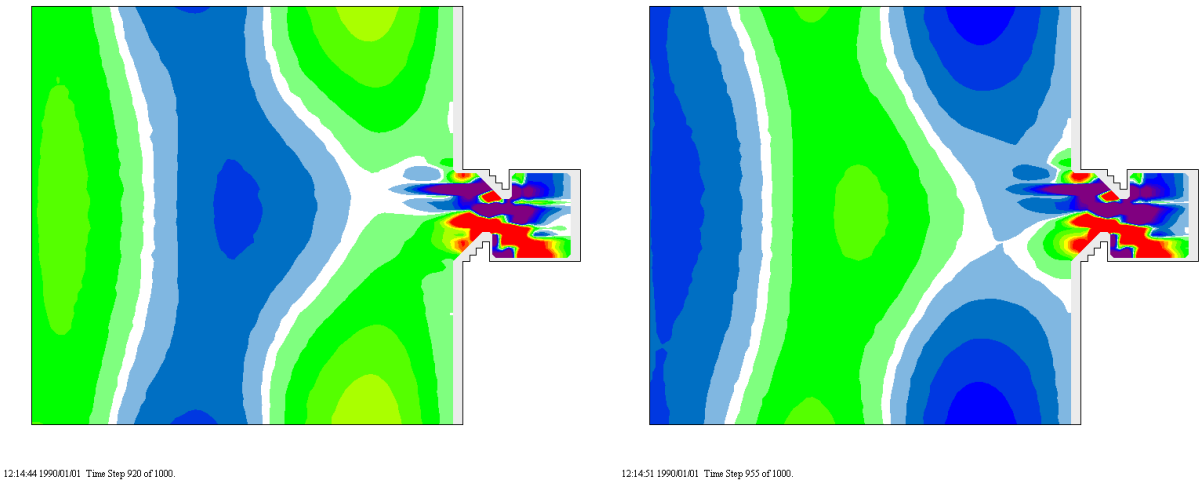

c) Q for two opposite phases.

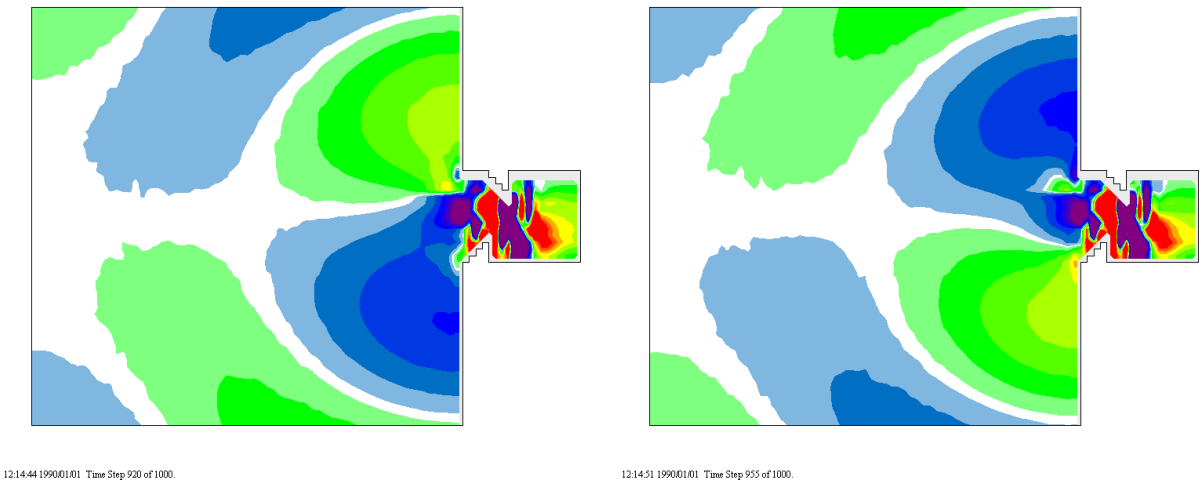

Figure C.19: Surface elevation η, flux P, flux Q for $T = 14.0s$.

a) η for two opposite phases.

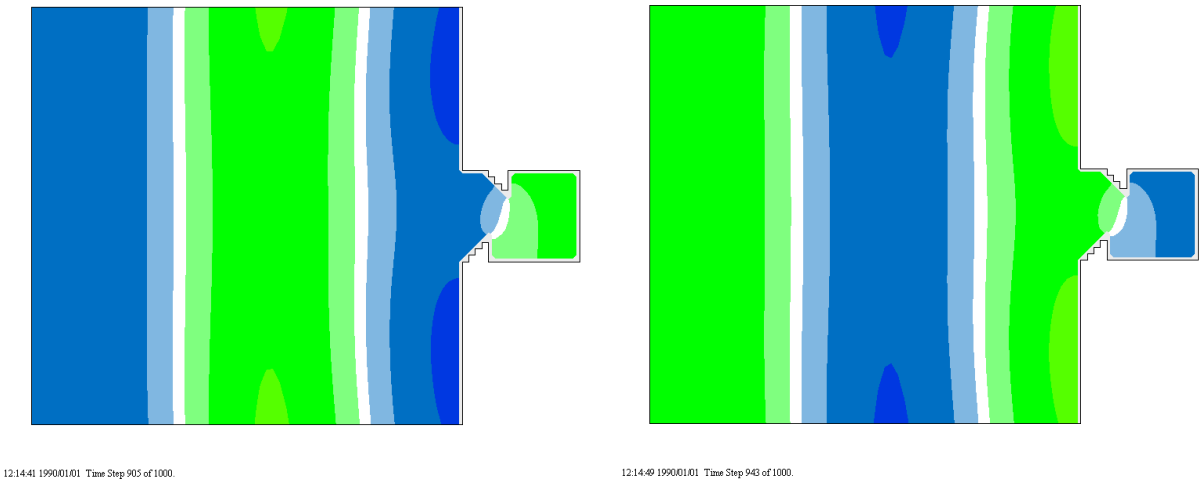

b) P for two opposite phases.

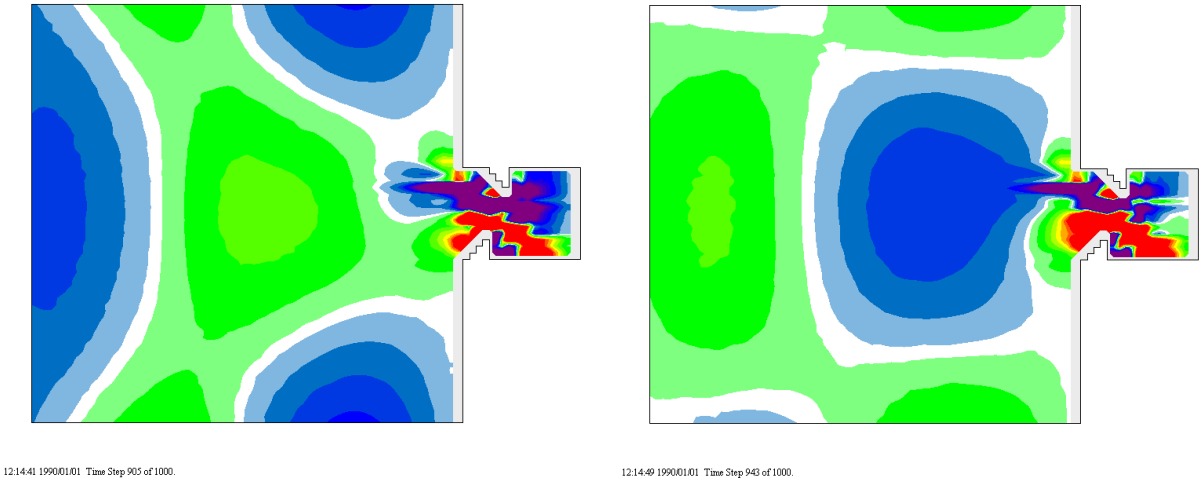

c) Q for two opposite phases.

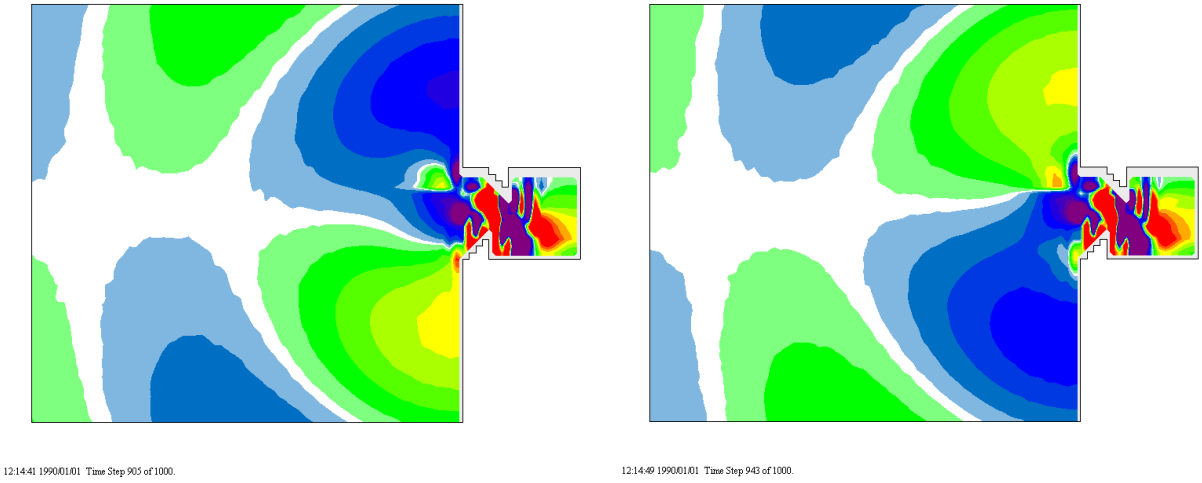

Figure C.20: Surface elevation η, flux P, flux Q for $T = 15.0s$.

a) η for two opposite phases.

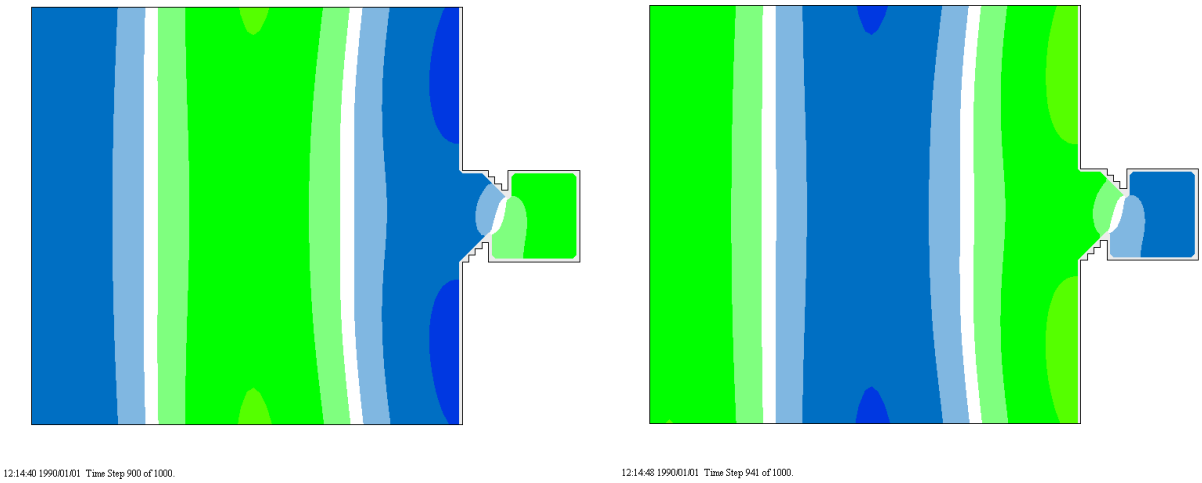

b) P for two opposite phases.

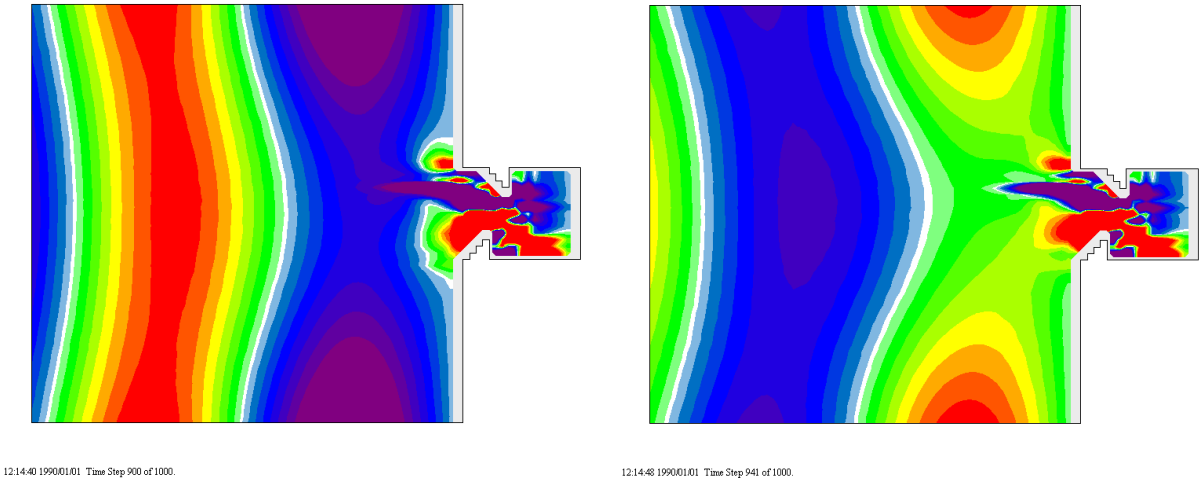

c) Q for two opposite phases.

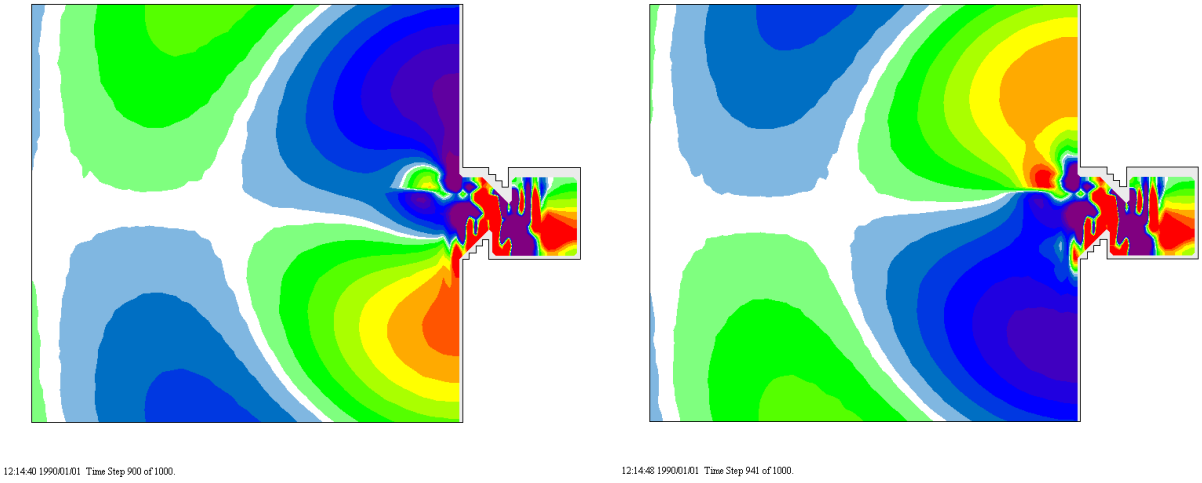

Figure C.21: Surface elevation η, flux P, flux Q for $T = 16.0s$.

List of References

Ambli, N., Bonke, K., Malmo, O. and Reitan, A. (1982). The Kvaerner multiresonant OWC. In: *2nd International Symposium on wave energy utilization*, pp. 275–295.

Arlitt, R., Tease, K., Starzmann, R. and Lees, J. (2007 September). Dynamic system modeling of an oscillating water column wave power plant based on characteristic curves obtained by computational fluid dynamics to enhance engineered reliability. In: *7th European Wave and Tidal Energy Conference*. Porto, Portugal.

Barstow, S. (2008). *Ocean wave energy. Current status and future perspectives*, chap. 4 The wave energy resource, pp. 93–132. Green Energy and Technology. Springer.

Bellotti, G. (2007). Transient response of harbours to long waves under resonance conditions. *Coastal Engineering*, vol. 54, pp. 680–693.

Black, K. and Mead, S. (2009). Design of surfing reefs. *Reef Journal*, vol. 1, pp. 177–191.

Brito-Melo, A., Hofman, T., Sarmento, A., Clement, A. and Delhommeau, G. (2000). Numerical modelling of owc-shoreline devices including the effect of the surroundings coastline and non-flat bottom. In: *Proc 10th Int offshore polar eng conf.*, vol. 1, pp. 743–748. Seattle, USA.

Brooke, J. (2003). *Wave Energy Conversion*. Elsevier Ocean Engineering Series. Elsevier Science.

Carrier, G., Shaw, R. and Miyata, M. (1971). The response of narrow mouthed harbours in a straight coastline to periodic incident waves. *Journal of Applied Mechanics*, pp. 335–344.

CDIAC (2007). Carbon dioxide information analysis center: Ranking of the world's countries by 2007 total carbon dioxide emissions from fossil fuel burning, cement production, and gas flaring [online]. Available: http://cdiac.ornl.gov/ [2011, January 7].

CEM (2006). *Coastal Engineering Manual*. US Army Corps of Engineers, Washington D.C. (in 6 volumes).

Chen, M. and Mei, C. (2000). Long-period oscillations in a harbour excited by broad-banded random sea waves. In: *Conference Of Global Chinese Scholars on Hydrodynamics*, pp. 3–8.

Clark, C. (2008 May). Constant-scale natural boundary map. ocean watersheds. Available at: `http://rightbasicbuilding.com/ [2011, October 25]`

Clement, A., McCullen, P., Falcão, A., Fiorentino, A., Gardner, F., Hammarlund, K., Lemonis, G., Lewis, T., Nielsen, K., Petroncini, S., Pontes, M., Schild, P., Sjöström, B.-O., Sørensen, H. and Thorpe, T. (2002). Wave energy in Europe: current status and perspectives. *Renewable and Sustainable Energy Reviews*, vol. 6, pp. 405–431.

Cossalter, V., Liberatore, G. and Toffolo, F. (1982). On the possibility of extracting power from resonant harbour oscillations. *Meccanica*, vol. 17, pp. 222–229. ISSN 0025-6455. 10.1007/BF02128315.
Available at: `http://dx.doi.org/10.1007/BF02128315`

Count, B.M. and Evans, D.V. (1984). The influence of projecting sidewalls on the hydrodynamic performance of wave-energy devices. *J. Fluid Mech.*, vol. 145, pp. 361–376.

Cruz, J. (2008). *Ocean Wave Energy. Current status and future perspectives.* Springer, Berlin.

DHI (2009). *MIKE 21 BW. Boussinesq waves module. Users Guide.* Danish Hydraulic Institute.

DoE (2010). Executive summary of the draft integrated electricity resource plan for South Africa 2010 to 2030. Draft, compiled by the Department of Energy. 22 October 2010.

Evans, D. (1982 June). Wave-power absorption within a resonant harbour. In: *Proc., 2nd Int. Symposium on wave energy utilization*, pp. 371–378. Trondheim, Norway.

Evans, D. (1988). The maximum efficiency of wave-energy devices near coast lines. *Applied Ocean Research*, vol. 10, no. 3, pp. 162–164.

Falcao, A. (2010). Wave energy utilization: A review of the technologies. *Renewable and Sustainable Energy Reviews*, vol. 14, no. 3, pp. 899–918.

Falcao, A.d.O. (2000 December). The shoreline owc wave power plant at theAzores. In: *Fourth European Wave Energy Conference.* Aalborg, Denmark.

Falnes, J. (2002). *Ocean waves and oscillating systems. Linear interactions including wave energy extraction.* Cambridge University Press.

Falnes, J. (2005 February). Havbolgje-energi havbï¿½lgje-energi. Presentation.

Falnes, J. (2007). A review of wave-energy extraction. *Marine Structures*, vol. 20, pp. 185–201.

Falnes, J. and Budhal, K. (1978). Wave power conversion by point absorbers. *Norwegian Maritime Research*, vol. 4, pp. 2–11.

Falnes, J. and Hals, J. (1999 June). Wave energy and its utilisation: A contribution to the EU Leonardo pilot project 1860 Alter ECO. http://www.ntnu.no/.

Folley, M. and Whittaker, T. (2009). Analysis of the nearshore wave energy resource. *Renewable Energy*, vol. 34, pp. 1709–1715.

Gierlevsen, T., Hebsgaard, M. and Kirkegaard, J. (2001 October). Wave disturbance modelling in the Port of Sines, Portugal with special emphasis on long period oscillations. In: *International Conference on Port and Maritime R&D and Technology*. Singapore.

Gouaud, F., Rey, V., Piazzola, J. and Hooff, R.V. (2010). Experimental study of the hydrodynamic performance of an onshore wave power device in the presence of an underwater mound. *Coastal Engineering*, vol. 57, no. 11-12, pp. 996 – 1005. ISSN 0378-3839.
Available at: `http://www.sciencedirect.com/science/article/pii/S0378383910000979`

Hagerman, G. (1992). Wave energy resource and economic assessment for the State of Hawaii. Tech. Rep., SEASUN Power Systems.

Holthuijsen, L. (2007). *Waves in oceanic and coastal waters*. Cambridge, UK.

Huang, L. and Tuck, E. (1970). On the oscillations of harbours of arbitrary shape. *Journal of Fluid Mechanics*, vol. 42, pp. 447–464.

IEA (2010). Power generation from coal. Measuring and reporting efficiency performance and carbon dioxide emissions. Tech. Rep., International Energy Agency.

James, W. (1968 August). Rectangular resonators for harbour entrances. In: *11th International Conference on Coastal Engineering*, 11, pp. 1512–1530. London.

James, W. (1970 September). Spectral response of harbour resonator configurations. In: *12th Conference in Coastal Engineering*, pp. 2181–2194. Washington D.C.

James, W. (1971 February). Two innovations for improving harbour resonators. *Journal of Waterway, Port, Coastal, and Ocean Engineering*, vol. WW1, pp. 115–122.

James, W. (1980). Power from waves using harbour resonators. *Journal of Waterway, Port, Coastal, and Ocean Engineering*, vol. 106, pp. 99–113.

Joubert, J. (2008). *An investigation of the wave energy resource on the South African coast, focusing on the spatial distribution of the South West coast.* Master's thesis, University of Stellenbosch, South Africa.

Karambas, T. and Gousidou, M. (2006). Modelling wave attenuation by submerged resonators. *Maritime Engineering*, vol. 159, no. MA2, pp. 45–53.

Khan, J. and Bhuyan, G. (2009 March). Ocean energy: Global technology development status, report. Tech. Rep. IEA-OES Document No.: T0104, Powertech Labs for the IEA-OES.
Available at: `www.iea-oceans.org`

Kofoed-Hansen, H., Kerper, D., Sorensen, O. and Kirkegaard, J. (2005). Simulation of long wave agitation in ports and harbours using a time-domain Boussinesq model. In: *Fifth International Symposium on Ocean Wave Measurement and Analysis WAVES.* Madrid, Spain.

Kramer, M. and Frigaard, P. (2002). Efficient wave energy amplification with wave reflectors. In: *Twelfth International Offshore and Polar Engineering Conference*, pp. 707–712.

Le-Mehaute, B. (1961 March). Theory in wave agitation in a harbor. *Journal of the Hydraulics Division*, vol. 87, no. HY 2, pp. 31–50.

Lee, J. (1969). Wave induced oscillations in harbors of arbitrary shape. Tech. Rep. Rep. No. KH-R-20, W. M. Keck Lab. Of Hyd. and Water Res., California Institute of Technology, Pasadena, California.

Lee, J. and Raichlen, F. (1971). Wave induced oscillations in harbors with connected basins. Tech. Rep. Rep. No. KH-R-26, W. M. Keck Lab. Of Hyd. and Water Res., California Institute of Technology, Pasadena, California.

Leppeletier, T. and Raichlen, F. (1987). Harbour oscillations induced by nonlinear transient long waves. *Journal of Waterway, Port, Coastal and Ocean Engineering*, vol. 113, pp. 381–400.

Li, D. (2002). *Los Angeles Long Beach Harbour pier 400. Harbour resonance study using numerical model CGWAVE.* Ph.D. thesis, The University of Maine.

Liu, P. (1986). Effects of depth discontinuity on harbour oscillations. *Coastal Engineering*, vol. 10, pp. 395–404.

Malmo, O. and Reitan, A. (1986*a*). Wave-power absorption by a finite row of oscillating water columns in a reflecting wall. *Applied Ocean Research*, vol. 8, no. 2, pp. 105–109.

Malmo, O. and Reitan, A. (1986*b*). Wave-power absorption by an oscillating water column in a reflecting wall. *Applied Ocean Research*, vol. 8, no. 1, pp. 42–48.

Marcos, M., Monserrat, S., Medina, R. and Lomónaco, P. (2005). Resonse of a harbour with two connected basins to incoming long waves. *Applied Ocean Research*, vol. 27, pp. 209–215.

Martins-Rivas, H. (2008 June). *Power extraction from an oscillating water column along a coast*. MSc, Department of Aeronautics and Astronautics, Massachusetts Institute of Technology.

Martins-Rivas, H. and Mei, C. (2007). Diffraction effects near Foz do Douro breakwater. *7th EuropeanWave and Tidal Energy Conference*, vol. 36, pp. 426–433.

Martins-Rivas, H. and Mei, C. (2009). Wave power extraction from an oscillating water column along a straight coast. *Ocean Engineering*, vol. 36, pp. 426–433.

McCormick, M. (2007). *Ocean Wave Energy Conversion*. Dover ed.

McIver, P. and Evans, D.V. (1988). An approximate theory for the performance of a number of wave-energy devices set into a reflecting wall. *Applied Ocean Research*, vol. 10, no. 2, pp. 58–65.

Mei, C. and Petroni, R. (1973). Waves in a harbour with protruding breakwaters. *Journal of the Waterways Harbour and Coastal Engineering Division*, vol. 99, pp. 209–229.

Miles, J. and Munk, W. (1961 August). Harbour paradox. *Waterways and Harbors Division*, vol. 87, pp. 111–130.

Miles, M. (1997). Gedap user's guide for Windows NT. Tech. Rep. HYD-TR-021, Canadian Hydraulics Centre.

Nakamura, T. (2005). Sheltering of long period waves to a rectangular harbor by a resonator. In: *Proc. 5th International Symposium WAVES 2005*, 82, pp. 1–10. Madrid.

Nakamura, T. and Latt, N. (2008). Effectiveness of a resonator under breaking and non-breaking wave conditions. In: *Coastal Engineering*, pp. 4751–4764.

Pitt, E. (2009). Assessment of wave energy resource. Marine renewable energy guides, European Marine Energy Centre (EMEC).

Polinder, H., Damen, M. and Gardner, F. (2005). Design, modelling and test results of the aws pm linear generator. *European Transactions on Electrical Power.*, vol. 15, pp. 245–256.

Previsic, M. (2004 June). E2i epri assessment. offshore wave energy convertion devices. Tech. Rep. E2I EPRI WP-004-US-Rev.1, E2I EPRI.

Rabinovich, A. (2010). *Handbook of coastal and ocean engineering*, chap. Seiches and Harbour Oscillations, pp. 193–236. World Scientific.

Raichlen, F. (1966). *Estuary and coastline hydrodynamics*, chap. Harbour Resonance, pp. 281–340. Engineering Societies Monographs. McGraw-Hill.

Raichlen, F. and Ippen, A. (1965 March). Wave induced oscillations in harbours. *Journal of the Hydraulics Division*, vol. 91, no. HY2, pp. 1–26.

Retief, D., Muller, J. and Prestedge, G. (1982). A proposal for wave energy conversion near Cape Town. In: *18th International Conference on Coastal Engineering*, pp. 245–260. ICCE, Cape Town.

Salter, S. (1974). Wave power. *Nature*, vol. 249, pp. 720–724.

Sorensen, H., Friis-Madsen, E., Panhauser, W., Dunce, D., Nedkvintne, J., Frigaard, P., Kofoed, J., Knapp, W., Rieman, S., Holmen, E., Raulund, A., Praest, J., Hansen, L., Christensen, L., Nohrlind, T., Bree, T. and McCullen, P. (2003). Development of wave dragon from scale 1:50 to prototype. In: *Fifth European Wave Energy Conference*. Available at: `www.wavedragon.net`

Spiers, T. (1976 April). *Experimental Study of Return Flow Drawn from Harbour Resonators*. Ph.D. thesis, McMaster University, Hamilton, Ontario.

Tease, W., Lees, J. and Hall, A. (2007 September). Advances in oscillating water column air turbine development. In: *7th European wave and tidal energy conference*. Porto, Portugal.

Thompson, E.F., Chen, H. and Hadley, L. (1996 September/October). Validation of numerical model for wind waves and swell in harbors. *Journal of waterway, port, coastal, and ocean engineering*, vol. 122, no. 5, pp. 245–257.

Thorpe, T. (1999 May). A brief review of wave energy. A report produced for the UK Department of Trade and Industry. Final ETSU Report R-122., AEA Technology plc. Produced for The UK Department of Trade and Industry, UK.

Tomisawa, Y., Ikoma, T., Masuda, K., Osawa, H., Ito, K. and Maeda, H. (2008). Wave energy absorption performance of P.W.-OWC type by harbor resonance. In: *Energy and Climate Change*. Pacific Congress on Marine Science and Technology (PACON), Honolulu, Hawaii.

Torre-Enciso, Y., Ortubia, I., Lopez de Aguilera, L. and Marquez, J. (2009). Mutriku wave power plant: from thinking to reality. In: *8th European Wave and Tidal Energy Conference*, pp. 319–329.

Tseng, R., Wua, R. and Huang, C. (2000). Model study of a shoreline wave-power system. *Ocean Engineering*, vol. 27, pp. 801–827.

Twu, S.W. and Liou, C. (2003). Damping long waves by a multi-channel structure. *Ocean Engineering*, vol. 30, pp. 351–367.

Valembois, J. (1953). Etude de l'action d'ouvrages resonants sur la propagation de la houle. investigation of the effect of resonant structures on wave propagation. In: *Minnesota International Hydraulics Convention*. Minnesota.

Van der Molen, V., Rossouw, M., Phelp, D., Tulsi, K. and Terblanche, L. (2010). Innovative technologies to accurately model waves and moored ship motions. Available at: `http://www.conference.csir.co.za/`

Wang, D., Katory, M. and Li, Y. (2002). Analytical and experimental investigation on the hydrodynamic performance of onshore wave-power devices. *Ocean Engineering*, vol. 29, pp. 871–885.

Wang, G., Dong, G., Perlin, M., Ma, X. and Ma, Y. (2011*a*). An analytic investigation of oscillations within a harbour of constant slope. *Ocean Engineering*, vol. 38, pp. 479–486.

Wang, S., Yuan, P., Li, D. and Jiao, Y. (2011*b*). An overview of ocean renewable energy in China. *Renewable and Sustainable Energy Reviews*, vol. 15, no. 1, pp. 91–111.

Wavegen (2002a). Islay limpet project monitoring final report. Tech. Rep. ETSU V/06/00180/00/Rep.

Wavegen (2002b). Research into the further development of the limpet shoreline wave energy plant. Tech. Rep. ETSU V/06/00183/REP URN 02/1487.

Weinstein, A. (2006). Harvesting the motion of the ocean. presentation. AquaEnergy Group.

Whittaker, T., Langston, D., Fletcher, N., Shaw, M. and Falcao, A.O. (2002 1 November 1998 to 30 April 2002). Islay limpet wave power plant. Tech. Rep. Contract JOR3-CT98-0312, The Queens University of Belfast in partnership with Wavegen Ireland Ltd., Charles Brand Ltd, Kirk McClure Morton and I.S.T. Portugal.

Wilson, B. (1954). The mechanism of seiches in Table Bay Harbour, Cape Town. In: *Proc. 4th Conf. Coastal Engineering*, pp. 52–77. Berkeley.

Wu, Y. (1992 June). A theoretical study of end effects for rectangular resonators on narrow channels. *Applied Math. Modelling*, vol. 16, pp. 307–313.

Xing, X. (2009). *Computer modeling for wave oscillation problems in harbours and coastal regions*. Master's thesis, University of Southern California.

Xing, X., Lee, J. and Raichlen, F. (2010). Harbor resonance: A comparison of field measurements to numerical results. In: *ICCE*, pp. 1–12.

Zelt, J. (1986 June). Tsunamis: The response of harbours with sloping boundaries to long wave excitation. Tech. Rep. KH-R-47, W. M. Keck Laboratory of Hydraulics and Water Resources, Div. of Eng. and Appl. Sci., California Institute of Technology, Pasadena, Calif.